Modelling and Measurement Analysis of the Satellite MIMO Radio Channel

Unwana M. Ekpe

Submitted for the Degree of
Doctor of Philosophy
from the
University of Surrey

Centre for Communication Systems Research
Department of Electronic Engineering
Faculty of Engineering and Physical Sciences
University of Surrey
Guildford, Surrey GU2 7XH, UK

January 2012

Abstract

The increasing demand for terrestrial and satellite delivered digital multimedia services has precipitated the problem of spectrum scarcity in recent years. This has resulted in deployment of spectral efficient technologies such as MIMO for terrestrial systems. However, MIMO cannot be easily deployed for the satellite channel using conventional spatial multiplexing as the channel conditions here are very different from the terrestrial case, and it is often dominated by line of sight fading. Orthogonal circular polarization, which has long been used for increasing both frequency reuse and the power spectral density available to earth-bound satellite terminals, has recently been recommended for directly increasing the throughput available to such devices. Following that theme, this thesis proposes a novel dual circular polarisation multiplexing (DCPM) technique, which is aimed at the burgeoning area of throughput-hungry digital video broadcasting via satellite to handheld devices (DVB-SH) and digital video broadcast to the next generation of handheld (DVB-NGH) systems.

In determining the working limits of DCPM, a series of measurement campaigns have been performed, from which extensive dual circular polarised land mobile satellite (LMS) channel data has been derived. Using the newly available channel data and with the aid of statistical channel modelling tools found in literature, a new dual circular polarised LMS MIMO channel model has been developed. This model, in contrast with previously available LMS MIMO channel models, is simpler to implement since it uses a distinct state-based empirical-stochastic approach. The model has been found to be robust and it easily lends itself to rapid implementation for system level MIMO and DCPM analysis.

Finally, by way of bit error rate (BER) analysis in different channel fading conditions, it has been determined when best to implement polarisation multiplexing or conventional MIMO techniques for DVB-type land mobile receivers. It is recommended that DCPM be used when the channel in predominantly Ricean, with co-polar channel Rice factors and sub-channel cross correlation values greater than 1dB and 0.40 respectively. The recommendations provided by this research are valuable contributions, which may help shape the evolving DVB-NGH standardisation process.

Key words: Multiple-input multiple-output, dual circular polarisation multiplexing, bit error rate, Rice factor, channel correlation, DVB-SH, DVB-NGH.

Email: U.Ekpe@surrey.ac.uk

Acknowledgments

Sincere thanks goes to my principal supervisor, Dr Tim Brown, for his steady support and direction throughout my research journey in the Centre for Communication Systems Research (CCSR). A big thank you also goes to my co-supervisor, Prof Barry Evans, most especially for giving me a firm foundation to embark on this research during my MSc. project days. I would also like to thank Dr P. R. King for showing me the ropes in executing land mobile satellite measurement campaigns and for providing me his channel data for further scrutiny.

I would like to thank the management and staff of the Akwa Ibom State University (AKSU), who have provided 'timely' funds to enable me embark on and complete this research work. I am also grateful to my CCSR colleagues, who have directly contributed to enriching my research experience; most notable among them is Mr Fais Mansor.

I would also like to thank my parents, Mr and Mrs M. J. Ekpe, and my elder brother, Mr Ini-Abasi Ekpe, for their guidance and unyielding support.

Finally and most importantly, I give thanks to God for his gracious sustenance and comforting presence throughout the period of my research.

Contents

List of Figures

List of Tables

Glossary of Terms

AFD	Average Fade Duration
APSK	Amplitude Phase Shift Keying
AWGN	Additive White Gaussian Noise
BER	Bit Error Rate
BPSK	Binary Phase Shift Keying
CDF	Cumulative Distribution Function
CGC	Complementary Ground Component
CSI	Channel State Information
dB	Decibel
D-BLAST	Diagonal Bell Labs Layered Space Time
DVB-H	Digital Video Broadcast-Handheld
DVB-NGH	Digital Video Broadcasting-Next Generation Handheld
DVB-SH	Digital Video Broadcasting via Satellite to Handheld
DVB-T2	Digital Video Broadcast-2nd generation Terrestrial
E_b/N_0	Energy per bit over noise power spectral density
ETSI	European Telecommunications Standards Institute
GEO	Geosynchronous or Geostationary Orbit

HEO	Highly Elliptical Orbit
HZF-SIC	Hybrid Zero Forcing/Maximal Ratio Combiner Successive Interference Cancellation
ISI	Inter Symbol Interference
LCR	Level Cross Rate
LEO	Low Earth Orbit
LHCP	Left Hand Circular Polarised
LMS	Land Mobile Satellite
LOS	Line Of Sight
Mbps	Megabits per second
MEO	Medium Earth Orbit
MFC	Multi-frequency Network
MIMO	Multiple-Input Multiple-Output
MISO	Multiple-Input Single-Output
MLSE	Maximum Likelihood Sequence Estimation
MMSE	Minimum Mean Squared Error
MMSE-OSIC	MMSE-Ordered Successive Interference Cancellation
MRC	Maximum Ratio Combining
NLOS	Non Line of Sight
OFDM	Orthogonal Frequency Division Multiplexing

OLOS	Obstructed Line Of Sight
OSIC	Ordered Successive Interference Cancellation
PDA	Personal Digital Assistant
PDF	Probability Density Function
PSK	Phase Shift Keying
QPSK	Quadrature Phase Shift Keying
RHCP	Right Hand Circular Polarised
RMS	Root Mean Squared
RMSE	Root Mean Squared Error
SC	Satellite Component
SFN	Single Frequency Network
SIMO	Single-Input Multiple-Output
SISO	Single-Input Single-Output
SINR	Signal to Interference plus Noise Ratio
SNR	Signal to Noise Ratio
SSE	Sum of Squares due to Errors
SVD	Singular Value Decomposition
USIC	Unordered Successive Interference Cancellation
V-BLAST	Vertical Bell Labs Layered Space Time

XPC	Cross Polar Coupling
XPD	Cross Polar Discrimination
ZF	Zero Forcing
ZF-OSIC	Zero Forcing Ordered Successive Interference Cancellation

List of Symbols and Maths Operators

C	Channel capacity
$\mathbf{C}_{CP}$	Diagonal matrix containing co-polar channel cross correlation coefficients
$\mathbf{C}_{XP}$	Diagonal matrix containing cross-polar channel cross correlation coefficients
C_{DCPM}	Capacity of dual circular polarisation multiplexing
c	Coefficient of curve fitting polynomial equation
$\mathbf{D}$	Diagonal matrix
f_C	Centre frequency
$\mathbf{G}_i$	General matrix of channel weights
γ_{spec}	Spectral efficiency
h_{ij}	Instantaneous channel coefficient
$\mathbf{H}$	Matrix of instantaneous channel coefficients
$\mathbf{H}^H$	ian transposed **H**
$\mathbf{H}^*$	Conjugation of **H**
$\mathbf{H}^+$	Moore-Penrose pseudo-inversed **H**
$\mathbf{H}_{corr}$	**H** in which correlation has been artificially induced
$\mathbf{H}_{iid}$	**H** with independent identically distributed elements

$\mathbf{H}_{\text{LOS}}$	Matrix of coherently received signal
$\mathbf{H}_{\text{RaylF}}$	Matrix of Rice factor components for multipath signal
$\mathbf{H}_{\text{RiceF}}$	Matrix of Rice factor components for coherently received signal
$\mathbf{H}_{syn}$	Synthetically generated **H**
$\mathbf{H}_{\text{XPD-XPC}}$	Matrix of antenna XPD and channel XPC factor
i,j	General variables
m,n	General variables representing number of receive and transmit antennas respectively
K	Rice Factor
λ_i	Eigenvalue
m_1, m_2, m_3	Coefficients of curve fitting polynomial equation
M	Polarisation rejection scaling factor
$\boldsymbol{n}$	noise vector
η_0, η_1, η_2	Coefficients of curve fitting polynomial equation
$\text{P}_{i\|j}$	Probability of transiting from state i to state j
ρ	Signal to noise ratio
ρ_{12}	Complex correlation coefficient
ρ_e	Envelope correlation coefficient
ρ_p	Power correlation coeffient

rx, tx	Variables respectively representing receive and transmit link-ends
S_i	Singular value
S_m	Relative mean large scale fading level
σ	Standard deviation
σ_m	Empirical standard deviation
T_C	Channel correlation distance
t	Time variable
τ	Excess delay variable
τ_{MAX}	Maximum excess delay
τ_{MED}	Measurement excess delay
θ_i, ψ_i	Phase angles of receive signal
u, v	Complex variables representing instantaneous channel voltages
V_C	Velocity of light
ω	Independent variable of curve fitting polynomial
$\boldsymbol{w}_{MM}$	MMSE weights matrix
$\boldsymbol{w}_{ZF}$	Zero forcing weights matrix
$\boldsymbol{x}$	Transmit signal vector
x	Independent variable of fitted polynomial

y	Dependent variable of fitted polynomial
$\boldsymbol{y}$	Receive signal vector
$\boldsymbol{y}_{\text{eq\_ML}}$	MLSE equalised receive signal vector
$\boldsymbol{y}_{\text{eq\_MM}}$	MMSE equalised receive signal vector
$\boldsymbol{y}_{\text{eq\_ZF}}$	ZF equalised receive signal vector

Mathematical Operators

$\odot$	Hadamard (element-wise) multiplication
$\otimes$	Kronecker product

General Note

In this thesis, bold face lowercase letters denote vectors while boldface upper case letters represent matrices.

Chapter 1

1 Introduction

It has been established both theoretically and practically in the last two decades that multiple-input multiple-output (MIMO) can increase the capacity of communication systems without the need for additional spectrum. This increase is usually dependent on the presence of a rich scattering environment between the multiple transmit and receive antennas. However, most Land Mobile Satellite (LMS) two-way communication and broadcast systems spend most of their time in the line of sight (LOS) channel, where there is limited scattering, and are therefore in the danger of missing out on the MIMO advantage. Despite this drawback, some research [1],[2],[3],[4],[5] aimed towards implementing MIMO in the LMS channel have recently been conducted and the results of most of these, especially that of [4], point towards marginal capacity increase of MIMO over single-input single-output. However, there are a few promising results, as can be found in the work of Ozcelik [6], which actually predict increased MIMO capacity when the LOS channel is diagonally correlated. An example of such a channel is the dual orthogonally polarised LMS LOS channel. Therefore, since orthogonal circular polarisation has been proposed as a panacea that allows for MIMO sub-channel independence, permits the co-location of transmit-end and receive-end multiple antennas and then ultimately guarantees the workability of MIMO techniques in the LMS LOS channel [7], it is not trivial to investigate the limits of such MIMO operation. This thesis thus sets out to answer to questions of why it is necessary to bother with MIMO in the multipath-poor LMS LOS channel and when exactly can MIMO be beneficial in such channels. The questions will be answered in terms of commonly used empirical channel parameters including signal to noise ratio (SNR), channel correlation and channel Rice factor; and the answers would help determine if there are lower effort alternatives to conventional MIMO and how these lower effort schemes can be implemented. Thus all the analysis in this thesis except otherwise stated is based on a single satellite single user and dual polar 2×2 MIMO channel having orthogonal circular polarized antennas co-

located at the transmit link-end and used in communicating with closely spaced mobile receive antennas. This configuration fits into the on-going Digital Video Broadcasting-Next Generation Handheld (DVB-NGH) project, where it is envisaged that compatible satellite delivered broadcast services will complement terrestrial services by providing coverage in sparsely populated rural environments where satellite delivery provides better economies of scale.

1.1 Motivations and Objectives

With spectral efficient MIMO techniques successfully implemented in fourth generation terrestrial cellular systems, the main motivation of this research is the prospect of extending this MIMO advantage to LMS applications like vehicle-mounted or handheld communication and entertainment devices, along the lines of Digital Video Broadcasting via Satellite to Handheld (DVB-SH) specifications. Achieving this would entail measuring, characterising and modelling the dual circular polarised land mobile satellite MIMO radio channel for subsequent analysis of the performance of new alternative schemes to MIMO. Therefore, the main objectives of the research work include:

- Identification of gaps in the measurements and modelling aspects of the satellite MIMO radio channel.
- Investigation of the effects of antenna polarisation on MIMO channel capacity using statistical and numeric methods, and then derivation of appropriate metrics to estimate such capacity.
- Derivation of a simpler/low effort solution, termed dual circular polarisation multiplexing (DCPM), which gives comparable throughput to MIMO.
- Organisation and implementation of measurement campaigns to provide data that is more representative of the dual circular polarised LMS MIMO channel than was previously available.
- Fine tune old models and/or derive a new dual circular polarised LMS MIMO channel using the more realistic data from new measurement campaigns.
- Verify and validate the new model's reliability using branch power distributions, eigen value distribution, and bit error rate (BER) analysis.

- Identify the effects of parameters such as SNR and the related energy per bit over noise ratio (E_b/N_0), Rice factor and correlation on the BER performance and capacity of the modelled channel and its polarisation multiplexing advantage when using zero forcing, minimum mean squared error and maximum likelihood channel equalisation schemes.
- Application of polarisation multiplexing to the satellite component of the upcoming standards for digital video broadcasting to the next generation of handheld (DVB-NGH) devices.

1.2 Original Contributions and Achievements

The original and novel contributions of this work include the following:

- A new low effort polarisation MIMO scheme, termed dual circular polarisation multiplexing (DCPM), has been proposed for use in the high Rice factor LOS LMS channel. This proposal has already been published in a conference paper titled "Unleashing the polarisation domain for land mobile satellite MIMO systems." Also derived is a metric for computing the capacity of zero-forcing based DCPM.
- An updated and more accurate multi-state channel model for the dual circular polarised LMS MIMO channel has also been proposed. This model follows the physical statistical approach, is highly tractable and better renders dual polarised LMS MIMO channels than previously available channel models.
- Relevant to coding techniques in DVB-SH/NGH, the limits for which DCPM is practicable has been determined by way of BER analysis using the proposed channel model.

1.3 Publications

The following journal publication has been written and is awaiting submission:

- U. M. Ekpe, T. W. C. Brown, B. G. Evans, “Dual Circular Polarization Multiplexing for DVB-SH/NGH Applications”

The following conference papers have been published:

- **U. M. Ekpe**, T. Brown, and B. G. Evans, "Unleashing the polarisation domain for land mobile satellite MIMO systems," *in 3rd European Conference on Antennas and Propagation*, Berlin, Germany, 2009, pp. 2288-2291.
- **U. M. Ekpe**, T. W. C. Brown, and B. G. Evans, "Markov chain analysis for land mobile satellite MIMO channels," *in The 27th IET and AIAA International Communications Satellite Systems Conference*, Edinburgh, UK, 2009
- T. W. C. Brown and **U. M. Ekpe**, "When is Clarke's Approximation Valid?," *IEEE Antennas and Propagation Magazine*, vol. 52, pp. 171-181, 2010.
- **U. M. Ekpe**, "Dual Circular Polarisation Multiplexing for the Satellite Component of DVB-NGH Systems, 1st CCSR Research Symposium, June 2011
- **U. M. Ekpe**, T. W. C. Brown, and B. G. Evans, "Channel characteristics analysis of the dual circular polarized land mobile satellite MIMO radio channel," *in IEEE-APS Topical Conference on Antennas and Propagation in Wireless Communications*, Turin, Italy, 2011, pp. 781-784.

1.4 Structure of Thesis

Chapter 2 deals with background theory to the MIMO radio channel and channel modelling issues. It explains using diagrams and equations the meaning of instantaneous channel gain and relevant MIMO channel metrics including channel correlation, capacity, singular values and singular vectors. A brief description of available LMS MIMO channel models is given followed by the potential applications of MIMO technology in the LMS channel.

Chapter 3 starts off by providing a background to MIMO transceivers, with emphasis on how zero forcing, minimum mean squared error and maximum likelihood detection equalisation are done. With this safely covered the chapter then introduces the concept of dual circular polarisation multiplexing (DCPM), which is an alternative to conventional MIMO, and makes a connection on how DCPM is dependent on receiver architectures. Using simple models that allow for channel properties like Rice factor, channel correlation and XPD to be varied, the capacity potentials of DCPM and conventional

MIMO are investigated. The chapter is rounded off by BER simulations of different channel types and equalisation schemes.

Chapter 4 gives a detailed account of previous dual circular polarised LMS measurement campaigns that have been previously carried out by others and the recent measurements that have been undertaken to provide realistic channel data for the subsequent development of a new channel model. A method of extracting relevant statistics from the huge volume of measured channel data is also provided.

Chapter 5 presents the building blocks and methodology of modelling the dual circular polarised LMS channel. It divides the modelling process into two parts: the large scale fading part, which is modelled using Markov state switching, and the small scale fading aspect, modelled using an empirical based stochastic approach.

Chapter 6 employs the developed channel model to implement BER simulations and analysis on different channel fading states. These help in determining the channel conditions suitable for DCPM operation and the most practical candidates for channel equalisation.

Finally, chapter 7 concludes the findings by listing the major research contributions and giving pointers to future work.

Chapter 2

2 MIMO and LMS Channel Modelling Issues

This chapter reviews literature on multiple-input multiple-output (MIMO) channel modelling as applied in relevant terrestrial and land mobile satellite (LMS) systems. Starting with the overall MIMO input-output relationship, the effects of channel coefficients and additive white Gaussian noise on the received signal of the MIMO channel is explained. Also discussed are some important and widely used MIMO channel terms such as correlation, capacity and eigenvalue distribution. Then using data that has been obtained from a previous measurement campaign, it is graphically shown how MIMO channel eigenvalues and branch powers are distributed when signal propagation is in line-of-sight (LOS) and non-line-of-sight (NLOS) conditions. The two main methods of modelling the land mobile satellite (LMS) channel, namely: deterministic and stochastic channel modelling is thoroughly reviewed in order to determine which modelling method is more suitable for the LMS MIMO channel. Having revealed that the stochastic modelling approach is the better alternative, the channel fading phenomena of large- and small scale fading is also reviewed. The chapter ends by examining previous stochastic channel models with the aim of determining if they adequately render the dual polarised LMS MIMO channel and are tractable enough for use in designing LMS MIMO systems of the future.

2.1 The MIMO Radio Channel

MIMO systems are an outgrowth of multi-element antenna systems in which multiple antennas are placed at both the transmitting and the receiving link-ends. The multiple antennas at both link-ends can be used to increase system reliability (i.e. reduce the probability of the signal to noise ratio fading below a required threshold) through diversity techniques or to increase system capacity (i.e. increase data throughput over the same bandwidth and transmit power) using multiplexing techniques. A detailed treatment

of the many diversity techniques, which make use of space, time, frequency, angle, polarisation or channel coding, can be found in [8]. Multiplexing on the other hand entails transmitting independent information through the multiple antennas for increased system capacity. The channel conditions and the number of transmit-receive antenna pairs being used dictates how much increase in capacity is achievable. One of the earliest investigations by [9] uncovered a linear relationship between capacity increase for MIMO systems and the number of transmit-receive antenna pairs used. The influence of the channel condition on the predicted capacity increase or spectral efficiency is such that MIMO systems must operate in either the beamforming or multiplexing modes (using spatial, polarisation multiplexing or space-time coding) [10-12]. Figure 2.1 shows a schematic of the wireless MIMO channel including ancillary equipment.

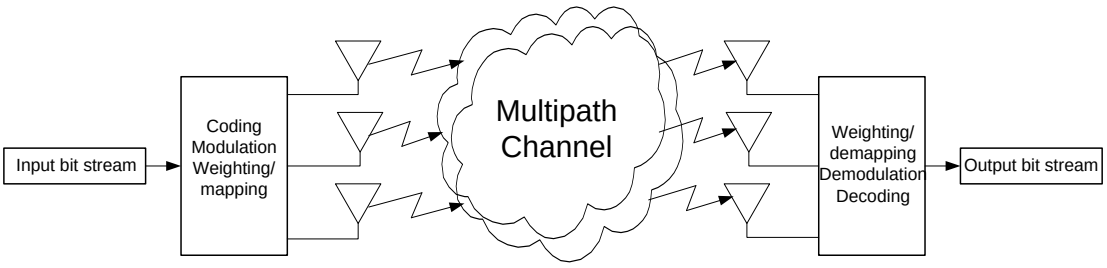

Figure 2.1: The wireless MIMO channel

The overall input-output relationship of the MIMO system of Figure 2.1 can be represented by a simplified time-invariant frequency-flat fading channel model given as:

$$\boldsymbol{y} = \mathbf{H}\boldsymbol{x} + \boldsymbol{n}, \tag{2.1}$$

where $\boldsymbol{y}$ is a $j\times1$ received signal vector, with j being the number of receive antennas. $\boldsymbol{x}$ is a $k\times1$ transmit signal vector, with k being the number of transmit antennas. Therefore $\mathbf{H}$ is a $j\times k$ channel coefficient matrix representing the channel attenuation terms between receive antenna j and transmit antenna k. $\boldsymbol{n}$ indicates an additive white Gaussian noise component at each of the receive antennas. Since $\mathbf{H}$ is a matrix, it is generally represented as:

$$\mathbf{H} = \begin{bmatrix} h_{11} & h_{12} & \cdots & h_{1k} \\ h_{21} & h_{22} & \cdots & h_{2k} \\ \vdots & \vdots & \ddots & \vdots \\ h_{j1} & h_{j2} & \cdots & h_{jk} \end{bmatrix}. \tag{2.2}$$

In an environment where there is a good line of sight (LOS) between the transmit and the receive terminals and where there are few interacting objects (in the form of scatterers) to create rich scattering, it is usually more beneficial to orient the main beams of both the transmitter and the receiver at each other. This in effect creates a single-input single-output (SISO) channel and increases the channel gain. To implement beamforming, the same signal is transmitted through all the multiple antenna elements but with different phase weightings applied to each of the antenna elements. This steers the created beam towards the desired direction while placing nulls in the direction of interferers. Beamforming has been used extensively in the downlink macrocell channels of mobile cellular communication systems to provide sectoring and improved frequency reuse [13].

To benefit from spatial multiplexing there needs to be a rich scattering environment between the communicating MIMO terminals [14],[15]. In spatial multiplexing, a high data rate bit stream is divided into several independent lower bit rate streams and simultaneously transmitted and received using multiple antenna elements without the need for additional spectrum and power. Spatial multiplexing can be easily implemented in terrestrial channels found in micro-, pico- and femto-cells, as the rich scattering in such environments ensure that correlation between the MIMO channels at the transmit and receive link-ends is minimal and within acceptable thresholds (i.e. the envelope correlation coefficient must be less than 0.7 [8]). The rich scattering environment sometimes allows the antennas to be placed as close as ¼ wavelengths [8], thus making MIMO feasible for devices with small form factors such as laptops and handhelds.

Implementing spatial multiplexing MIMO in the case of LMS systems is much more challenging mainly due to the asymmetric nature of LMS channels and the huge distances between land mobile and satellite terminals. Channel asymmetry refers to the lack of scatterers within the vicinity of the satellite to adequately de-correlate propagating signals. This creates a scenario whereby antennas at the satellite link-end need to be separated by several hundreds of wavelengths to achieve the required correlation

requirements. To implement spatial multiplexing in LMS systems, some authors including [3],[16],[17] have suggested the use of two or more satellites located in different orbital slots. However, several factors militate against implementing such spatially separated LMS MIMO systems. One mitigating factor is the need to compensate for the huge propagation delay difference that can arises when bits of the same code-word is split between multiple satellite transmitters. These bits will have to travel different distances to the land mobile receiver, which may not be able to compensate for the delay. Even when compensation is possible, complex synchronisation and scheduling arrangements is required at both the satellite and mobile link-end. This can make the cost of implementing MIMO prohibitive.

A more promising MIMO technique for LMS systems is the use of a single satellite with orthogonally polarised antennas [3],[18]. Single satellite LMS MIMO removes the need for synchronisation between two or more satellites and allows for the orthogonally polarised antennas to be co-located since orthogonal polarisations alone can effectively create independently fading channels. For a 2×2 LMS MIMO system, a pair of right hand circular polarised (RHCP) and left hand circular polarised (LHCP) antennas is used at both the satellite and land mobile terminals as illustrated in Figure 2.2. Satellite communication systems use circular polarisation in order to counter various adverse ionospheric effects, chief among with is Faraday rotation. For example, if linear polarisation is employed alongside a centre frequency of 1GHz and an elevation angle of 30^{o}, it has been reported in [19], pp. 101 that up a 108^{o} polarisation rotation is possible. This rotation causes a mismatch between communication antennas and results in extra path loss. Also, in the case of a geostationary satellite where orbital dynamics results in the satellite's position, although fixed within an orbital slot, to continually change (tracing a figure eight) relative to a fixed point on the earth's surface. A changing satellite position affects the polarisation alignment between the satellite and land-based antennas and the use of circular polarisation can minimise any adverse effects.

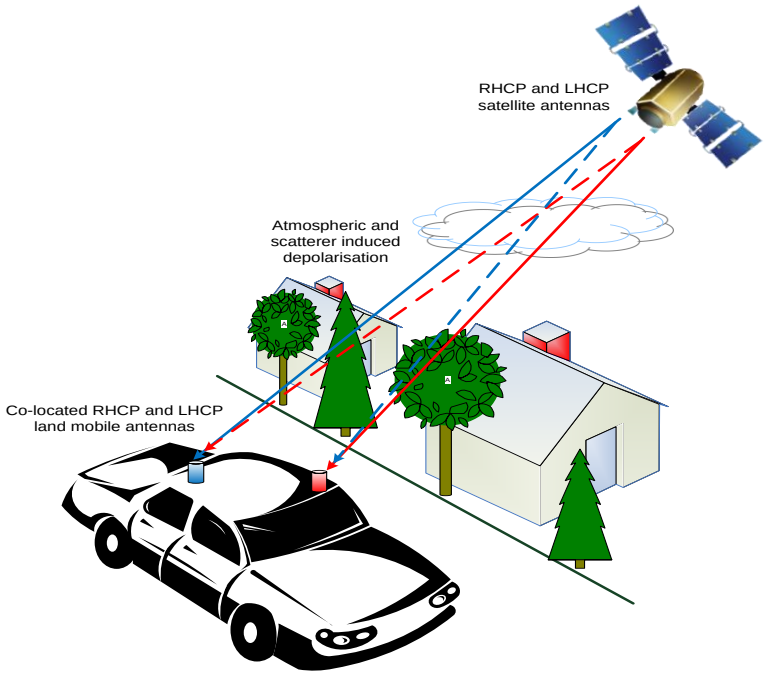

Figure 2.2: Single satellite dual circular polarised LMS MIMO channel

However advantageous the use of single satellite dual orthogonal polarisation MIMO looks, there are numerous gaps in knowledge that this thesis sets out to fill before the technique can be implemented. Subsequent sections of this chapter will review some important metrics used in characterising the performance of MIMO systems in general, and with the scarcity of dual polarised LMS MIMO channel data, the strengths and weaknesses of some widely used terrestrial and LMS MIMO channel models will be investigated. This will then give a solid footing to analyse the newly available dual polarised LMS MIMO channel data obtained in the measurement campaigns described in chapter 3.

2.2 Modelling Challenges

A channel model is a mathematical expression describing radio propagation. The attenuating effects suffered by a propagating radio wave include those resulting from path loss absorption as well as reflection and diffraction, both of which cause the phenomenon called scattering. Two main modelling approaches have emerged to predict these attenuating effects. The first being a deterministic approach which employs solutions or approximate solutions of Maxwell's propagation equations to predict the individual

contributions arising from the attenuating effects of the various propagation phenomena. The second main method, known as stochastic modelling, employs a statistical approach based on probabilistic (stochastic) methods to predict the level of a radio signal at given points in the propagation medium. The advantages and disadvantages choosing any of the modelling approaches have been exhaustively treated by [8],[20]. Whereas the computational complexity of deterministic models makes them unattractive for large scale LMS simulations, their accuracy (depending on the underlying database) and relatively easier implementation compared to undertaking real measurements make them the best candidates for simple point to point channel analysis. Also, deterministic models can allow for specific small scale channel attenuation effects to be closely studied. On the other hand, when large scale channel knowledge is required, especially in the case of highly mobile systems, stochastic models offer a better alternative. This is due to the ease with which stochastic models can predict signal levels propagating over very large areas.

The two main modelling approaches earlier mentioned holds for both SISO and MIMO systems. However for MIMO systems there is an increased channel modelling complexity since there is at least an $m \times n$ fold increase in the number of individual propagation channels to be modelled. This increased complexity has made the simpler statistical based modelling approach more attractive for the MIMO case. This is especially true in the area of LMS MIMO as most of the models developed in recent years [3],[18],[21] have leaned towards statistical implementation. Additionally, an important consideration in MIMO channel modelling is to determine if there exist relationships between the attenuation effects affecting the individual MIMO sub-channels. To this end, various modelling studies including [20] and [22] have shown that simple relationships hardly ever exist. What suffices is an environment dependent joint variation of parameters like the correlation and distribution of individual channel powers, and the eigenvalue distribution of the MIMO channel. Thus a challenging task in MIMO channel modelling, especially for the LMS case, is to simultaneously estimate the value of each of these parameters for the multiple sub-channels and also determine their joint and independent environment-induced evolution. The following sections will treat the parameters used in characterising the channels and proceed to look at some popular approaches to MIMO channel modelling as applicable to the terrestrial and LMS channels.

2.2.1 Channel Coefficients

Channel coefficients give an indication of the time (or frequency) evolution of the channel's attenuating effects as the channel-sounding or information-carrying signals propagate from transmit to receive antennas. Since this thesis focuses on the radio channel, it is assumed that all antenna effects except for polarisation have been normalised out from the channel coefficient, therefore the terms channel coefficient and received signal power will be used interchangeably. In the time domain, channel coefficients can be determined by probing the channel using narrowband or wideband channel sounders. Figure 2.3 shows cumulative distribution plots of normalised channel coefficients of a 2×2 obstructed line-of-sight (OLOS) MIMO channel plotted from the dual circular polarised land mobile satellite measurement campaign data reported in [1]. The diagram indicates that co-polar channel coefficients are usually similarly distributed and distinct from the cross-polar channel coefficients. The channel coefficient matrix of a MIMO channel is also called an H-matrix and this was earlier shown in equation (2.2).

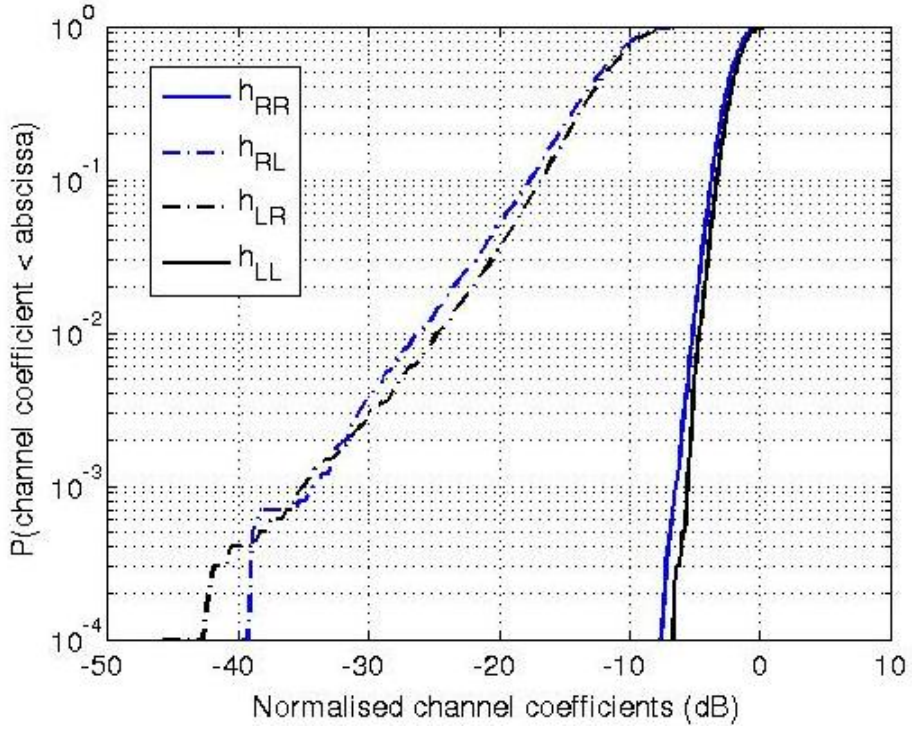

Figure 2.3: CDF plots of normalised channel coefficients for a 2x2 OLOS dual circular polarised MIMO channel

2.2.2 Channel Correlation

The cross correlation between the multiple sub-channels of a MIMO system is one of the most important parameters for MIMO channel characterisation. The correlation coefficient gives a measure of independence (or lack of it) of the individual MIMO sub-channels as they traverse the propagation medium and it directly affects the capacity supportable by such channels. The effects of channel correlation on indoor MIMO channels has been investigated in [23], where the correlation coefficient is defined and calculated in three different forms, namely: the complex, envelope and power forms. If u and v are complex variables respectively sampled from the fading signals of two individual MIMO sub-channels, their complex correlation coefficient, ρ_{12}, is defined as:

$$\rho_{12} = \frac{E[uv^*] - E[u]E[v^*]}{\sqrt{(E[|u|^2] - |E[u]|^2)(E|v|^2 - |E[v]|^2)}}, \tag{2.3}$$

where * denotes complex conjugation. Similarly, the envelope and power correlations of u and v are respectively given by:

$$\rho_e = \frac{E[|u||v|] - E[|u|]E[|v|]}{\sqrt{E[|u|^2 - (E[|u|])^2]\, E[|v|^2 - (E[|v|])^2]}}, \tag{2.4}$$

$$\rho_p = \frac{E\left[|u|^2|v|^2\right] - E\left[|u|^2\right]E[|v|^2]}{\sqrt{E[|u|^4 - (E[|u|^2])^2]\, E[|v|^4 - (E[|v|^2])^2]}}. \tag{2.5}$$

This thesis will only make use of the complex correlation coefficient since its formulation compares both the magnitude and phase of the fading signals.

It well known that the correlation coefficient calculated using the power and envelope formulations will give similar results. Also, the squared value of the complex correlation coefficient is equivalent to the envelope correlation of a Rayleigh channel [24]. These relationships have been investigated for both the Rayleigh and Ricean channels using synthetic and measured channel data in [25] and it was concluded that the relationships hold provided a sufficient number of samples is used in computing the correlation coefficients. Numerous studies including [26-28] of multi-antenna systems have shown that correlation can adversely affect channel capacity; hence for most channels it is

desirable to keep correlation to a minimum while in a few other channels, like the diagonally correlated channel, the effects of correlation can be beneficial [6],[29]. This thesis will explore the effects of correlation and provide in fine details its impact on MIMO channel capacity and bit error rates (BER).

2.2.3 Channel Capacity

Another metric to characterise the performance of MIMO channels is the Shannon channel capacity metric. Shannon in [30] defined capacity as the maximum data rate a channel can support at an arbitrarily low error probability. The capacity of a single-input single-output memoryless channel in bits per second per Hertz is given in [9] as:

$$C = \log_2(1 + \rho), \tag{2.6}$$

where ρ is the signal to noise ratio (SNR) at the receive antenna. The channel coefficient, h, which should have been included in (2.6), has been dropped since it is assumed to have been normalised to unity. The well-known expression for the channel ergodic capacity of MIMO systems was then derived from (2.6) in [9] and is given as:

$$C = \log_2 \left[\det\left(\mathbf{I}_n + \frac{\rho}{N}\mathbf{H}\mathbf{H}^H\right)\right], \tag{2.7}$$

where $\mathbf{I}_n$ is an $n \times n$ identity matrix, N is the number of transmit antennas and $\mathbf{H}^H$ is the Hermitian transpose of $\mathbf{H}$. Equation (2.7) is often the preferred metric to test how good a model represents the wireless channel and has also been derived in terms of the eigenvalues (λ_i) of $\mathbf{H}\mathbf{H}^H$ by [31] as:

$$C = \sum_{i=1}^{m} \log_2\left(1 + \frac{\rho}{N}\lambda_i\right). \tag{2.8}$$

In equation (2.8), m represents the smaller of either number of transmitters or number of receivers. For completeness, the capacity of single-input multiple-output (SIMO) and that of multiple-input single-output (MISO) channels are given in [32] as:

$$C_{SIMO} = \log_2(1 + \rho \sum_{i=1}^{m} |h_i|^2), \tag{2.9}$$

$$C_{MISO} = \log_2\left(1 + \frac{\rho}{N}\sum_{i=1}^{n} |h_i|^2\right), \tag{2.10}$$

where *n* and *m* represent the number of transmit and receive antennas respectively. Capacities that can be supported by ergodic and non-ergodic channel conditions and the effect of presence of channel state information (CSI) both at the transmitter and the receiver can be found in most MIMO texts including [11], [33] and [34]. Except otherwise stated, all capacity computations in this thesis will assume perfect CSI at both the transmit and receive antennas.

2.2.4 Singular Values and Singular Vectors

Since the focus of this thesis is on MIMO for LMS systems, it is important to know the number of independent channels that can be practically supported by the available transmit–receive antenna pairs. This is realised by decomposing the MIMO channel into independent sub-channels using the singular value decomposition (SVD) [35]. From equation (2.1) the SVD is operated on the MIMO channel matrix **H** as follows:

$$\boldsymbol{y} = \mathbf{H}\boldsymbol{x} + \boldsymbol{n} = \mathbf{U}\mathbf{S}\mathbf{V}^{\boldsymbol{H}}\boldsymbol{x} + \boldsymbol{n}, \tag{2.11}$$

$$\boldsymbol{y} = \mathbf{U}\mathbf{S}\begin{bmatrix} v_1^H \\ v_2^H \\ \vdots \\ v_m^H \end{bmatrix} + \boldsymbol{n} = \mathbf{U}\begin{bmatrix} s_1 & \cdots & 0 & \cdots & 0 \\ \vdots & \ddots & \vdots & \vdots & \vdots \\ \vdots & \cdots & s_k & \cdots & 0 \\ \vdots & \cdots & \cdots & \ddots & \vdots \\ 0 & \cdots & \cdots & \cdots & 0 \end{bmatrix}\begin{bmatrix} v_1^H \\ v_2^H \\ \vdots \\ v_m^H \end{bmatrix} + \boldsymbol{n}, \tag{2.12}$$

$$\boldsymbol{y} = [u_1 \;\; u_2 \;\; \cdots \;\; u_n]\begin{bmatrix} s_1 v_1^H \\ s_2 v_2^H \\ \vdots \\ s_m v_m^H \end{bmatrix} + \boldsymbol{n}, \tag{2.13}$$

$$y = \sum_{i=1}^{\min(n,m)} u_i s_i v_i^H \, x + n. \tag{2.14}$$

In equations (2.11) to (2.13), **H** is decomposed into *k* parallel sub channels (s_1 to s_k) as indicated by the elements of the diagonal matrix **S. U** and **V** are the left and right singular vectors of **H** which indicate the array weights to be applied on the transmit and receive signal streams respectively. Looking at equation (2.14), we notice that the maximum diversity or multiplexing order that can be achieved is equal to *k*, which is the smaller of either the number of transmitters or receivers. Note that *k* is also equal to the rank of **H**. Singular values (and singular vectors) are related to eigenvalues (and eigen vectors) by:

$$s_i = \sqrt{\lambda_i}\ . \tag{2.15}$$

In equation (2.15), s_i represents the singular values of **H** and λ_i the eigenvalues of $\mathbf{HH}^H$. It is interesting to note that Weichselberger in [36] used the eigenvalue distribution to estimate the order of diversity and beamforming present in the MISO channel. A good explanation of the effects the eigenvalue distribution has on the MIMO channel, i.e. whether beamforming or spatial multiplexing would be more favourable, can be found in [11]. Also, recent work by Webb in [37] has studied the effects of the channel eigen-coherence time and the performance of different MIMO schemes in terms of capacity and bit error rates (BER). Both the eigen-coherence time and the eigenvalue (or singular value) distribution of a channel directly depend on the prevailing channel propagation conditions. A CDF plot of eigenvalues obtained from the same measurement as in Figure 2.3 is shown in Figure 2.4, where the red plots indicate when the channel is more multiplexing friendly and the blue and black plots show when the channel would be more diversity friendly.

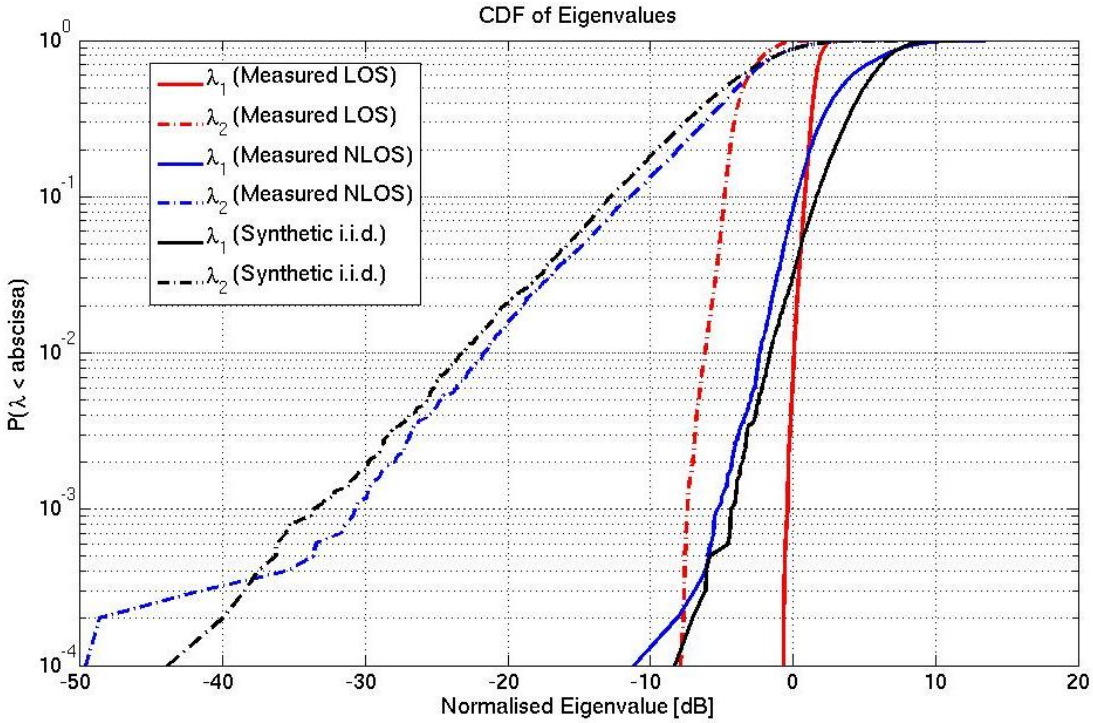

Figure 2.4: CDF plots of Eigenvalue distribution for MIMO channel favouring multiplexing (red plots) and diversity (blue and black plots)

Questions arising from the multiplexing-diversity dilemma which has not been conclusively treated for the dual polarised LMS MIMO channel include the following:

- When precisely does the eigenvalue distribution of a dual polarised LMS MIMO channel show that it would be more beneficial to implement multiplexing than diversity?
- In addition to the eigenvalue distribution, what other channel parameters are required to make the choice between diversity and multiplexing?
- What effects do the channel parameters have on channel performance metrics like channel capacity and bit error rate?

A good understanding channel attenuation effects is necessary in order to answer some of the above multiplexing-diversity questions. Also, since LMS MIMO channel modelling is dependent upon a sound knowledge of channel attenuation, the next section provides a brief background on these phenomena.

2.2.5 Channel Fading

Channel fading is the random attenuation a signal suffers as it traverses the propagation medium. In terms of the time (or distance) scales at which this random attenuation is observed, channel fading is of two main types: large scale fading and small scale fading. Large scale fading, also called shadowing, is noticed as a slow variation in the local mean of the received signal power. It is caused by different degrees of attenuation the propagating signal suffers as it propagates through, reflects off or diffracts past large objects such as buildings, vegetation and terrain. Assuming a fixed terminal is transmitting to a mobile receiving terminal, large scale fading encountered by the mobile terminal may be observed over a distance of a few metres to tens or even hundreds of metres. On the other hand, small scale fading or fast fading manifests as a rapid fluctuation in the amplitude of the received signal power. It is caused by constructive or destructive addition of numerous multipath components reaching the receiver. Constructive addition happens when the arriving multipath components at the receiver have the same phase. Destructive addition happens when multipath components arrive out of phase at the receiver after having propagated through paths of different lengths. According to Brennan in [38], the time scales over which small scale fading occurs must

be short compared to the time it takes for the amplitude of the received signal to appreciably change, but long when compared to the period of the lowest frequency of the transmitted signal.

2.2.6 Narrowband and Wideband Channels

The definition of whether a channel is narrowband or wideband depends on the relationship between the duration of a symbol transmitted through the channel and the time it takes for multiple copies of the symbol, after having travelled through paths of different lengths, to arrive at the receiver. To illustrate further, we extract from equation (2.1) a SISO channel and fully notate it by adding t and τ to respectively represent the transmit time and encountered delay, we have:

$$y(t) = h(t,\tau) * x(t) + n(t) = \int_{-\infty}^{\infty} x(t-\tau)h(t,\tau)d\tau + n(t), \tag{2.16}$$

where * represents convolution. The convolution of the channel coefficient $h(t,\tau)$ and the transmitted symbol $x(t)$ gives the channel impulse response and included in the measured impulse response, $y(t)$, is an additive noise component $n(t)$. Note that numerous copies of a transmission symbol will arrive with delays of between $-\infty$ and ∞ and are scaled differently according to their respective $h(t,\tau)$.

Let us assume in the time domain that there are N multipath copies of a transmit symbol, $x(t)$, that possess significant energy. The first copy of $x(t)$ to reach the receiver, having probably travelled along an LOS path, will arrive after a delay of τ_1 and its last copy will arrive after a delay of τ_N. If the difference between τ_1 and τ_N is much less than the duration of $x(t)$, transmitted at time t =1, the channel is considered to be narrowband. On the other hand, a channel is wideband if the difference in time between τ_1 and τ_N is greater than or of similar magnitude as the duration of $x(t)$. Wideband channels cause the late arriving multipath copies of $x(t;\ t$ =1) to arrive at similar times with trailing symbols transmitted at time t >1. The overlapping arrival times of copies of a prior transmitted symbol, say $x(t;\ t$ =1), with early copies of a later transmitted symbol, say $x(t;\ t$ =2), is known as intersymbol interference (ISI).

A channel may either be narrowband or wideband depending on the signal transmission rate, mobility of the communicating terminals or changes within the channel itself. Significantly increasing the transmission rate in a channel that was previously narrowband may make it become wideband. This is because an increase in transmission rate amounts to a reduction in symbol duration, which may cause late arriving copies of earlier transmitted symbols to interfere with later transmitted symbols. Transmission rates and symbol durations used in LMS (MIMO) channels where interacting objects are within a few meters of the land mobile receiver do not usually cause enough delay that result in the wideband channel phenomenon of ISI. Hence, except otherwise stated, the discussion in this thesis assumes all LMS MIMO channels to be narrowband. This assumption is based on the fact that previous S-Band wideband LMS measurements by [1] and [39] revealed that multipath components with significant energy arrived after delays of 140ns and 153.5ns respectively. This delay is far less than 115.5μs, which according to ETSI [40] is the shortest symbol duration for the 8MHz channel designed for DVB satellite service delivery to handheld devices below 3GHz.

2.3 Modelling the LMS MIMO Channel

All land mobile satellite channels, whether originating from satellites placed in the geostationary, highly elliptic, medium earth, or low earth orbits, exhibit the same asymmetric configuration due to the absence of interacting objects (scatterers) within the vicinity of the satellite. Apart from the effects of Faraday rotation, which occurs in the ionosphere, and the deterministic path loss effects resulting from gaseous absorption, it is only the environmental effects of shadowing and multipath that adversely affects the propagation of satellite signals. The effects of Faraday rotation can be resolved by using circular polarisation while attenuation due to atmospheric gases and hydrometeors can be mitigated by avoiding certain frequencies for satellite communications. It is the asymmetric nature of the channel that makes the adoption of conventional MIMO difficult for LMS communications since the satellite link-end would require antennas to be spatially separated by several kilometres to achieve uncorrelated fading. This has led some authors [3],[16],[17] to suggest the use of multiple satellites located in different orbital slots. The large area covered by a satellite footprint, called a megacell, can only be

realistically modelled using statistical methods since deterministic methods would incur very huge computational resources. On this premise, the next sections will review in greater depth the deterministic and stochastic modelling methods as applicable to LMS MIMO (and SISO) channels. Compared with SISO channels, an additional requirement of LMS MIMO channel modelling is to simultaneously describe the propagation effects encountered by the individual MIMO sub-channels and to accurately represent the channel fading relationships existing between the sub-channels using the simplest possible means.

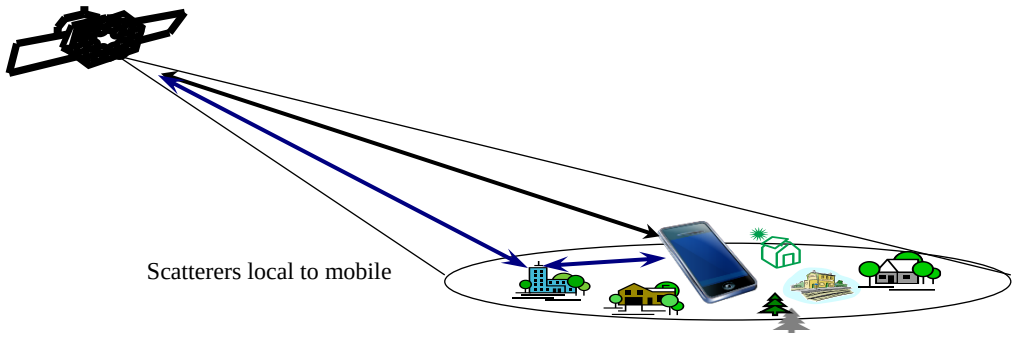

Figure 2.5: The Land Mobile Satellite radio channel

2.3.1 The Deterministic Modelling Approach

Deterministic models rely on numerical methods to accurately predict the effects of electromagnetic interactions (reflection and diffraction) on a signal as it propagates through an environment. For LMS systems, the propagation environment of concern can be several hundreds of square kilometres and to reliably model the boundary conditions between different media in this large area and computing all the attenuation effects is usually prohibitive. Even when the area of concern is reduced to only a few metres radius of the receive/transmit terminal, the use of direct deterministic methods may still not be practical as there are limitations to how precise the environmental boundary conditions can be electromagnetically described.

Examples of deterministic models include ray tracing and ray launching, both of which are mainly used for small scale indoor measurements. To apply the deterministic modelling approach for LMS channels requires breaking the channel down into different sections exhibiting distinct characteristics. As has been done by Frigyes in [41], in order

to model satellite to indoor propagation, the channel is divided into three parts. The first part is of free space propagation from the satellite to the first interacting object, which can be conveniently modelled deterministically. The second and third parts comprise the path from the first interacting object to the land mobile receiver. These two sections are better modelled statistically. Other attempts at deterministically modelling the LMS channel by [3],[42-44] involve a lot of approximations, and such modelling approach can be called semi-deterministic or physical-statistical.

2.3.2 The Stochastic Modelling Approach

Stochastic models, whether SISO, MIMO, terrestrial or LMS, take a simpler probabilistic approach to predict the characteristics of signals reaching a receive terminal using geometric, parametric or correlation based methods. In the geometric-stochastic case as done in [45-47], scatterers or buildings are placed at defined geometric locations or placed following observed distributions within the propagating path of the radio wave. The signal at the receiver is then made up of the sum total of direct, reflected, diffracted and scattered waves, with each contribution computed according to electromagnetic principles. Parametric-stochastic models on the other hand use parameters such as mean angles of arrival and departure and their corresponding spreads, and the Doppler frequency to estimate the spatio-temporal cross correlations existing between the sub-channels of a MIMO channel [48]. For the correlation-stochastic MIMO models, the aim is to use from measurements the correlation that exists between each of the receive-end (and transmit-end) antennas to impress upon an independent identically distributed matrix the desired correlation through pre- and post-multiplication by an appropriate transformation matrix. The transformation matrices being derived from the receive-end and transmit-end correlation values respectively. Two groups of correlation-stochastic MIMO models exist – one group [28],[49],[50], referred to as Kronecker models, considers the correlation of the receivers and transmitters to be independent of each other while the other group [51] considers a joint correlation at the two link-ends.

Literature reveals the Kronecker modelling approach to be the most popular method of stochastic MIMO channel modelling and it has been shown in [20],[52] to give good estimates of channel capacity provided the channel matrix is not greater than 2×2 and the

correlation between antenna elements is low. The ease of channel representation and its relative accuracy makes the Kronecker model a good candidate for analysing the LMS MIMO channel. However, there are certain drawbacks in using the Kronecker modelling approach; these include the assumption that the correlation at the channel link-ends is completely separable and the requirement for correlation matrix to always be positive semi-definite. These assumptions/requirements are not a problem for Rayleigh channels, for which MIMO was originally conceptualised, but very much hampers the usability of the Kronecker model in the asymmetric and correlated LOS MIMO channel. Even with the adoption of orthogonal polarisations [21],[18],[53-58] to reduce channel cross-correlation, it was observed as far back as 1955 [59] that channels can still remain correlated at certain frequencies.

From the foregoing, and pertaining to the time scales in which channel fading and cross-correlation is characterised, the next two sections of this chapter reviews large scale and small scale LMS channel modelling. Two stochastic channel models, the Loo and the Fontan models, representative of the large scale models are examined in greater detail. Regarding small scale modelling, aspects treated include Rice and Rayleigh distributions, the Kronecker model and the use of Cholesky factorisation to induce correlation.

2.3.3 Large Scale LMS Channel Modelling

Large scale fading, when viewed over spatial dimensions ranging from several tens to a few hundreds of signal wavelengths, is observed as a slow variation in the local mean of the received signal power. As far as the mobile stays within a distance for which the local variation stays within the same mean value, all propagation paths to the mobile in this period are said to possess some level of large scale correlation [13].

In order to model large scale fading in LMS channels, the receive signal power (in decibels) first needs to be averaged over periods corresponding to the observation distance/time scales earlier mentioned. The second step involves subtracting from the received signal the computed average signal power and then plotting the probability density function of the resultant signal. It has been reported in [60] that in addition to modelling the large scale fading of an LMS channel by means of the log-normal

distribution, the observed local variability can be modelled using the standard deviation computed from a fitted theoretical log-normal distribution.

Although the large scale fading of an LMS channel can be partially described by the log-normal distribution, more than one distribution is needed to completely describe the range of fading a mobile terminal experiences as LMS propagation conditions change from LOS to OLOS and NLOS. To this end, the following subsections will review the Loo model, which uses a single log-normal distribution, and the Fontan model, which relies on the Loo model and uses multiple distributions to model the LMS channel.

2.3.3.1 The Loo Model

The Loo model is a stochastic model based on empirical data. In [61], Loo describes the SISO land mobile satellite channel in terms of its first order statistics by way of the probability density function, and in terms of second order statistics using the level crossing rate and average fade duration. This model is given as:

$$r = \exp(j\theta) = Z\exp(j\bar{\varphi}) + W\exp(j\tilde{\varphi}), \tag{2.17}$$

where the received signal *r* is the sum of a slowly varying log-normally distributed LOS component, *Z*, and a faster varying Rayleigh distributed multipath component, *W*. The phases $\bar{\varphi}$ and $\tilde{\varphi}$ are uniformly distributed over [0, 2π]. If *Z*, is kept constant, the probability of *r* reduces to that of a Ricean vector, given by:

$$p(r|Z) = \frac{r}{b_0}\exp\left[\frac{-r^2+Z^2}{2b_0}\right] I_0\left(\frac{rz}{b_0}\right), \tag{2.18}$$

where b_0 is the received power from multipath sources, I_0 is the modified Bessel function of zeroth order. Since *Z* has been assumed to be log-normal, its probability is given by:

$$p(Z) = \frac{1}{\sqrt{2\pi d_0 Z}}\exp\left[\frac{-(lnZ-\mu)^2}{2d_0}\right], \tag{2.19}$$

where $\sqrt{d_0}$ and μ are the standard deviation and mean of *Z*. From the assumption that *Z* can be fixed as well as log-normally distributed, the total probability theorem reveals that:

$$p(r) = \int_0^\infty p(r,Z)dZ = \int_0^\infty p(r/Z)p(Z)dZ, \tag{2.20}$$

$$p(r) = \frac{r}{b_0\sqrt{2\pi d_0}}\int_0^\infty \frac{1}{Z}\exp\left[\frac{-(lnZ-\mu)^2}{2d_0} - \frac{r^2+Z^2}{2b_0}\right] I_0\left(\frac{rZ}{b_0}\right) dZ. \quad (2.21)$$

Equations (2.17)–(2.21) hold for a single land mobile satellite SISO channel in LOS conditions and can be extended to represent a MIMO channel by adding the required number of sub-channels and including factors to account for the relationships that exist between the various sub-channels.

2.3.3.2 The Fontan model

The Fontan model [62] is a stochastic LMS SISO channel model. It models the propagating LMS signal by subsuming the slowly varying environmental effects of large scale fading into three Markov states. Within each Markov state, large scale fading and multipath (small scale fading) effects are described by a Loo distribution and are correspondingly modelled using different parameters. The 3-state approach, which gives three different distributions, is adopted because single distributions cannot adequately describe the range of fading experienced in most LMS channels. The first state of the Fontan model represents LOS fading conditions, while the second and third states represent periods of moderate shadowing and deep large scale fading respectively. This model describes the SISO channel, *h*, using:

$$h(\tau;t) = \sum_i a_i(t)e^{j\varphi_i(t)}\delta(\tau-\tau_i(t)), \quad (2.22)$$

where a_i represents the amplitude of a single direct, specularly reflected, or diffuse multipath signal. The multipath signal may be due to either the direct or the specularly reflected signal. $e^{j\varphi_i(t)}$ represents the associated phase shifts. The individual delta functions $\delta(\tau-\tau_i(t))$ represent the delays while *t* indicates that all the functions are time varying.

Also given in the Fontan model are state probability and state transition probability matrices which respectively give an indication of how long the signal stays in a given state and the probability of transiting from one state to the other. This model can be easily expanded to represent the MIMO channel by adding as many individual paths as there are antenna pairs using equation (2.22) and also including parameters to depict the relationships that exist between the individual paths.

The Fontan model has been recently revised in [60],[63] to better characterise OLOS and NLOS conditions. The revised version reduces the number of fading states from three to two and uses a more versatile set of Loo distribution parameters to describe each state. State changes are implemented using a semi-Markov model, where the fade distribution in one of the states (the 'good' state) is described by a power law distribution and in the other state (the 'bad' state) the fading signal is log-normally distributed.

2.3.4 Small Scale LMS Channel Modelling

Small scale fading, when viewed over spatial dimensions much smaller than the large scale correlation distance, is a rapid fluctuation in the amplitude of the received signal power. The signal fluctuation is so rapid that the only practical way of modelling it is by stochastic means. Literature [13] reveals three methods of stochastically modelling the small scale fading in LMS channels as: additive white Gaussian (AWGN), Ricean and Rayleigh.

A channel is modelled as AWGN when the mobile terminal is stationary and in line-of-sight, with the surrounding scatterers being also stationary. This results in the received signal power being of fixed amplitude and perturbed only by an additive white Gaussian noise component arising from extremely weak multipath components (relative to the LOS component) and electronic noise within the receiver itself. AWGN small scale fading, being the least adverse fading that can be experienced by a channel, is usually modelled only for comparison purposes since mobile terminals and scatterers are much more likely to be in motion than stationary.

Small scale fading in an LMS channel is usually modelled using a Ricean distribution when there is a dominant LOS component in addition to significant multipath contributions. If a mobile then moves from an LOS to an NLOS location, the channel can now be better modelled using a Rayleigh distribution since all the power that arrives at the receiver now only come from numerous multipath sources. Stochastic methods, using the Ricean and Rayleigh probability density functions allows the receive signal power to be more easily predicted than with deterministic methods. Note that signal power prediction using deterministic means would require complete knowledge of the

propagation environment and including the electromagnetic and boundary properties of all the elements within the environment. The probability density function of the Ricean distribution was earlier given in equation (2.18) while that of a Rayleigh distribution, *r*, is given as:

$$p(r) = \frac{r}{\sigma^2}\exp\left(\frac{-r^2}{2\sigma^2}\right), \tag{2.23}$$

where σ is the standard deviation of either the real or imaginary parts of *r*.

In relation to MIMO channels and staying within the domain of small scale fading, correlation existing between individual MIMO sub-channels has always been a cause of concern in terms of channel capacity [18-22], and bit error rates [64]. These concerns are even more acute for single satellite LMS MIMO channels due to their propensity to accentuate both large scale and small scale channel cross correlation [3]. This being the case, the next section reviews the Kronecker model, which is the most popular method of statistically modelling correlation in MIMO channels.

2.3.5 Channel Correlation and the Kronecker Model

Channel correlation as discussed in the rest of this thesis, except otherwise stated, is within the dimensions of small scale fading. This section will examine the Kronecker model, which is defined in [65] as:

$$\mathbf{H} = \mathbf{R}_{rx}^{1/2}\mathbf{H}_{iid}\mathbf{R}_{tx}^{1/2}, \tag{2.24}$$

where $\mathbf{H}_{iid}$ is a 2×2 matrix made up of uncorrelated identically distributed elements, $\mathbf{R}_{rx}^{1/2}$ and $\mathbf{R}_{tx}^{1/2}$ are respectively the Cholesky factorised matrices of the receive-end and transmit-end correlations. Equation (2.24) shows that the Kronecker model considers the receive-end and transmit-end correlation to be completely separable. This is not always the case. Also to be gleaned from the equation is the fact that Cholesky factorisation provides a convenient means to induce correlation on $\mathbf{H}_{iid}$. Another expression for the Kronecker model is:

$$\mathrm{vec}(\mathbf{H}_{iid}) = \mathbf{R}^{1/2}\mathrm{vec}(\mathbf{H}_{iid}), \tag{2.25}$$

where vec($\mathbf{H}_{iid}$) stacks $\mathbf{H}_{iid}$ into a column-wise vector and $\mathbf{R}^{1/2}$ is an upper triangular matrix derived from Cholesky factorising matrix **R**, which is obtained from the Kronecker product of receive-end and transmit-end correlation matrices, and is expressed as:

$$\mathbf{R} = \mathbf{R}_{tx} \otimes \mathbf{R}_{rx}. \tag{2.26}$$

A necessary condition for (2.26) to be used in (2.25) is that **R** must be symmetric and positive definite or semi-definite. This cannot always be achieved especially when the complex correlation function is used in obtaining the link-end correlation coefficients. Hence this thesis will avoid the stringent requirement of obtaining positive definite or semi-definite matrices and will instead propose a simpler and more efficient correlation inducing scheme for its channel modelling.

2.3.6 MIMO for Land Mobile Satellite Systems

LMS systems have been designed over the years for optimum operation in LOS conditions. This is especially necessary due to link budget restrictions arising from the limited power of small handheld LMS terminals such as in devices being proposed for DVB-SH and DVB-NGH systems [40]. Local scatterers, which cause NLOS propagation are on one hand undesirable due to the severe reduction in signal power they cause while on the other hand they create NLOS conditions which is more suitable for MIMO implementation. Apart from LOS propagation or the lack of it, another important phenomenon is the influence of LMS channels on the polarisation orientation of propagating radio waves. Having found in the 1950s [66] that signals of orthogonal linear polarisation exhibit independent fading at frequencies of a few megahertz and as such were proposed for use in diversity systems, it was only recently that orthogonal circular polarization was introduced for use in LMS MIMO systems. It is therefore necessary for this thesis to review literature regarding the very important LOS propagation metric of Rice factor, how it is estimated and its influence on the application of MIMO for LMS systems. Also, a paragraph has been devoted to defining the characteristics of polarisation in the form of antenna and channel cross polar discrimination (XPD).

2.3.6.1 The Rice Factor and Its Influence of MIMO Capacity

The Rice factor, *K*, gives a measure of the severity of fading of a wireless channel. It is defined as the ratio of arriving LOS components, a, to the multipath components, σ [13] Hence when $K = \propto$ there are no multipath components and no fading whatsoever. On the other end of the scale, when $K = 0$, the fading is at its most severe and the channel can be better described by a Rayleigh distribution. Methods proposed in literature for estimating the Rice factor include the maximum likelihood estimation (MLE) method of [67], the probability distribution fitting method of [68] and the moment based estimation method of [69]. This thesis will only use the MLE method since it gives very good estimates of a and σ. Although the MLE method has been reported in [69] as being of high computational complexity because it uses a unique expectation/maximisation algorithm, the variant employed in this thesis makes use of a simple MATLAB algorithm.

The influence of LOS propagation, and inherently the Rice factor, on MIMO channel capacity has been not been conclusively investigated for LMS systems. We can only infer from investigations conducted in terrestrial systems [54],[70] that high Rice factors will adversely affect LMS MIMO channel capacity if MIMO is implemented in its spatial dimension form. The use of orthogonal polarisation and the subsequent diagonalisation of the MIMO channel [6],[29] makes it necessary to use a capacity metric different from equations (2.7) and (2.8) to predict the MIMO channel capacity. This metric will be developed in chapter 3 of this thesis.

2.3.6.2 Channel Cross-Polarisation Coupling and Antenna Cross-Polarisation Discrimination

The polarisation sense of an electromagnetic wave is defined by the trace of its electric field vector relative to the direction of wave propagation. Depolarisation occurs when the propagation medium alters the polarisation sense of a propagating wave. This phenomenon is referred to as cross-polarisation coupling (XPC). For example, a wave transmitted with pure right hand circular polarisation may end up at the receiver with some components being left hand circular polarised. This depolarisation phenomenon can also be measured in terms of, and relative to, an antenna's cross-polar discrimination (XPD) [13]. XPD is the ratio of the received co-polarised signal power to the received

cross-polarised signal power. It gives an indication of an antenna's ability to reject oppositely polarised signals. Using h_{RR} and h_{LL} to represent the co-polarised RHCP and LHCP channels respectively, while h_{RL} and h_{LR} represent their cross-polarised components, the XPD in decibels is defined as:

$$\text{XPD} = 10\log\left(\frac{h_{RR}}{h_{LR}}\right) = 10\log\left(\frac{h_{LL}}{h_{RL}}\right). \tag{2.27}$$

The XPD as used in this thesis is assumed to be only antenna dependent while XPC has only channel dependence. Hence the channel model to be developed will use a joint XPD-XPC term since it is the channel that causes the depolarisation in the first place while the antenna possesses a finite ability to accept or reject signals of certain polarisations.

2.4 Existing LMS MIMO Channel Models

A good number of land mobile satellite MIMO channel models adopt the stochastic approach because of the ease with which stochastic methods describe the small and large scale fading effects experienced by land mobile terminals. Also, electromagnetic ray tracing over huge areas covered by a satellite's footprint would be computationally prohibitive as there are millions, if not billions of diffraction, reflection, and other boundary conditions to consider. This section presents some of such recently developed channel models.

2.4.1 The King Models, University of Surrey

King, in his University of Surrey Ph.D. thesis [3], has proposed two models for the LMS MIMO channel. The first model adopts a physical-statistical approach and has been formulated for both multiple and single satellite scenarios. This model is based on the ray tracing algorithm and it employs a scatterer cluster-centre approach to define whether signals propagating from the satellite to the land mobile terminal are either reflected, diffracted or completely blocked. Time series data of instantaneous branch power is generated for each receive-transmit (*M*,*N*) left and right hand circular polarised antenna pair using the following parameters:

$$\alpha_{M,N} = \begin{cases} P_{M,N}e^{jkd_{M,N}} + b\sum_{i=1}^{n} T_i\,\Gamma_i P_{M,N,i}e^{jkd_{M,N,i}} & clear\ co-polar\ path \\ b\sum_{i=1}^{n} T_i\,\Gamma_i P_{M,N,i}e^{jkd_{M,N,i}} & clear\ cross-polar\ path \\ D_{M,N}P_{M,N}e^{jkd_{M,N}} + b\sum_{i=1}^{n} T_i\,\Gamma_i P_{M,N,i}e^{jkd_{M,N,i}} & blocked\ co-polar\ path \\ S_b D_{M,N}P_{M,N}e^{jkd_{M,N}} + b\sum_{i=1}^{n} T_i\,\Gamma_i P_{M,N,i}e^{jkd_{M,N,i}} & blocked\ cross-polar \\ T_{M,N}P_{M,N}e^{jkd_{M,N}} + b\sum_{i=1}^{n} T_i\,\Gamma_i P_{M,N,i}e^{jkd_{M,N,i}} & co-polar\ via\ trees \\ S_t T_{M,N}P_{M,N}e^{jkd_{M,N}} + b\sum_{i=1}^{n} T_i\,\Gamma_i P_{M,N,i}e^{jkd_{M,N,i}} & cross-polar\ via\ trees \end{cases} \quad (2.28)$$

The parameters in equation (2.28) are defined as follows: $P_{M,N}$ represents the mobile-satellite antenna path loss, *k* represents the wave number, *n* represents the number of scatterers, *T* is tree attenuation, Γ is the reflection coefficient, *d* represents distance, *D* is diffraction loss and *S* represents cross-polar attenuation terms. This model has been validated against measured data and its first order and correlation statistics have been found to be relatively accurate. However the model has some draw backs which include:

- The use of numerous parameters including diffraction loss and tree attenuation, which is usually calculated from the averages of edges grazed and in lengths (in metres) of tree matter (vegetation) traversed. These numerous parameters greatly increase computational complexity of the model.

- In a bid to reduce the computational complexity, the model replaces real scatterers like irregularly shaped trees and buildings with spherical clusters. This inadvertently over simplifies the channel and incurs a huge penalty in prediction accuracy.

The second of King's LMS MIMO models in [3], of which a stepwise implementation has been given and validated in [71],[72], employs an empirical-stochastic approach and has

been generated both for narrowband and wideband dual polarised 2×2 MIMO channels. In the narrowband case, large scale correlated Gaussian channel data samples having zero mean and unit standard deviation are generated and passed through a first order recursive filter to impose the appropriate temporal fading (memory). The recursive filter's parameters include variables representing the mobile terminal's velocity, channel sampling rate and the channel coherence distance and are given by:

$$h_{i,j|corr(n)} = h_{i,j|uncor(n)} + \exp\left(-\frac{v_m \Delta t}{r_c}\right) h_{i,j|corr(n-1)}, \tag{2.29}$$

where $h_{i,j|corr(n)}$represents a channel sample in which large scale correlation has already been induced. $h_{i,j|uncor(n)}$ indicates an uncorrelated narrowband channel sample and the recursive filter terms v_m, Δt and r_c represent the mobile's velocity, sample time and channel coherence distance respectively.

Prior to equation (2.29), large scale correlation of the individual MIMO channels $h_{i,j|corr(n)}$ is induced by way of Cholesky factorising a 4×4 large scale correlation matrix of the channel and multiplying that with a vectorised 4×1 stack of the 2×2 channel matrix. Different large scale correlation matrices are created for LOS periods and OLOS/NLOS periods. As with the large scale correlation, small scale correlation between the individual MIMO channels is then added to the generated channel data based on values extracted from measurements. A detailed treatment of the small scale modelling aspects of this model has recently been published in [71]. Finally, four large scale fading states are defined and a Markov model is used in switching between these fading states. For a 2x2 channel, this model is formulated as:

$$\mathbf{H} = \bar{\mathbf{H}} + \tilde{\mathbf{H}} = \begin{bmatrix} \bar{h}_{11} & \bar{h}_{12} \\ \bar{h}_{21} & \bar{h}_{22} \end{bmatrix} + \begin{bmatrix} \tilde{h}_{11} & \tilde{h}_{12} \\ \tilde{h}_{21} & \tilde{h}_{22} \end{bmatrix}, \tag{2.30}$$

where $\bar{h}_{ij}$ (i,j = 1,2) represents the log-normally distributed large scale fading components, while $\tilde{h}_{ij}$ represents the Ricean distributed small scale fading components. This model represents one of the first attempts at empirical based dual polarised LMS MIMO channel modelling. However, due to its novelty, it suffers from some of the accuracy limitations of the earlier physical-stochastic model including:

- The use of very low elevation (7^o – 18^o) channel data to determine the model parameters which makes the model only valid for that environment. Most practical LMS systems operate at elevations much higher than 18^o and as such contributions from multipath components are very low relative to the LOS components. This is especially true for suburban and open environments.

- The Markov switching process generates abrupt and rapid transitions between channel states which is not very consistent with measurements.

- The choice of four fading states is rather cumbersome. Recent channel data analysis has revealed that some of the fading states are extremely unlikely, hence the need to reduce the states to a more realistic number.

Fixed correlation coefficients were used for both the large and small scale fading matrices. This creates some inaccuracy in the model as MIMO channels in real environments have variable correlation coefficients.

2.4.2 The Sellathurai Model, Communications Research Centre of Canada

While with the Communications Research Centre of Canada in Ottawa, Sellathurai in [21] proposed a polarisation scattering model for investigating different space-time coding techniques for land mobile satellite systems. The model builds a 2x2 horizontal and vertical polarised MIMO channel using:

$$\mathbf{H} = \mathbf{L}\begin{bmatrix} \sqrt{\frac{K_{11}}{K_{11}+K_{12}+1}} & 0 \\ 0 & \sqrt{\frac{K_{21}}{K_{21}+K_{22}+1}} \end{bmatrix} + \mathbf{S}\begin{bmatrix} \sqrt{\frac{K_{12}}{K_{11}+K_{12}+1}} & 0 \\ 0 & \sqrt{\frac{K_{22}}{K_{21}+K_{22}+1}} \end{bmatrix} + \mathbf{D}\begin{bmatrix} \sqrt{\frac{1}{K_{11}+K_{12}+1}} & 0 \\ 0 & \sqrt{\frac{1}{K_{21}+K_{22}+1}} \end{bmatrix}, \tag{2.31}$$

where K_{11}, K_{21} and K_{12}, K_{22} are the Rice factors of the direct and specula reflected components respectively. Note that K_{11} and K_{12} represent the Rice factors for the co- and cross-polar vertical components respectively while K_{21} and K_{22} represent the cross- and co-polar horizontal components respectively. **L**, **S** and **D** are 2x2 matrices representing

the power in the LOS, specula and diffuse components respectively. They give an indication of the antennas XPD. Typical Rice factors for this model vary from 7 to 10 in suburban/ rural environments up to about 100 in open environments [21]. In urban areas the channel usually exhibits Rayleigh distribution and the available signal power is inadequate for LMS applications.

A limitation of the Sellathurai model is the assumption that the cross-polarised channels in all three environments studied (urban, suburban/rural and open) has correlation coefficient values of between 0.3 and 0.7. This is not usually the case as higher correlation coefficients ranging from 0.76 to 0.92 have been reported in [3], even when orthogonally polarised antennas are employed. Another drawback of this model, despite its simplicity, is its lack of experimental validation.

2.4.3 The Liolis Model, European Space Agency

Liolis in [18],[73] proposed his dual polarised LMS MIMO channel model while working with the European Space Agency's Research and Technology Centre (ESA/ESTEC) in Noordwijk, The Netherlands. The Liolis model is a statistical model derived from LMS SISO and terrestrial MIMO measurements and it uses a Markov chain process and the Loo distribution to describe the huge range of fading effects experienced in a typical LMS channel. Included in the model are parameters to account for polarisation and temporal correlation, LOS shadowing, elevation angle effects, antenna XPD and user environment effects as parameterised by the cross-polar coupling (XPC).

To induce the required large scale fading correlation, the model proceeds by generating a 4×4 positive semi-definite covariance matrix, $\mathbf{H}_{cov,large}$, based on measurement results. Examples of such measurement results can be found in [3],[1] Next, a 2×2 matrix, $\mathbf{H}_{iid}$ made up of identically distributed and circularly symmetric Gaussian elements with a given mean, α, and standard deviation, ψ, values is generated. The large scale correlation is then incorporated into $\mathbf{H}_{iid}$ using equation (2.25). The large scale correlated vector (now a vector since it has been stacked by the *vec* function), $\mathbf{H}_{corr,large}$, is then exponentiated to give it a log-normal (Loo) distribution.

The Liolis model uses the Kronecker approach to induce correlation on the small scale fading components. A semi-definite covariance matrix, as done in the large scale case, is generated but this time the matrix is built using the Kronecker product as shown:

$$\mathbf{H}_{cov,small} = \mathbf{R}_{tx}^{T} \otimes \mathbf{R}_{rx}^{T}, \tag{2.32}$$

where the superscript *T* indicates that the positive semi-definite covariance matrices of the transmit link end, $\mathbf{R}_{tx}$, and the receive link end, $\mathbf{R}_{rx}$, have been transposed. The small scale correlation is then induced on a second $\mathbf{H}_{iid}$ matrix following equation (2.25). Or, in the Kronecker form [50],[65],[74] , this correlation induction is expressed as:

$$\mathbf{H}_{corr,small} = \mathbf{R}_{rx}^{1/2}\mathbf{H}_{iid}\mathbf{R}_{tx}^{1/2}. \tag{2.33}$$

Using the Liolis model, it has been shown that increasing antenna XPD leads to improved channel capacity. However, one of the major handicaps of the Liolis model is its dependence on a 4×4 positive semi-definite covariance matrix, which as explained in section 2.3.5, may be difficult to formulate.

2.4.4 The King-Brown-Kyrgiazos Model, University of Surrey

The King-Brown-Kyrgiazos model was recently proposed in [71] to more robustly model the small scale fading aspect of the King model [72]. Its strength lies in the description of the small scale fading of a dual polarised LOS MIMO channel in LOS channels. In such scenarios, the channel correlation is not separable and hence the popular Kronecker approach cannot be applied. Otherwise, as with the Sellathurai model, this model is made up of three main components as shown below:

$$\mathbf{H} = \sqrt{\frac{K_1}{K_1+K_2+1}}\mathbf{A} + \sqrt{\frac{K_2}{K_1+K_2+1}}\mathbf{S} + \sqrt{\frac{1}{K_1+K_2+1}}\mathbf{L}, \tag{2.34}$$

where K_1 and K_2 represent the Rice factor or the direct co-polar and direct cross-polar components respectively, **A** is a 2x2 matrix whose diagonal elements represent the two co-polar channels while its off-diagonal elements are equal to zero. **S** is also a 2x2 matrix representing the direct cross-polar components. Its diagonal elements are made equal to zero while its off-diagonal elements contain the two cross-polar channels. **L** is a matrix

representing the diffuse multipath components and as such it is made up of zero mean circular symmetric complex Gaussian elements.

The main difference between this model and other stochastic based LMS MIMO models is the way it applies complex correlation on the small scale fading component (matrix **L**) of both the co- and cross-polar channels. Firstly, using values extracted from measured channel data, it respectively defines the co- and cross-polar correlation matrices as:

$$\mathbf{R}_{c-pol} = \begin{bmatrix} 1 & r_{CP}^{*} \\ r_{CP} & 1 \end{bmatrix} \text{ and } \mathbf{R}_{x-pol} = \begin{bmatrix} 1 & r_{XP}^{*} \\ r_{XP} & 1 \end{bmatrix}. \tag{2.35}$$

In the case of dual circular polarisations, matrix **L** is defined as:

$$\mathbf{L} = \begin{bmatrix} h_{RR} & h_{RL} \\ h_{LR} & h_{LL} \end{bmatrix} \tag{2.36}$$

and the correlation procedure is performed in three steps given by:

$$\begin{bmatrix} h_{RR|corr1} \\ h_{LL|corr1} \end{bmatrix} = \mathbf{R}_{c-pol}^{1/2} \begin{bmatrix} h_{RR} \\ h_{LL} \end{bmatrix}, \tag{2.37}$$

$$\begin{bmatrix} h_{RR|corr2} \\ h_{RL|corr2} \end{bmatrix} = \mathbf{R}_{x-pol}^{1/2} \begin{bmatrix} h_{RR|corr1} \\ h_{RL} \end{bmatrix}, \tag{2.38}$$

$$\begin{bmatrix} h_{LL|corr2} \\ h_{LR|corr2} \end{bmatrix} = \mathbf{R}_{x-pol}^{1/2} \begin{bmatrix} h_{LL|corr1} \\ h_{LR} \end{bmatrix}. \tag{2.39}$$

Lastly, the correlated **L** matrix is assembled as shown below:

$$\mathbf{L}_{corr} = \begin{bmatrix} h_{RR|corr2} & h_{RL|corr2} \\ h_{LR|corr2} & h_{LL|corr2} \end{bmatrix}. \tag{2.40}$$

The above three steps avoid the problem of having to Cholesky factorise a 4×4 matrix as is required in the Kronecker approach. This represents a convenient work around since for Cholesky factorisation to be easily implemented 4×4 matrices must always be positive semi-definite, which in practice is not always the case. Using measured channel data, the model has been validated both for first order statistics and eigenvalue distribution.

However, more empirical data is needed to fine tune and validate the correlation, Rice factor and polarisation properties as described by the model.

The King-Brown-Kyrgiazos model's adoption of different Rice factor and correlation values to describe the small scale fading statistics of the co-polar and cross-polar channels makes it especially suitable for analysing new alternative schemes to conventional MIMO. This is especially true since the workability of MIMO schemes depend on the level of correlation that exist between the MIMO sub-channels and a model that isolates these two terms to describe its small scale fading aspect comes in very handy. Therefore, adopting the King-Brown-Kyrgiazos model in addition to the multistate modelling approach of Fontan [62], which handles the large scale fading aspects, allows all the possible fading characteristics of the dual polarised LMS MIMO channel to be isolated and their effects on the capacity and BER of MIMO and alternative schemes studied in very fine detail. With the availability of new empirical data, the relationship between Rice factor and correlation in the small scale fading domain can be uncovered and fed into the King-Brown-Kyrgiazos model or used in developing a new model for the dual circular polarised LMS channel.

2.5 Potential Applications for LMS MIMO: Digital Video Broadcasting Services (DVB-SH and DVB-NGH)

DVB-SH refers to the European Telecommunications Standards Institute (ETSI) broadcast standard for the satellite delivery of video, audio and data services to small mobile and fixed devices including vehicle mounted infotainment devices and personal mobile communication and entertainment devices like telephones, personal digital assistants (PDAs), laptops and palmtops [40],[75]. The DVB-SH system is essentially a satellite-terrestrial hybrid network operating at frequencies below 3GHz. Its satellite component (SC) provides coverage to very large areas since satellite is often the most economical means to reach sparsely populated rural areas. The terrestrial coverage of DVB-SH is made up of cellular-type complementary ground components (CGC) that fill the gaps left off by the SC. The DVB-SH hybrid transmission set up shown in Figure 2.6 [76],[77] allows for continuity of service at acceptable QoS levels.

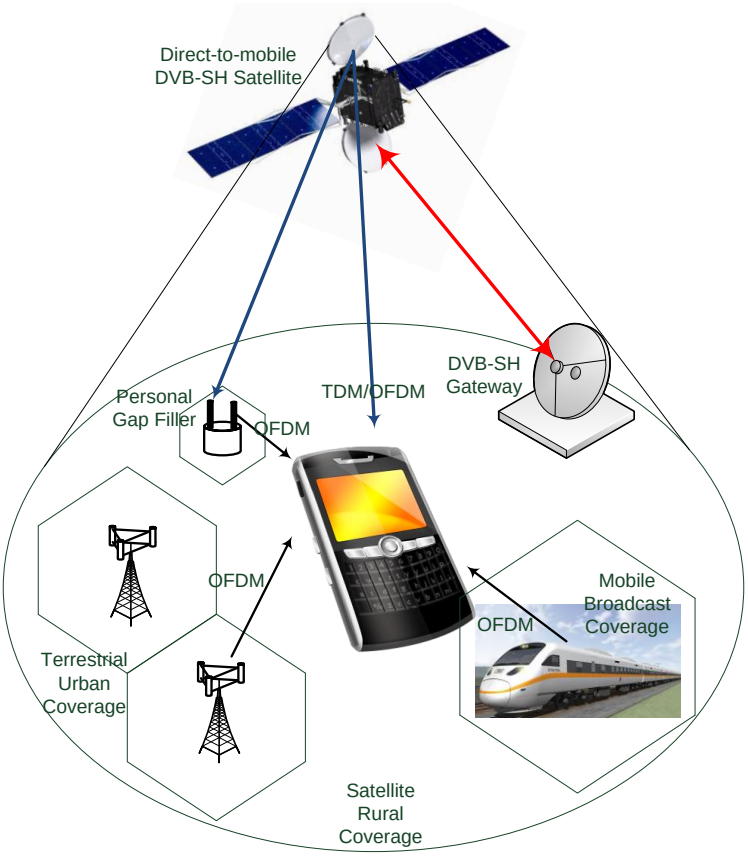

Figure 2.6: DVB-SH system architecture

Two transceiver classes have been defined for the ground terminals of the DVB-SH system [75]. They are SH-A transceivers which can handle only orthogonal frequency division multiplexing (OFDM) on both the satellite and terrestrial links, and SH-B transceivers which use time division multiplexing (TDM) on the satellite link and OFDM for the terrestrial link. According to recommendations given in [77], the typical and maximum bit rates for the hybrid DVB-SH system is given in Table 2-1, while the transceiver structure showing demodulation modules of its SH-B transceiver is shown in Figure 2.7. Note that the SH-A transceiver is also contained within the SH-B transceiver and both transceivers are currently designed to reliably handle a minimum bit rate of 2.2Mbps per 5MHz bandwidth when in satellite-only reception mode.

Table 2-1: Typical and maximum net bit rates in Mbps for the DVB-SH system in satellite-only and terrestrial-only coverage

Hybrid network frequency configuration		**Transceiver Architecture**					
		SH-A				**SH-B**	
		SFN		**MFN**		**MFN**	
		Typ	Max	Typ	Max	Typ	Max
3×5MHz beam satellite	Satellite-only beam rate	2.5	10.0	2.5	10.0	2.7	10.6
	Terrestrial-only beam rate	10.0	30.0	7.5	20.0	7.4	20.5
4×5MHz beam satellite	Satellite-only beam rate	2.5	10.0	2.5	10.0	2.7	10.6
	Terrestrial-only beam rate	13.7	40.0	11.2	30.0	11.1	30.4

In Table 2-1, 3×5MHz represents a 3 colour reuse – i.e. when a 15MHz bandwidth is divided into three sub-bands of 5MHz each. Both the SH-A and SH-B transceiver architectures have been designed to work in single frequency network (SFN) and multi-frequency network (MFN) configurations. For SFN, the same sub-band is used by the transmitting SC and CGC while transmission in MFN configuration respectively is done on two separate frequency sub-bands.

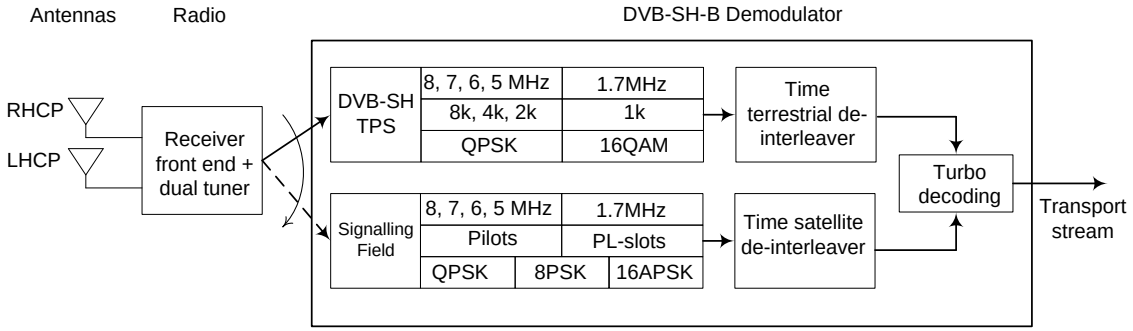

Figure 2.7: Transceiver structure of DVB-SH showing modules of the SH-B demodulator

The demodulator modules of the SH-B transceiver indicate that frequency sub-bands ranging from 1.7MHz to 8MHz are capable of being handled in the DVB-SH system. Whereas satellite only TDM reception (the lower blocks of the demodulator in Figure 2.7) can support quadrature phase shift keying (QPSK), 8PSK and 16PSK modulation formats, the terrestrial receiving mode is designed for OFDM modulation using QPSK or 16QAM (16 quadrature amplitude modulation) constellations. While the DVB-SH receiver is in MFN configuration (SH-B), the SC and CGC transmitters are capable of using any of the 8k, 4k, 2k or 1k OFDM modes to respectively obtain 6817, 3409, 1705 or 853 carriers [40].

Orthogonal circular polarisation in satellite-earth communications has traditionally been used for reducing the effects of inter-beam interference and to promote a high order of frequency reuse by multi-beam satellites [19]. However, DVB-SH being a hybrid satellite-terrestrial system that would most likely employ multi-beam satellites, there is an overriding need to employ orthogonal circular polarisation to improve spectral efficiency in order to meet the minimum bit rate requirements. Methods of dealing with the expected increased inter-beam and inter system interference is a subject which this thesis will partially address. Therefore, in the example of a hypothetical 3-colour 6-beam satellite given in [77], the polarisation reuse mode where each European country (or sub region) is covered by two beams of orthogonal circular polarisations is chosen in this thesis according to recommendations in [77] as the de facto standard for the satellite component of DVB-SH systems. Figure 2.8 pictorially represents this concept and given that spectral efficiency is: $\gamma_{spec} = \left(\frac{Number\ of\ beams}{Number\ of\ colours} \times frequency\ reuse\ factor\right)$, there is an eight fold increase in spectral efficiency compared with a satellite employing a single beam. The frequency reuse factor (i.e. the number of times a frequency sub-band is reused over the total coverage area of the satellite) increases to 4 compared with 2 as when orthogonal polarisation is employed in its traditional role of increasing inter-beam isolation. The only downsides of this choice are increased satellite payload complexity, increased inter-beam interference and an increased likelihood of causing harmful interference to other wireless systems.

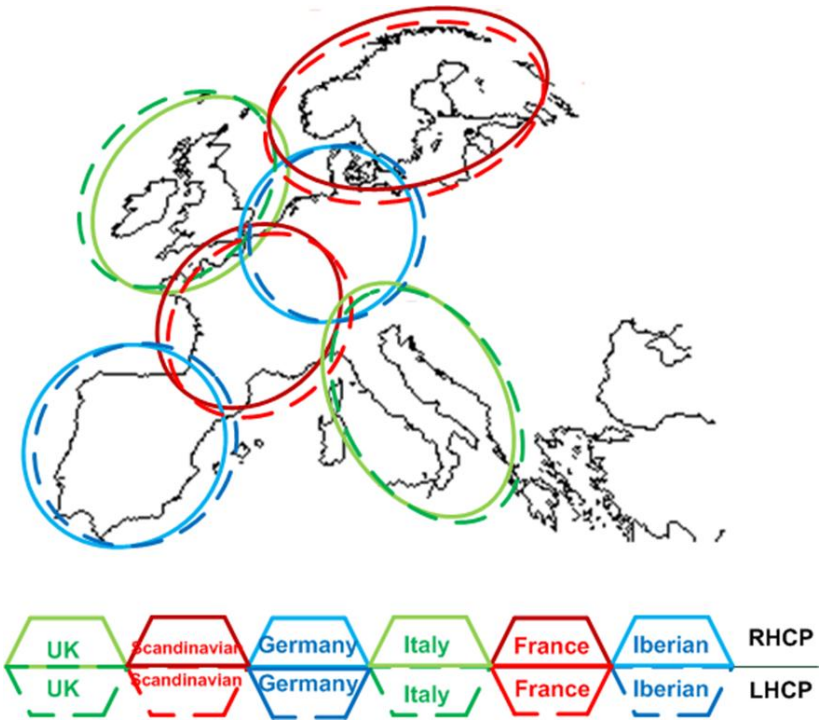

Figure 2.8: Example of a multi-beam 3-colour dual circular polarised satellite coverage of Europe

Each of the colours in Figure 2.8 represents a frequency band 5MHz wide. The bold lines represent RHCP coverage while the broken lines represent LHCP coverage. It is apparent that the 6-beam 3-colour satellite coverage scheme allows the bandwidth of each beam to be doubled, which can in turn support higher bit rates or can be used in improving the QoS through conventional MIMO diversity methods. This thesis in chapter 6 will determine what channel conditions can make the multiplexing of two circular orthogonally polarised signals more viable than conventional MIMO diversity techniques when compared within the context of DVB-SH systems.

The demand for rich wirelessly delivered multimedia applications is expected to increase several-fold in the near future and the current systems of delivery may not be able to cope with this demand. This has prompted ETSI to seek for possible enhancements (in terms of a reduction in signal processing overheads and the use of multi-antenna techniques like MIMO) to the current DVB-H, DVB-SH and DVB-T2 standards so as to meet the predicted demand. The enhancement activities, which included a Call for Technologies [78], a Study Mission Report [79], and a commercial requirements specification [80] are expected to cumulate in the publication of a new ETSI digital video broadcasting via

satellite standard applicable to the next generation of handhelds (DVB-NGH). According to [80], the type of devices to be addressed in the DVB-NGH standard include small wearable receivers like mobile phones and video players capable of indoor and outdoor TV signal reception, portable devices like laptops, notebooks, netbooks and vehicle mounted devices. The DVB-NGH standard is bound to offer smooth degradation mechanisms in areas of poor network coverage and allow for receivers to seamlessly switch to other available systems like LTE if the QoS of NGH falls below acceptable levels. The QoS for NGH services in ideal conditions has been defined in [78] as a quasi-error free quality of service which amounts to not more than one uncorrected error per hour. Since open source literature is lacking on acceptable QoS levels of DVB-SH and DVB-NGH systems, the BER analysis carried out in chapter 6 of this thesis is the first time at which the propagation environment-dependent QoS characteristics of such services are thoroughly determined; these are done via simulations using measured and modelled dual circular polarised LMS MIMO channel data. The BER analysis will determine if polarisation multiplexing meets the QoS requirements for both DVB-SH and DVB-NGH services.

2.6 Conclusions

This chapter has presented various metrics used in characterising wireless MIMO channels and models derived from measurements. Reasons have been given why most LMS MIMO channel models prefer the stochastic modelling approach. Various stochastic and polarisation based LMS MIMO channel models have been reviewed with an in-depth look on how they capture and present the large scale and small scale channel fading effects. This has revealed some weaknesses in previous modelling attempts and has highlighted the need to develop better and more accurate channel models that take into account earlier overlooked aspects like the relationship between the cross-correlation of orthogonally polarised MIMO sub-channels and their Rice factors, the branch power ratio of MIMO sub-channels as propagation conditions change from LOS to OLOS/NLOS and vice versa and the influence of antenna and environment dependent XPD on the signal power received the antennas. Fully incorporating these factors in a tractable channel

model would help in uncovering the true potentials of MIMO in orthogonally circular polarised LMS channels.

Finally, since satellites have much larger footprints than terrestrial broadcast systems and can offer more economical broadcast solutions to highly dispersed users, literature concerning the newly proposed DVB-SH and DVB-NGH systems has been reviewed. With MIMO being proposed for adoption in future DVB systems, there is an open research question as to whether MIMO is really necessary in the LMS channel and under what propagation conditions can MIMO be implementable. Thankfully, there are indications that with slight increase in the complexity of present satellite broadcast systems and with the use of dual orthogonal circular polarisations, it is feasible to implement MIMO (at least in its polarisation multiplexing mode) in the LMS channel. Such MIMO implementations may help deliver high bit rate (and spectral efficient) services to dispersed land mobile satellite users. Therefore, it is necessary for the next chapter to review literature on popular transceiver structures since transceivers are vital to wireless communication systems and without their optimal operation, the potentials of MIMO diversity or MIMO multiplexing cannot be realised.

Chapter 3

3 MIMO Transceiver Techniques and Dual Circular Polarisation Multiplexing

The previous chapter reviewed literature relating to multiple-input multiple-output (MIMO) channel modelling for terrestrial and land mobile satellite (LMS) channels with particular emphasis on how available models describe the polarisation characteristics of LMS MIMO channels. The insight derived from chapter 2 thus lays a good foundation to embark on a brief review of different practical MIMO transceiver techniques in this chapter. Transceiver techniques deserve to be given much attention since one of their paramount roles, without which MIMO would remain an academic exercise, is their ability to identify and utilise the additional spatial and/or polarisation domains of MIMO even in the presence of increased inter-channel interference. Hence, one of the outcomes of chapter 3 is the proposal of a dual circular polarisation multiplexing (DCPM) scheme. DCPM is a low effort alternative to MIMO and has been found to yield comparable capacity to conventional MIMO at low signal to noise ratio (SNR) values and in channel conditions of sufficient polarisation purity.

3.1 Background to MIMO Transceiver Architectures

By transceiver architecture, this thesis refers a terminal capable of performing both the operations of transmission and reception. Due to the plethora of transceiver techniques available in literature, this chapter will only examine the receiver aspects of a transceiver system and in doing so will stick to the discrete time domain. Readers interested in the frequency domain aspects are encouraged to use the Fourier transform relationship between time and frequency to extend the analysis if needed. The receiver-only description adopted here, in addition to keeping the discussion brief is justifiable because wireless propagation channels obey the theory of reciprocity [13]. Channel reciprocity

allows for the convenience of viewing a channel in transmit mode while doing computational analysis and then assuming the same channel to be in the receiving mode while measuring the channel. The reciprocity principle is the premise on which linear receiver structures like Zero Forcing (ZF), Minimum Mean Squared Error (MMSE) detection and the non-linear Maximum Likelihood Sequence Estimator (MLSE) will be studied in this chapter. Matched filtering, a precursor to the linear receiver structures is also treated before examining how the linear transceivers can be used in highly correlated LMS channels to improve the performance of communication systems.

It is important to emphasise that since a receiver's main job on sensing the transmitted signal is to remove the channel attenuation effects and correctly detect the transmitted information, it can also be referred to a channel equaliser. Hence, the rest of the thesis will use receiver architectures and channel equalisation techniques interchangeably.

3.1.1 Zero Forcing

Zero forcing (ZF) is the simplest of the linear channel equalisation techniques. It operates on the assumption that the MIMO channel matrix, **H**, is fully invertible and the product of the received signal and the coefficient of inverted channel must fulfil the criteria:

$$[\mathbf{w}_{ZF}(t)\boldsymbol{y}(t)]_{t=iT_s} = \begin{cases} 1 & i = 0 \\ 0 & otherwise \end{cases} \tag{3.1}$$

and $$\boldsymbol{w}_{ZF} = \mathbf{H}^{+}, \tag{3.2}$$

where in the case of a 2×2 channel, $\boldsymbol{y}(t)$ represents a 2×1 received signal vector, $\mathbf{W}_{ZF}(t)$ is a 2×2 matrix of the Zero Forcing complex weights produced by inverting **H** using the Moore-Penrose pseudo-inversion process ($\mathbf{H}^{+}$) [35], and T_s represents the duration of the received symbol. Equation (3.1) means that the output of the channel equaliser will be forced to zero at all instants except when $t = 0$. The expression in (3.1) also assumes that the channel is narrowband. If the channel happens to be wideband, multiple taps are needed and $w(t)$ for each of the taps are scaled corresponding to their level of contribution to the overall received signal power.

ZF is optimal in removing interference but in the process of channel inversion it enhances background channel noise [8],[13],[34]. However, despite the noise enhancement drawback, ZF's simplicity makes it well suited for the LOS scenario of the dual polarised LMS MIMO channel since noise is such channels is usually minimal. The only significant channel distortion comes from the interference of depolarised signals and the receiving antennas inability to completely reject signals of orthogonal polarisation. It is then important that achievable bit error rate (BER) of the dual polarised LMS MIMO channel when using the ZF receiver be thoroughly investigated. This is the main crux of chapter 6 of this thesis.

3.1.2 Minimum Mean Square Error Detection

The minimum mean square error (MMSE) detection criterion for linear channel equalisers goes a step further than ZF by trying to simultaneously minimise the effects of both interference and channel noise. The objective of this equaliser is to choose a matrix, **M** that minimises the error ϵ, given by:

$$\epsilon^2 = E[(\boldsymbol{x} - \overline{\boldsymbol{x}})^T(\boldsymbol{x} - \overline{\boldsymbol{x}})] = [(\boldsymbol{x} - \boldsymbol{y}\boldsymbol{w}_{MM})^T(\boldsymbol{x} - \boldsymbol{y}\boldsymbol{w}_{MM})], \tag{3.3}$$

where $\boldsymbol{x}$ is the transmitted signal vector and $\overline{\boldsymbol{x}}$ is the signal vector estimated by the equaliser to have been transmitted. The other terms are as previously defined and since we are dealing with a 2×2 MIMO channel, $\boldsymbol{x}$ and $\boldsymbol{y}$ are both 2×1 vectors. The MMSE complex channel weights are contained in the 2×2 dimensional $\mathbf{w}_{\boldsymbol{MM}}$, which is arrived at by inverting both the channel matrix, **H**, and the noise contributions (in the SNR term), and is defined in [34] as:

$$\boldsymbol{w}_{\boldsymbol{MM}} = \left(\mathbf{H}^H\mathbf{H} + \frac{1}{SNR}\mathbf{I}_m\right)^{-1}\mathbf{H}^H, \tag{3.4}$$

where **I** is an identity matrix with a dimension equal to the number of receive antennas, *m*, superscript *H* indicates Hermitian transposition.

MMSE equalisation strives for a compromise between interference elimination and noise removal, making its implementation is more challenging than that of ZF. Provided there are no transceiver power constraints to hamper the increased complexity, MMSE is a

better candidate to equalise dual polarised LMS MIMO channels experiencing OLOS fading due to its ability to deal with increased channel noise.

3.1.3 Maximum Likelihood Detection

Receivers based on the maximum likelihood (ML) detection criterion are optimum because they exhaustively search through complete sets of code words or symbols to determine (in the particular case of ML Sequence Estimators (MLSEs)) the sequence in which they were most likely transmitted. Assuming that the transmitted data stream, $\boldsymbol{x}$, is temporally uncoded, the MLSE criterion is defined in [34],[81] as:

$$\bar{\boldsymbol{x}} = \arg_{\boldsymbol{x}}\min\|\boldsymbol{y} - \mathbf{H}\boldsymbol{x}\|^2, \tag{3.5}$$

where $\bar{\boldsymbol{x}}$ is the estimated symbol vector obtained after exhaustively searching through all the vector constellations for the most probable transmitted vector. Due to the exhaustive search they perform, ML receivers are highly complex and not feasible to implement in most cases. They will only be used in this thesis to benchmark against the BER performance of the more practical ZF and MMSE transceivers and for constellation sizes not greater than QPSK.

3.1.4 Matched Filtering

At the front of every linear receiver is a filter that is matched to the convolution of the channel coefficient, $h(t,\tau)$, and the transmitted symbol, $x(t)$. The main function of such filters is to limit the amount noise and interference that is sampled from the channel. Looking from the transmit link-end, match filtering entails the application of precoder weights to the transmit signal so as to enforce channel orthogonality, which in turn supports eigen mode transmission. Recall in section 2.2.4 that eigen mode transmission is dictated by the eigenvalue distribution of the given MIMO channel. Therefore MIMO channel matched filtering is a system whereby multiple equivalent channels are created by matching each transit beam to a receive beam and sending independent bit streams through the matched beams. The enforced channel orthogonality eliminates inter bit stream interference, which implies that matched filtering is optimal when the channel is orthogonal. However, for conventional MIMO systems, eigen mode transmission via

matched filtering requires a very rich scattering environment, which is not usually the case in LMS channels. Luckily, the use of orthogonal circular polarised antennas with high XPDs has been recently shown to provide a good level of orthogonality and capacity [3],[82],[83], a phenomenon this thesis aims to explore further.

3.2 Dual Circular Polarisation Multiplexing – An Application of Receiver-based Processing for the LMS Channel

Dual circular polarisation multiplexing has been proposed by the author as a technique to optimally combine two orthogonally polarised channels for increased throughput when the LMS channel is mainly LOS and with highly correlated fading statistics. The choice of polarisation multiplexing is based on the findings of [84] which revealed that conventional equal power allocation MIMO becomes increasingly inefficient as the MIMO channel gets more correlated. Hence dual circular polarisation multiplexing, being an offshoot of beamforming, is proposed as a more appropriate MIMO technique to implement in such correlated channel conditions. A schematic diagram of the DCPM architecture is shown in Figure 3.1, where there is a 2×2 MIMO link between a satellite and a land mobile terminal. The RHCP and LHCP antenna pairs at both the satellite and the mobile terminal link-ends as shown in Figure 3.1 and previously explained in section 2.5 are for the purposes of simultaneously transmission and reception two independent and parallel bit streams. Channel equalisation is performed only at the mobile while the satellite may be periodically updated of the large-scale fading statistics of the channel. It is important to emphasise that DCPM is fundamentally different to MIMO which applies weights processing at both the satellite and LMS terminal so as to enforce channel orthogonality.

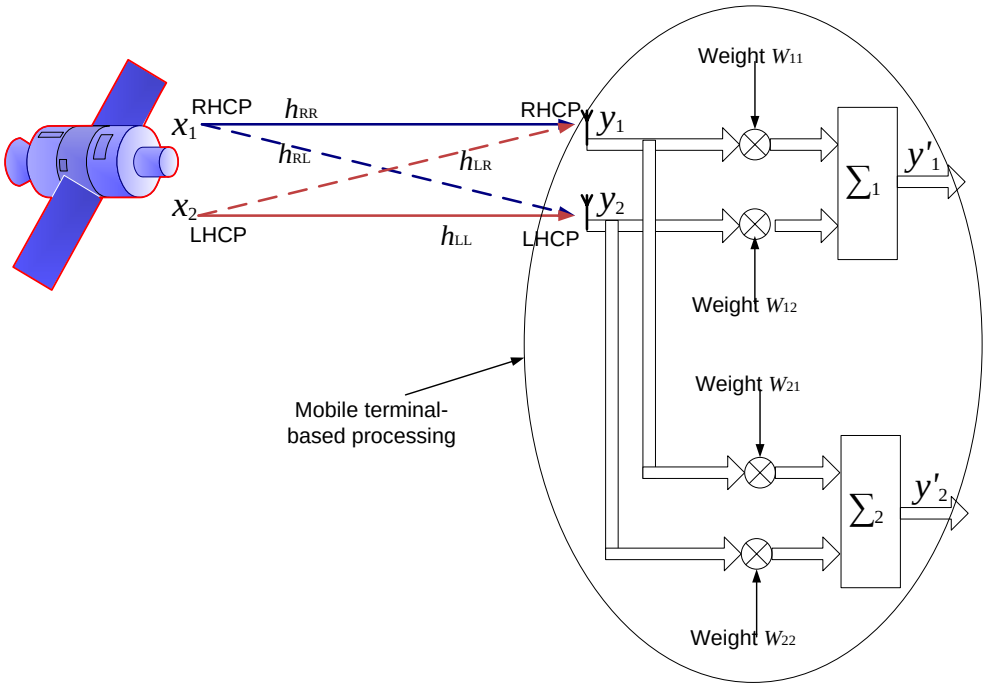

Figure 3.1: DCPM architecture showing receiver based channel equalisation

3.2.1 Iterative Receivers and Applications

ZF and MMSE linear receiver techniques earlier described can be made to work in iterative designs to successively eliminate interference and channel noise. Iterative channel distortion elimination is the basis upon which popular transceiver architectures like the Diagonal Bell Labs Layered Space Time (D-BLAST) [85] and Vertical Bell Labs Layered Space Time (V-BLAST) [86],[87] channel equalisation schemes operate. Since the multiple channels of a MIMO communications system usually encounter different levels of channel interference, two types of iterative channel equalisation designs–ordered and unordered successive interference cancellation (OSIC or USIC)–have been proposed and implemented over the years.

Selection order in OSIC transceivers is achieved by first choosing the MIMO sub-channel with the strongest signal to interference plus noise ratio (SINR), then estimating (using ZF or MMSE) and removing the contribution of this sub-channel in the overall received signal. Successive iterations are then performed on the depleted MIMO channel to estimate and remove the contributions from progressively weaker MIMO sub-channels. In the simpler USIC, sub-channels are chosen at random for first stage estimation and

elimination. This comes with certain drawbacks, chief among which is the higher probability of error propagation between iteration stages given the increased likelihood of a weaker MIMO sub-channel to be chosen for first stage estimation. First stage estimation errors would then be propagated to the second stage leading to higher error rates for USIC. Details of SIC transceivers can be found in [34],[88]. The BER performance of OSIC compared with SIC [89],[90] makes it a more favoured candidate for use in dual polarised LMS MIMO systems because of its reduced incidence of error propagation. Especially for LOS conditions characterised by high SINRs and minimal interference, the advantages of OSIC can be exploited and used with the simpler ZF equalisation (ZF-OSIC) as compared to the more cumbersome MMSE-OSIC.

Implementing ZF-OSIC in a dual polarised MIMO system would be a two-step operation which involves firstly estimating the stronger of the two co-polar channels (RHCP or LHCP) and removing its effect from the total **H** matrix and secondly estimating the transmitted symbols in the depleted **H** matrix. Although many different OSIC algorithms have been proposed for use in different environments [87],[91],[92] and the effect of the ordering criteria extensively studied [93], only one preliminary study [4] has looked at the influence of orthogonally polarised data-streams on the BER rates of LMS MIMO schemes.

Since LMS communication systems mainly operate in the LOS mode and antenna co-location remains the only practical means to implement MIMO in such systems, the correlation between supposedly independent MIMO sub-channels is bound to be very high. Therefore the effect of this high correlation on the transceiver bit and symbol error rates is very important and needs to be exhaustively studied. Up until now, only a few researchers have taken on this task. One of such studies was done by Akhtar and Gesbert in [94], where they proposed a hybrid ZF/maximal ratio combiner with SIC (HZF-SIC) to combat the adverse effects of channel correlation. In the said reference, the MIMO channel is represented by a matrix, **R**, made up of large scale correlation coefficients and known only to the transmitter. A second part of the channel that is added to **R**, is an iid matrix, $\mathbf{H}_{iid}$, which this time is known only by the receiver. The assumption is that the **R** changes slowly enough for it to be regularly fed back to the transmitter. Since $\mathbf{H}_{iid}$ is well-conditioned and easy to invert, the zero forcing criteria is used in estimating this part of

the channel while the ill-conditioned **R** is handled using maximal ratio combining, which estimates the strongest of the multiple MIMO sub-channels. Successful estimation is followed by removing the effects of the estimated channel from the rest of the MIMO channel matrix. As with the recursive ZF technique, interference is successively cancelled by estimating and removing the effects of second, third, etc of the MIMO sub-channels. The main difference lies in not re-inverting the depleted MIMO channel each time but only performing MRC combinations instead. Additionally, a BER balancing criterion (BBC) is defined, giving rise to a pre-coder weighting scheme used in controlling the transmit-end large scale correlation. The benefit of the pre-coder design is such that the channel can either operate in full MIMO mode using spatial multiplexing when channel correlation as defined by **R** is low, or when **R** is high such that the entire MIMO channel is fully correlated, the scheme can operate in SIMO mode using constellation multiplexing to maintain predefined data rates.

The improved BER performance of HZF-SIC in comparison with linear ZF and HZF-SIC without pre-coding points to the fact that ZF, if implemented in well-conditioned MIMO channels can be quite beneficial. However, apart from the tractability of using closed form expressions to handle individual channel components as done in [94], there is significant difficulty in separating dual polarised LMS MIMO channels into well-conditioned small scale fading and ill-conditioned large scale fading components. Therefore, with diagonally correlated MIMO sub-channels being reported to achieve higher capacities than independently faded channels [6], and considering the works of Sarris [70], Arapoglou [58] and the references mentioned earlier in this section, this thesis proposes the use of Dual Circular Polarisation Multiplexing (DCPM) [95] for the highly correlated LMS MIMO channels.

3.2.2 DCPM Capacity, Interference Mitigation and Channel Weighting

Even though two orthogonal circular polarisations have been used to ensure independent small-scale fading of MIMO sub-channels, their large scale fading is known to be highly correlated [3]. It is thus necessary that such characteristics alongside any equalisation schemes are included in the metrics derived for testing the viability of DCPM. Supportable channel capacity is one of such metrics that can be used as a first step to test

DCPM. The following channel capacity derivation is based on the assumption that the satellite shown in Figure 3.1 does not require any channel state information (CSI) fed back to it and the channel weights used in nulling out interference are derived from a simple receiver-based linear ZF equalisation technique. Thus, starting from the overall input output relationship for MIMO channels, we have:

$$\boldsymbol{y} = \mathbf{H}\boldsymbol{x} + \boldsymbol{n}. \tag{3.6}$$

Looking at Figure 3.1, observe that the signal vectors at the mobile terminal receive antennas are:

$$y_1 = x_1 h_{RR} + x_2 h_{LR}; \quad y_2 = x_1 h_{RL} + x_2 h_{LL}. \tag{3.7}$$

Introducing the complex weights, the output of the two combiners (labelled Σ_1 and Σ_2) is given by:

$$y = y_1' + y_2' = (y_1 w_{11} + y_2 w_{12}) + (y_1 w_{21} + y_2 w_{22}). \tag{3.8}$$

Substituting (3.7) into (3.8) results in:

$$y = (x_1 h_{RR} + x_2 h_{LR}) w_{11} + (x_1 h_{RL} + x_2 h_{LL}) w_{12} + (x_1 h_{RR} + x_2 h_{LR}) w_{21} + (x_1 h_{RL} + x_2 h_{LL}) w_{22} \tag{3.9}$$

and rearranging (3.9) gives:

$$y = (h_{RR} w_{11} + h_{RL} w_{12}) x_1 + (h_{LR} w_{11} + h_{LL} w_{12}) x_2 + (h_{RR} w_{21} + h_{RL} w_{22}) x_1 + (h_{LR} w_{21} + h_{LL} w_{22}) x_2. \tag{3.10}$$

The first two terms in equation (3.10) are the output from the top combiner in Figure 3.1. This is made up of the signals emanating from the RHCP antenna, which have been equalised by the complex weights w_{11} and w_{12}. The last two terms in (3.10) are output by the lower combiner.

3.2.3 Channel Capacity Potentials of the ZF-based DCPM

To derive the capacity metric within the ZF channel equalisation context, the method explained in [13] is adopted in performing the following:

1. Assuming that the channel matrix is correctly normalised, the coefficient of x_1 in (3.10) is equated (forced) to one while the coefficient of x_2 is forced to zero in order to obtain the capacity contribution emanating from the satellite's RHCP antenna.

$$h_{RR}w_{11} + h_{RL}w_{12} = 1;\ \ h_{LR}w_{11} + h_{LL}w_{12} = 0. \tag{3.11}$$

2. In a second separate step, the contribution from the satellite's LHCP antenna is obtained by forcing the coefficient of x_1 to zero while the coefficient of x_2 is forced to one.

$$h_{RR}w_{21} + h_{RL}w_{22} = 0;\ \ h_{LR}w_{21} + h_{LL}w_{22} = 1. \tag{3.12}$$

The resulting sets of equations of (3.11) and (3.12) are respectively solved simultaneously to obtain the ZF complex phase weights given by:

$$w_{11} = \frac{h_{LL}}{h_{RR}h_{LL} - h_{RL}h_{LR}} = \frac{h_{LL}}{\Delta H}, \tag{3.13}$$

$$w_{12} = \frac{h_{LR}}{h_{RL}h_{LR} - h_{RR}h_{LL}} = \frac{-h_{LR}}{\Delta H}, \tag{3.14}$$

$$w_{21} = \frac{h_{RL}}{h_{RL}h_{LR} - h_{RR}h_{LL}} = \frac{-h_{RL}}{\Delta H}, \tag{3.15}$$

$$w_{22} = \frac{h_{RR}}{h_{RR}h_{LL} - h_{RL}h_{LR}} = \frac{h_{RR}}{\Delta H}, \tag{3.16}$$

$$\text{where } \Delta H = h_{RR}h_{LL} - h_{RL}h_{LR}. \tag{3.17}$$

Assuming that the derived ZF complex weights do a good job at cancelling out the interfering cross-polar signals (since the antennas cannot themselves completely reject

signals of orthogonal polarisation [13]), observe in Figure 3.1 that there are two SINRs respectively defined as:

$$\text{SINR}_1 = \frac{|h_{RR}w_{11}+h_{RL}w_{12}|^2}{|h_{LR}w_{11}+h_{LL}w_{12}|^2+\sigma_{n1}^2}, \text{ and } \text{SINR}_2 = \frac{|h_{LR}w_{21}+h_{LL}w_{22}|^2}{|h_{RR}w_{21}+h_{RL}w_{22}|^2+\sigma_{n2}^2}, \quad (3.18)$$

where the noise contribution in SINR_1 and SINR_2 are respectively represented by:

$$\sigma_{n1}^2 = \frac{|h_{RR}|^2}{\text{SNR}} \text{ and } \sigma_{n2}^2 = \frac{|h_{LL}|^2}{\text{SNR}}. \quad (3.19)$$

The capacity of DCPM is then given as:

$$C_{DCPM} = \log_2(1 + \text{SINR}_1) + \log_2(1 + \text{SINR}_2). \quad (3.20)$$

The derivation of equation (3.20) then paves the way for preliminary channel capacity analysis in order to determine the conditions under which DCPM would work. For the preliminary analysis carried out in the course of this research, use was made of a simple statistical channel model, which specifically included a Rice factor component, *K*, and a depolarisation factor, *M*. The depolarisation factor allowed the author to uncover the effects of polarisation on the capacity of dual circular polarised LMS MIMO channels. Details of the simple channel model adopted can be found in chapter 10 of [13] and a circuit diagram for implementing a single branch of the Ricean LMS MIMO channel has been reproduced from [13] in Figure 3.2. The simple channel model was a necessity for the DCPM proof of concept due to the limited available data on measured dual circular polarised LMS MIMO channels. Details of this first stage analysis has been published in [95] and some of the assumptions adopted and initial results are given in the following paragraphs.

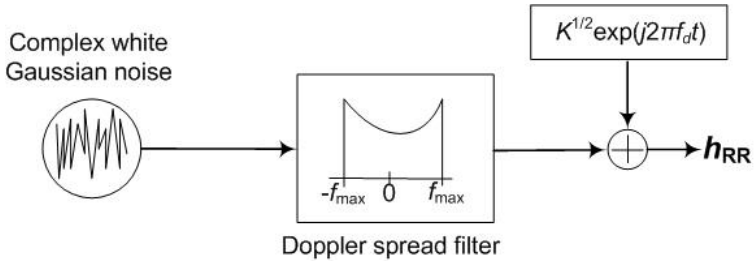

Figure 3.2: Circuit diagram for implementing a simple Rice-fading channel

The channel capacity analysis of ZF-based DCPM described in [95] is based on the assumption that a dual circular polarised LMS channel can be adequately represented by a synthetic 2×2 matrix, $\mathbf{H}_{syn}$, whose elements have unit mean values but different randomly distributed phases. The off-diagonal elements of $\mathbf{H}_{syn}$ are scaled by a factor, M, representing a combination of channel induced depolarisation (also called cross polarisation coupling) and the receive antennas inability to completely reject signals of opposite polarisation. These off-diagonal elements are regarded as interference, and are thus defined as the square root of the power that leaks from right hand circular polarisation to the left hand circular polarisation or from the left hand circular polarisation to the right hand circular polarisation. These leakages are usually assumed to be the same for both polarisations and the transceiver's duty in this case is to eliminate them using linear ZF channel equalisation. Mathematically,

$$\mathbf{H}_{syn} = \begin{bmatrix} h_{RR} & \frac{h_{RL}}{M} \\ \frac{h_{LR}}{M} & h_{LL} \end{bmatrix}. \tag{3.21}$$

Elements of $\mathbf{H}_{syn}$ in (3.21) are inserted into equations (3.13) – (3.20) in order to arrive at the appropriate capacity expression for DCPM. This setup allows for the magnitude of M to be adjusted in order to determine its effect on channel capacity. For comparing the achieved DCPM capacity with that of equal power allocation MIMO, equation (2.7) is used on a Rayleigh distributed channel data that has been appropriately scaled to render the same Frobenius norm as that of the dual polarised channel. The Frobenius norm of a channel $\mathbf{H}$ is defined in [35] as:

$$\|\mathbf{H}\|_F = \sqrt{\sum_{i=1}^{m}\sum_{j=1}^{n}\left|h_{ij}\right|^2}, \tag{3.22}$$

where m and n respectively represent the number of receive and transmit antennas. The Frobenius norms of the two channels types - $\mathbf{H}_{syn}$ and the appropriately normalised Rayleigh distributed channel–for the whole range of M are plotted in Figure 3.3.

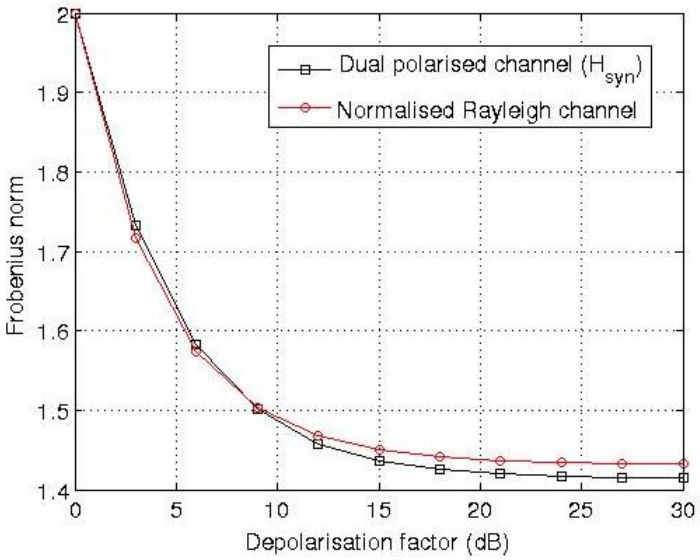

Figure 3.3: Computed Frobenius norms of synthetic dual polarised Ricean (H_{syn}) and normalised Rayleigh channels

The very close fit between the two plots indicate that the capacity of the two channels independently computed using the DCPM capacity as expressed in equation (3.20) and the equal power allocation MIMO capacity of (2.7) can be directly compared. Examples of such comparisons are given in Figures 3.4(a) to (d), which at Rice factor values of 6dB, 10dB, 15dB and 100dB show the influence of SNR on MIMO and DCPM capacities when *M* is kept at 10dB. In the figures, the equal power allocation MIMO capacity of the normalised Rayleigh channel is labelled as "MIMO Rayleigh" while the single-input single-output capacities for equivalent Ricean and Rayleigh channels are labelled as "SISO Rice" and "SISO Rayleigh" respectively; these were only included for benchmarking purposes. As reported in [6],[29], the diagonally correlated Ricean dual polarised LMS channel (MIMO Rice) achieves a slightly higher capacity than its Rayleigh counterpart at SNR values above 0dB. This implies that the channel model produces accurate capacity statistics and can be used with confidence to analyse the potentials of DCPM. Therefore, Figures 3.4(a) to (d) show that at a fixed *M* value of 10dB and with increasing Rice factor, DCPM capacity, labelled "DCPM Rice" steadily increases, approaching that of conventional MIMO. Since *M* is fixed, the observed improvement in DCPM capacity is solely due to the increasing efficiency of the receiver based channel weighting. Note specifically in Figures 3.4(a) and (b) that the DCPM capacity curves begin to widen away from that of MIMO at SNRs above 20dB. This phenomenon highlights the fact that SNR needs to be low for DCPM and MIMO to

achieve comparable capacity and low SNRs are typical of LMS systems. Figure 3.4(c) was included because 15dB is the average Rice factor value that was recorded in the dual circular polarised LMS channel measurements of chapter 4. Lastly and on the other end of the scale, Figure 3.5(d) shows an extremely high Rice factor of 100dB and as can be observed, DCPM capacity is almost equal to that of MIMO for the full SNR range.

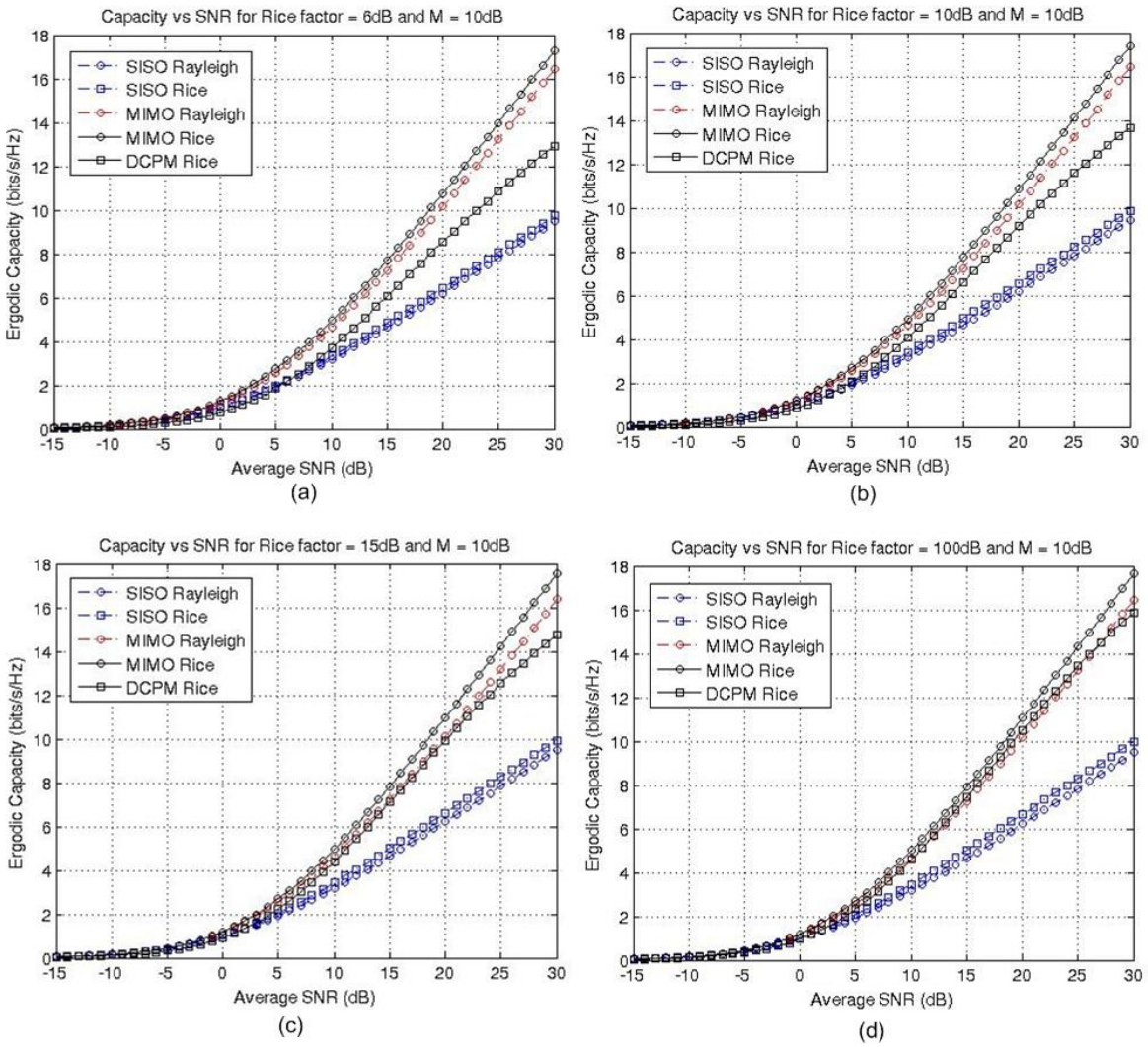

Figure 3.4: DCPM and MIMO capacities versus SNR for M = 10 dB at (a) Rice factor of 6dB, (b) Rice factor of 10dB, (c) Rice factor of 15dB and (d) Rice factor of 100dB

Figures 3.5(a) to (d) show the influence of the depolarisation factor, M, at Rice factor values of 6dB, 10dB, 15dB and 100dB. Observe that DCPM capacity becomes equal to that of conventional MIMO when M approaches 20dB and at very high channel Rice factor values (100dB). However, at a minimum M value of 10dB, which can be achieved

by most commercial grade antennas, and with high enough Rice factors (a minimum of around 6dB or a typical value of 15dB), DCPM gets to within 1bit/s/Hz the capacity of MIMO. This represents a very significant result because DCPM relies only on receiver based processing to achieve the capacity increase while conventional MIMO relies on both transmitter and receiver based processing. Since *M* has a joint channel and antenna dependence and the depolarisation effects of the channel cannot be controlled, much emphasis should be placed on designing antennas that possess very high polarisation purity. However, antenna design and testing is beyond the scope of this thesis and interested readers are referred to [96] and [97], which chronicle some of the recent attempts at designing antennas that may be suitable for the proposed DCPM scheme.

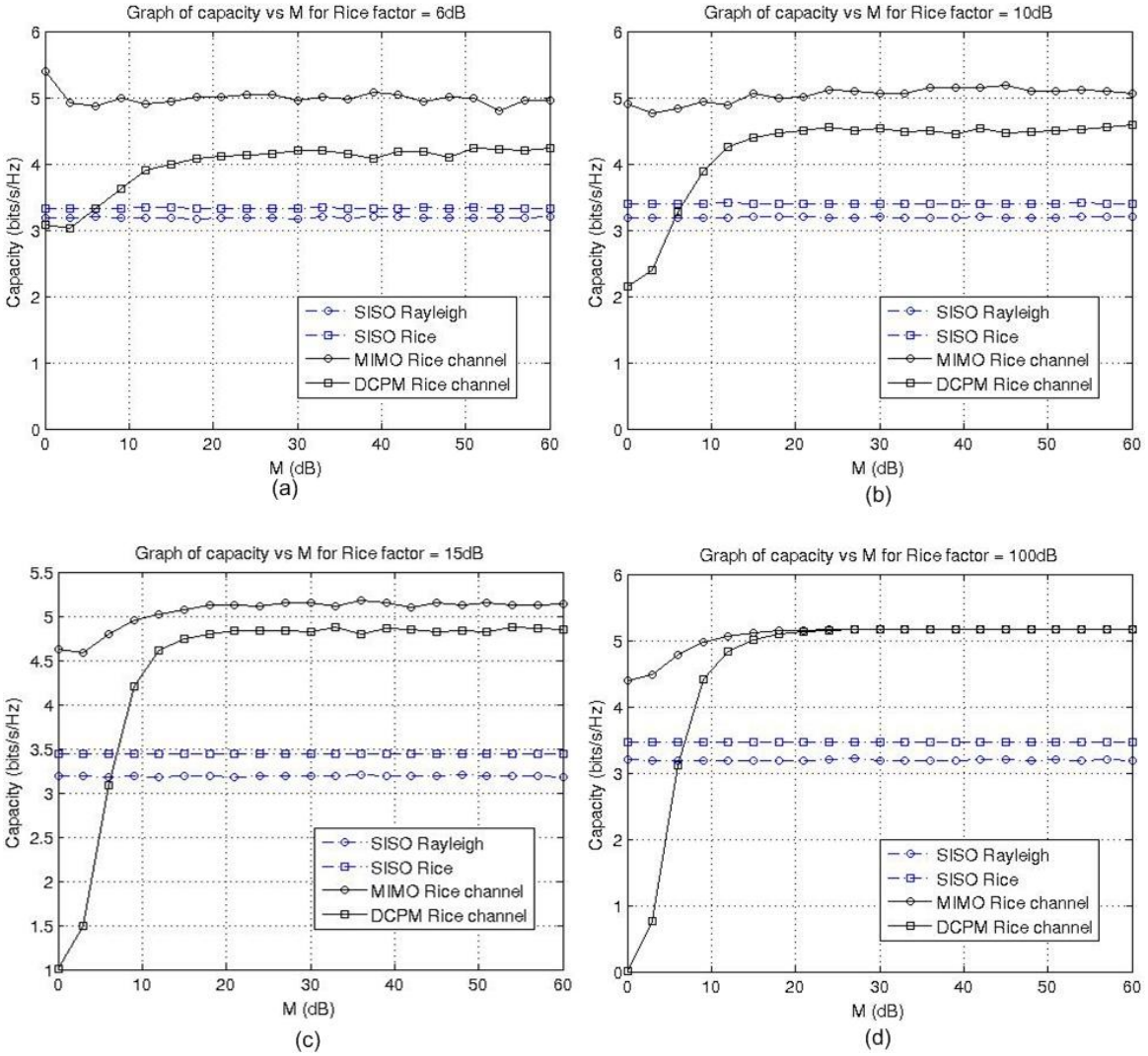

Figure 3.5: DCPM and MIMO capacities versus *M* for SNR = 10dB at (a) Rice factor of 6dB, (b) Rice factor of 10dB, (c) Rice factor of 15dB and (d) Rice factor of 100dB

The above results point to the fact that when polarisation rejection is good, which usually occurs in dual polarised systems operating under LOS conditions, DCPM can approach the capacities achievable using conventional equal power allocation MIMO. However, as can be observed in Figure 3.5(c), it is vital for the appropriate polarisation purity threshold to be set for DCPM implementation; else DCPM capacity can even become worse than that of SISO. Finally, Figure 3.4(c) indicates that even when the LMS channel is highly Ricean and with good polarisation purity, DCPM only achieves comparable capacity to MIMO at low SNR values.

Therefore, following the presented low SNR based DCPM capacity results of the synthetic channel simulations, the next section uses a more detailed channel model to validate the effects of channel Rice factor and the combined effects of antenna cross polar discrimination (XPD) and channel cross polar coupling (XPC) on the capacities of DCPM and that of equal power allocation MIMO. On successfully validating the DCPM capacity characteristics, it then becomes imperative to test its bit error rate performance when using the recommended linear ZF equalisation scheme, which is the simplest of the popular channel equalisation techniques, and compare the results with bit error rates of more complex equalisation schemes such as MMSE and MLSE.

3.2.4 Dual Circular Polarisation Multiplexing versus Equal Power Allocation MIMO: Additional Capacity Simulations

Having found out in the previous section that DCPM can only deliver comparable capacities to equal power allocation MIMO when the channel has good polarisation purity – represented by an XPD of at least 10dB, this section explores the specific effects of XPC, XPD, channel Rice factor and SNR on deliverable capacity. The following analysis uses a more detailed channel model that explicitly defines antenna XPD, channel XPC and the Rice factor terms. The model is based on Oestges's [98] multi-linear polarised channel model, which is given by:

$$\mathbf{H} = \begin{bmatrix} h_{RR} & h_{RL} \\ h_{LR} & h_{LL} \end{bmatrix}, \tag{3.23}$$

where the two co-polar components, h_{RR} and h_{LL}, are Gaussian distributed, having values less than or equal to 1. h_{LL} is a phase-shifted and attenuated version of h_{RR}, given as:

$$h_{LL} = h_{RR}\mu\exp(-j\theta). \tag{3.24}$$

In (3.24), μ accounts for the difference in the amplitude of the RHCP and LHCP channel coefficients and θ is a zero mean random variable. Similarly, the cross-polar components are defined as:

$$h_{RL} = h_{RR}\chi\exp(-j\phi) \text{ and } h_{LR} = h_{LL}\chi\exp(-j\phi). \tag{3.25}$$

with χ accounting for the imbalance between the co-polar and cross-polar terms and ϕ being independently and uniformly distributed over [0 2π]. This imbalance directly results from the channel's XPC ratio and the antennas XPD values. A close look reveals that the models of equations (3.21) and (3.23) are basically the same; the only difference is that in the former, an additional channel attenuation factor is externally applied by way of straight-forward division to represent the different states of channel XPC and antenna XPD. The earlier used depolarisation factor, *M*, is related to χ as follows:

$$M = \frac{1}{\sqrt{\chi}}. \tag{3.26}$$

Note that *M* in (3.26) above is in linear form, not in decibels (dB). A more formal approach following the method of [99] is to decompose the channel two parts as follows:

$$\mathbf{H} = \begin{bmatrix} 1 & \sqrt{\chi} \\ \sqrt{\chi} & 1 \end{bmatrix} \odot \bar{\mathbf{H}}, \tag{3.27}$$

where ($0 < \chi < 1$) account for the XPD and XPC effects while $\bar{\mathbf{H}}$ represents the Ricean correlated channel components whose amplitudes are defined by μ in (3.24) and $\odot$ indicates Hadamard (element-wise) multiplication. Including a Rice factor component in (3.27) following the Sellathurai model [21] and adding on a second matrix that only contains diffuse multipath components gives:

$$\mathbf{H} = \begin{bmatrix} 1 & \sqrt{\chi} \\ \sqrt{\chi} & 1 \end{bmatrix} \odot \left(\sqrt{\frac{K}{K+1}}\bar{\mathbf{H}} \right) + \sqrt{\frac{1}{1+K}}\tilde{\mathbf{H}}, \tag{3.28}$$

where K is the Rice factor in linear scale and $\tilde{\mathbf{H}}$ is the matrix of diffuse multipath components whose elements are zero mean, circularly symmetric and have different randomly distributed phases. Equation (3.28) represents the building blocks for the new/updated model, which will be explained in greater detail in chapter 5.

To determine the effect of χ on the ergodic channel capacity, (3.28) was coded in MATLAB and 10^4 channel instances (coefficients of **H**) produced. Equations (2.7) and (3.20) were then used in respectively computing the DCPM and equal power allocation MIMO ergodic channel capacities. The result of this is shown in Figure 3.6 where SISO capacities have again been included for comparison and benchmarking.

Observe in Figure 3.6(a) that DCPM capacity decreases with increasing χ. At $\chi = 0.22$, the capacity of DCPM reduces to that of a SISO channel and it is no longer advantageous to implement DCPM in such channels. The important point in the capacity versus χ curves of Figure 3.6(a) is that at an SNR as low as 10dB and a Rice factor of 10dB, DCPM achieves a capacity of 5.2bits/s/Hz, which is equal to the capacity of equal power allocation MIMO. This is possible only when χ approaches 0. Exactly how small χ needs to be in order for DCPM to achieve MIMO capacity has already been given using its equivalent M value in Figure 3.5(c). In the said figure it is shown that at an M of about 20dB (equivalent to a χ of 0.01), DCPM capacity becomes equal to that of MIMO but at a very high Rice factor of 100dB.

Since the value of χ has been tentatively chosen to be 0.01 for good DCPM capacity, the next task is to determine the range of Rice factors for which DCPM capacity is comparable to that of MIMO. The result of this is shown in Figure 3.69(b) where it can be observed that DCPM capacity comes within 0.4bits/s/Hz of MIMO capacity at a Rice factor of 20dB and at a low SNR of 10dB. As the Rice factor increases beyond 50dB, MIMO and DCPM capacity become indistinguishable. Note that 10dB SNR and 20dB Rice factor values have been used as capacity comparison reference points because these Rice factor values can be easily achieved by typical LMS broadcast systems. Also note in Figure 3.69(b) that even though the Rice factor region between 0dB and 10dB shows a very large MIMO capacity compared with DCPM, this type of channel may be practically

impossible to achieve since high polarisation purity of dual polarised channels in reality only correspond to LOS propagation, with the attendant high Rice factor values.

In concluding the MIMO and DCPM capacity comparison, Figure 3.6(c) shows the ergodic capacity versus average SNR curves for DCPM (implemented with the recommended zero forcing complex weights), DCPM (implemented without the ZF weights, only relying on orthogonal polarisations), equivalent Ricean channel MIMO and SISO capacities. With χ set at 0.01 and a Rice factor of 10dB, it can be observed that DCPM with the channel weights always comes within 1.4bits/s/Hz of MIMO capacity for SNR values less than 10dB. Beyond this SNR, DCPM capacity starts falling further and further behind that of MIMO. The effect of increasing the Rice factor while keeping the SNR fixed is to improve DCPM capacity, thereby allowing it to become equivalent to that of MIMO as can be seen in Figure 3.4(c). At 20dB SNR, Figure 3.6(c) shows that ZF equalisation gives DCPM a 2.5bits/s/Hz advantage over DCPM when implemented without ZF weighting. This implies correct receiver based channel weighting is perhaps the most important aspect of DCPM as even in spite of using orthogonal circular polarisations, DCPM would never achieve acceptable channel capacity – observe that DCPM without channel weighting gives less capacity than SISO at 20dB SNR.

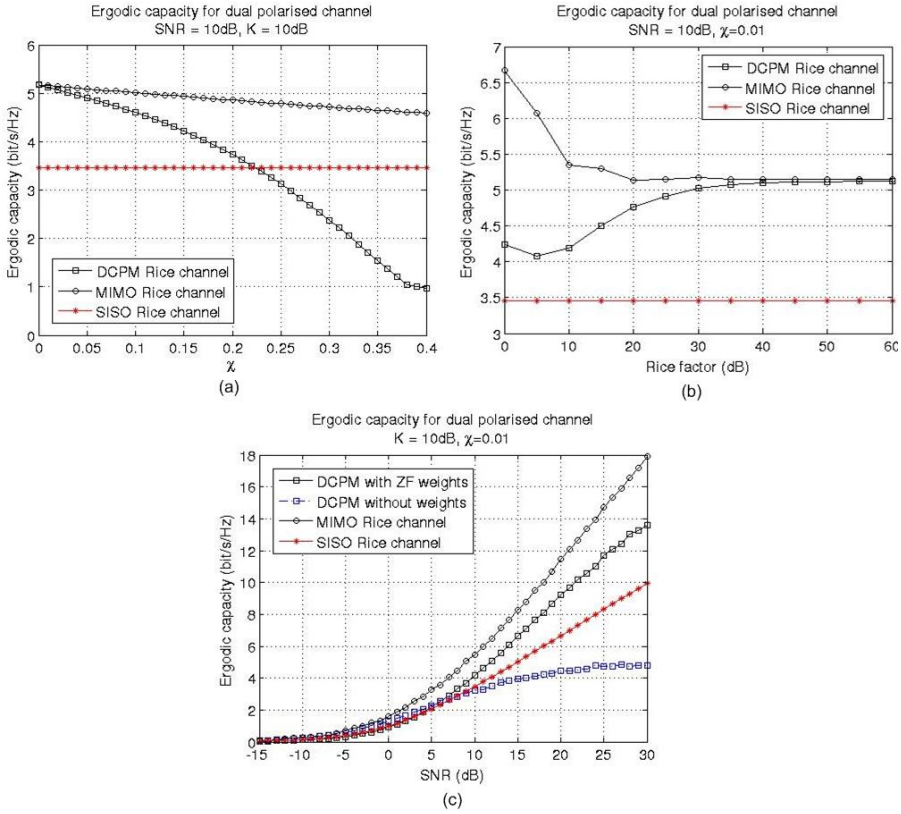

Figure 3.6: DCPM and equal power allocation MIMO ergodic capacities versus (a) χ, which is an XPD-XPC factor, (b) Rice factor and (c) SNR

The fact that Figure 3.6(c) essentially follows the same pattern as the capacity versus SNR curves of Figure 3.4 is enough prove that the effects of Rice factor, XPD and XPC on DCPM and MIMO capacity has been validated since the two sets of results have been obtained using two different channel models. It is important to point out that in the results of Figures 3.4 to 3.6, only the capacity advantage of using ZF channel equalisation scheme was considered. It has been assumed that similar capacities would be achieved if other more complex (and perhaps better) channel equalisation schemes such as MMSE or MLSE are considered. However, this would entail a very tedious process that is beyond the scope of this research. A more feasible way to determine the effects of the other equalisation schemes and if the choice of ZF over them is justified is through bit error rate analysis. Therefore the next section alters the parameters of the channel model of (3.28) to represent three channel fading states that are broadly defined as LOS, OLOS and NLOS/Rayleigh, and uses these to determine the comparative BER advantage of the using any of the three equalisation schemes.

3.2.5 BER Characteristics of the Dual Orthogonal Circular Polarised Channel: Numeric Examples and Simulations

In order to provide a better understanding of the effects of orthogonal circular polarisation on the transceiver scheme chosen for DCPM, three channel types with parameters given in Table 3-1 have developed based on the model of (3.28) for bit error rate analysis. For each channel type a random sample from the 10^4 generated by a MATLAB implementation of the channel model is chosen for numeric analysis. In each of these cases, ZF and MMSE channel weights are obtained using equations (3.2) and (3.4), while MLSE decoding employs exhaustive search to determine the most likely transmitted symbols.

Table 3-1: Table showing Rice factor and the XPC-XPD factor different channel types

Channel type	**Average co-polar Rice factor (*K*)**	**Average XPC-XPD factor (χ)**
LOS	10 dB	0.02
OLOS	6 dB	0.01
NLOS/Rayleigh	-4 dB	1.0

3.2.5.1 LOS Channel

The channel type chosen for this example is when polarisation purity is high and this corresponds to situations where χ in (3.27) approaches zero. The dual circular polarised MIMO channel rendered in this case is shown in Figure 3.7 and is given as:

$$\mathbf{H} = \begin{bmatrix} 1.0777 - j0.0553 & 0.3935 - j0.0939 \\ 0.4666 - j0.0276 & 0.8674 - j0.1029 \end{bmatrix}. \tag{3.29}$$

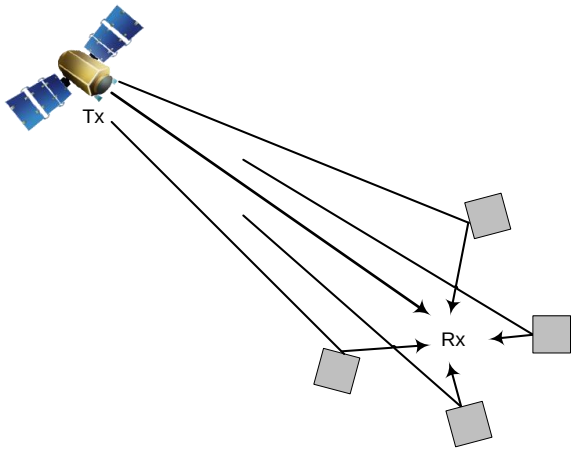

Figure 3.7: Illustration of a LOS LMS channel

The matrix of (3.29) contains relatively low values of the off-diagonal elements (h_{RL} and h_{LR}), which are at least 7dB below the elements in the main diagonal (h_{RR} and h_{LL}). To induce channel fading, the channel matrix is multiplied by independently transmitted data streams from each of the two circular polarised antennas. Using an example with QPSK modulated signals of 0+*j*1 transmitted from the RHCP antenna and 1+*j*0 transmitted from the LHCP antenna, and employing the nomenclature of (3.6), the effect of the channel on the transmitted bits is given by $\mathbf{y}_{dual\ pol} = \mathbf{H}\boldsymbol{x} + \boldsymbol{n}$, which is:

$$\mathbf{y}_{dual\ pol} = \begin{bmatrix} 1.0777 - j0.0553 & 0.3935 - j0.0939 \\ 0.4666 - j0.0276 & 0.8674 - j0.1029 \end{bmatrix} \begin{bmatrix} -0.7071 + j0.7071 \\ 0.7071 - j0.7071 \end{bmatrix} + \begin{bmatrix} -0.0843 - j0.0534 \\ 0.2537 - j0.4119 \end{bmatrix}. \quad (3.30)$$

In equation (3.30), the energies of the transmitted bits ($\boldsymbol{x}$) have been normalised to 1, hence 0+*j*1 = –0.7071+*j*0.7071 while 1–*j*0 = 0.7071–*j*0.7071. The noise ($\boldsymbol{n}$) is composed of complex valued pseudorandom numbers drawn from a standard normal distribution and is appropriately scaled to obtain a nominal energy per bit over noise ratio (E_b/N_0) of 5dB. Note that E_b/N_0 is a normalised version of the SNR and it is a more appropriate metric for characterising the performance of digital systems. This is because each bit is transmitted with a certain amount of power and multiplying the bit's power by its duration (time) gives the energy carried by that particular bit. The noise power spectral density is equal to its power divided by the bandwidth. Chapter 3 of [100] provides more details on why E_b/N_0 is preferable to SNR for BER analysis.

For ZF equalisation whose aim is to completely eliminate interference, **H** is inverted using the Moore-Penrose pseudo-inversion method [35] of (3.2), giving the channel weights as:

$$\mathbf{W}_{ZF} = \begin{bmatrix} 1.1487 - j0.0096 & -0.4947 - j0.1877 \\ -0.6134 - j0.0413 & 1.3970 + j0.2508 \end{bmatrix}. \quad (3.31)$$

While for MMSE equalisation the target is to simultaneously minimise the errors due to both interference and noise. Thus the matrix to be inverted is given by (3.4), which produces the following channel weights:

$$\mathbf{W}_{MM} = \begin{bmatrix} 0.5518 - j0.0121 & 0.0030 - j0.0373 \\ -0.0433 - j0.0341 & 0.5561 + j0.0861 \end{bmatrix}. \tag{3.32}$$

The channel is then equalised by multiplying the received signal with the weights, and the signal presumed to be received via ZF and MMSE are respectively given by

$$\mathbf{y}_{eq\_ZF} = \mathbf{W}_{ZF}\mathbf{y}_{dual\ pol} = \begin{bmatrix} -0.8000 + j0.5953 \\ 1.0073 - j0.9756 \end{bmatrix} \tag{3.33}$$

$$\text{and } \mathbf{y}_{eq\_MM} = \mathbf{W}_{MM}\mathbf{y}_{dual\ pol} = \begin{bmatrix} -0.2440 + j0.1574 \\ 0.3157 - j0.3250 \end{bmatrix}. \tag{3.34}$$

In the case of MLSE, an exhaustive search is performed over the entire constellation of the received QPSK signal according to (3.5) in order to determine which symbol was most likely transmitted. The MLSE algorithm implemented for this particular scenario correctly decodes the received signal as:

$$\mathbf{y}_{eq\_ML} = \begin{bmatrix} -0.7071 + j0.7071 \\ 0.7071 - j0.7071 \end{bmatrix}. \tag{3.35}$$

To check the errors of the equalisation schemes, the transmitted symbols are subtracted from the decoded symbols, giving:

$$\mathbf{y}_{ZF} = \left\|\mathbf{y}_{eq\_ZF} - \boldsymbol{x}\right\|^2 = \begin{bmatrix} 0.0211 \\ 0.1622 \end{bmatrix}, \tag{3.36}$$

$$\mathbf{y}_{MM} = \left\|\mathbf{y}_{eq\_MM} - \boldsymbol{x}\right\|^2 = \begin{bmatrix} 0.5167 \\ 0.2992 \end{bmatrix}, \tag{3.37}$$

$$\text{and } \mathbf{y}_{ML} = \left\|\mathbf{y}_{eq\_ML} - \boldsymbol{x}\right\|^2 = \begin{bmatrix} 0 \\ 0 \end{bmatrix}. \tag{3.38}$$

Observe in (3.36 – 3.38) that the error due to ZF is slightly better than the supposedly superior MMSE. MLSE in this case does not produce any errors. However, the computation burden for full search MLSE is very high and this limits its practical application in many cases.

3.2.5.2 OLOS Channel

The channel realisation chosen for this example is when antenna XPD is high. This corresponds to situations where χ approaches 0 and the channel as rendered by the model of (3.27) is illustrated in Figure 3.8 whiles its channel matrix is given as:

$$\mathbf{H} = \begin{bmatrix} 0.8383 + j0.1020 & 0.1455 + j0.0632 \\ 0.3554 - j0.0426 & 0.8683 + j0.1223 \end{bmatrix}. \tag{3.39}$$

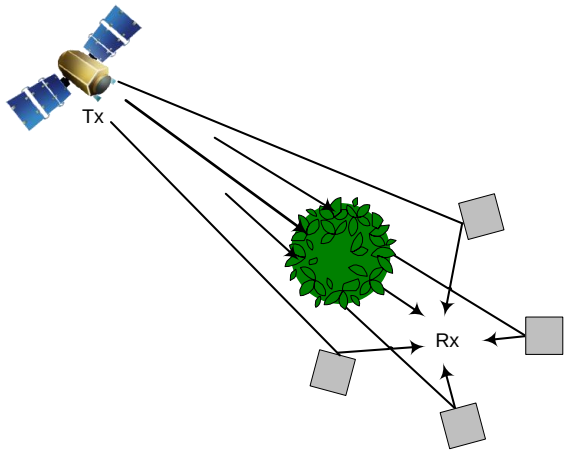

Figure 3.8: Illustration of an OLOS LMS channel

As with (3.29) the matrix of (3.39) contains very low values of the off-diagonal elements (h_{RL} and h_{LR}) relative to the main diagonal elements (h_{RR} and h_{LL}). In this particular case, the difference between h_{RR} and h_{RL} is about 15dB while the difference between h_{RL} and h_{LR} is about 8dB. To induce channel fading, the channel matrix is multiplied by independently transmitted data streams from each of the two circular polarised antennas. Using an example with QPSK modulated signals of $1+j1$ transmitted from the RHCP antenna and $1+j0$ transmitted from the LHCP antenna, and employing the nomenclature of (3.6), the effect of the channel on the transmitted bits is given by

$$\mathbf{y}_{dual\ pol} = \begin{bmatrix} 0.8383 + j0.1020 & 0.1455 + j0.0632 \\ 0.3554 - j0.0426 & 0.8683 + j0.1223 \end{bmatrix} \begin{bmatrix} 0.7071 + j0.7071 \\ 0.7071 - j0.7071 \end{bmatrix} + \begin{bmatrix} -0.2509 - j0.2079 \\ 0.3961 - j0.4380 \end{bmatrix}. \tag{3.40}$$

The energy in the transmitted bits have been normalised to 1 while the noise is composed of complex valued pseudorandom numbers drawn from a standard normal distribution and is appropriately scaled to obtain a nominal E_b/N_0 of 5dB.

The Moore-Penrose pseudo-inversion of **H** gives the ZF weights as:

$$\mathbf{W}_{ZF} = \begin{bmatrix} 1.2734 - j0.1519 & -0.2294 - j0.0348 \\ -0.4865 + j0.1932 & 1.2235 - j0.1694 \end{bmatrix}. \tag{3.41}$$

While for MMSE the weights are given by

$$\mathbf{W}_{MM} = \begin{bmatrix} 0.5918 - j0.0713 & 0.0618 + j0.0056 \\ -0.0712 + j0.0265 & 0.5895 - j0.0823 \end{bmatrix}. \tag{3.42}$$

The channel is then equalised and the signal presumed to be received via ZF and MMSE are respectively given by

$$\boldsymbol{y}_{eq\_ZF} = \mathbf{W}_{ZF}\mathbf{y}_{dual\ pol} = \begin{bmatrix} 0.0428 + j0.3601 \\ 1.0727 - j1.0503 \end{bmatrix} \tag{3.43}$$

$$\text{and } \mathbf{y}_{eq\_MM} = \mathbf{W}_{MM}\mathbf{y}_{dual\ pol} = \begin{bmatrix} 0.2180 + j0.0807 \\ 0.5673 - j0.4855 \end{bmatrix}. \tag{3.44}$$

MLSE performs an exhaustive search over the entire constellation of the received QPSK signal and correctly decodes the received signal as:

$$\mathbf{y}_{eq\_ML} = \begin{bmatrix} 0.7071 + j0.7071 \\ 0.7071 - j0.7071 \end{bmatrix}. \tag{3.45}$$

To check the errors of the equalisation schemes, the transmitted symbols are subtracted from the decoded symbols, giving:

$$\mathbf{y}_{ZF} = \left\|\mathbf{y}_{eq\_ZF} - \boldsymbol{x}\right\|^2 = \begin{bmatrix} 0.5617 \\ 0.2515 \end{bmatrix}, \tag{3.46}$$

$$\mathbf{y}_{MM} = \left\|\mathbf{y}_{eq\_MM} - \boldsymbol{x}\right\|^2 = \begin{bmatrix} 0.6316 \\ 0.0686 \end{bmatrix}, \tag{3.47}$$

$$\text{and } \mathbf{y}_{ML} = \left\|\mathbf{y}_{eq\_ML} - \boldsymbol{x}\right\|^2 = \begin{bmatrix} 0 \\ 0 \end{bmatrix}. \tag{3.48}$$

Observe in (3.46 – 3.48) that the errors due to MMSE in the RHCP channel (the top right hand side of (3.47)) is greater that due to ZF for the same channel (the top right hand side of (3.46)). Recall that the difference between the co- and cross-polar components of the RHCP channel was about 15dB. The result indicates that instances of high polarisation purity, ZF can prove to be better than MMSE. However, for the LHCP channel where the difference between its co-and cross-polar components was measured at 8dB, the error due to MMSE is less than that due to ZF. Finally and in line with expectation, MLSE gives an errorless performance. When the results of the LOS and OLOS channels are taken together, it can be concluded that during periods of good polarisation purity, ZF is more likely to outperform MMSE. Whether this scenario repeats itself in significant durations in real dual circular polarised LMS MIMO channel will be determined from the analysis of measured channel data.

3.2.5.3 NLOS/Rayleigh Channel

In this case the channel tends towards being Rayleigh, is illustrated in Figure 3.9 and represented by the matrix of (3.49). The procedure used in the two previous sections for the LOS and OLOS channels is employed to determine the following errors:

$$\mathbf{H} = \begin{bmatrix} -0.0354 - j0.1051 & 0.0331 - j0.0639 \\ 0.0058 + j0.0852 & -0.0299 - j0.0276 \end{bmatrix}, \tag{3.49}$$

$$\mathbf{y}_{ZF} = \left\|\mathbf{y}_{eq\_ZF} - \boldsymbol{x}\right\|^2 = \begin{bmatrix} 3.1147 \\ 36.8305 \end{bmatrix}, \tag{3.50}$$

$$\mathbf{y}_{MM} = \left\|\mathbf{y}_{eq\_MM} - \boldsymbol{x}\right\|^2 = \begin{bmatrix} 0.9904 \\ 0.9311 \end{bmatrix}, \tag{3.51}$$

and $$\mathbf{y}_{ML} = \left\|\mathbf{y}_{eq\_ML} - \boldsymbol{x}\right\|^2 = \begin{bmatrix} 2.0 \\ 0 \end{bmatrix}. \tag{3.52}$$

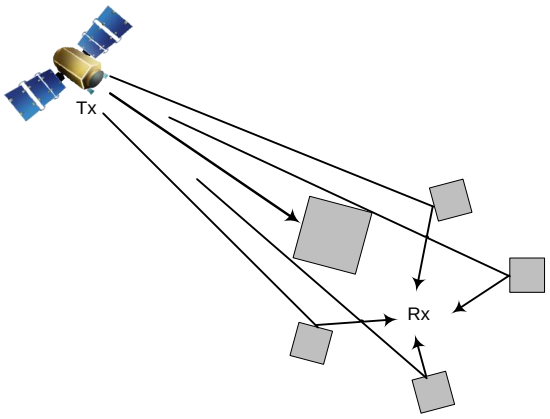

Figure 3.9: Illustration of NLOS/Rayleigh LMS channel

This particular channel shows that MLSE (3.52) is after all not infallible as it has incorrectly decoded the sign of the QPSK symbol transmitted from the RHCP antenna, which gives rise to the huge error of 2.0. There are also random but significant errors by the MMSE decoder while zero forcing gives the worst performance as shown in (3.50) and (3.51) respectively.

3.2.6 Monte Carlo simulations using variable E_b/N_0 on different channel types

Finally, to gain broader insight into the performance of the three equalisation schemes of ZF, MMSE and MLSE, Monte Carlo simulations with 10^4 channel realisations were performed and the E_b/N_0 varied from -15 to 25dB for the three dual polarised channel types described in the previous section. A case where no equalisation is performed has also been included for bench marking purposes. In all four cases, the bit streams are uncoded and hard decision decoding is employed at the receiver. A 'maximum likelihood' algorithm is used for decoding where for example, if the QPSK symbol 0+*j*0 were to be decoded, the logic used for determining the boundary conditions is coded in MATLAB as follows:

```
for ii = 1: number of channel samples
     for row = 1:2
          if    real(Yeq_zf(row,1,ii))    <    0    &&
          imag(Yeq_zf(row,1,ii)) < 0;
```

```
            zf_decode(row,1,ii) = - 0.7071- j0.7071;
        end
    end
```

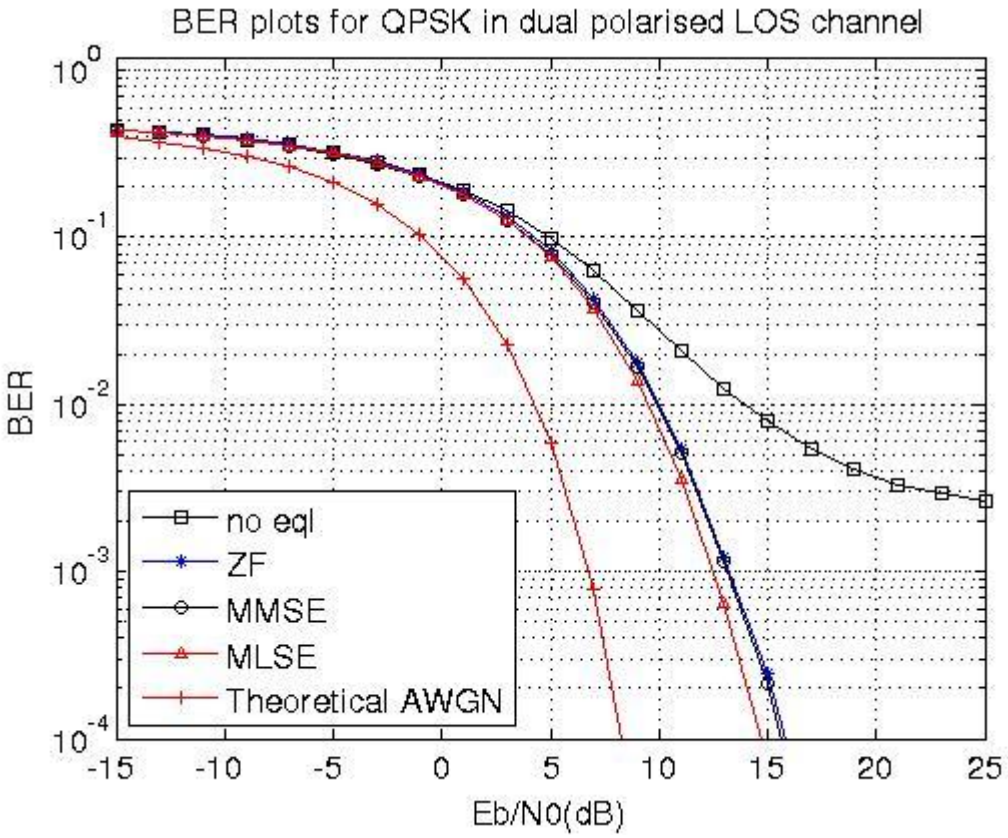

Figure 3.10 BER curves for QPSK modulation in a simulated dual circular polarised LOS channel

For the simulations carried out in this chapter, the effects of variable channel correlation and successive interference cancellation using recursive designs have not been explored and are left for chapter 6. The results are shown in Figures 3.10 – 3.12, where the BER of a theoretical additive white Gaussian noise (AWGN) channel are also included for benchmarking. According to [8],[100], the theoretical BER of QPSK modulation in an AWGN channel is the same as that of BPSK and can be computed using $Q\left(\sqrt{2E_b/N_0}\right)$.

It can be observed in Figure 3.10 that for the dual circular polarised LOS channel the BER due to orthogonal circular polarisations (no eql) alone equals that of MMSE and MLSE for Eb/N_0 values below 3dB. The difference between the BER of ZF and MMSE is marginal for all E_b/N_0 values and these two compare favourably with the computationally

more complex MLSE. The results indicate that it is not necessary to bother with the complexities of equalisation in such channels since exploiting polarisation orthogonality alone can be enough to achieve the desired BER rates when SNR or E_b/N_0 is low. Note that the convergence of all the BER curves at low E_b/N_0 values to the theoretical maximum value of 0.5 for QPSK modulation (see chapter 3, pp 219-220 of [100]) indicates the accuracy of the simulations.

As the channel deteriorates and become obstructed by vegetative matter, we get into the OLOS channel. The BER curves for the dual circular polarised OLOS channel using the three equalisation schemes and no equalisation is shown in Figure 3.11. It is interesting to observe that the error rates in this channel are not very different from the LOS scenario. The only difference is the slight degradation of the BER for all three equalisation schemes. MLSE consistently gives the best results while MMSE and ZF follow very closely behind.

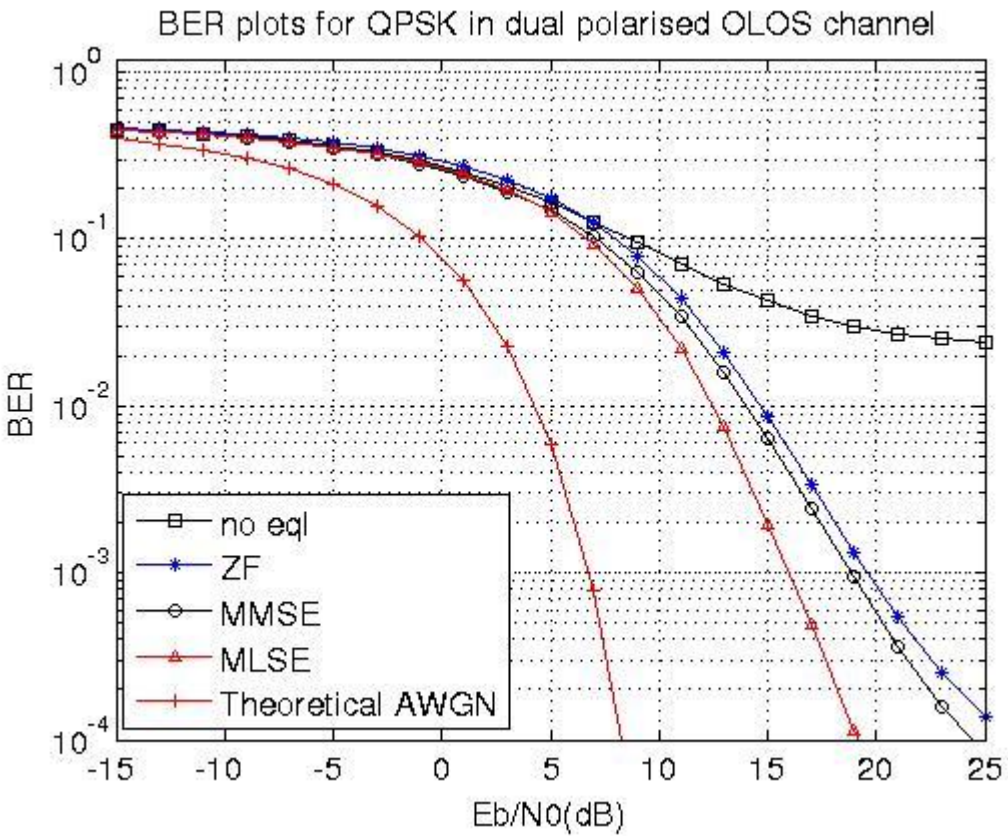

Figure 3.11: BER curves for QPSK modulation in a simulated dual circular polarised OLOS channel

In Figure 3.12 where the same equalisation schemes have been implemented on an NLOS/Rayleigh channel, and it can be observed that when no equalisation is used, the probability of decoding a bit in error is only slightly lower than the worst case value of 0.5 at an E_b/N_0 of 25dB. MLSE is only better than MMSE for E_b/N_0 values above 17dB while ZF is about 3dB worse than MMSE.

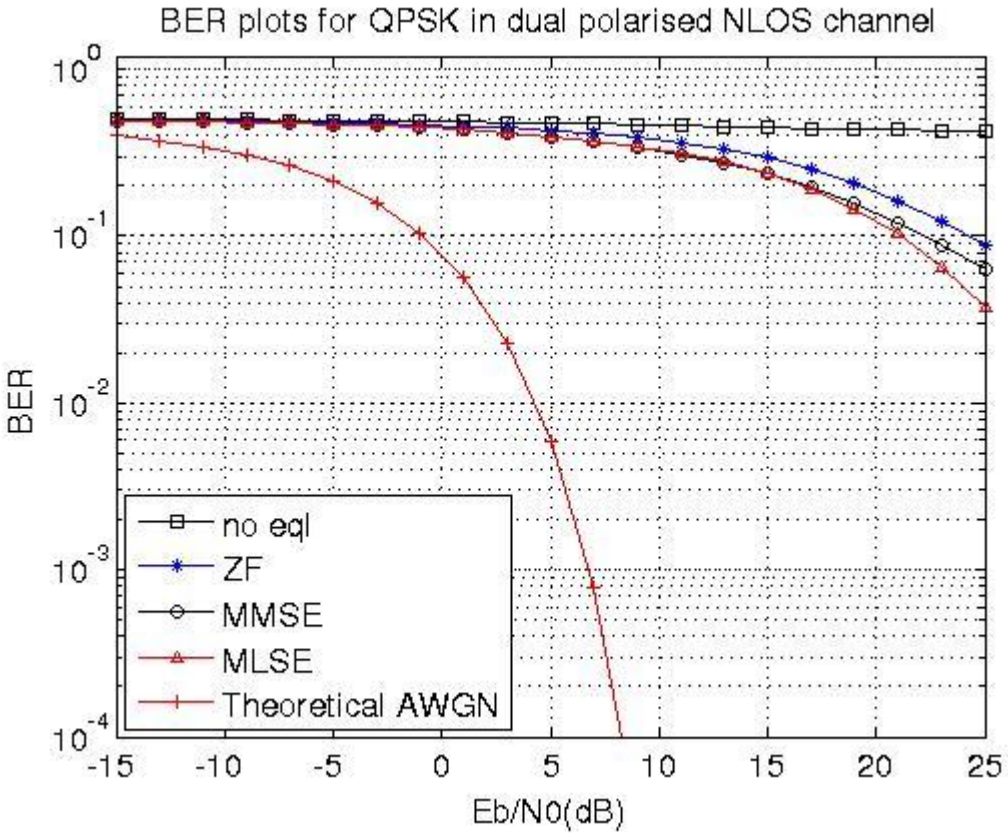

Figure 3.12: BER curves for QPSK modulation in a simulated dual circular polarised Rayleigh/NLOS channel

The marginal BER improvement of the highly complex MLSE over MMSE and ZF, and most especially 'no equalisation' in the low E_b/N_0 region of the dual circular polarised LOS channel makes a good case for simple transceiver schemes like DCPM to be adopted for such channels. If and when equalisation is to be adopted, the fourth order complexity of MMSE [101] can be prohibitive given that it is just marginally better than the much simpler ZF. For MLSE equalisation, its complexity increases exponentially with the constellation size, making it impractical for constellation sizes larger than QPSK. Even though there exists exact MLSE algorithms that do not perform exhaustive searches (like

the Kannan algorithm [102], the KZ algorithm [103] and the sphere decoding algorithm [104],[105]), their complexity is still very high and implementing them for comparison with ZF is beyond the scope of this thesis.

From the foregoing, the choice then to adopt the simpler ZF based DCPM is even more compelling when the BER results are view vis-à-vis the improved capacity results brought about by polarisation multiplexing (as shown in Figures 3.4 and 3.6).

3.3 Conclusions

In this chapter, the three main transceiver building blocks of ZF, MMSE and MLSE equalisation have been presented in order to understand how they are applied in the receive-only linear equalisation mode to mitigate the effects of interference and noise in the dual circular polarised LMS MIMO and Rayleigh channels. Also discussed was how the equalisation schemes can be applied in recursive designs to improve their performance.

Due to the lack of channel metrics to properly characterise polarisation-MIMO schemes, a new metric based on ZF channel equalisation has been formulated to compute the capacity derivable from dual circular polarisation multiplexing (DCPM). Ideas behind DCPM have been published in a conference paper titled "Unleashing the Polarisation Domain for Land Mobile Satellite MIMO Systems [95]", where initial results on achievable capacity were presented and repeated here, though in a slightly different formulation.

Using an adapted version of the dual polarised terrestrial channel model, the BER of the dual polarised LMS channel under LOS, OLOS and NLOS/Rayleigh fading conditions have been analysed by way of numerical comparisons and Monte Carlo simulations. Among the characteristics found to greatly influence the practical application of DCPM are the channel XPC and antenna XPD, the channel Rice factor and the received SNR.

Finally, since there are inherent limitations to the modelled channel data used in the initial DCPM capacity analysis, there is need for an extensive measurement campaign to make available more realistic channel data. One of such aspects which the channel model

completely ignored is the time evolution of the received signal powers of the dual polarised channels and their corresponding co- and cross-polar cross-correlation coefficients. Hence, the next chapter will describe the measurement campaigns that have been performed to obtain, understand and subsequently model the missing parameters.

Chapter 4

4 Measuring the Dual Circular Polarised LMS MIMO Channel

The best way to understand the dual polarised land mobile satellite (LMS) multiple-input multiple-output (MIMO) channel is to directly measure the channel matrix **H**. A few MIMO and multiple-input single-output (MISO) LMS measurements including that of [1],[3],[5],[106],[107] have been conducted to determine the instantaneous channel coefficient, channel correlation, capacity and rank among other LMS MIMO channel parameters. Direct measurements help uncover not only the propagation channel effects but also the effects of the measurement antennas as it is through the antennas that the measurement equipment excite and sample the effect of the channel on the excitation signal. However, channel measurements can only be truly representative of the particular channels in which the measurements are taken and cannot conveniently be extended to portray different channel scenarios. Therefore several measurement campaigns are usually needed to completely characterise different environment types for which wireless communications or broadcast services are planned to be implemented. This chapter uses two sections to describe some of the measurement campaigns that have been performed to characterise the dual circular polarised LMS MIMO. The first section describes previous and new measurement campaigns while the second section explains in detail the new measurements that have been performed and the procedures undertaken to extract the first order channel statistics.

4.1 Previous Measurements

Most research in the area of dual polarised LMS MIMO systems have up until now depended on a single set of channel data obtained from the measurement campaigns of P. King [1],[3]. The measurements, which were conducted in the summer of 2005 around

the town of Guildford, UK, made use of hill top mounted directional antennas and vehicle mounted omnidirectional antennas to respectively emulate satellites transmitting from geostationary orbits to a land mobile receiving unit. The transmit antennas at the top of the hill were mounted such that a first pair of left and right hand circular polarised antennas were co-located and a second co-located antenna pair (also of RHCP and LHCP) were separated from the first pair by about 10 wavelengths. As graphically illustrated in Figure 4.1, this configuration emulated a two-satellite dual circular polarised LMS MIMO channel and also provided data for the more viable one-satellite LMS MIMO system. The measurement routes covered tree lined roads, suburban and urban environments and the topography ensured that satellite elevation angles varied from 5^{o} to 18^{o}.

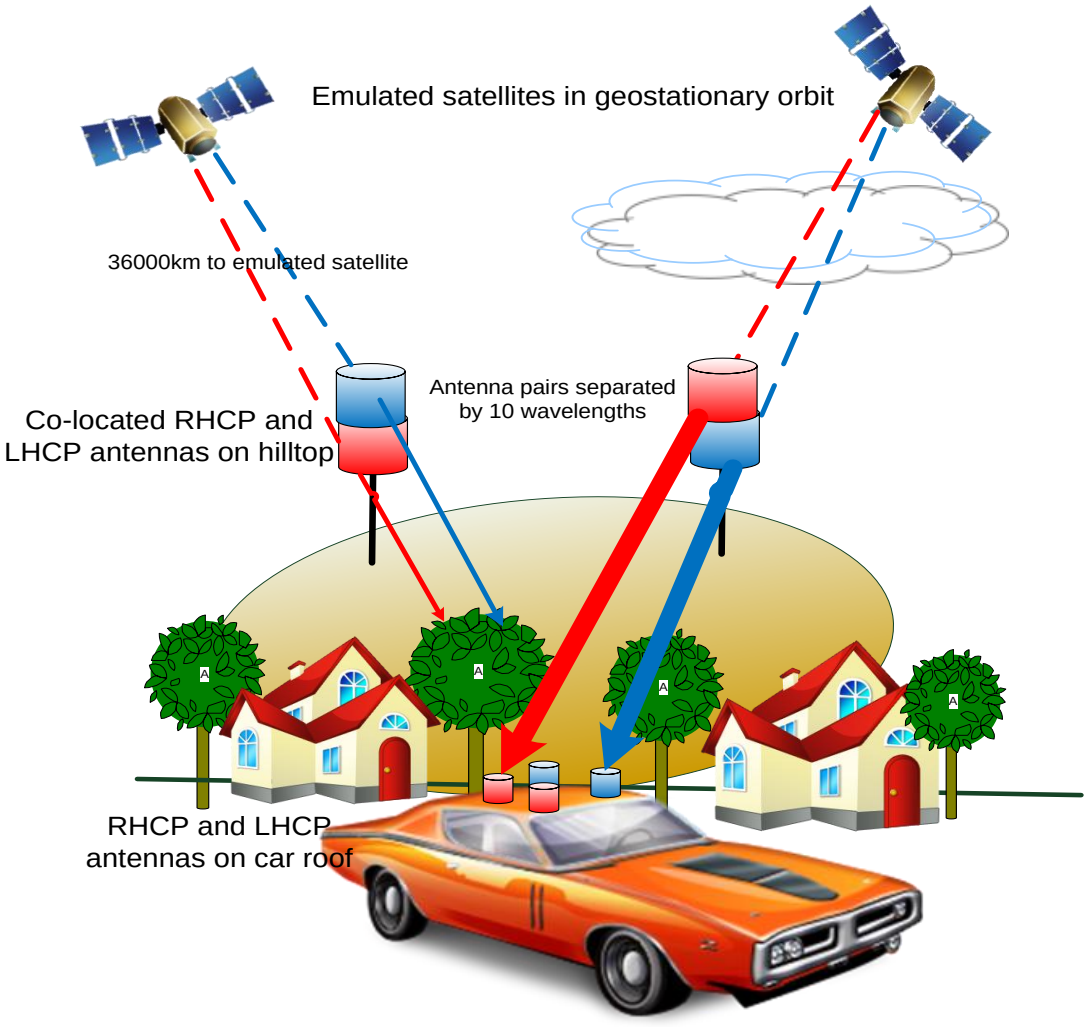

Figure 4.1: Graphic illustration of P.King's dual circular polarised LMS MIMO measurement campaign setup.

The Elektrobit wideband channel sounder was the main equipment used for King's measurement campaigns. This sounder was set to operate at a centre frequency 2.45GHz with a null to null bandwidth of 200MHz. Its transmit unit sent to the four transmit antennas a set of direct sequence spread spectrum signals produced from binary phase shift keyed (BPSK) modulated pseudo-noise codes. The receive unit used fast synchronised sequential switching to sample the channel from each of the four receive antennas. The sampling rate and switching allowed the 4×4 MIMO channel to be completely sampled well within the channel coherence time. The novelty of this measurement limited it to very low elevation angles whose characteristics cannot reliably be extrapolated to channels with higher elevation angles. Hence, more realistic measurements at higher elevation angles are needed.

King's emulated LMS MIMO channel measurements inadvertently excludes both tropospheric and ionospheric effects since the transmit antennas were mounted on a hill instead of being located thousands of kilometres away in orbit. Tropospheric effects include depolarisation [108] and attenuation due to gases, clouds, precipitation, sand and dust storms while ionospheric effects include Faraday rotation, propagation delay, dispersion and scintillation [13]. According to [19], ionospheric effects progressively decrease with increasing radio frequency while tropospheric effects increasingly become significant above 3GHz. Tropospheric effects is also known to become very severe at certain frequencies above 40GHz due to increased absorption by atmospheric oxygen and water vapour. To accommodate the adverse ionospheric and tropospheric effects, fade margins are usually added to the link budgets of LMS communication systems and analysts of emulated LMS channel data should always be aware of such needed fade margins.

The other LMS measurement campaigns of higher elevation, though of the MISO type, that deserves the attention of this thesis were carried out in 2008 and 2009 under the MiLADY project [106],[107]. The objective of this set of measurements was to study the angle diversity derivable from multiple real satellites that may in future support multimedia satellite broadcast services to small handheld devices. Unlike King's measurements, the MiLADY measurements sampled data from satellites at high elevation angles (23^o to 83^o) and the fade distribution statistics of its suburban environment was

found to closely match that of the Fontan models [60],[62], which have been recommended for DVB-SH systems in [63] and [77]. One of the conclusions of this set of measurements was that there is a good business case for satellite delivered services to land mobile terminals and that mobile reception strongly depends on environmental factors close to the mobile devices. This gives rise to a clear distinction between the effects of urban, suburban and rural-type environments on mobile satellite reception.

The MiLADY measurements led on to the very recent (August 2010 and May 2011) dual polarised single and multiple satellite MIMO MIMOSA measurement campaigns reported in [5]. This measurement campaign made use of a set of RHCP and LHCP car-roof mounted mobile antennas and a set of stationary antennas of the same polarisation to receive right and left hand polarised 2.187 GHz centre frequency signals from a satellite in orbit. A small frequency offset was applied between the orthogonally polarised RHCP and LHCP signals to make the process of separating them at the receiver somewhat easier. The statistics derived from the MIMOSA measurements allowed for the effects of the environment on channel and antenna parameters like Rice factor, XPD and large scale correlation to be studied. The findings of this measurement campaign generally agree with that of earlier measurements by P. King in the following aspects:

- Co-polarised signals are always stronger than cross-polarised signals during LOS propagation. This relationship was observed in both measurement campaigns to sometimes reverse during OLOS conditions or during periods of deep shadowing.
- The signal XPD level, computed from the receive power levels at the RHCP and LHCP antennas, was found to strongly depend on environmental conditions – with the urban and suburban environments causing more signal depolarisation than the tree lined road/rural environment.
- The large scale fading of single satellite dual polarised MIMO channels were found to be highly correlated, more so during LOS fading. This impacted negatively on the capacity predictions of King's measurement whereas its impact on the MIMOSA measurements is yet to be ascertained.

Given the unique characteristics of the dual polarised MIMO channel and due to the fact that in-depth characteristics analysis of such channels is at its infancy and has so far

depended on just two measured channel data sets, it is necessary that more measurement campaigns be executed to provide the much needed channel data. From the measured data, newer and better channel models that can more robustly relate the effects of XPD, Rice factor and channel correlation (among other parameters) on the achievable channel capacity and bit error rates of MIMO techniques in the dual polarised LMS channel can then be derived. The next section gives a brief description of additional channel measurements that have been conducted by the author to provide the much needed data to further the analysis into dual polarised multiplexing systems earlier started in section 3.2 of this thesis.

4.2 New Measurements

This section discusses additional measurements that have since been carried out to shed more light on the dual circular polarised LMS MIMO channel. Two environment types similar to the ones in [3] but at higher elevation angles have been investigated. The first environment can be described as rural while the second is characterised as suburban. Both measurements were carried out in summer when trees and shrubs are in full foliage so as to capture the worst case attenuation.

4.2.1 Measurement Campaign I

The first measurement campaign was carried out in the summer of 2009 with the aim of recording LOS and OLOS propagation scenarios where obstruction in the channel is mainly caused by tree matter and occasional rural buildings. The measurement route chosen for this campaign was the Newlands Corner area of Guildford, U.K., a location that can be described as being predominantly rural. As shown in Figure 4.2, the route traverses a large area densely vegetated by tall road side trees and low growing crops interspaced with occasional farm houses. This allowed the receiver, which was roof mounted on a mobile vehicle to experience a channel that varies from LOS to OLOS and vice versa. This location was chosen to enable extensive propagation data to be collected such that LMS MIMO broadcasts to rural environments can be characterised and the expected large scale MIMO channel fading possibly modelled using a Markov switching

process. A schematic cross-section of the measurement campaign environment showing Fresnel zone clearance and elevation angle range is shown in Figure 4.4.

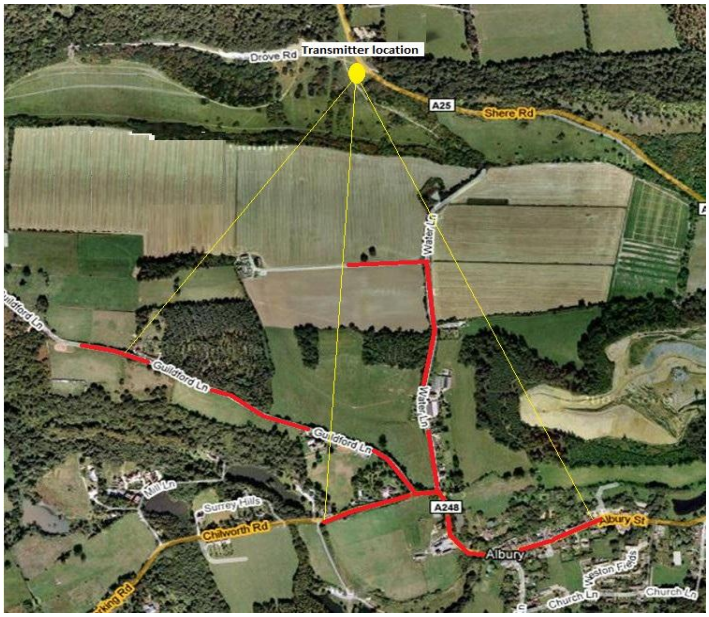

Figure 4.2: Satellite image showing measurement route (in red)

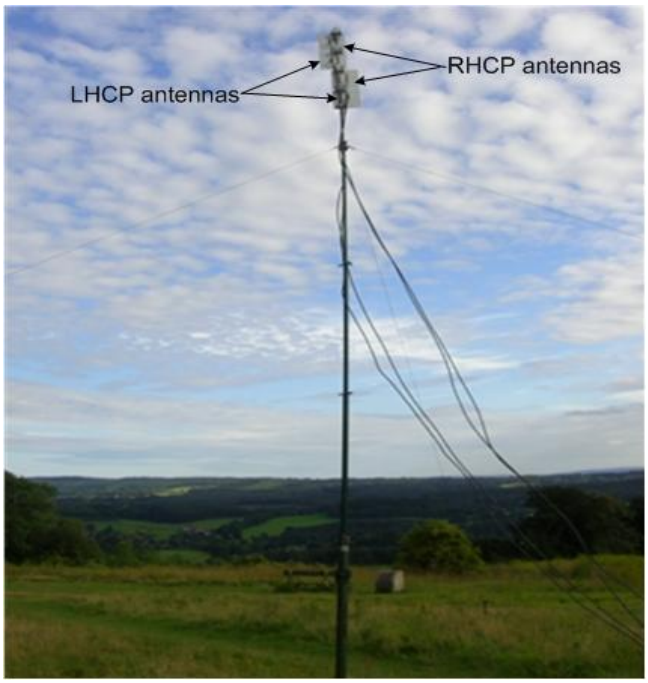

Figure 4.3: Directional circular polarised transmit antennas mast-mounted on a hill and pointing down towards a valley

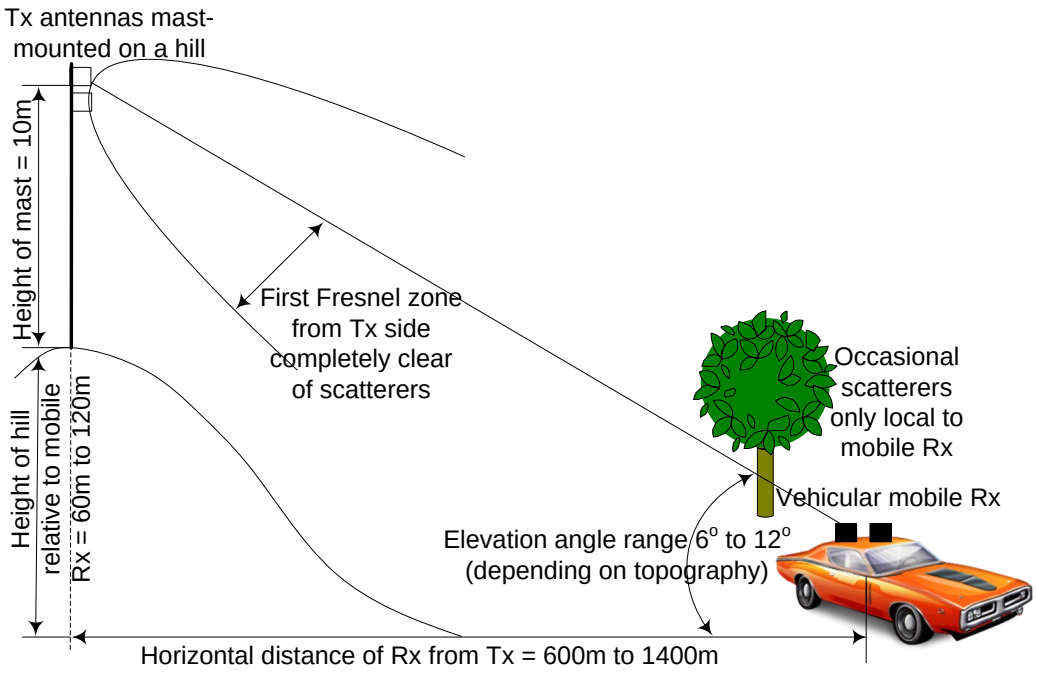

Figure 4.4: Schematic cross-section of measurement campaign setup for rural environment

4.2.1.1 Summary of Equipment and Measurement Parameters

The equipment used in measuring the MIMO channel was the Elektrobit Propsound, a correlation-based wideband channel sounder, manufactured by Elektrobit of Finland. The parameters of the channel sounder were set as follows:

- Basic parameters: 2.43GHz carrier frequency, 23dBm transmit power, 50MHz null to null bandwidth and a sensitivity of -94dBm.
- Delay resolution parameters: 25×10^6 chips/s, a pseudorandom code length of 63, a delay resolution of 40ns ($1/25\times10^6$ chips/s) and the length of impulse response = 2.52μs (code length/25×10^6 chips/s).
- Measurement distance parameters: a path loss exponent of 2.1, nearest distance between transmitter and receiver to maintain synchronisation was chosen as 600m, transmitter and receiver gain were 13dBi and 0dBi respectively. Maximum impulse response dynamic range was set at 35dB.
- Spatial resolution parameters: number of transmit and receive antennas were 4 and 6 respectively, giving 24 MIMO channels plus 4 guard channels making a total of

28 channels. Since the pseudorandom code length used was 63, it took the sounder 70.56μs to scan the 28 MIMO channels. Maximum mobile speed was set at 96km/h, which directly affects the choice of MIMO channel sample rate as explained in the next section.

The Elektrobit Propsound has only one RF chain and as such it can only sample MIMO channels by switching between all transmit-receive antenna pairs. It is thus important to ensure that the delay domain and spatial resolution parameters chosen for the Newlands Corner measurements enables all 28 channels to be sampled well within the channel coherence time. Details of the switching, synchronisation and timing of the Elektrobit sounder as used in a previous wideband measurement campaign can be found in [3] and for this measurement is explained in the next section.

4.2.1.2 Channel Measurement Set-up and Procedure

The Newlands Corner measurement campaign took advantage of the local topography and the routes covered as shown in Figure 4.2 are Water Lane, Guildford Lane and Chilworth Road. The transmitting antennas in this case were mast-mounted on a hill (see Figure 4.3 and 4.4) while the receiving antennas were placed on the roof-top of a measurement vehicle as shown in Figure 4.5 and driven along a preselected route in the valley beneath. This configuration ensured that the elevation angle was never less than 6^o and not more than 12^o, which not only adequately emulates a geostationary satellite viewed from high latitude cities but also ensures that the propagating signals are intermittently shadowed by the foliage from roadside trees.

Four directional circular polarized (two LHCP) and two RHCP) transmit antennas were co-located on a mast to emulate a single satellite transmitting to four spatially separated omnidirectional receive antennas and two co-located experimental quadrifilar helix antennas. Thus a 4×6 MIMO channel was captured from which data from the first 2×2 dual polarised MIMO channel (consisting of one each of an RHCP and an LHCP commercial type antenna pair) is analysed in this thesis. The second 2×2 MIMO channel from the commercial type antennas served as a backup to check for inconsistencies, if any, in the channel data emanating from the first set of antenna pairs. The remaining two 2×2 channels, received using the experimental quadrifilar helix antennas have been used

for other analyses beyond the scope of this thesis. The spatial separation between the commercial type receive antennas was set at 4 wavelengths with the antennas placed in the same configuration as was done in [3]. Table 4-1 shows a matrix of the antenna pairs, where the commercial type antennas are labelled R(L)HCP 1 and 2 while the experimental quadrifilar helix receive antennas are labelled Q-RHCP and Q-LHCP.

Table 4-1: Channel matrix and antennas used for the Newlands Corner measurements

The 1st 2×2 MIMO channel is in bold fonts and shaded grey. The 2nd 2×2 MIMO channel is shaded green		Receive Antennas					
		RHCP 1	RHCP 2	LHCP 1	LHCP 2	Q-RHCP	Q-LHCP
Transmit Antennas	RHCP 1	**1,1**	1,2	**1,3**	1,4	1,5	1,6
	RHCP 2	2,1	2,2	2,3	2,4	2,5	2,6
	LHCP 1	**3,1**	3,2	**3,3**	3,4	3,5	3,6
	LHCP 2	4,1	4,2	4,3	4,4	4,5	4,6

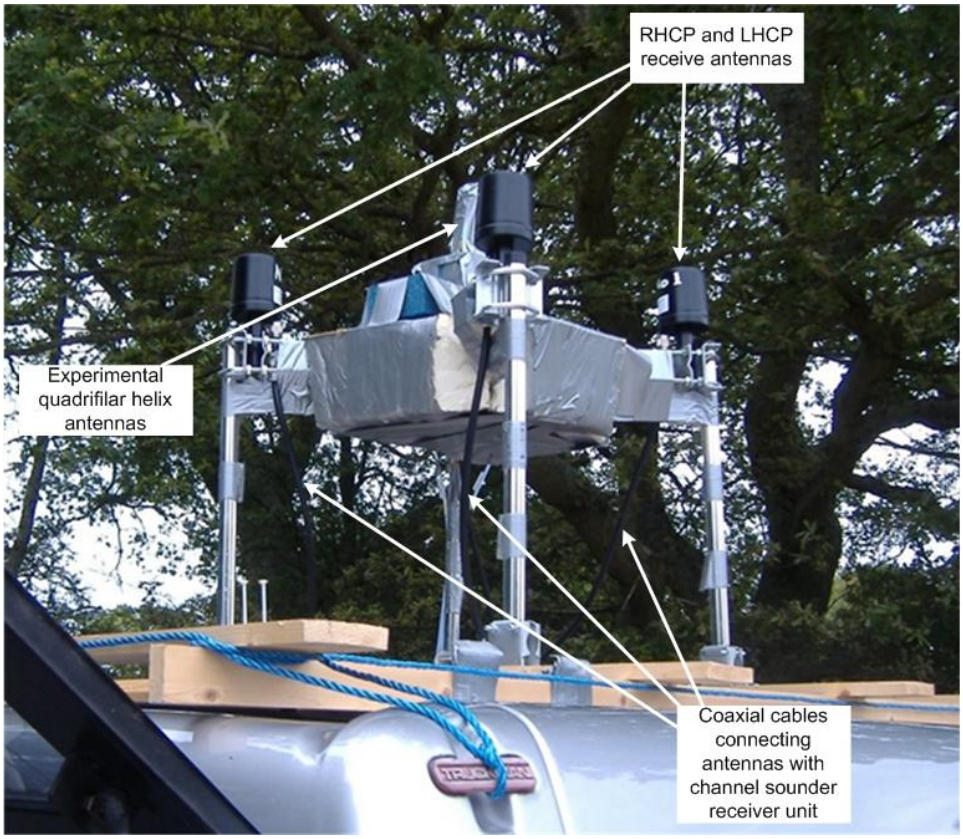

Figure 4.5: Omnidirectional receive antennas roof-mounted on measurement campaign vehicle

The channel switching frequency of the transmitter and receiver units of the Elektrobit Propsound channel sounder was synchronised prior to commencing each measurement campaign. This is because Elektrobit Propsound measures the MIMO channel by sequentially switching between all the transmit and receive antenna pairs and the penalty for lack of switching synchronisation can result in the power delay profile exiting the sounder's power delay profile display window during measurement.

Pre-measurement channel sounder calibration involves matching both the switching frequency and the pseudorandom code cycles at the transmitting and receiving units using in-built rubidium clocks through a measurement setup wizard that runs from a control laptop. A screenshot of the wizard for setting the measurement distance parameters is shown in Figure 4.7 and a link budget analysis to determine the feasibility of the measurement campaign is given in Appendix I. Since the channel sounder is correlation based, for the Newlands Corner measurements, the channel is measured by transmitting a BPSK modulated pseudorandom code sequence of predetermined length and at the receiver the received signal is cross-correlated with a locally generated pseudorandom code sequence of the same length. The pseudorandom codes are designed to have near perfect autocorrelation properties but very low cross-correlation properties when correlated against random channel noise. Cross-correlation at the receiver enables the amplitude and phase of the transmitted signal and hence the channel impulse response to be determined. Due to the difference in distance that signals propagate from the transmitter to the receiver (see Figure 4.2), the delay resolution of the channel sounder, which is determined by the pseudorandom code length, must be set such that the last arriving multipath component is captured well within the delay window. In other words, since the mean delay changes as a measurement campaign progresses, the delay resolution of the sounder must be greater than the total expected excess delay and also make allowance for the movement of the RMS delay spread up and down the delay window. Knowing from previous measurements [1],[39] that the maximum expected delay for LMS systems is about 153ns, the appropriate code length is determined with the aid of an in-built measurement calibration wizard, which specifically takes into account the effects of the mobile receiver velocity. This is because the relative velocity between

the transmitter and receiver affects the correlation distance, T_C, of the channel. T_C is estimated using [8]:

$$T_C \leq \frac{V_c}{2f_c v_{\max}}, \tag{4.1}$$

where V_C is the velocity of light, f_C is the centre frequency and v_{max} is the maximum velocity of the receiver. For a maximum velocity of 96km/h (26.7m/s), the coherence time is 2.3ms. Hence the switching must be fast enough to completely sample the MIMO channel well within its coherence time.

In rural outdoor environments where scatterers are not very closely spaced, a low delay domain spatial resolution in the order of a few MHz is enough to capture all relevant multipath components [109]. A choice of 50MHz is adequate for the Newlands Corner measurements, and this gives a chip frequency of 25×10^6chips/s (MHz) following the Nyquist criterion which specifies that null to null bandwidth must be twice the chip frequency. This gives a chip duration of 40ns and a choice of 63 chips per code (63 being the length of the pseudorandom codes) as shown in Figure 4.6 ensures that the complete 4×6 MIMO channel is captured in 70.56µs. A choice of 708.62Hz MIMO channel sampling frequency means that the MIMO array is completely captured every 1/708.62Hz = 1.4ms + 70.56µs. This is well within the channel coherence time, estimated at 2.3ms when the maximum receiver velocity is 96km/h. Also, the maximum resolvable Doppler shift for the channel sounder setup is 354.31Hz. The captured wideband complex channel impulse response is stored in real time and written to the hard drive unit of the channel sounder shown in Figure 4.8.

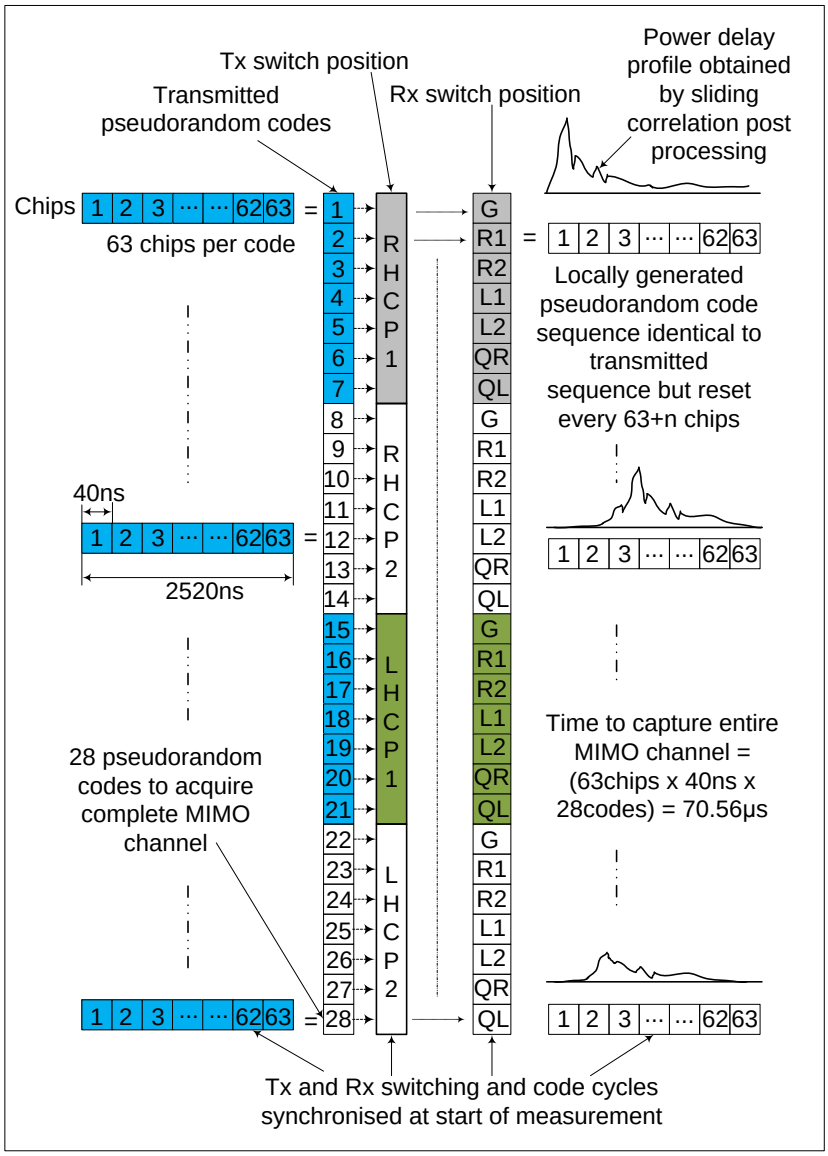

Figure 4.6: Timing diagram of the switch-based Elektrobit wideband channel sounder as used in the rural environment measurement campaign

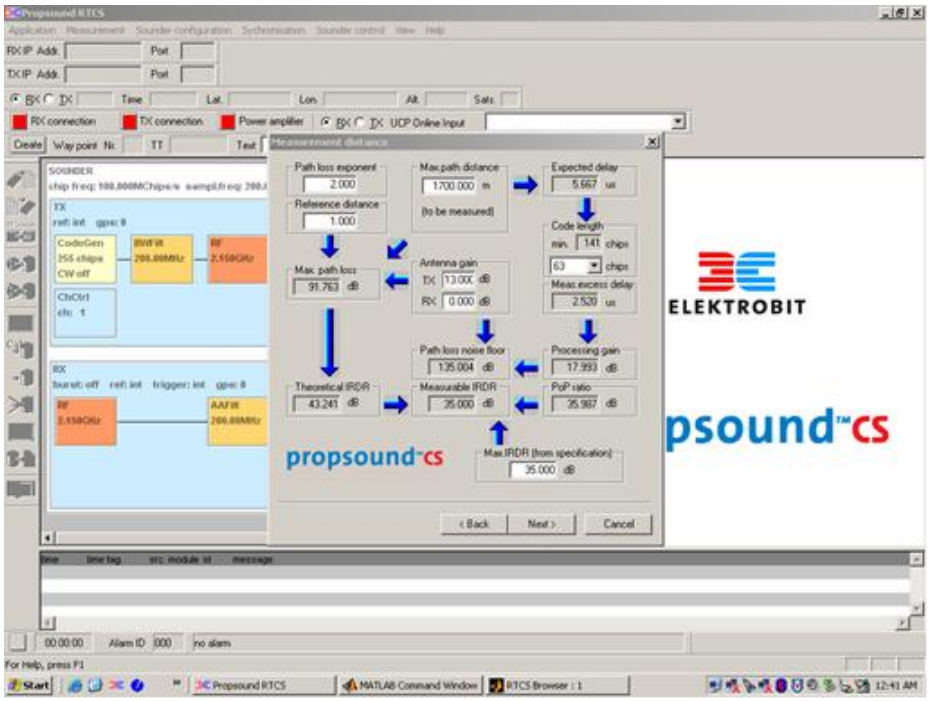

Figure 4.7: Screenshot of Elektrobit's measurement calibration wizard

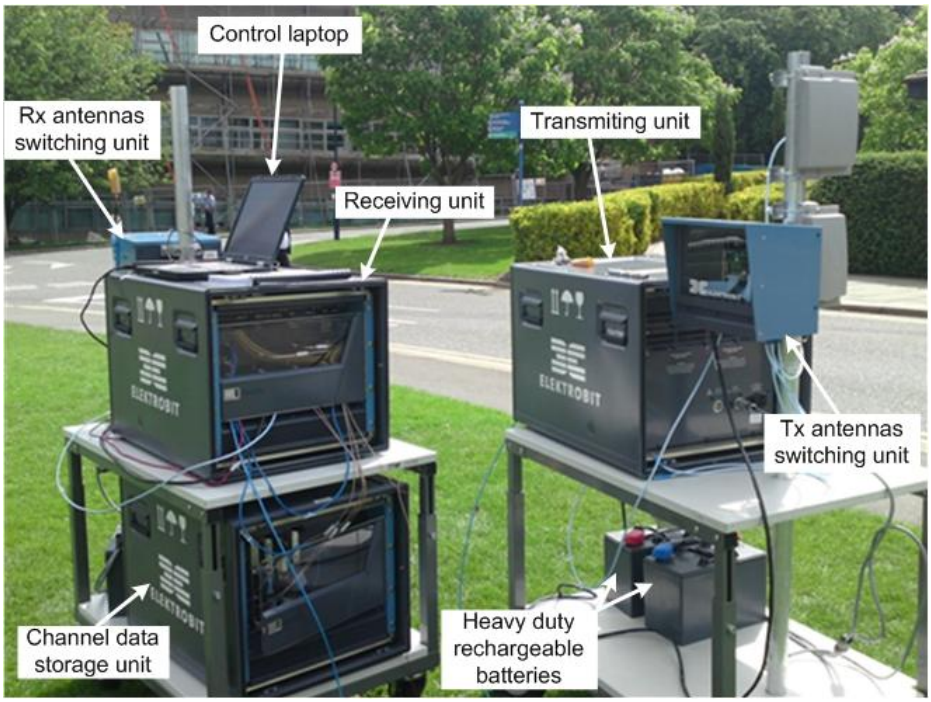

Figure 4.8: The Elektrobit Propsound channel sounder units during pre-measurement calibration

4.2.2 Measurement Campaign II

The second measurement campaign carried out in the summer of 2010 aimed to uncover the characteristics of the dual circular polarised LMS MIMO channel in a suburban environment. A low density residential area in the town of Guildford, U.K. was chosen for this measurement campaign and the routes were specifically selected so that the mobile receiver views the emulated satellite from higher elevation angles than was achieved in previous measurements such as [1] and [3]. Routes covered in this suburban environment measurement campaign as shown in Figure 4.9 are Millmead Terrace, Portsmouth Road and Bury Fields. Figure 4.10 shows a schematic cross-section of the measurement campaign environment while Figure 4.11 gives a pictorial view of the satellite emulated by tower block-mounted transmitting antennas and the vehicular mobile receiver.

Figure 4.9: Satellite image showing suburban measurement route (in red)

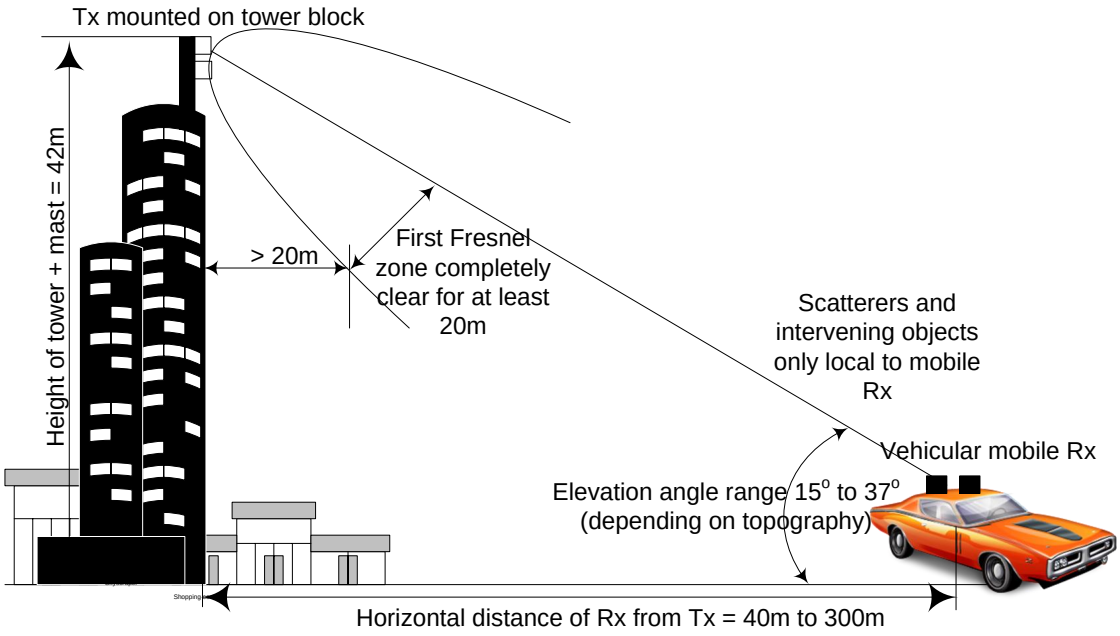

Figure 4.10: Schematic cross-section of measurement campaign setup for suburban environment

Figure 4.11: Pictorial view of tower block mounted emulated satellite transmitter and vehicular mobile receiver

4.2.2.1 Summary of Equipment and Measurement Parameters

The same equipment used for the Newlands Corner measurements were used for this second measurement campaign. The channel sounder parameters were set as follows:

- Basic parameters: 2.5GHz carrier frequency, 23dBm transmit power, 200MHz null to null bandwidth and a sensitivity of -88dBm.
- Delay resolution parameters: 100×10^6 chips/s, a pseudorandom code length of 2047, a delay resolution of 10ns ($1/100\times10^6$ chips/s) and the length of impulse response = 20.47μs (code length/100×10^6 chips/s).
- Measurement distance parameters: a path loss exponent of 2.1, nearest distance between transmitter and receiver to maintain synchronisation was chosen as 50m, transmitter and receiver gain were 13dBi and 0dBi respectively. Maximum impulse response dynamic range was set at 35dB.
- Spatial resolution parameters: number of transmit and receive antennas were 2 and 6 respectively, giving 12 MIMO channels plus 2 guard channels making a total of 14 channels. Since the pseudorandom code length used was 2047, it took the sounder 286.58μs to scan the 14 MIMO channels. Maximum mobile speed was set at 50km/h, which directly affects the choice of MIMO channel sample rate as earlier explained for the previous measurement campaign.

4.2.2.2 Channel Measurement Set-up and Procedure

As shown in Figures 4.9 - 4.11, the transmitting antennas were placed on the roof of a 40m high tower block while the receive antennas were mounted on the roof of a vehicle, in the same configuration as was done in the Newlands Corner measurements, and driven along a preselected route. This geometry emulates a satellite located at between 15^o and 37^o elevation, i.e. depending on where the receiver was located with respect to the transmitter. The route was designed such that these elevation angle bounds were never exceeded and also so that there would be periods of distinctly LOS, OLOS and NLOS propagation.

The measurement route composed tarmac covered road of about 8m wide in most places and was bordered by single to three storey buildings interspaced with occasional tree matter. The buildings were traditional English buildings with walls made from fired

bricks and mortar while the roofs were made from slate. These man-made physical structures formed the bulk of the scatterers within the vicinity of the receiving antennas. Due to the nature of the scatterers, theory [8] predicts that the reflection and diffraction in OLOS and NLOS conditions would ensure low Rice factor with corresponding low correlation between the individual orthogonally polarised MIMO sub-channels. These channel fading characteristics will be investigated using first and second order statistics in subsequent sections of this chapter.

To emulate a single satellite transmitting dual polarised signals, one RHCP and one LHCP antenna were co-located on the tower block mounted mast and direct sequence pseudorandom codes were transmitted to six vehicle mounted receive antennas. Thus a 2×6 MIMO channel was captured from which data from a 2×2 dual polarised channel is analysed in this thesis. The configuration and spatial separation of the receive antennas in the suburban measurements were exactly the same as that of the rural Newlands Corner measurement campaign.

Channel sounder calibration for this measurement campaign involved inserting a 20dB attenuator between the receive antennas and the Elektrobit receiver unit to avoid RF overload due to the relatively short distance between the transmit and receive antennas and the presence of wireless local area network (WLAN) signals leaking out from the surrounding residential buildings. A notable difference between the rural and the suburban measurement campaigns is the choice of a larger (200MHz) sampling bandwidth. This is to improve the delay resolution of the channel sounder and allow for multipath contributions from more closely spaced scatterers to be resolved. Note that there are more scatterers in an urban environment than a rural environment, necessitating a finer delay domain resolution which in turn enables all the significant multipath contributions to be determined. The delay resolution needed for an indoor measurement campaign where the scatterers are very close together would even be higher [109].

Since each delay domain chip must be sampled at least twice following the Nyquist criterion, the chip frequency for a 200MHz sampling resolution equals 100×10^6chips/s (MHz). This implies that the duration of each chip will be 10ns long. A choice of 2047 for

the code length ensures that the measurement excess delay, τ_{MED}, is 20.47μs, which computed from:

$$\tau_{\mathrm{MED}} = \frac{\text{code length}}{\text{chip frequency}}, \tag{4.2}$$

is in excess of the maximum expected delay (τ_{MAX}), given by:

$$\tau_{\mathrm{MAX}} = \frac{\text{maximum measurement distance}}{C}. \tag{4.3}$$

C in (4.3) is the velocity of light. It is recommended in [109] that for correlation based channel sounding, τ_{MED} should be ideally greater than τ_{MAX}.

The time it takes for the complete 2×6 MIMO channel to be sounded is given by 2047chips × 10ns × (12 pseudorandom codes + 2 guard channel codes) = 286.58μs. A choice of 488.77Hz MIMO channel sampling frequency means that the MIMO array is completely captured every 1/488.77Hz = 2ms + 286.58μs. This is well within the channel coherence time, estimated at 4.3ms using (4.1) when the maximum receiver velocity is 50km/h (13.39m/s). Also, the maximum resolvable Doppler shift for the channel sounder setup is 244.38Hz. These parameters were inserted into the measurement set up wizard at the start of the campaign and the impulse response of the sounded channel written to the receiver hard disc storage unit in real time during the course of the measurements.

Preliminary real time visual power delay profile inspection of the measured channel showed that a lot of interfering WLAN signals was also picked up and a technique for filtering out the interfering signals had to be developed. As with all wireless communications, antennas provide a means through which the channel can be excited (sounded) and the influence of the channel on the excitation signals measured. The next section will describe the antennas used for channel sounding.

4.2.3 Measurement Campaign Antennas

The antennas used for both measurement campaigns were right and left hand circular polarised commercially manufactured directional patch antennas (for the satellite

transmitter) and omnidirectional dipole antennas. Below are summarised the main characteristics of the antennas.

4.2.3.1 Directional Transmit Antennas

- Optimal frequency range of operation: 2.400 – 2.485GHz
- Average co-polar boresight gain (elevation and azimuth): 12dBi
- Average co-polar 3dB beamwidth (elevation and azimuth): 30^o
- Average cross-polar boresight gain (elevation): -10dBi
- Average cross-polar boresight gain (azimuth): - 14dBi
- Average antenna boresight XPD: 24dBi

The average refers to mean values of the RHCP and LHCP antennas. Other details of this antenna including its elevational and azimuthal gain pattern can be found in [3].

4.2.3.2 Omnidirectional Receive Antennas

- Optimal frequency range of operation: 2.35 – 2.55GHz
- Average co-polar gain over 360^o (azimuth): 0dBi
- Average cross-polar gain over 360^o (azimuth): -15dBi

For more details about the co- and cross-polar elevation and azimuth gain patterns of the omnidirectional receive antennas, the reader is referred to [97], where they are referred to as reference antennas and compared with a co-located dual polarised quadrifilar helix antenna. Also, a look at the antenna elevation gain patterns shown in Figures 4.12 and 4.13 reveal that the ratio between the co-polar and cross-polar antenna gains in excess of 10dB for the 6^o to 37^o elevation angle range. This is the range within which the two measurement campaigns were performed. Thus assuming equal powers in the arriving co- and cross-polarised signals, the antenna relative difference between the receive antennas co- and cross-polar gains on its own should theoretically provide enough polarisation discrimination to make DCPM viable. This will be investigated in chapter 6.

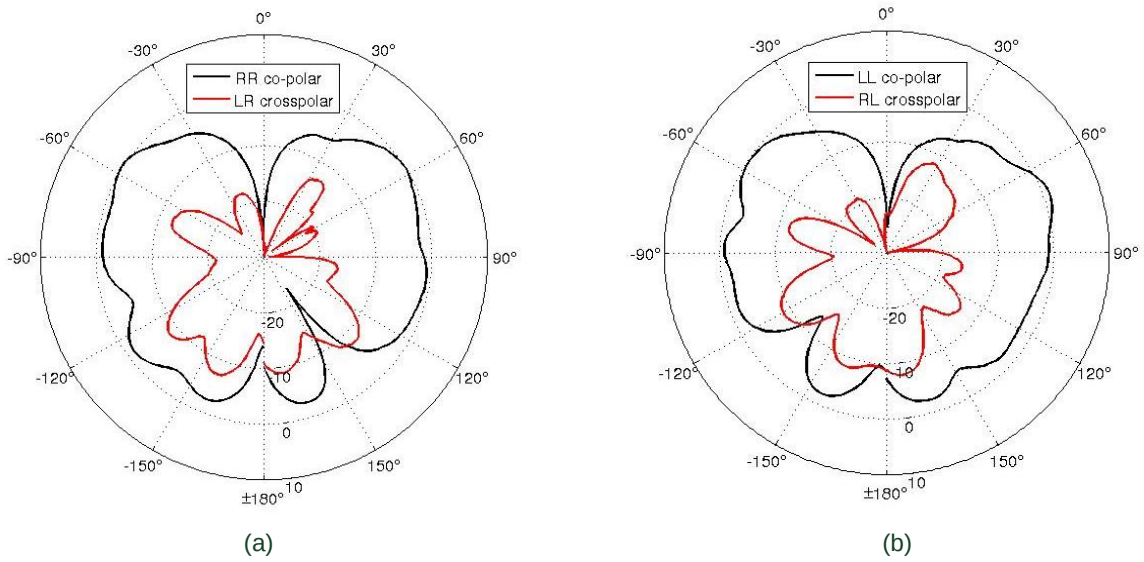

Figure 4.12: Elevation gain pattern for (a) RHCP and (b) LHCP receive antennas

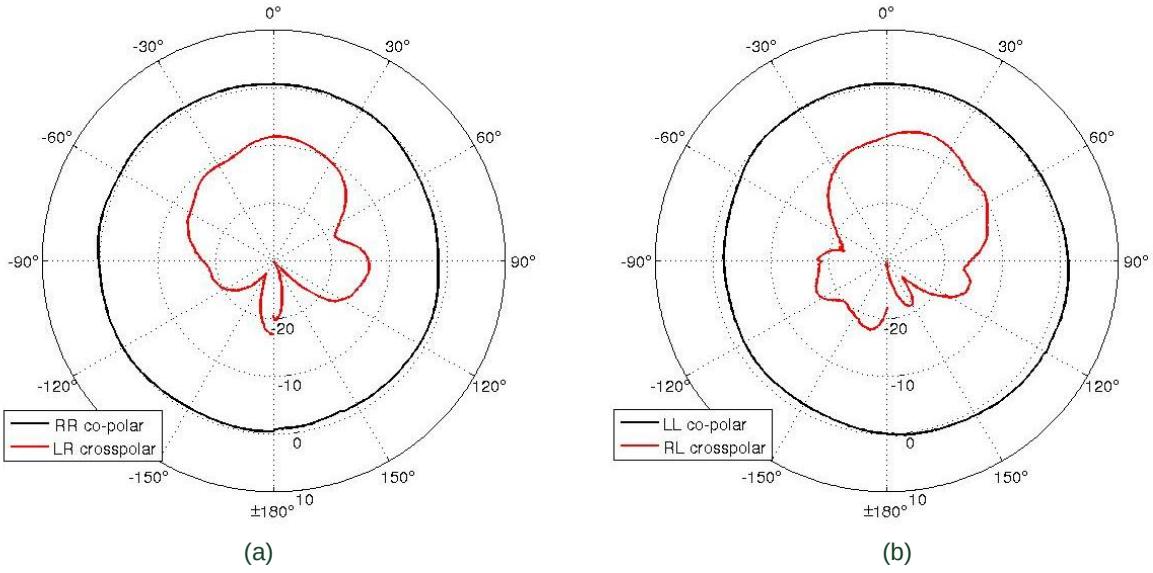

Figure 4.13: Azimuth gain pattern for (a) RHCP and (b) LHCP receive antennas

4.2.4 Extraction of Narrowband Channel Data and First Order Statistics

Channel data obtained using the Elektrobit channel sounder was of the wideband type and in the case of the Newlands Corner measurements the delay resolution was 2520ns divided into 63 delay bins of 40ns each. Due to the change in the distance between the

transmit and the receive antennas and a possible loss of Tx-Rx synchronisation as the measurement campaign progressed, the arrival time of the first channel impulse response varied by a few tens of nanoseconds. This variation in arrival time of impulse responses of significant power was the reason why a larger than necessary delay resolution was chosen (maximum delay in the earlier measurements of [1] and [39] awas 153ns). Figure 4.14(a) shows the power delay profile of the h_{RR} co-polar channel for a small section of the Newlands Corner measurement run. Observe that significant multipath contributions all arrive within a few nanoseconds of the first impulse response. In Figure 4.14(b), all contributions below the -90dBm level have been filtered out. This is because the channel sounder's sensitivity for this measurement run was set at -94dBm and any impulses below the -94dBm level is as a result of residual noise in the sounder's correlation computation process.

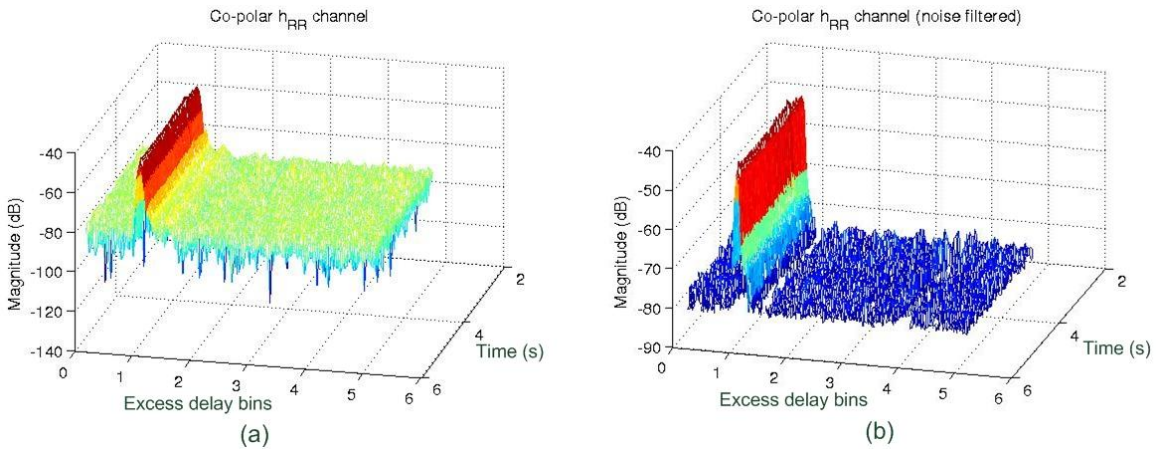

Figure 4.14: Power delay profile of co-polar h_{RR} channel (a) with background channel noise and (b) with background channel noise < 90dBm filtered out

The narrowband component was obtained by performing an FFT operation across the delay domain and then filtering out all frequencies apart from the centre frequency components. Note that the FFT operation on the delay bins implements a vector addition of all the arriving multipath components and transforms from the time to frequency domain. Figure 4.15 shows the spectrum of the wideband channel impulse response (power delay profile) of Figure 4.14. To complete the narrowband data extraction, centre frequency component extraction was then carried out for all the co-polar and cross-polar channels in all the measurement runs.

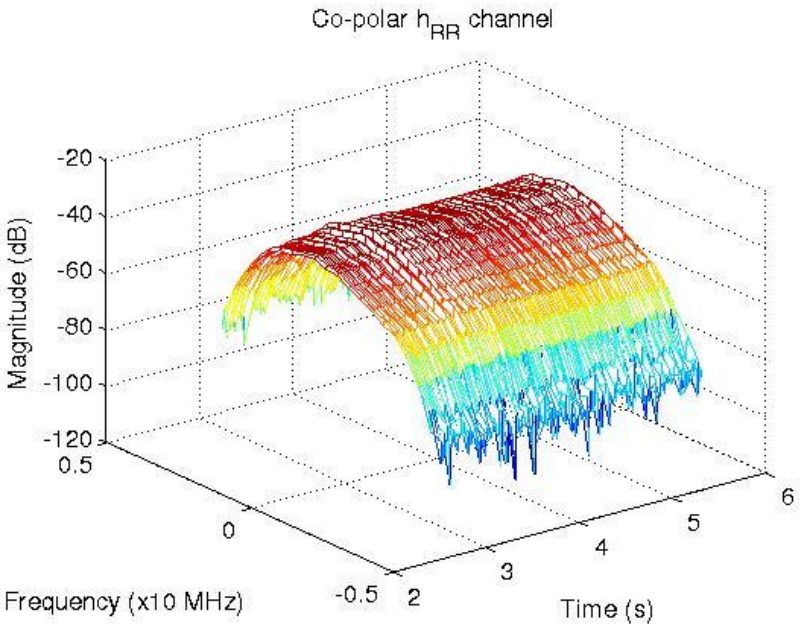

Figure 4.15: Spectrum of co-polar h_{RR} channel without filter correction

Sections of extracted narrowband time-series of co- and cross-polar received signal power from a single measurement run are shown in Figure 4.16. Observe in Figure 4.16 (a) that in the region marked LOS to OLOS, the co-polar signal powers (both h_{RR} and h_{LL}) are much stronger than their cross-polar counterparts, sometimes exceeding the latter by more than 10dB in pure LOS conditions. As channel fading gradually changes from pure LOS to OLOS, the cross-polar signals progressively experience deeper fades and the difference between the co- and cross-polar powers reduces. In Figure 4.16 (b) where it is shown a section of OLOS fading, the difference between the co- and cross-polar signal powers further diminishes and the co-polar signals begin to exhibit deeper fading. Figure 4.16 (c) shows a section of OLOS to NLOS fading, where the co-polar powers become comparable with the cross-polar powers. Since the antenna XPD value stays constant, the sections of comparable co- and cross-polar powers indicate very rich scattering environments which in turn cause several polarisation reversals due to the numerous instances of scattering, reflection and diffraction of the propagating signals. The observations are in agreement with other LMS measurements of [5] and the emulated satellite measurements of [3].

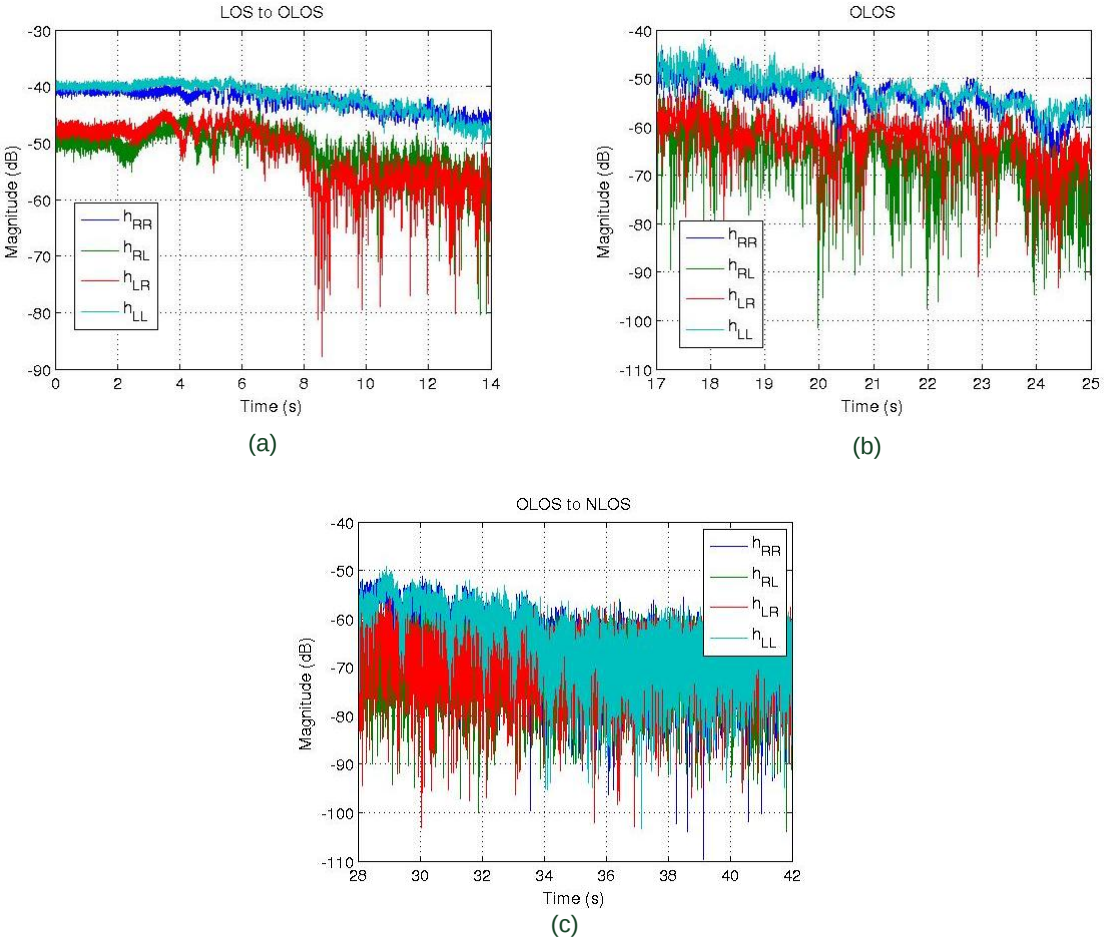

Figure 4.16: Received co- and cross-polar signal power in a single measurement run showing (a) LOS to OLOS fading, (b) OLOS fading and (c) OLOS to NLOS fading

4.2.4.1 Normalisation

The recorded channel data was normalised with respect to the LOS level and performed in such a way that the branch power ratio of the MIMO channel was maintained at all times. The first step of the normalisation process was both tedious and manual and involved classifying the channel data into LOS, OLOS and NLOS sections. This was done by matching the recorded channel data with GPS data of the receiver's position and then comparing this with the most recent open sourced Google Earth maps. These sections, which were made to be multiples of the channel coherence distance (since the sampled time series channel data could easily be converted to position series) were then normalised one section at a time to preserve their respective MIMO branch power ratio.

The normalisation factor used was the total average power from the co-polarised RHCP received signal for each of the sections and is defined as:

$$N_F = \left(\frac{1}{n_{tx}^R n_{rx}^R}\sum_{i=1}^{n_t}\sum_{i=1}^{n_r} E\left\{|h_{ij}^{RR}|^2\right\}\right)^{1/2}, \tag{4.4}$$

where $n_{tx,rx}^R$ represents the number of RHCP transmit and receive antennas, and h_{ij}^{RR} is the co-polar RHCP channel coefficient. The normalisation can be viewed as a demeaning process in which the 2×2 MIMO channel is divided through by the mean signal level of the RHCP (or LHCP) co-polar channel. Note that the mean is computed using the same number of samples as the LOS, OLOS or NLOS fading sections.

4.2.4.2 Channel Cross-polar Discrimination (XPD)

Correct normalisation of the recorded channel data allows for the channel cross-polar discrimination ratios to be computed with good accuracy. These ratios are defined as:

$$\text{XPD}_1 = 20\log\left(\frac{h_{RR}}{h_{LR}}\right) \text{ and } \text{XPD}_2 = 20\log\left(\frac{h_{LL}}{h_{RL}}\right). \tag{4.5}$$

It was observed that XPD_1 is not always equal to XPD_2 as given by Stutzman in [110]. This is partly as a result of the slight disparity in the radiation patterns of the RHCP and LHCP antennas. Figure 4.17 shows a CDF graph of the XPD for one of the Newlands Corner measurement runs where the propagation condition changed from pure LOS to OLOS.

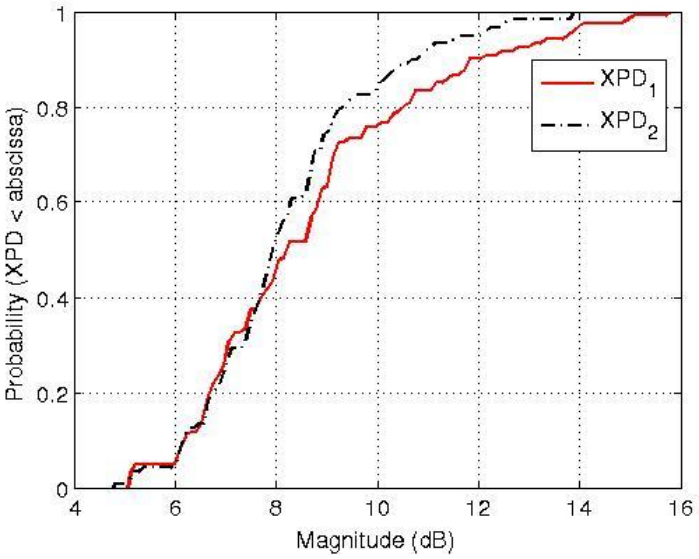

Figure 4.17: CDF plots of XPD for LOS and OLOS channel conditions

4.2.4.3 Large Scale Fading Characteristics

Large scale fading results from signal attenuation by large intervening objects between the satellite transmitter and the land mobile receiver. For signal attenuation to be attributable to large scale fading, the received signal must be viewed over spatial dimensions ranging from several tens to several hundreds of wavelengths. Following the classification in section 4.2.4.1 of signal attenuation into LOS, OLOS and NLOS regions, this section characterises the observed large scale fading within these predefined regions using empirical and theoretical probability density function plots.

Starting with a predominantly LOS fading region, Figure 4.18 shows probability density function (PDF) plots of large scale fading for RHCP and LHCP co- and cross-polar received signals. It is evident that the distributions of all four signals (channels) are characteristically lognormal – i.e. they follow a normal distribution over a logarithmic (dB) scale. Thus it is safe to conclude that the large scale fading in an LOS fading dual circular polarised LMS MIMO channel is lognormal since their empirical PDF plots very closely match their theoretical PDF plots. Note that on determining the mean level of the dB-valued received signal power, the theoretical PDF was computed from the normal (Gaussian) probability density function, defined in [111] as:

$$P_{\mathrm{NORM}} = \frac{1}{\sigma\sqrt{2\pi}} \exp\left(\frac{-(x-\mu)^2}{2\sigma^2}\right), \tag{4.6}$$

where $\sigma > 0$ is the standard deviation of the instantaneous received signal, x, and μ is its mean value over the large scale fading spatial dimension. The theoretical PDF plots of Figure 4.18 also give the same result if the received signal is converted into a linear scale and the lognormal probability density function employed in computing the PDF. The lognormal density function is given in [111] as:

$$P_{\mathrm{LGNM}} = \frac{1}{x\sigma\sqrt{2\pi}} \exp\left(\frac{-(\log x-\mu)^2}{2\sigma^2}\right). \tag{4.7}$$

An important point to observe about Figure 4.18 is that the co- and cross-polar LHCP signals have been shifted by 3dB to the left away from their respective RHCP values for increased clarity. If this was not done, the two co-polar and the two cross-polar signals would almost exactly overlap. The LOS fading channel has also been referred to as Channel Fading State1 and the mean values of the co-polar and cross-polar signals for this channel are respectively 0dB and -7dB.

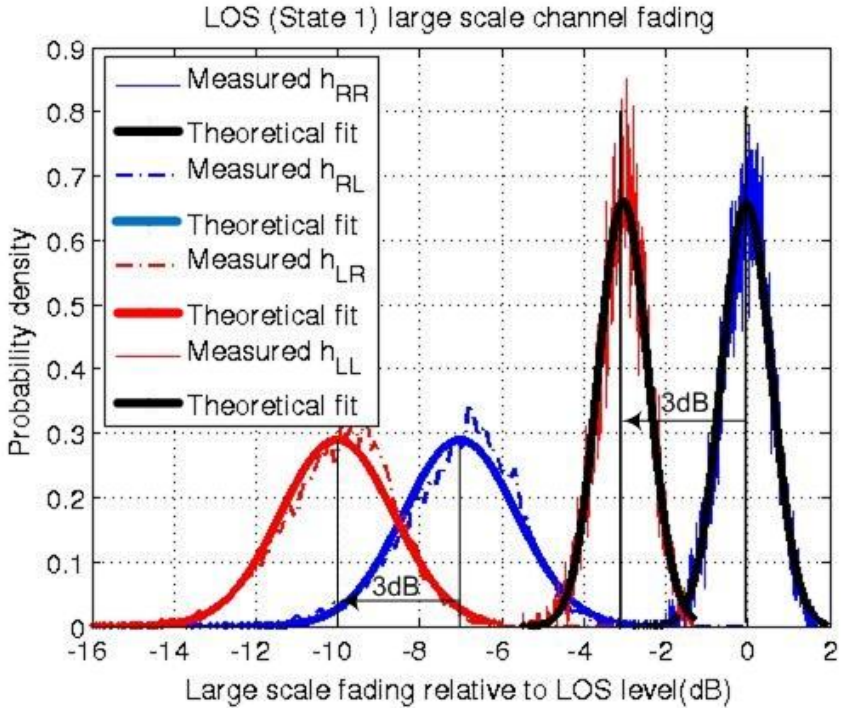

Figure 4.18: Empirical and theoretical fit of lognormally distributed large scale fading of LOS received signal

The second channel type that has been characterised is described as obstructed line of sight (OLOS). Since there are different levels or depths of obstruction that is experienced in the LMS channel, this channel type has been split into two main types: OLOS1 and OLOS2. OLOS1 represents a channel that is lightly shadowed, where the co-polar signals are greater than the cross-polar signals (and similar to the LOS case) while OLOS2 represents a channel that is predominantly deeply shadowed and the cross-polar signals stronger than their co-polar counterparts for a greater percentage of time. The OLOS1 channel is also called Channel Fading State2 and its empirical and theoretical signal PDFs are shown in Figure 4.19.

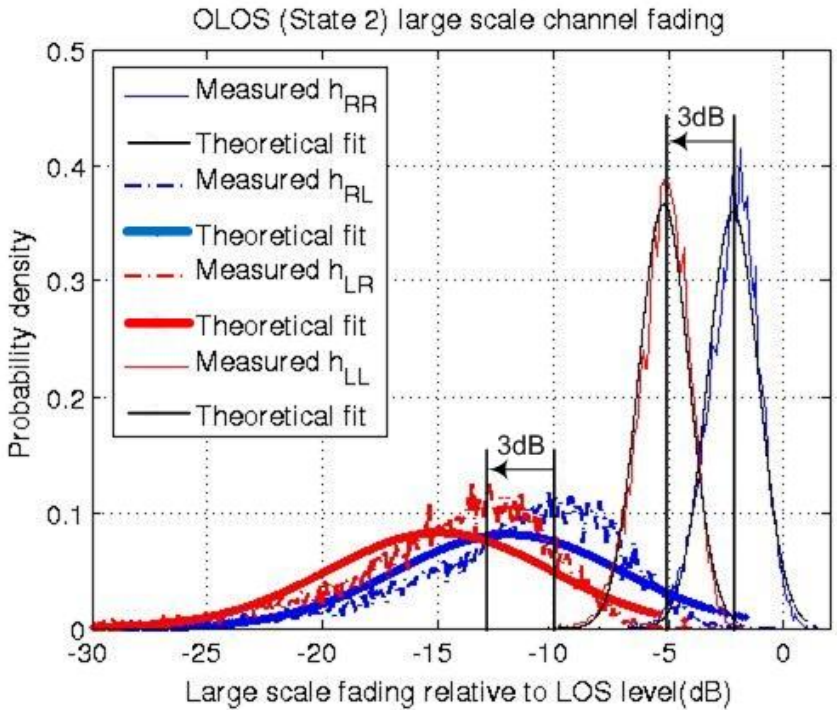

Figure 4.19: Empirical and theoretical fit of lognormally distributed large scale fading of OLOS received signal

As with the previous figure, the co- and cross-polar LHCP signals of the OLOS1 channel in Figure 4.19 have been shifted to the left by 3dB from their respective RHCP counterparts for better clarity. It is observed that the co-polar channels are lognormally distributed as indicated by the good match between their empirical and theoretical PDF plots. Also, although the cross-polar channels follow a lognormal distribution, their empirical values are not as well matched with their theoretical values as is the case in the LOS channel.

Figure 4.20 shows the large scale fading characteristics of the OLOS2 channel. In this case, the co- and cross-polar signals have been displaced to the right and left of their observed mean values by 5dB to 10dB. Otherwise, the PDF plots would have clustered around -6dB and -7dB for the cross-polar and the co-polar signals respectively. As observable, all distributions are approximations of the lognormal distribution, each with different degrees of deviation.

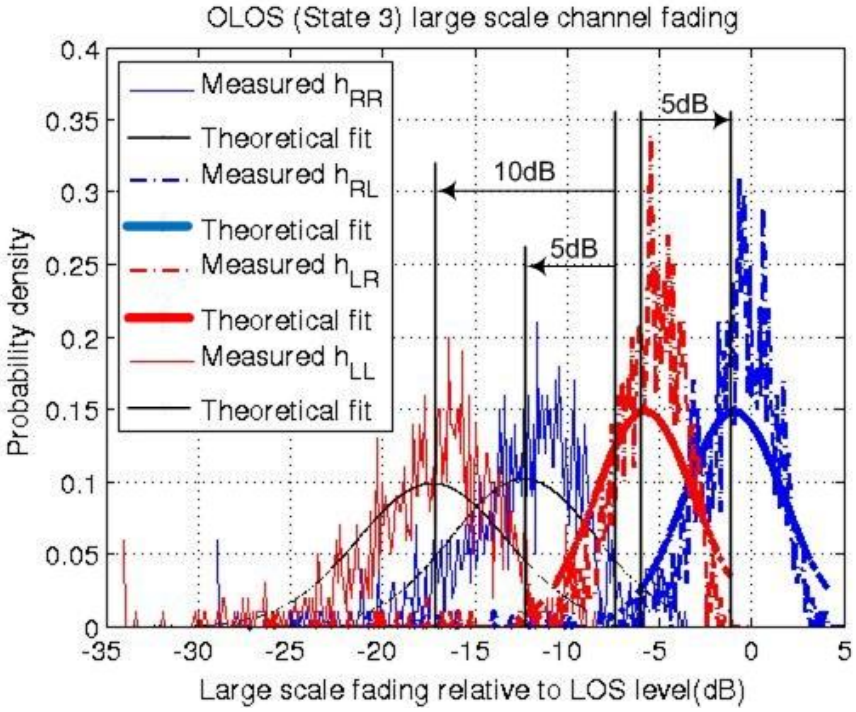

Figure 4.20: Empirical and theoretical fit of lognormally distributed large scale fading of a different OLOS received signal

The last of the large scale fading characteristic is shown for a channel that is predominantly in the non-line of sight mode (NLOS), which is given in Figure 4.21. In this channel type, all four sub-channels of the dual circular polarised LMS MIMO channels have the maximum density of their empirical PDFs hovering around -17dB while their maximum empirical PDF values are about -20dB. All four channels in this state (Channel Fading State4) are still relatively lognormal. A summary of the large scale fading characteristics of the four defined channel states of the dual circular polarised LMS MIMO channel is given in Table 4-2.

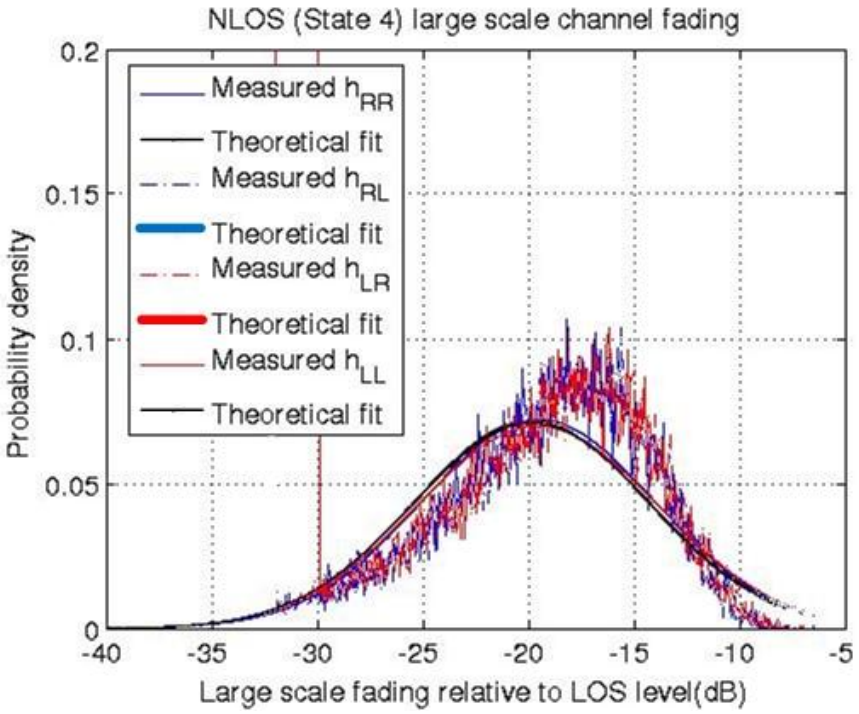

Figure 4.21: Empirical and theoretical fit of lognormally distributed large scale fading of signal receive in NLOS conditions

Table 4-2: Large scale fading statistics for dual circular polarised LMS channel

Channel State	**Received signal power (Path loss component)**			
	Co-polar channel		**Cross-polar channel**	
	Mean value (dB)	**Standard deviation (dB)**	**Mean value (dB)**	**Standard deviation (dB)**
State1 (LOS)	-0.04	0.61	-7.04	1.37
State2 (OLOS1)	-3.20	1.09	-11.98	4.89
State3 (OLOS2)	-9.79	3.93	-7.87	2.18
State4 (NLOS)	-19.76	5.47	-19.53	5.57

A phenomenon worth further investigation is the disparity that sometimes exists between the mean and standard deviation values of the co-polar RR and the co-polar LL channels even when the channel data comes from the same measurement run. As earlier mentioned, this may have to do with the slightly different radiation patterns of the orthogonally polarised antennas. The extracted mean and standard deviation values of Table 4-2 are averages of the two co-polar and two cross-polar channels for each of the channel fading states. These values are in close agreement with those published in [72]. The statistics

shown in Figures 4.18 to 4.21 and Table 4-2 were estimated using a MATLAB maximum likelihood estimation algorithm and at 99% confidence intervals.

4.2.4.4 Small Scale Fading Statistics - Rice Factor and Channel Cross Correlation

The importance of classifying of the recorded channel data into their correct fading states is once again emphasised here as this strongly determines if the Rice factor can be computed with reasonable accuracy. The Rice factor, defined as the ratio of the direct signal component to its multipath component, is determined using statistical maximum likelihood estimation on one section (a section comprising multiple of the channel correlation distance) at a time. LOS sections are expected to have higher Rice factors than OLOS and NLOS sections, and the distributions of obstructed propagation periods should tend towards being more Rayleigh than Ricean distributed. The use of large scale fading data sections to determine the small scale Rice and Rayleigh fading statistics ensure that sections of mixed distributions (e.g. when conditions change from LOS to OLOS and vice versa) are avoided and also helps to confirm that the Lee sampling criterion [112] is obeyed within the chosen data sections. Therefore, while not violating the Lee sampling criterion, the Rice factor computed using different numbers of data samples should remain relatively unchanged if all the samples chosen are within the same channel fading section.

Figure 4.22 shows a scatter plot of the estimated Rice factor and the normalised average received signal power of a mostly LOS fading channel. The received signal power has been normalised with respect to the path loss component of a purely LOS fading channel, which itself has been given the value of 0dB. The normalisation can be referred to as a localised averaging process whereby the path loss component has been removed for each small scale fading section. Since the path loss has been removed, the remaining signal in the case of the LOS channel shown in the x-axis of Figure 4.22 is the average received signal resulting from localised scattering. Therefore each plotted point in the scatter diagram represents a Rice factor value and its corresponding average scattering loss component, and these are both computed from a section of sequentially recorded narrowband channel coefficients. As earlier explained, a section of channel coefficients is

composed of single length or multiple lengths of the minimum correlation distance. The choice of using single or multiple lengths depends on the Lee sampling criterion, that is, how fast the average value of the path loss component is changing.

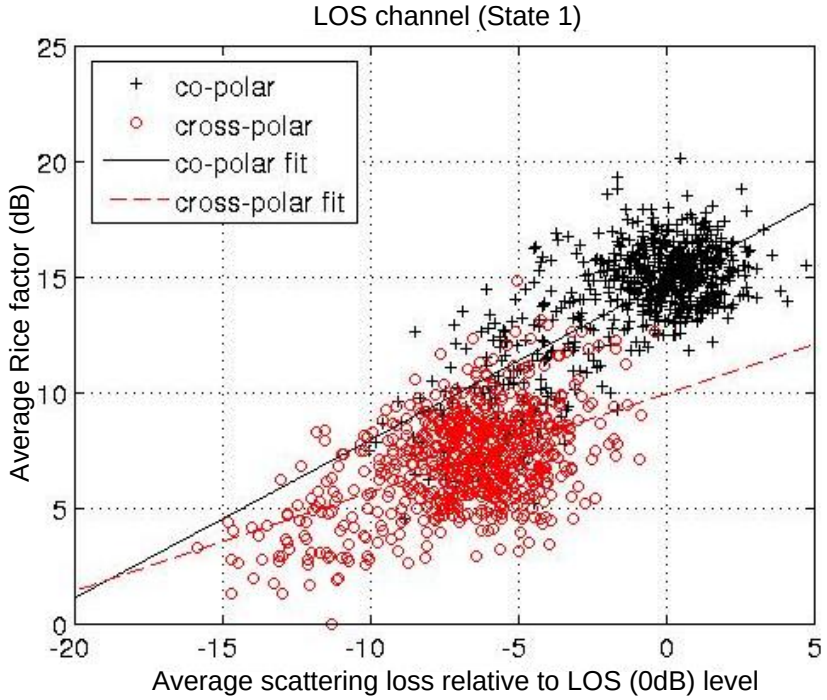

Figure 4.22: Average Rice factor versus normalised average scattering loss relative to LOS level for the LOS channel fading state

As shown in Figure 4.22, the average scattering loss of the co-polar channel is lower than that of the cross-polar channel and their difference in dB is equal to the average channel and antenna dependent polarisation discrimination ratio (denoted as M and χ in the previous chapter). Increasing the clutter/scatterers in the channel (e.g. the OLOS or NLOS channels) can only serve to increase the scattering loss and reduce the corresponding Rice factor values as is shown in the OLOS-type and NLOS channels of Figures 4.23 to 4.25. Note that in the OLOS-type and NLOS channels, in addition to an increase in the localised scattering loss, there is also a shadowing loss component in the received signal level due to the presence of large intervening objects. The localised normalisation applied to these channels only removes the average path loss component one small scale fading section at a time. Therefore the x-axis of Figures 4.23 to 4.25 represent the average scattering plus shadowing loss relative to the LOS channel fading level.

A convenient way to analyse the trend behind scatter diagrams is by way of curve fitting and in the LOS channel fading state as shown in Figure 4.22, there is an underlying linear relationship between channel Rice factor and the corresponding path loss component.

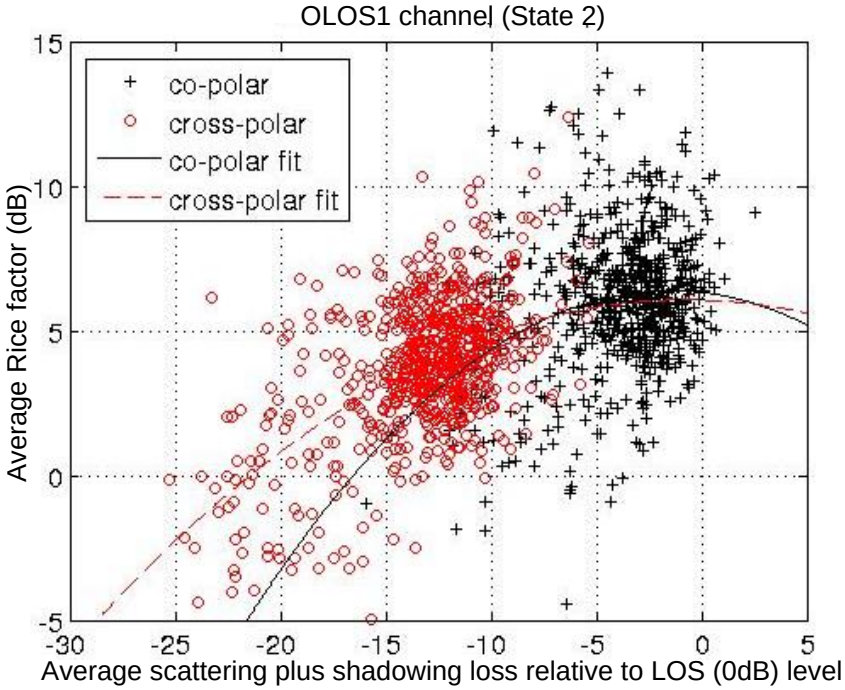

Figure 4.23: Average Rice factor versus normalised average scattering plus shadowing loss relative to LOS level for the OLOS1 channel fading state

A straight line equation is usually described as:

$$y = c + m_1 x, \tag{4.8}$$

where c and m_1 are coefficients representing the intercept and the slope respectively. It is usually assumed that the independent variable, x (which in this case is the average Rice factor), is measured without any error and all the errors reside in the dependent variable, y (being the average path loss). Note that the choice of dependent or independent variable for the purpose of determining the underlying trend behind the Rice factor versus path loss scatter diagram in this thesis is arbitrary. Therefore, employing the linear least squares estimation method [113], the first order polynomial of equation (4.8) was used in fitting the scatter plots of Figure 4.22. Note also that the fit may not always be linear and of first order, as is the case with the co-polar Rice factor fit of the OLOS1 channel in Figure 4.23; hence the required polynomial for curve-fitting can have more than two

coefficients and be of second or higher order. Therefore polynomial equations used in the curve fitting in this thesis are more generally represented by:

$$y = c + m_1 x + m_2 x + \cdots + m_j x, \tag{4.9}$$

where j represents the number of independent variables; or in the case where j represents the order of polynomial, the equation can take the form of:

$$y = c + m_1 x^j + m_2 x^{j-1} + \cdots + m_j x. \tag{4.10}$$

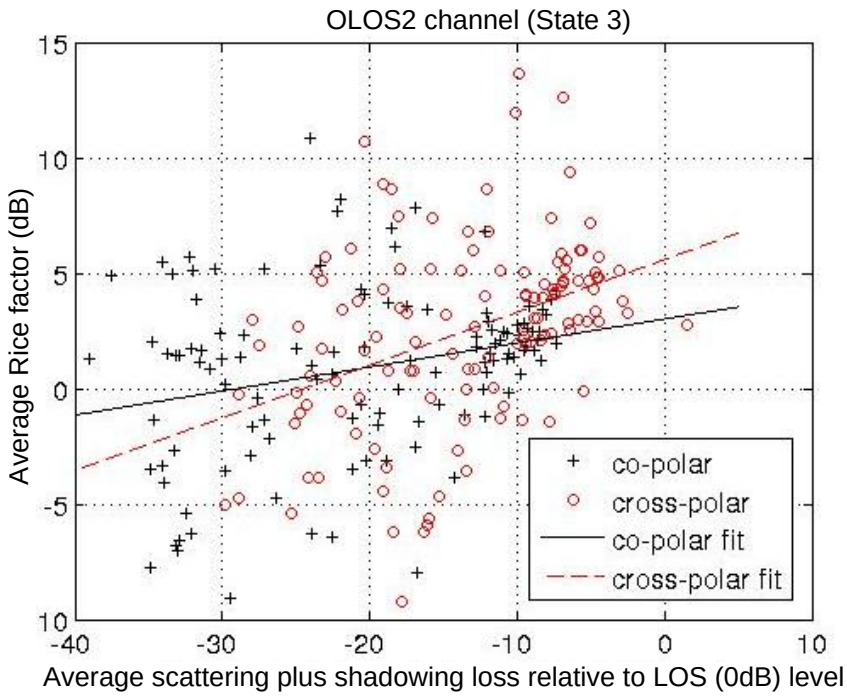

Figure 4.24: Average Rice factor versus normalised average scattering plus shadowing loss relative to LOS level for the OLOS2 channel fading state

Shown in Figures 4.24 and 4.25 are the scatter diagrams and their respective fitted plots for the predominantly OLOS2 and NLOS dual circular polarised LMS MIMO channels. In all cases, the least squares method serves to estimate the coefficients in the polynomial fitting equations by minimising the sum of the squares of residuals. Residuals are the differences between observed values (the provided scatter points) and the fitted values. Observe in Figures 4.24 and 4.25 that there is a wider scattering of average Rice factors and average scattering plus shadowing loss compared with the LOS and OLOS1 channel

states. A summary of empirical parameters derived from the state based small scale channel data analysis of Figures 4.22 to 4.25 is given in Table 4-3.

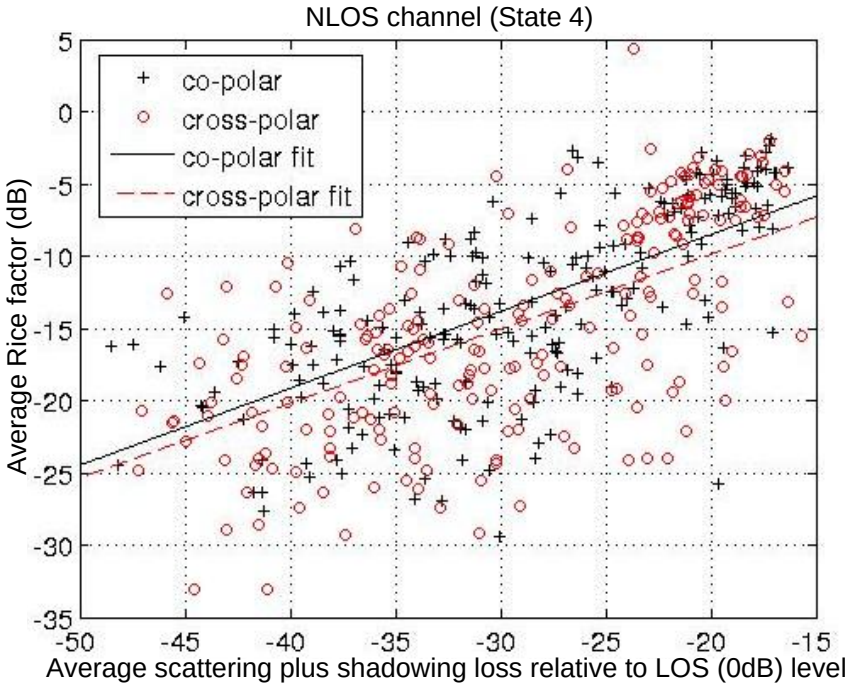

Figure 4.25: Average Rice factor versus normalised average scattering plus shadowing loss relative to LOS level for the NLOS/Rayleigh channel fading state

Table 4-3: Mean polarisation discrimination factor and average channel Rice factor

Channel type	**Mean channel and antenna polarisation discrimination factor (dB)**	**Average Rice factor (dB)**	
		Co-polar channel	**Cross-polar channel**
LOS (State 1)	7	15	7
OLOS 1 (State 2)	9	6	4
OLOS 2 (State 3)	-2	2	4
NLOS (State 4)	0	-4	-8

Lastly for this section and explained below is the relationship between the channel Rice factor and the mean co- and cross-polar channel correlations of the dual circular polarised LMS MIMO channel. This small scale first order channel statistics has not yet been fully published (see [114]) and this thesis, including a written up journal article [115] by the author, represents the first time that this is being presented and thoroughly analysed. The relationship in question is shown in Figure 4.26, having derived it from channel data

from the two measurement campaigns of this thesis and the previous channel measurements of P. King [3].

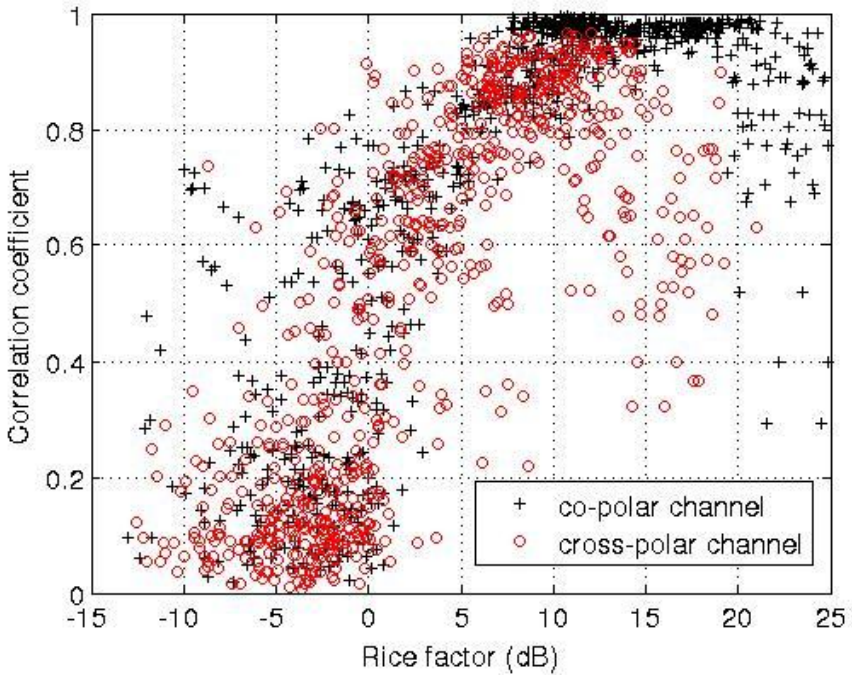

Figure 4.26: Scatter diagram showing the Rice factor–channel correlation relationship for the dual circular polarised LMS MIMO channel

A first step towards understanding and subsequently modelling the Rice factor–channel correlation relationship of Figure 4.26 is to choose the correct equation, whose parameters when estimated with minimal error would closely fit the observed distribution. One of such equations is a second order polynomial derived from (4.10). Hence the polynomial fitted curves for the Rice factor–channel correlation statistics of the co- and cross-polar channels is shown in Figure 4.27 and the equation used is given in Table 4-4, where the Rice factor is in dBs.

Although Figure 4.27 provides a general trend of the Rice–correlation relationship, it is most likely misleading since it predicts that correlation would fall as Rice factor increases beyond 15dB. This is at variance with theory and a plausible explanation for this is the inherent errors within the Rice factor and correlation coefficient estimation algorithms. For the sake of completeness, Table 4-4 contains the estimated parameters of the polynomials used in fitting the Rice distributions of Figures 4.22-4.25 and Figure 4.27.

Also included is their goodness of fit statistics, which helps one to decide how good the models are at predicting the dependent variables.

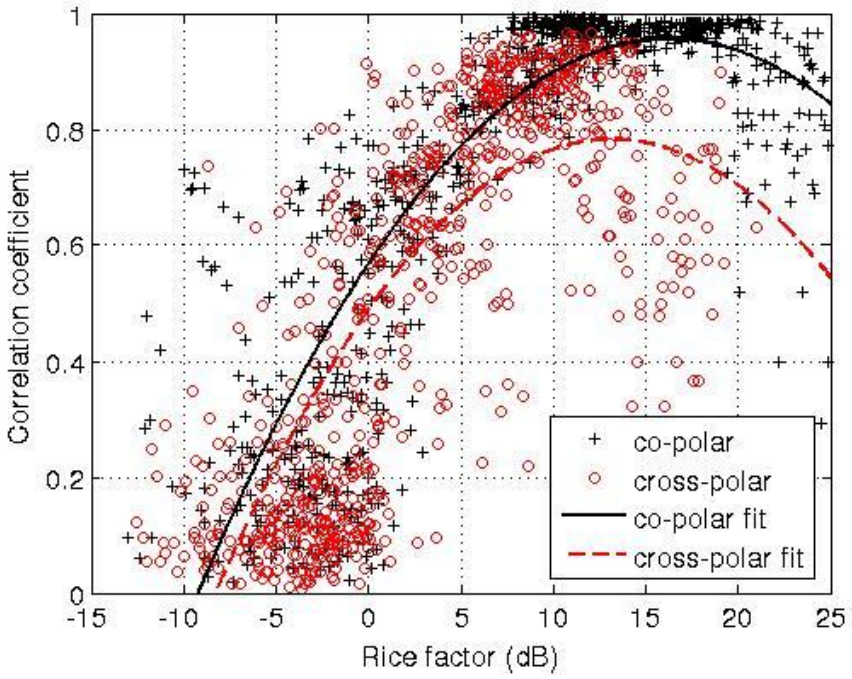

Figure 4.27: Rice factor–channel correlation relationship with polynomial fits showing general trend

Table 4-4: Estimated coefficients and goodness of fit statistics for small scale fading

Channel type		**Polynomial fit equation**	**Least squares coefficient estimates**			**Goodness of fit statistics**		
			c	***m*$_1$**	***m*$_2$**	**SSE**	**r^2**	**RMSE**
LOS (State1)*	Co-pol	$c + m_1x$	14.720	0.6612	-	2.12e+3	0.5311	1.7208
	X-pol	$c + m_1x$	9.673	0.4079	-	2.14e+3	0.2503	1.7787
OLOS1 (State2)*	Co-pol	$c + m_1x + m_2x$	6.427	-0.0514	-0.0256	4.26+3	0.0581	2.4381
	X-pol	$c + m_1x + m_2x$	6.277	-0.0162	-0.0151	3.68e+3	0.2843	2.2663
OLOS2 (State3)*	Co-pol	$c + m_1x$	3.801	0.1508	-	1.50e+3	0.1360	3.6460
	X-pol	$c + m_1x$	6.782	0.2712	-	1.45e+3	0.2328	3.4333
NLOS (State4)*	Co-pol	$c + m_1x$	1.777	0.5016	-	4.63e+3	0.4381	4.6072
	X-pol	$c + m_1x$	0.5089	0.5321	-	7.43e+3	0.3661	5.8390
All States†	Co-pol	$c + m_1x + m_2x^2$	0.5676	4.78e-2	-1.47e-3	26.92	0.6976	0.1628
	X-pol	$c + m_1x + m_2x^2$	0.4883	0.0448	0.04883	38.7	0.5744	0.2062

In Table 4-4, * indicates the linear fits to the average Rice factor versus average path loss while † indicates the fit to the Rice-channel correlation curve. SSE stands for sum of

squares due to error, also called the residual sum of squares. This statistic gives a measure of the squared scatter of the observed values around those calculated by the fitted equation [113]. An SSE approaching zero indicates that the model has very small random errors and the fit will predict the dependent variable with good accuracy. As can be observed, the SSEs for the individual channels are quite large, only those for the prediction of the Rice-channel correlation relationship are in the double digits. However, these are still very poor fits. $\mathbf{r}^2$ measures how successful the fit is in explaining the variation within the data, while RMSE is the standard error of regression. An RMSE close to zero indicates that the fit is very useful in predicting the dependent variable.

An aspect of the scatter plot of Figure 4.27 that is detrimental to polynomial curve fitting is the issue of clusters. As can be observed, the correlation versus Rice factor values are sparsely clustered at both the upper and lower end of the Rice factor range relative to the middle section. This results from the overwhelming majority of the channel data having Rice factors of between -5dB and 15dB, hence the channel correlation coefficients are more densely clustered in this region. Ordinarily, the extreme isolated sparse values (otherwise called outliers) outside the main trend would have been ignored since they tend to have a greater influence on curve fitting algorithms than the centrally clustered values [113], but these values can only be ignored at our peril if the real cause of their existence is unknown. Besides, outliers have been known to be the source of a great many Nobel prizes. Therefore, even though there are doubts regarding the reduction in the cross correlation between the two cross-polar channels as Rice factor increases beyond 12.5dB, Figures 4.28 and 4.29 still include the negative slope for the sake of completeness. It is then recommended that with the availability of more channel data, efforts should be made to conclusively uncover the reason behind the observed negative slope.

Therefore, following the method of [116], a better way to understand the trend behind the Rice factor–correlation data is to slice down the data into different Rice factor class sizes and obtain unique mean and standard deviation values for the Rice factors and correlation coefficients of each of these class sizes. The width of the class size, or granularity, depends on the area of interest and for the dual circular polarised LMS-type propagation the 0dB to 10dB region is of significant interest. This is because apart from the ‘good’ LOS (State1) propagation scenarios with Rice factor values beyond 10dB as indicated in

chapter 3, users of satellite enabled land mobile receivers may spend considerable time in shadowed (OLOS1 – State2) channel conditions. These users would still expect good quality service delivery in these conditions and an understanding of the channel characteristics in this scenario is invaluable. Hence, Table 4-5 contains the mean and standard deviation values of Rice factor and co- and cross-polar channel correlation coefficients for Rice factor granularities of 1dB and 5dB. The variable granularity also ensures that enough samples are available to get statistically significant results.

Table 4-5: Mean and standard deviation values of complex correlation for varying Rice factors from measured channel data

Rice factor range (dB)	**Co-polar channels (h_{RR} and h_{LL})**				**Cross-polar channels (h_{RL} and h_{LR})**			
	Rice factor		Channel cross-correlation		Rice factor		Channel cross-correlation	
	Mean value	Std dev	Mean value	Std dev	Mean value	Std dev	Mean value	Std dev
-15 – -10	-11.8673	0.7121	0.2390	0.1560	-11.1773	0.7830	0.1219	0.0811
-10 – -5	-7.1666	1.3743	0.2845	0.2103	-6.9810	1.4682	0.1593	0.1297
-5 – 0	-2.2235	1.3727	0.3195	0.2244	-2.3535	1.3489	0.2478	0.2065
0 – 1	0.5092	0.3003	0.4155	0.2377	0.3987	0.2653	0.4253	0.2357
1 – 2	0.5606	0.3099	0.5883	0.1854	1.4995	0.2966	0.5796	0.1962
2 – 3	2.4775	0.3126	0.6208	0.1773	2.4738	0.2961	0.6609	0.1448
3 – 4	3.5198	0.2478	0.7019	0.0874	3.5779	0.2776	0.6583	0.1774
4 – 5	4.6708	0.3064	0.7354	0.0753	4.4908	0.2766	0.6964	0.1527
5 – 10	8.1670	1.3614	0.9142	0.0690	7.3792	1.4044	0.7988	0.1562
10 – 15	12.0055	1.3425	0.9655	0.0299	12.1205	1.3960	0.8294	0.1419
15 – 20	17.4473	1.3857	0.9619	0.0389	17.0814	1.1805	0.5383	0.2371

It is observed in Table 4-5 that the Rice factor region of interest is further reduced to 0dB to 5dB for ease of Rice factor–channel correlation modelling and for reasons that will be stated later. Using the data from Table 4-5, Figure 4.28(a) is produced. Compare this with Figure 4.28(b), which is plotted with an increased granularity for the -5dB to 10dB Rice factor range. Observe that the difference in their middle section slopes is insignificant and the use of Figure 2.28(b), while simplifying channel characteristics analysis, also helps speed up the detailed channel correlation-dependent BER simulations of chapter 6.

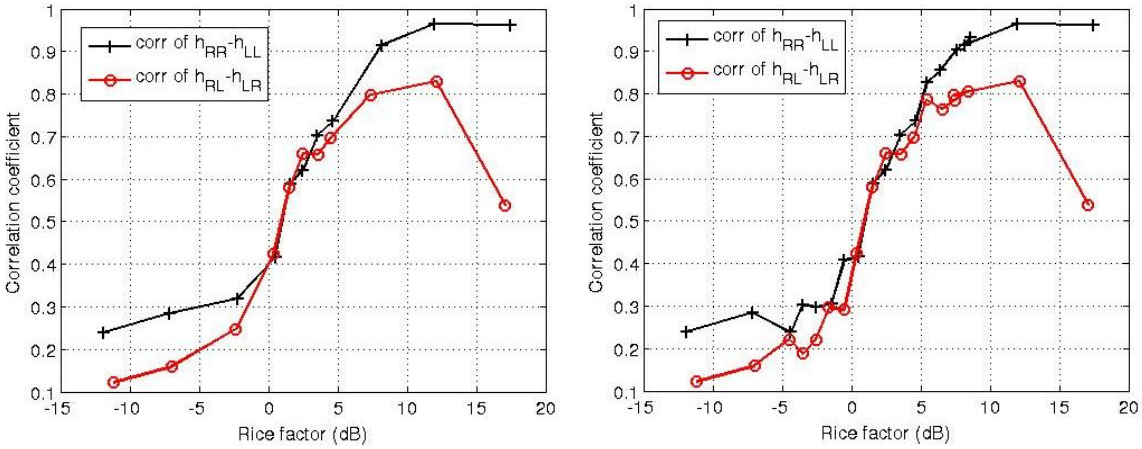

Figure 4.28: Rice factor–channel correlation relationship mean values (a) emphasising Rice factor range of 0dB to 5dB (b) emphasising Rice factor range of -5dB to 10dB

In Figure 4.29, the values of Table 4-5 have been rounded to two decimal places and incorporated in a so called centipede diagram in order to highlight the cross-correlation and Rice factor characteristics of the dual circular polarised LMS MIMO channels. Observe that from a Rice factor of -2.5dB up to 12.5dB, the characteristics of the co- and cross-polar channels are very similar. There is an almost linear increase of correlation coefficient with increasing Rice factor. This presents a very interesting modelling clue that wouldn't have been possible just relying on the goodness of fit statistics from polynomial fit curves. The actual modelling attempt is a subject for chapter 5.

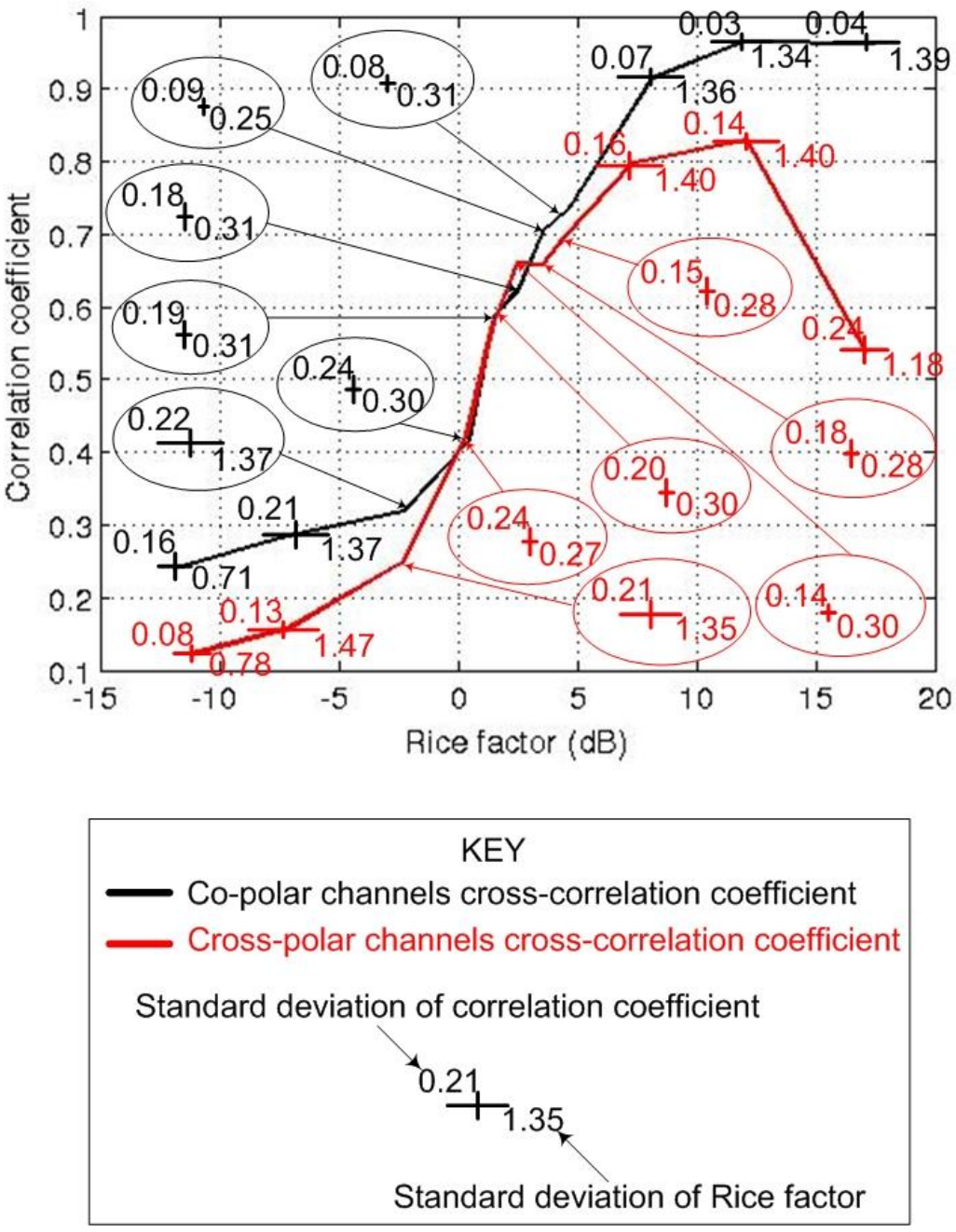

Figure 4.29: Rice factor–channel correlation relationship with details of mean and standard deviation values of correlation coefficients and dB-valued Rice factors

4.3 Conclusions

It can be conclusively inferred from the data of Figures 4.22 to 4.27 and Table 4-4 that the use of orthogonal circular polarisation, though providing some level of channel independence, cannot provide the independent fading needed to implement conventional MIMO techniques in LMS channels. Hence in order harness the proposed advantages of MIMO in this exacting channel, other techniques which take into cognisance the peculiar characteristics of the dual polarised LMS channel need to be developed. One of these new techniques proposed in this thesis is DCPM. However, to fully test the workability of DCPM, channel data with realistic statistics (XPD, XPC, correlation and Rice factor) for different fading conditions is needed. Using measurements alone to provide such data would be too cumbersome, time consuming and expensive. Only a well-developed channel model having the flexibility to easily tune between different channel parameters can allow for the workability of DCPM to be properly tested.

In arriving at the above conclusion, this chapter first of all laid down the details of previous dual circular polarised LMS measurement campaigns and two additional measurements campaigns that were carried out by the author. The measurement campaign procedure and equipment used in channel sounding have been explained in great detail. Channel characterisation, which involved extracting the narrowband first order channel characteristics, is the other important aspect that was discussed in this chapter. It was shown with the help of PDF and polynomial fits to scatter plots that most of the channel statistics follow expected theoretical trends and are similar to results obtained in earlier measurements. Finally, in the course of channel characterisation, a new relationship, the Rice factor-channel correlation statistics, was uncovered for the dual circular polarised LMS MIMO channel. This relationship, which has been partly published in a conference paper, “Channel Characteristics Analysis of the Dual Circular Polarized Land Mobile Satellite MIMO Radio Channel [114]”, is used as a guide in chapters 5 and 6 to aid in channel modelling and uncovering the BER characteristics of the dual polarised LMS MIMO channel.

Chapter 5

5 Modelling the Dual Circular Polarised LMS MIMO Channel

Channel models are very important tools used by satellite radio network operators, communication standards developers and system optimisation engineers for various purposes ranging from planning and rolling out of new services to trouble-shooting and optimisation of network system resources. A simple and generic channel model that may be very useful to network planning engineers may be grossly inadequate for system optimisation engineers. It is therefore necessary for the land mobile satellite (LMS) multiple-input multiple-output (MIMO) channel model to be developed in this thesis to be based on empirical results obtained from channel measurements and for it to simple and generic yet accurate enough to represent average characteristics of large scale channel conditions and at the same time and to possess additional tuneable parameters that can be adjusted in order to portray specific small scale channel fading conditions. The tuning flexibility built into the model would make it suitable for use by a wide range of wireless communication practitioners. Thus in line with the modelling trend found from extensive literature survey, the model to be developed in this thesis will follow a correlation based stochastic approach and use a few controlling parameters. These parameters include the channel Rice factor and cross-polar coupling ratio, the antenna cross polar discrimination ratio and the cross-correlation coefficients of the co- and cross-polar channels of the dual circular polarised LMS MIMO channel.

5.1 Proposed Channel Model

The model proposed in this thesis follows the stochastic approach as with most LMS models. The asymmetric nature of the LMS channel, with scatterers only located within the vicinity of the land mobile receiver, ensures that time dispersion of the channel is

minimal. Hence it is reasonable for the model presented here to only consider the narrowband aspects as the channel coherence bandwidth of satellite systems is in most cases always greater than their system bandwidths. Where larger system bandwidths are required, the orthogonal frequency division multiplexing (OFDM) technique can be used to slice the system bandwidth down into narrower frequency chunks with multiple sub-carriers and thus eliminating wideband channel effects. The stochastic modelling approach adopted here can also be referred to as an empirical-stochastic or a physical-statistical approach since the model's parameters are tuned with respect to measurements (empirical) from real (physical) channels. The only aspect of this model, which could have easily been modelled using a deterministic approach is the free space path loss between the satellite and the land mobile terminal. However, this is not necessary because there is very little difference in the path loss within a satellite's footprint/coverage area, and as such the model only concerns itself with statistically describing the attenuation effects of the environment within the vicinity of the land mobile receiver – i.e. all propagation interactions happening between the first scatterer and the receive antenna. It is assumed that effects of the deterministic path loss component have been completely normalised out of the proposed channel model and the different states of the model are described with respect to the LOS state.

The dual circular polarised LMS MIMO channel model in this thesis follows the four-state approach of [72] to model large scale fading (shadowing) while an empirical-statistical approach is used in modelling the observed small scale fading. Each of the states represents a combination of high or low co-polar and cross-polar signal powers. Since the interdependence of fading between the orthogonally polarised co-polar and the cross-polar channels of the dual circular polarised MIMO channel is initially ignored, modelling them using the well-established SISO approach of [63],[117] suffices for a start. Note that the SISO approach to LMS MIMO channel modelling has recently been gaining critical acclaim as it has been the method of choice in [3],[18],[73] and [118] and simplified versions of it have recently been used in [71],[72]. The next important modelling step is to impose onto the SISO sub-channels the large scale and small scale channel fading relationships uncovered during the measured channel data analysis. The proposed model simplifies and improves upon the previous models and the following

sections will explain how the model employs the Markov state approach to describe large scale fading (shadowing) before explaining the intricacies of modelling the small scale channel fading.

5.1.1 Modelling the Large Scale Fading – The Markov State Approach

The deep and shallow fades usually experienced in narrowband LMS channels make it impossible for single distributions to appropriately describe such channels. Hence, following the channel characterisation exercise of chapter 4, in which large scale fading of the dual circular polarised LMS MIMO channel was divided into sections of different average received signal powers, the proposed model follows the Markov chain approach of Fontan [60],[62],[63] and King [72] to model the large scale fading. The model is shown in Figure 5.1.

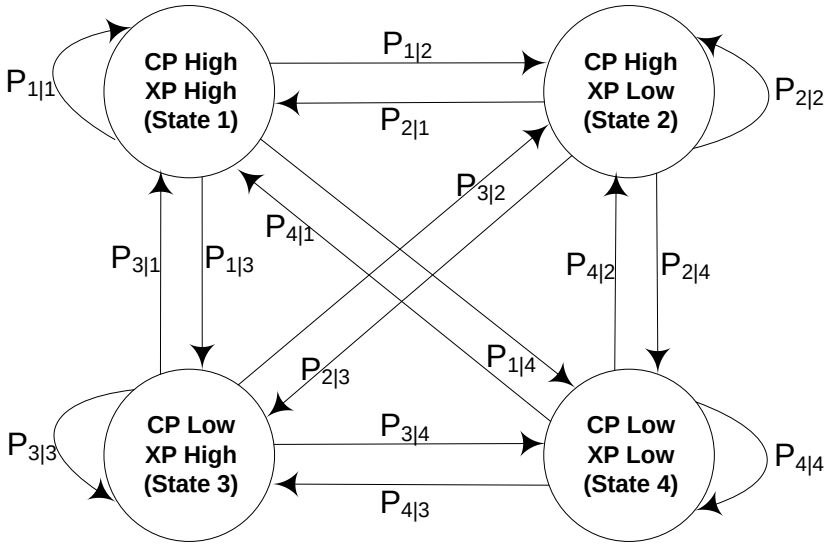

Figure 5.1: Four-state Markov model illustrating state change probabilities

In Figure 5.1, $P_{i|j}$ represents the probability of moving from state *i* to state *j*. The reasons for choosing the four state Markov model are as follows:

1. Based on empirical analysis of measured channel data, there are definite thresholds for when the received co-polar and cross-polar signal powers can be characterised as having dropped from their high LOS (State1) level to lower OLOS (States2 and 3) or NLOS (State4) levels or vice versa.

2. The received power levels of the cross-polar signals generally follow the time evolution (in the large scale fading domain) of the received co-polar signals. However, these are scaled by the propagation channel's cross polar coupling (XPC) ratio and the cross polar discrimination (XPD) ratio of the receive antennas.
3. Three different depths of large scale fading have been observed and relative to the LOS fade level, the fade depths of the co- and cross-polar signals have been characterised as OLOS1, OLOS2 and NLOS (see section 4.2.4.3).
4. OLOS1 or State2 type fading were found to occur in light shadowing conditions, wherein a drop in the received signal power mainly resulted from the attenuation effects of intervening vegetative matter. In this state, the co-polar component retains its property of being proportionally stronger than the cross-polar component; therefore it is labelled as 'CP High, XP Low' in Figure 5.1.
5. OLOS2 or State3 type fading was found to occur during brief periods of blocking by solid man-made objects. In addition to the drop in received signal power, a striking feature of this state is that the received cross-polar power becomes slightly greater than the received co-polar power. Therefore this state is labelled as 'CP Low, XP High.' Apart from [72], this type of fading in the dual circular polarised LMS channel has also recently been reported in [5].
6. NLOS or State4 type fading occurs when the direct LOS paths and specular reflected components have been completely blocked. Both the co- and cross-polar signal level in this state are at the lower end of the LMS receiver's dynamic range; therefore they are labelled as 'CP Low, XP Low'.
7. Since state transitions are never abrupt but are found to slowly evolve with time, a low pass infinite impulse response filter such as used in [3], is employed to impose the observed time evolution.
8. A state probability matrix is built by deriving probabilities of when the channel stays or transits from one state to another. Channel sampling in order to determine the large scale state probability matrix is done within the channel correlation distance.

Note that the state probability matrix specifies the interdependence between the mean co-polar and cross-polar signal levels, thereby removing the need for a large scale correlation matrix. A Markov model is suitable because it easily approximates the switching characteristics between the different channel fading states. One of the earliest uses of the Markov model for the LMS channel can be found in [119]. The Markov model described in steps 1 to 8 above is graphically illustrated in Figure 5.2 and the low pass filtering process of step 8 is given by:

$$y_n = \left(x_n + \exp\left(\frac{-vT}{T_C}\right) y_{n-1}\right) \odot \sigma_m \left(1 - \exp\left(\frac{-vT}{T_C}\right)\right) + S_m, \tag{5.1}$$

where y_n represents a normalised filtered sample of the of the average large scale fading level, x_n represents an unfiltered sample of the large scale fading level, v represents the mobile receiver's velocity, T is the sampling time, T_C is the channel correlation distance and n is the sample number of the large scale fading level. σ_m and S_m are respectively the empirical standard deviation and the relative mean large scale fading levels; both obtained from measured channel data. The terms on the right hand side of (5.1) but left of the Hadamard product operator, $\odot$, represent the low pass filter while the terms on its right are factors to normalise the filtered signal back to its required level.

When viewed in the log (dB) scale, the filtered and normalised large scale fading for each state result in the characteristic lognormal fading observed in chapter 4.

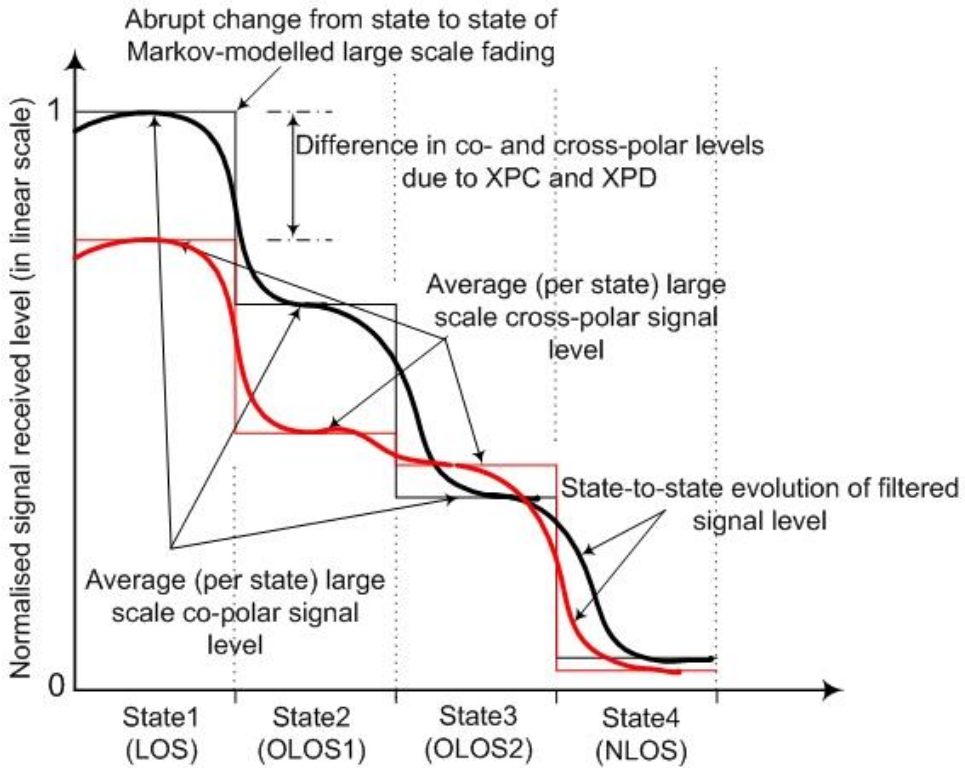

Figure 5.2: Illustration of relative mean signal levels/path loss (not to scale) of the large scale fading experienced in dual circular polarised LMS MIMO channels

5.1.2 Modelling the Small Scale Fading – The Empirical-Stochastic Approach

In the LMS channel, scatterers are only local to the land mobile receiver and as a result signals reach the receiver through direct paths or through paths involving single or several instances of reflections, diffractions and refractions. It is the constructive and destructive adding of these arriving signals, after having propagated through paths of different lengths that manifest as small scale fading. Since small scale fading phenomenon is random in nature and takes place over dimensions of a few wavelengths, it is usual practice to use the Rice probability distribution function to describe it.

As earlier explained, Rice factor is the ratio of received signal power arriving from a LOS path (or a dominant specular reflected path) to the sum of the signal power arriving from diffuse multipath reflections. Therefore since the modelling approach adopted in this thesis is state-based, with different levels of co- and cross-polar LOS components for each of the states, the Rice factor is bound to vary very widely from state to state. Also,

considering that multipath components arrive randomly from all directions with equal probability, a realistic way to model them is by way of an appropriately scaled (i.e. in terms of their mean value and standard deviation and with respect to the LOS/coherently received component) probability distribution. Finally, not forgetting to take into account the XPC and XPD effects of the dual circular polarised LMS MIMO channel and with emphasis on the small scale fading aspects, the proposed channel model is completely described as follows:

$$\mathbf{H}_{\text{DualCirc}} = \mathbf{H}_{\text{XPD}-\text{XPC}} \odot (\mathbf{H}_{\text{RiceF}} \odot \mathbf{H}_{\text{LOS}}) + (\mathbf{H}_{\text{RaylF}} \odot \mathbf{H}_{\text{MPC}}), \tag{5.2}$$

where $\mathbf{H}_{\text{XPD-XPC}}$ is the antenna XPD and channel XPC matrix, which contains elements χ_i, with subscript *i* representing distinct χ-values for each of the four states. This matrix was introduced in (3.26) and repeated here as:

$$\mathbf{H}_{\text{XPD}-\text{XPC}} = \begin{bmatrix} 1 & \sqrt{\chi}_i \\ \sqrt{\chi}_i & 1 \end{bmatrix}. \tag{5.3}$$

In equation (5.2), $\odot$ indicates a Hadamard multiplication operation and $\mathbf{H}_{\text{LOS}}$ is the mean level of the coherently received component in each channel fading state relative to the LOS level. $\mathbf{H}_{\text{RiceF}}$, $\mathbf{H}_{\text{RaylF}}$ and $\mathbf{H}_{\text{MPC}}$ respectively represent a Rice factor matrix for the coherently received signal, a Rice factor matrix for the multipath signals and a matrix containing the multipath components. As in (5.3) where *i* represents distinct values of their respective elements for each of the four states, these three channel model components are mathematically expressed as:

$$\mathbf{H}_{\text{RiceF}} = \begin{bmatrix} \sqrt{\left(\frac{K_{RR}}{K_{RR}+1}\right)_i} & \sqrt{\left(\frac{K_{RL}}{K_{RL}+1}\right)_i} \\ \sqrt{\left(\frac{K_{LR}}{K_{LR}+1}\right)_i} & \sqrt{\left(\frac{K_{LL}}{K_{LL}+1}\right)_i} \end{bmatrix}, \tag{5.4}$$

$$\mathbf{H}_{\text{RaylF}} = \begin{bmatrix} \sqrt{\left(\frac{1}{K_{RR}+1}\right)_i} & \sqrt{\left(\frac{1}{K_{RL}+1}\right)_i} \\ \sqrt{\left(\frac{1}{K_{LR}+1}\right)_i} & \sqrt{\left(\frac{1}{K_{LL}+1}\right)_i} \end{bmatrix}, \tag{5.5}$$

$$\mathbf{H}_{\mathrm{MPC}} = \begin{bmatrix} e^{-j\theta_{RR}} & e^{-j\theta_{RL}} \\ e^{-j\theta_{LR}} & e^{-j\theta_{LL}} \end{bmatrix}. \tag{5.6}$$

For equations (5.4)-(5.6), K_{RR} and K_{LL} represent Rice factors of co-polar RHCP and co-polar LHCP channels respectively, K_{RL} and K_{LR} are cross-polar Rice factors of signals respectively originating from an RHCP and an LHCP transmit antenna; θ_{ij} represent random phases of the narrowband channels. $\mathbf{H}_{\mathrm{MPC}}$ is of zero mean and specific but distinct standard deviation values for each of the channel states.

The channel model of equation (5.2) is a rather detailed expression and a simplified version of it, earlier published in [114], is given as:

$$\mathbf{H} = \begin{bmatrix} h_{RR} & h_{RL} \\ h_{LR} & h_{LL} \end{bmatrix} = \begin{bmatrix} \alpha + \sigma\exp(-j\theta_{RR}) & \beta + \sigma\exp(-j\theta_{RL}) \\ \beta + \sigma\exp(-j\theta_{LR}) & \alpha + \sigma\exp(-j\theta_{LL}) \end{bmatrix}, \tag{5.7}$$

where α and β are the large scale fading components and respectively represent the mean signal powers (per state) of the co-polar and cross-polar channels. These are respectively equivalent to the main diagonal terms and the off diagonal terms of the product of the first three terms on the right hand side of equation (5.2). $\sigma\exp(\theta_{\mathrm{i,j}})$ represents the multipath component, and is equivalent to the product of the last two terms on the right hand side of (5.2). Note that σ in this case is the standard deviation of the multipath components.

Finally, in dealing with channel correlation, this model simplifies previous channels models like the Liolis [18] and King's models [3],[72] by considering only the cross-correlation between the two co-polar channels, C_{CP}, and the cross-correlation between the two cross-polar channels, C_{XP}. The Cholesky factorisation product, defined in [120] as:

$$\mathbf{A} = \mathbf{R}^T\mathbf{D}\mathbf{R} \tag{5.8}$$

is for inducing the desired cross correlation. In (5.8), **A** is a Cholesky factorised symmetric matrix, **R** is a Cholesky product of **A**, $\mathbf{R}^T$ is **R** transposed and **D** is a diagonal matrix in which the correlation coefficients contained in **R** is imposed. Thus to induce correlation on the generated small scale channel data, we have:

$$\mathbf{H}_{COR} = \begin{bmatrix} h_{RR|COR} & h_{RL|COR} \\ h_{LR|COR} & h_{LL|COR} \end{bmatrix}, \tag{5.9}$$

$$\text{where} \begin{bmatrix} h_{RR|COR} & x_{off} \\ x_{off} & h_{LL|COR} \end{bmatrix} = \mathbf{C}_{CP}^{T} \begin{bmatrix} h_{RR} & 0 \\ 0 & h_{LL} \end{bmatrix} \mathbf{C}_{CP}, \tag{5.10}$$

$$\text{and} \begin{bmatrix} h_{RL|COR} & x_{off} \\ x_{off} & h_{LR|COR} \end{bmatrix} = \mathbf{C}_{XP}^{T} \begin{bmatrix} h_{RL} & 0 \\ 0 & h_{LR} \end{bmatrix} \mathbf{C}_{XP}. \tag{5.11}$$

In (5.10) and (5.11), the $h_{ij|COR}$ (i,j = R,L) terms on the left hand side represent the correlated co- and cross-polar channels of the overall $\mathbf{H}_{COR}$ channel matrix shown in (5.9). The off-diagonal terms, labelled x_{off} are unwanted products of the matrix multiplication on the right, which are discarded. Note that the co-polar and cross-polar cross-correlation matrices that have been Cholesky factorised as expressed in (5.8) are respectively defined by:

$$\mathbf{C}_{CP} = \begin{bmatrix} 1 & C_{CP} \\ C_{CP}^{*} & 1 \end{bmatrix}, \tag{5.12}$$

$$\text{and } \mathbf{C}_{XP} = \begin{bmatrix} 1 & C_{XP} \\ C_{XP}^{*} & 1 \end{bmatrix}. \tag{5.13}$$

Therefore, the model proposed in this thesis induces empirically obtained cross-correlation in a way that is similar to the King-Brown-Kyrgiazos model using an approach as simple as the Kronecker model but adopting a slightly different process. In contrasting this method with the Kronecker approach, it is worth pointing out that while the Kronecker method uses transmit-end and receive-end correlation coefficients to build positive semi-definite 4×4 matrices for correlation induction purposes, the new method uses two separate 2×2 matrices of cross-channel correlation coefficients. There is no requirement for these 2×2 matrices to be positive definite nor positive semi-definite. Finally, although the Kronecker method is adequate for 2×2 Rayleigh channels, it fails woefully to depict the correlation experienced in dual circular polarised LOS channels [65], therefore previous dual polarised LMS channel models that have followed this approach have done so at their own detriment.

After inducing correlation in the small scale fading data, the generated and consequently up-sampled large scale fading data is added to the small scale fading part as shown in (5.2). The next section provides directions on how this is achieved.

5.1.3 Step-wise Generation of Time Series Data for the Dual Circular Polarised LMS MIMO Channel

The following describes the steps used in generating the time series data for the large scale fading part of the dual circular polarised land mobile satellite channel:

1. Specify the centre frequency, the receiver velocity, the minimum duration of time or distance spent in one state, the sampling spacing in metres or seconds, the total travelled distance, the minimum channel correlation and the 4×4 state probability matrix. Also, for each of the four states, specify the matrix containing the XPD-XPC factors ($\mathbf{H}_{\text{XPD-XPC}}$), the matrix of mean co-polar and cross-polar Rice factors ($\mathbf{H}_{\text{RiceF}}$), and the matrix of mean co-polar and cross-polar signal levels relative to the LOS level ($\mathbf{H}_{\text{LOS}}$).
2. Using the state probability matrix, set up a loop to randomly draw from a set of numbers lying between 0 and 1. The number of iterations of this loop should be equal to the earlier specified total travel distance divided by the minimum duration (in metres) in each state. Each draw, when probability-tested against the state matrix, identifies which state has been chosen and specifies the time spent or distance travelled in that state. Subsequent draws allow one to move on to a different state or to remain in the same state.
3. Within the loop described above and according to (5.2), multiply out:
$$\mathbf{H}_{\text{LargeScale}} = \mathbf{H}_{\text{XPD}-\text{XPC}} \odot (\mathbf{H}_{\text{RiceF}} \odot \mathbf{H}_{\text{LOS}}).$$
4. Filter and normalise the co- and cross-polar large scale fading levels of $\mathbf{H}_{\text{LargeScale}}$ using equation (5.1).
5. Up-sample to match the finer resolution (in terms of sample spacing in time or distance) of the yet to be generated small scale fading.

Table 5-1 gives the empirical averages of the large scale fading parameters for the proposed model. These values were extracted after thorough analyses of data from several different measurement runs of the measurement campaigns described in chapter 4.

Table 5-1: Average parameter values for modelling large scale fading of the dual circular polarised channel

	χ (for $\mathbf{H}_{\text{XPD-XPC}}$)	$\mathbf{H}_{\text{RiceF}}$		$\mathbf{H}_{\text{LOS}}$	
		$K_{11} = K_{22}$	$K_{12} = K_{21}$	co-polar	x-polar
LOS (State 1)	0.2	12 dB	8 dB	1	1
OLOS 1(State 2)	0.1	6 dB	4 dB	0.9	0.9
OLOS 2 (State 3)	0.5	2 dB	4 dB	0.5	0.8
NLOS (State 4)	1	-4 dB	-8 dB	0.001	0.001

The parameters of Table 5-1 are average values and can range very widely in certain propagation conditions. However, for the purposes of channel modelling, strict thresholds had to be determined and the per-state average values computed from these. The process of extracting the values was both manual and tedious as it required comparing measured channel data (which in most cases came with GPS time-stamps) with detailed terrain maps and photographs to verify the type of fading being experienced. Then from the threshold values, first-order discrete-time Markov chain transitions (see [60],[117],[119]) are generated. These Markov four state transitions are defined by:

$$\mathbf{P} = \begin{bmatrix} P_{1|1} & P_{1|2} & P_{1|3} & P_{1|4} \\ P_{2|2} & P_{2|2} & P_{2|3} & P_{2|4} \\ P_{3|1} & P_{3|2} & P_{3|3} & P_{3|4} \\ P_{4|1} & P_{4|2} & P_{4|3} & P_{4|4} \end{bmatrix}, \text{ and } \mathbf{W} = \begin{bmatrix} W_1 \\ W_2 \\ W_3 \\ W_4 \end{bmatrix}, \tag{5.14}$$

where **P** is the state transition probability matrix that models the time spent (duration) in each of the states. $P_{i|j}$ is the probability of transiting from state i to state j and $\sum_{j=1}^{4} P_{i|j} = 1, \text{for } i = 1 \text{ to } 4$. **W** is the absolute state matrix which gives the probability of total time spent in the four states. $\sum_{i=1}^{4} W_i = 1$.

For the small scale channel fading, Gaussian random number generators are used following the method of Fontan [117] to generate the wanted length of complex valued random numbers. These are then filtered according to the observed Doppler spread before adding on the required standard deviation values, which are unique to each of the four Markov states. An appropriate filter is the Butterworth filter since it is has been generally accepted [117],[121], and based on observations from measurements performed by the author and P. King [3], that in LMS channels, multipath contributions mainly come from both sides of the travelled route (i.e. from the 0^o and 180^o azimuth direction assuming the

mobile travels in the 90^o direction as shown in Figure 5.3) causing the Doppler spread to cluster round the centre frequency as shown in Figures 6.67 and 6.68 of [3].

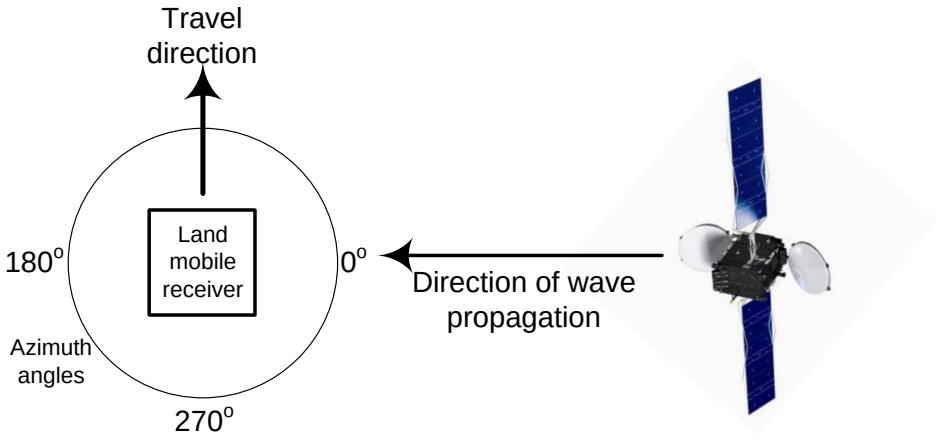

Figure 5.3: Land mobile receiver travel direction in relation to transmitting satellite

The other main aspect of small scale channel modelling is correlation induction, which is performed one correlation length at a time as explained in section 5.1.2. The model uses only the cross-channel correlations (i.e the correlation value between the two co-polar and the two cross-polar channels) since it has been proven in [122] that an increase in cross-channel correlation has more influence on, and positively affects, the MIMO channel capacity when compared with the effects of transmit-end or receive-end correlations.

Finally, the small scale fading, which has been generated at very fine sample spacing–in the order of fractions of wavelengths–is added to the up-sampled large scale fading data. In one of the measurement runs around Newlands Corner (an open/rural type environment), the following state transition matrix shown in Table 5-2 was extracted from the recorded channel data. Note that each of the rows all sum to one.

Table 5-2: Sample state transition probabilities for rural type environment

P			
$P_{1\|1}$ = 0.6942	$P_{1\|2}$ = 0.2413	$P_{1\|3}$ = 0.0098	$P_{1\|4}$ = 0.0547
$P_{2\|1}$ = 0.5670	$P_{2\|2}$ = 0.3941	$P_{2\|3}$ = 0.0107	$P_{2\|4}$ = 0.0282
$P_{3\|1}$ = 0.3187	$P_{3\|2}$ = 0.1445	$P_{3\|3}$ = 0.2396	$P_{3\|4}$ = 0.2972
$P_{4\|1}$ = 0.0956	$P_{4\|2}$ = 0.3786	$P_{4\|3}$ = 0.1872	$P_{4\|4}$ = 0.3386

A schematic diagram, based on the LMS channel model circuit diagrams in [117] and [119], showing how the proposed model generates time series channel data is given in Figure 5.4.

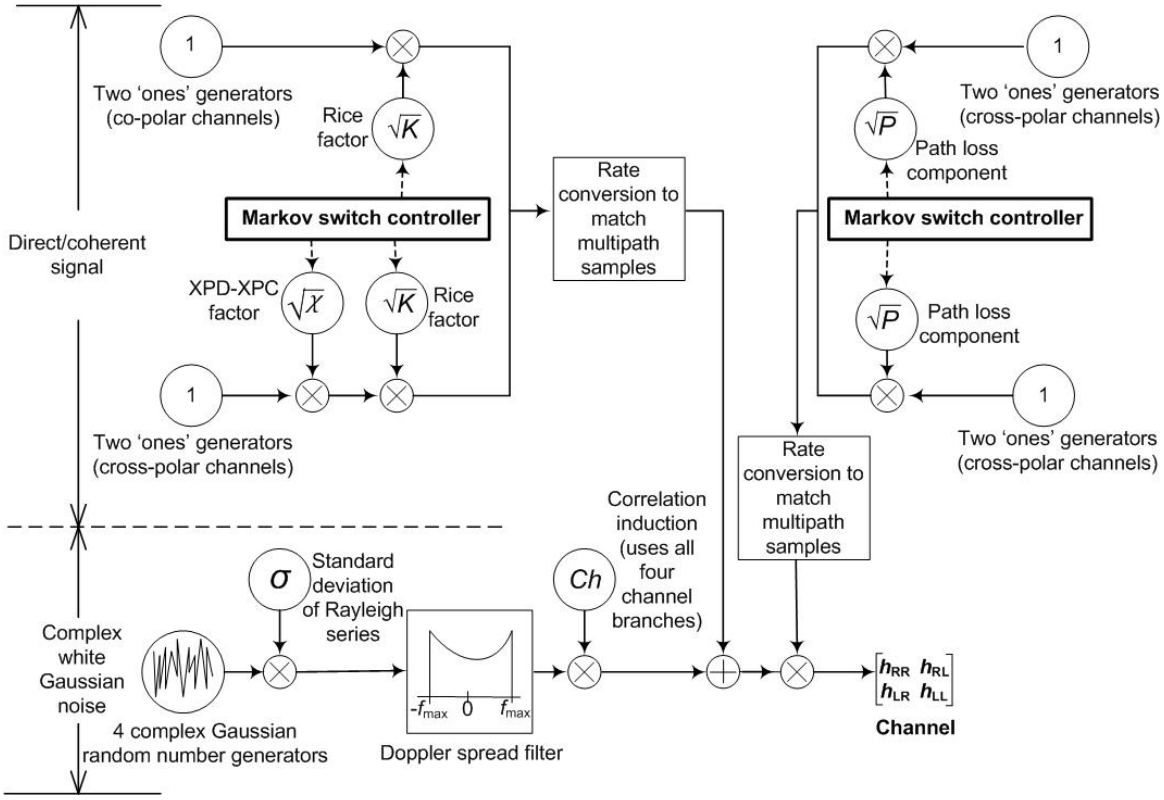

Figure 5.4: Circuit diagram for simulating the four-state Markov model of the dual circular polarised LMS MIMO channel

It is obvious from Table 5-2 that the probability of occurrence of State 3 is statistically very small; this is also true for the totality of measured channel results of chapter 4 and of the results obtained by [5]. However its inclusion in the four-state model makes for a complete description of the probable power levels of the dual circular polarised LMS MIMO channel.

A very interesting but previously ignored aspect of the dual circular polarised channel is the relationship between the Rice factor and the channel correlation. The next section of the thesis is devoted to modelling this phenomenon.

5.1.4 Modelling the Rice Factor–Channel Correlation Relationship

Following from section 4.2.4.4 where the general trend for the channel correlation–Rice factor relationship was established by way of Figure 4.29 and the equation in Table 4-4, it is necessary to develop a model to link these two parameters. Among the expected characteristics of the proposed model are the following:

1. To ensure the accurate prediction of the channel correlation within the Rice factor range of -15dB to 12.5dB.
2. To ensure the continuity of correlation prediction throughout the above state Rice factor range, even if it means using multiple slopes.
3. Expression of the model in a tractable form to allow for high speed execution in simulations.

The developed model ultimately aims to provide a better understanding of the dual circular polarised channel and enable such channels to be used in more efficient ways for present and future communication and broadcast systems. Going by the trend in Figure 4.29, the approach adopted is a two-slope linear regression method, where the model's coefficients are calculated using the least squares algorithm. The model is given as:

$$\rho_{12} = \begin{cases} \eta_0 + \eta_1 K & \text{for } (-15dB \leq K \leq x_b) \\ \eta_0 + \eta_1 K + \eta_2 K^2 & \text{for } (x_b \leq K \leq 12.5dB)' \end{cases} \quad (5.15)$$

where ρ_{12} is the channel correlation coefficient, η_0 is the constant parameter, η_1 is the slope coefficient, K is the channel Rice factor in dB and x_b is the Rice factor breakpoint in dB. Regression analysis is performed separately for either side of x_b and care must be taken to choose the right breakpoint to maintain function continuity. The algorithm for the least squares estimation works by first selecting prospective model coefficients that is deemed to fit the data. It then tests the 95% confidence bounds of the chosen coefficients and successively removes coefficients with very large bounds. Both linear and nonlinear fits are used according to the distribution of the fitted parameter. In the process of regression fitting for (5.15), outliers were treated with utmost caution because they are known to have a greater than necessary influence on the curve fitting process. Since the generally accepted methods of dealing with outliers (either by complete elimination or by

appropriate weighting [123]) are both are fraught with unique problems, this thesis adopts a simpler approach by only fitting the data within regions of relatively few extreme outliers. Apart from Figure 4.29, which identified outliers (in terms of the correlation axis) by way of their large standard deviation values, the Grubbs Test [124] can also be used. The regression fitted two-slope model of the Rice factor–channel correlation relationship is as follows:

$$\rho_{12|CPOL} = \begin{cases} 0.27 - 0.025K & \text{for } (-15dB \leq K \leq x_b) \\ 0.44 + 0.084K - 0.0033K^2 & \text{for } (x_b \leq K \leq 12.5dB) \end{cases}, \quad (5.16)$$

$$\rho_{12|XPOL} = \begin{cases} 0.24 + 0.0096K & \text{for } (-15dB \leq K \leq x_b) \\ 0.42 + 0.08K - 0.0037K^2 & \text{for } (x_b \leq K \leq 12.5dB) \end{cases}. \quad (5.17)$$

The appropriate choice of breakpoint, x_b, is determined through a recursive process; this lies between -2.5dB and -1.6dB. Using the models in (5.16) and (5.17), the co-polar and cross-polar channel cross correlations are superimposed on the Rice factor-channel correlation scatter diagrams and these are shown in Figures 5.5 (a) and (b). Figure 5.6(a) and (b) give an indication of the accuracy of the model by plotting the residuals of the curve fitting process. As can be observed by the decrease in the spread of the residuals at higher Rice factors (especially for the co-polar cross correlation fits), the model is fairly accurate. However its high residual spread at low Rice factors indicate that there are large errors, the causes of which need to be further investigated as more empirical channel data becomes available.

The simplified and novel channel modelling method implemented in this thesis aptly describes the large and small scale fading phenomena and also the relationship between the channel cross-correlation and the Rice factor. As is shown in the next section, the modelled channel's first and second order statistics stay consistent with measurements.

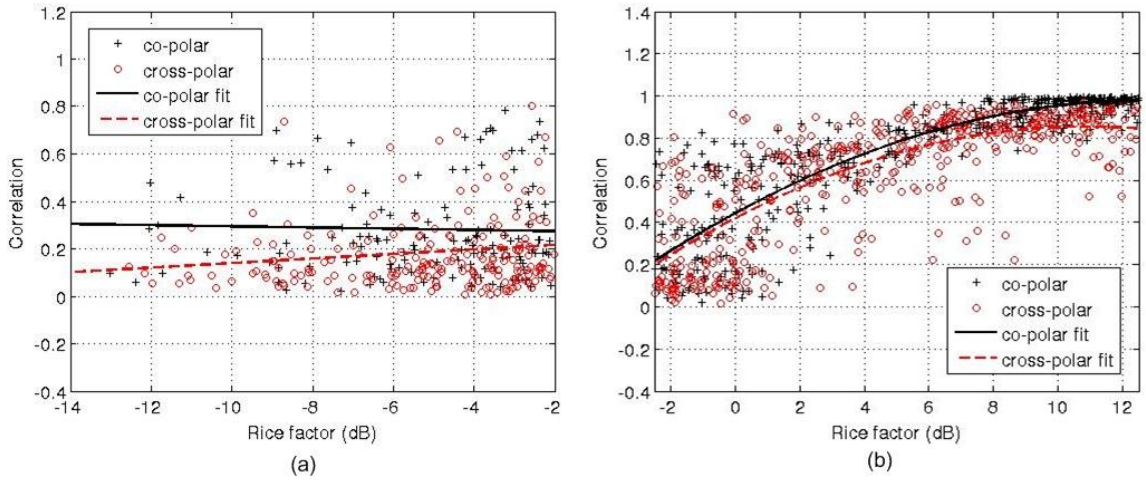

Figure 5.5: Modelled co-polar and cross-polar channels cross correlation fits for (a) lower Rice factor range and (b) upper Rice factor range

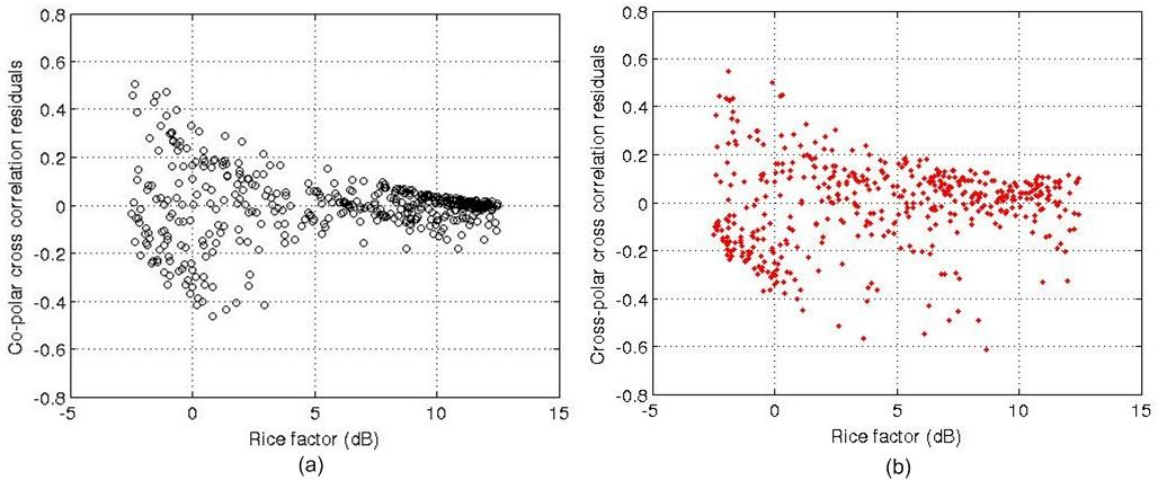

Figure 5.6: Residuals from curve fitting the upper Rice factor range for (a) co-polar channel cross correlation and (b) cross-polar channel cross correlation

5.2 Model Validation

The channel data generated from the proposed model needs to be compared against measured channel data in order to verify that the model accurately captures all the important characteristics of the measured dual circular polarised LMS MIMO channel. Resorting to use measured channel data from which the model was derived for validation purposes is because other sources of measured dual circular polarised LMS MIMO channel data (for example, [5]) were not readily available. The validation process adopted

here is worthwhile since apart from comparing direct channel characteristics like branch power distribution and Rice factor, validation involves the comparison of indirect parameters like eigenvalue distribution and channel capacity. For example, if the eigenvalue distribution of a section of measured channel data of a certain Rice factor is compared with modelled channel data of the same Rice factor and both their eigenvalue distributions match, it confirms that the model can accurately represent first and second order statistics of the LMS MIMO channel and any interdependences that exists between the individual MIMO sub-channels [72]. For first order channel characteristics, this thesis validates the model using CDF plots of branch power, eigenvalue and Rice factor distribution. Also compared for the purposes of channel model validation are the capacities of the modelled and measured channels. Validation of the second order statistics of the model is by comparing the level crossing rates and the average fade durations of the modelled channel with that of the measured channel. The recorded measured channel data used for model validation has been obtained from the measurement campaigns of King [3] and measurement campaigns I and II (see sections 4.2.1 and 4.2.2) whose elevation angles range from 5^o to 37^o.

5.2.1 Branch Power Distribution

Branch (MIMO sub-channels) power distribution of the 2×2 dual polarised LMS MIMO channel is a function of both the antenna and channel cross-polar discrimination. As a first step towards validating the channel model, CDF plots are used to compare the branch power distributions of the modelled and measured channel for different fading sections characterised in Table 5-3.

Table 5-3: Rice factor of measured and modelled channels for sections of LOS and OLOS1 fading used in Figure 5.7

	Rice factor in dB			
	LOS fading		**OLOS1 fading**	
	Co-polar channel	Cross-polar channel	Co-polar channel	Cross-polar channel
Measured channel	16.6	9.6	9.7	5.3
Modelled channel	17.2	9.9	10.1	5.6

The CDF plots are shown in Figure 5.7. Observe the very close match between the two data types for both LOS and OLOS1 fading. Note specifically that at a probability of 10^{-3}, the modelled receive signal power of the LOS fading is within 1dB of the measured channel for the co-polar MIMO sub-channels. Figure 5.7 only shows the co- and cross-polar RHCP MIMO sub-channels for LOS fading and shows only the LHCP co- and cross-polar sub-channel for OLOS1 fading for increased clarity of the plots. The close match between modelled and measured MIMO sub-channel power distributions and their Rice factor values, especially during LOS fading (which this thesis is more interested in), is a good proof that the model accurately reproduces the branch power ratios observed during measurements. OLOS2 type fading is not shown due to the limited available measured channel data while that of NLOS is omitted as this type of fading can be easily modelled using the popular Kronecker channel models. Besides, these fading conditions are not of much interest to this thesis since they do not reliably support dual circular polarisation multiplexing.

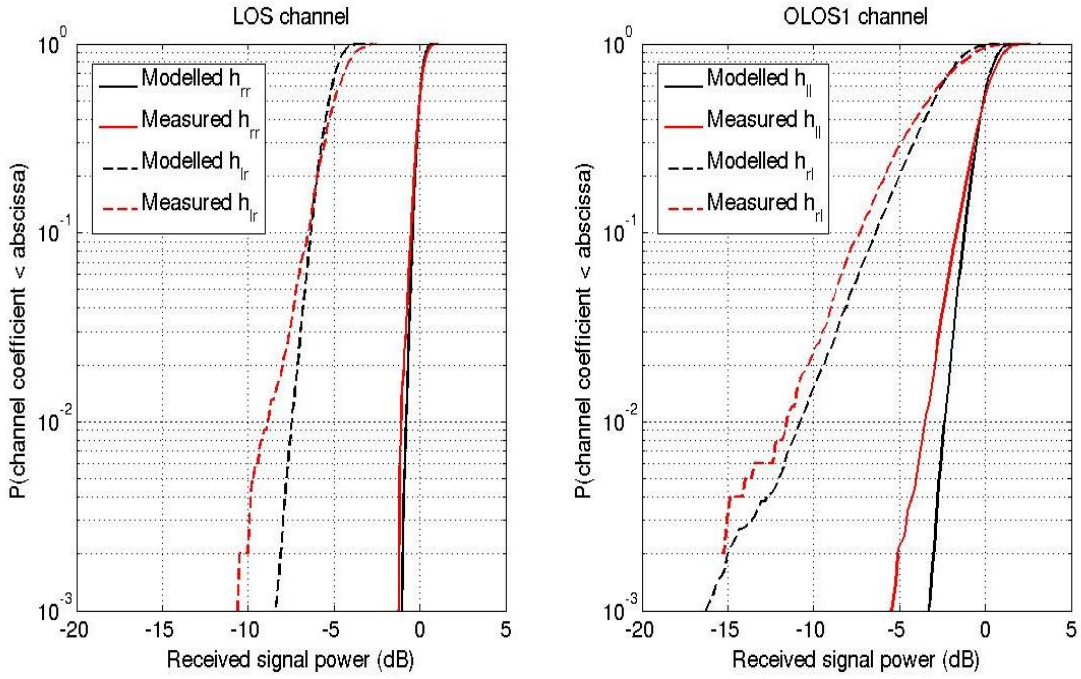

Figure 5.7: CDF plots of received signal power for LOS and OLOS1 channels

5.2.2 Eigenvalue Distribution

The distribution of eigenvalues of the dual polarised LMS channel indicates what MIMO mode–whether multiplexing or diversity–would be best suited for such a channel. A good match between the CDF of eigenvalues of the measured and modelled channel helps to confirm whether the interdependence between the MIMO sub-channels have been correctly preserved and are in line with channel fading conditions. Figure 5.8 compares the eigenvalue CDF plots of the measured and modelled channel for the same data sections that were used in generating Figure 5.7, and as can be observed, there is a very good match between the two. This serves as further proof of the accuracy of the proposed model and indicates that it can be reliably used to demonstrate the multiplexing or diversity capabilities of the dual polarised LMS MIMO channel. The left side of Figure 5.8 shows an LOS propagation scenario where the first and second eigenvalues are closely spaced with the second eigenvalue being about 6dB less than the first eigenvalue at a probability of 10^{-3}. Compare this with the plot on the right where there is about 30dB difference between the first and second eigenvalues of an OLOS1 channel. Such eigenvalue distributions point to a situation that is more suitable for diversity-combining MIMO techniques. For LOS propagation, it would be more spectrally efficient to transmit independent bit streams through the two available channels and multiplex the bit streams at the receiver. A scheme for implementing such multiplexing has been proposed in [95] and is the subject of chapter 6.

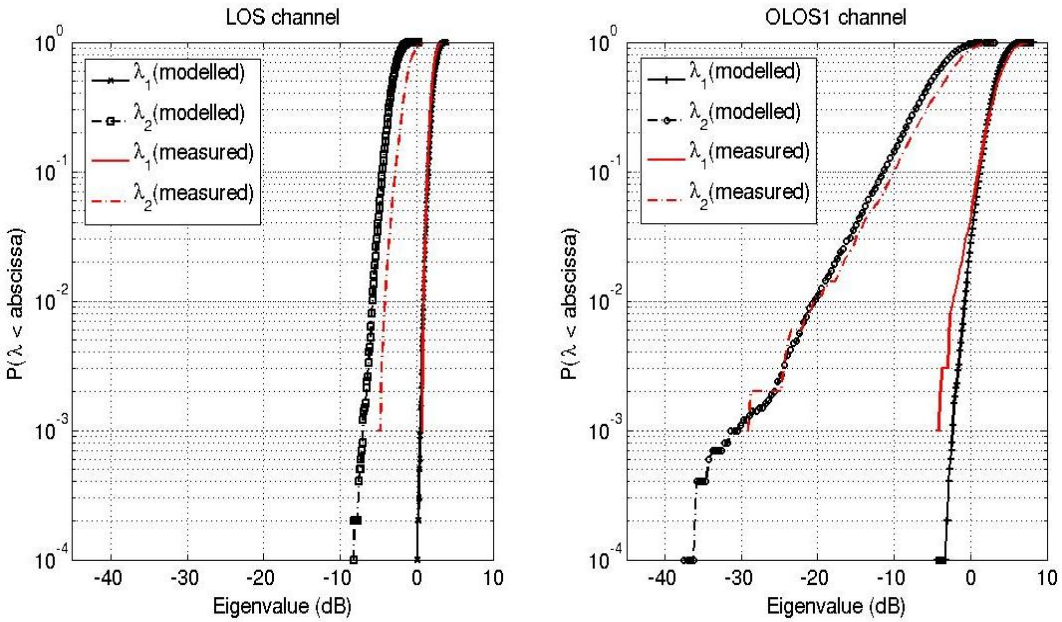

Figure 5.8: CDF plots of channel eigenvalues for LOS and OLOS1 channels

5.2.3 Channel Capacity

Another very important metric used in model validation is the Shannon channel capacity metric given in equation (2.7) for MIMO channels. Two realisations of channel capacity are used; the first of which is within the small scale fading wideband domain while the second considers the small scale fading narrowband aspects of the channel. In the small scale fading wideband domain, the channel coherence time is smaller than the duration of the transmitted codeword and as such the codeword experiences many different channel realisations. This implies that the capacity that can be supported by such a channel can only be computed as an ensemble average of its many fading instances. This average capacity is referred to as the channel ergordic capacity. In the small scale fading narrowband channel where the coherence time is much larger than the duration of the transmitted codeword, the classic assumption that the experiences channel block fading holds (i.e. the channel is quasi-static and stays the same throughout the duration of a codeword). Hence the appropriate channel capacity to use in this case is the outage capacity, which is defined as the percentage of time that a given information rate can be guaranteed by the channel [122].

For both the ergodic and the outage capacity in the ensuing comparisons of the modelled and measured channels, it is assumed that the transmit and receive link-ends both possess perfect channel knowledge and power is allocated equally to the two MIMO sub-channels. Hence in using the Shannon channel capacity equation given in (2.7), each channel matrix realisation, **H**, has been normalised with respect to the LOS signal level and the capacity computed for different SNR values. The result of this is given in Figure 5.9 where a very good fit can be observed between the measured and the modelled channel ergodic capacity predictions. The predicted SISO capacity is also included for benchmarking purposes. Note that predicted capacity of the proposed model (in its final version) given in Figure 5.9 is almost identical to that of the interim model provided earlier (see equation (3.27) and Figure 3.7). This is because channel cross correlation, which is not considered in the earlier model but is taken into account in the final model, has limited effects on the ergodic channel capacity.

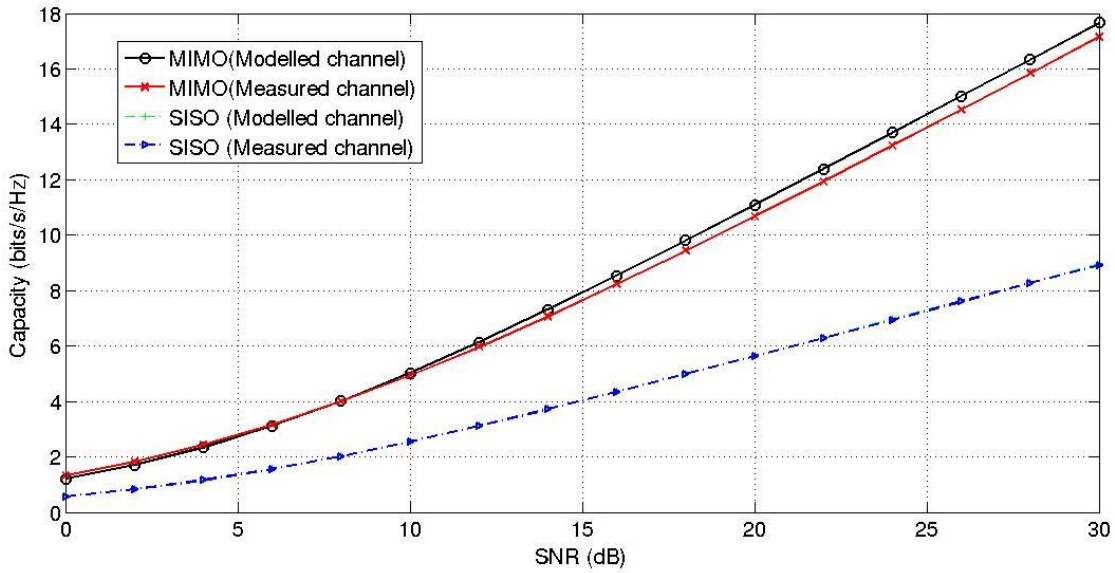

Figure 5.9: Ergodic channel capacity per SNR for modelled and measured channels

The average Rice factor of the data sections used in the ergodic capacity comparison in Figure 5.9 was 16dB. Whereas it would have been more interesting to compare modelled and measured channel capacity at different Rice factors (various levels of LOS or OLOS propagation), the aim of validating the channel model would have been defeated since variations within the Rice factor value of the measured channel data would have

introduced errors resulting from the conflicting effects of SNR and Rice factor on the channel capacity. This conflict has been explained by the ergodic capacity results in [122] (also see the analysis in section 3.2.4) where it has been shown that increasing the Rice factor decreases the channel capacity while and at the same time if transmit power is kept constant, the presence of a Ricean component (LOS) implies an increase in SNR which results in higher capacities than obtainable during periods when the channel is less Ricean (Rayleigh or OLOS).

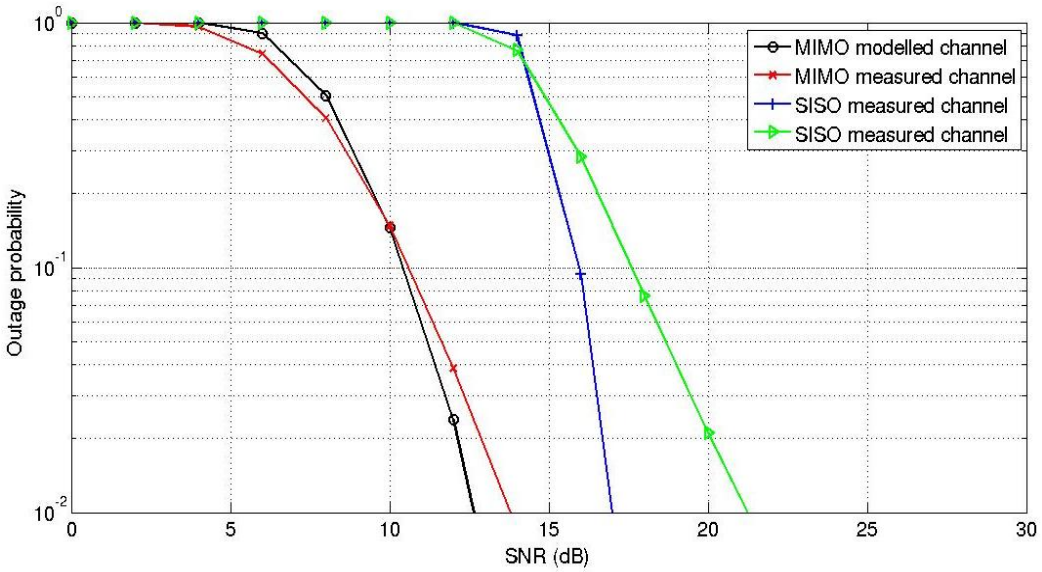

Figure 5.10: Outage probability at a capacity of 4b/s/Hz

The very good match between the measured and the modelled channel capacity is repeated in Figure 5.10 for the outage capacity predictions. When taken together, Figures 5.9 and 5.10 conclusively prove that the model can accurately predict the channel capacity.

5.2.4 Level Crossing Rate

The level crossing rate (LCR) is the rate at which a received signal crosses a specified level in the positive direction. It has great significance in the choice of transmission bit rates and coding schemes for LMS communication systems. The LCR is defined in [109] and [125] as:

$$LCR = \sqrt{2\pi} f_m r \, exp(-r^2), \tag{5.18}$$

where f_m is the maximum Doppler shift of the received signal *r*, which itself has been normalised by its RMS value. The Doppler shift component in (5.18) indicates that LCR has a dependence on the mobile terminal's velocity, making it a second order statistic. Since the modelled and measured channels in this thesis have already been normalised with respect to the LOS channel, the LCR for the co-polar channel can be computed from:

$$\frac{LCR}{f_m} = \sqrt{2\pi} |h_{RR}|^2 \, exp(-(|h_{RR}|^2)^2), \tag{5.19}$$

where $|h_{RR}|^2$ is the absolute value of RHCP co-polar channel. For a fair comparison, the LCR of measured channel data in Figure 5.11 is obtained from a single measurement run and is compared against modelled channel data that exhibits the same fading state evolution. An example of fading state evolution for the measured channel was earlier shown in Figure 4.16.

The good fit between the LCR of the co-polar and cross-polar modelled and measured channels of Figure 5.11 shows that this very important second order statistic has been accurately rendered by the proposed channel model. Observe that the highest rate of level crossings for the co-polar channels occur at around 0dB while that of the cross-polar channels occur at about -7dB. This indicates that for most of time, the value of the co-polar channel power stays at about 0dB while that of the cross-polar channel hovers around 7dB below.

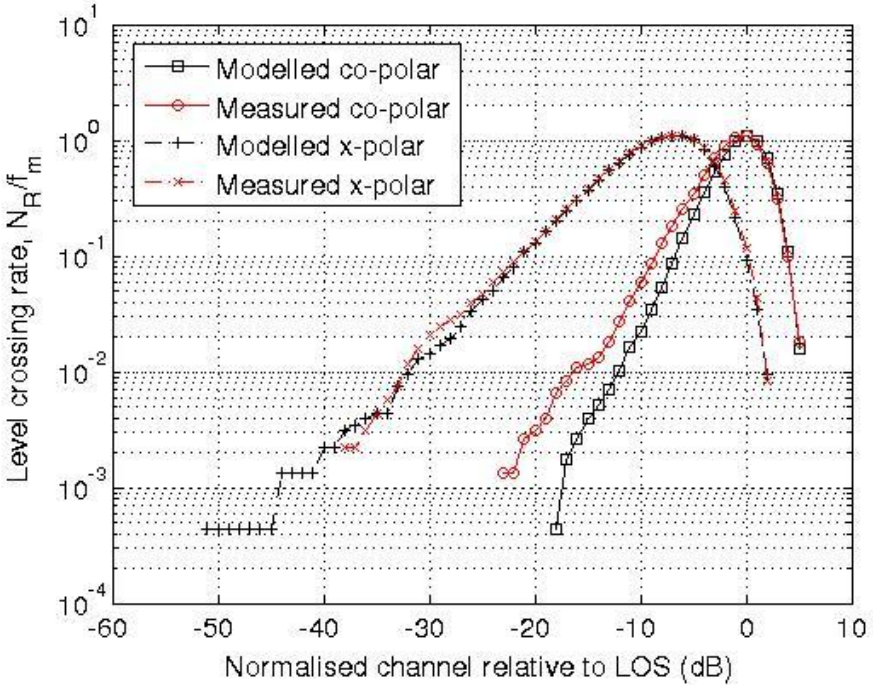

Figure 5.11: Normalised level crossing rates for co- and cross-polar measured and modelled channels

5.2.5 Average Fade Duration

In addition to the LCR, another very important second order channel statistic which needs to be represented accurately is the average fade duration (AFD), which is the length of time the received signal, r, stays below a given level, R. AFD is defined in [117] as:

$$AFD_R = \text{Prob}(r \leq R)/LCR, \tag{5.20}$$

where $\text{Prob}(r \leq R) = \sum_i t_i/T$ is sum of times (t) the signal crosses a level within the total period of observation (T). Hence the AFD can simply be computed by counting the total length of time the received signal stays below a given level and then dividing the value by the crossing rate at that signal level (the LCR).

As with the LCR, Figure 5.12 shows that the model is valid as it accurately predicts the AFD for different channel fading conditions. Observe that the length of time in seconds that the received cross-polar signal will stay below 0dB is greater than that of the co-polar channel.

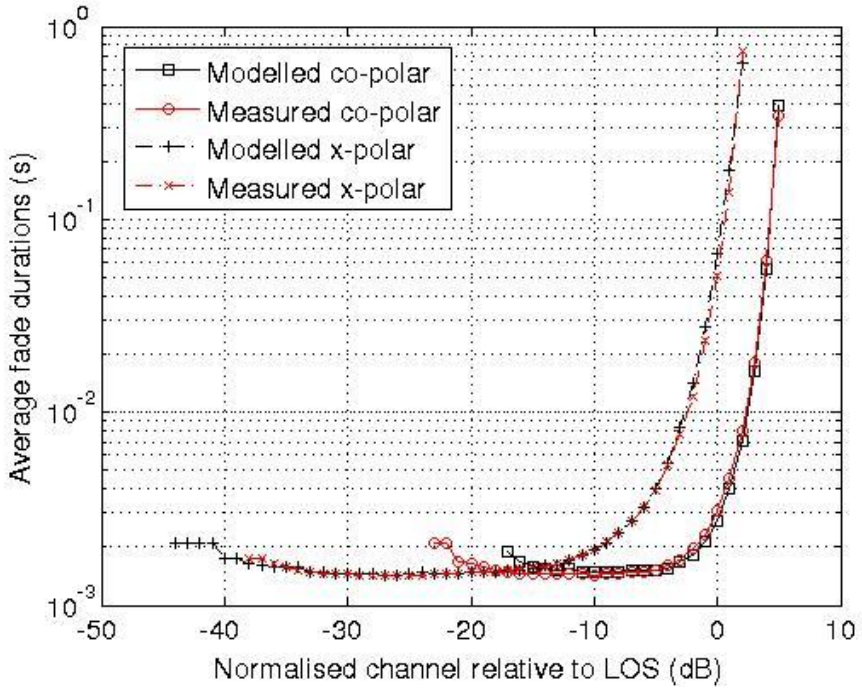

Figure 5.12: Normalised average fade duration for co- and cross-polar measured and modelled channels

5.3 Conclusions

A comprehensive model for simulating the dual circular polarised LMS MIMO channel has been presented. A stepwise procedure for building this model was also given alongside a high level schematic of its circuit diagram construct. The Rice factor-channel correlation relationship, which forms a cornerstone of the proposed model and which prior to now has never been investigated in any detail, has been presented in the form of a two-slope linear model. The values of the coefficients of the Rice factor-channel correlation model have been derived using a least squares estimation method and detailed statistical analysis has shown that given high Rice factor values, the correlation coefficient prediction of the model becomes more accurate.

Going back to the newly proposed model, by way of CDF plots comparing the branch power and eigenvalue distributions of the measured and the modelled channel, it has been shown that the model accurately predicts the first order statistics of the LMS MIMO channel. Also, to further verify the accuracy of the model, its predicted capacity and second order statistics of level crossing rates and average duration of fades have been

compared with that of the measured channel. The close agreement of all the compared modelled and measured channel parameters indicate that the model is indeed accurate and can be used with confidence to determine the effects of intervening objects within the close vicinity of the mobile terminal on the system level performance of communication systems designed for the dual circular polarised LMS MIMO channel. Among the system level indicators that may be of interest to developers of LMS MIMO systems, especially those working on the upcoming DVB-SH and DVB-NGH systems, include the effects channel cross-correlation and Rice factor on the bit error rates of various receive terminal-based channel equalisation schemes. These effects are investigated in the next chapter.

Chapter 6

6 BER Analysis of Equalisation Schemes Suitable for DCPM LMS Receivers

The potential of multiple-input multiple-output (MIMO) to achieve linear capacity increase per number of additional transmit-receive antenna pairs depends very much on the ability of the transceiver to exploit the additional spatial and/or polarisation dimensions. Having seen in chapter 3 that Dual Circular Polarisation Multiplexing (DCPM), being a simple receiver-based channel equalisation scheme, is capable of doubling the capacity of land mobile satellite (LMS) devices equipped with orthogonal circular polarised antennas, it remains to be seen how different channel fading conditions affect the bit error rates (BER) of such receivers. Therefore, this chapter uses the channel model proposed in chapter 5 alongside the channel correlation and Rice factor values obtained in chapter 3 and the proposed Rice factor-channel correlation model to determine the bit error rates achievable with practical zero forcing (ZF) and minimum mean squared error equalisation (MMSE) schemes. The results obtained and the analysis thereof help in determining how best to deploy DCPM in LMS environments. The analysis carried out is based on a Digital Video Broadcasting via Satellite to Handhelds (DVB-SH)/Digital Video Broadcasting to Next Generation of Handhelds (DVB-NGH) scenario where the satellite is the transmit link-end while the land mobile device is a receive-only terminal and the channel is assumed to be quasi-static with its coherence time long enough for several bursts of symbols to be fully transmitted and received. Parameters used and scenarios considered in this chapter are based on the DVB implementation guidelines published in [77] and the channel statistics earlier derived in chapter 4.

The BER is a particularly suitable metric for determining the best possible equalisation scheme for DCPM implementation. This is because BER measures the complete end-to-

end system performance–in terms of bits transmitted and bits correctly/incorrectly received–and takes into account the effects of noise (of the electronic and antenna subsystems), channel fading conditions and quantisation errors. Channel fading conditions relate to the level of signal obstruction and the presence of multipath components while quantisation errors depend on the modulation schemes employed; these last two parameters directly test the 'goodness' of the chosen equalisation scheme and how it influences the capacity doubling ambitions of DCPM.

6.1 DCPM System Aspects

Although orthogonal circular polarisation has long been used in multi-beam satellites for increasing the radiated power levels reaching earth terminals and inadvertently increasing the frequency reuse factor [19], [126], its use for capacity doubling has only recently been suggested and only a few papers including [2],[4] have attempted some preliminary investigation. As the name implies, DCPM is based on dual circular polarisation per satellite beam and it seeks to double the capacity of satellite broadcast systems but at the cost of increased inter-beam interference in multi-beam scenarios and/or increased intra-system interference in single (global) beam scenarios. Even though the following DCPM analysis is based on the DVB-SH and DVB-NGH framework, where it is envisaged that satellite services will be complemented by terrestrial broadcast, inter-beam interference from the same satellite or from complementary terrestrial sources is ignored and a global beam broadcast scenario is assumed in order to keep the analysis simple. Therefore in the analysis, DCPM employs practical linear channel equalisation schemes like ZF and MMSE to eliminate the intra-system interference caused by the orthogonally polarised S-band signals (2170 – 2200MHz) per satellite beam. Also, since the iterative use of linear equalisers such as V-BLAST [86] has been proven to improve interference elimination capabilities with marginal increase in system complexity, the operation of DCPM needs to be investigated using ordered successive zero forcing and ordered successive minimum mean squared error equalisation schemes. Also, BER simulations of DCPM operating under linear unordered ZF and MMSE modes in different fading conditions needs to be performed so as to determine its exact working limits.

To reveal the intricacies of the DCPM BER simulations carried out in this chapter, a high level block diagram of the mobile terminal-based DCPM equalisation architecture is provided in Figure 6.1. Here, a single user channel is assumed and shown in the diagram are the transmit data stream, available equalisation modes, the dual circular polarised channel and the composition of the received signals. A high bit rate data stream ($\boldsymbol{x}$) meant for a land mobile user is demultiplexed by the satellite into two sub-streams ($\boldsymbol{x}_1$ and $\boldsymbol{x}_2$) of lower bit rates, encoded into QPSK, 8PSK or 16APSK symbols and transmitted using each of the two orthogonally circular polarised satellite antennas. As with V-BLAST, the same constellation is used for the two sub-streams and transmission is done in bursts of L symbols. The total available transmit power is shared equally between the two antennas.

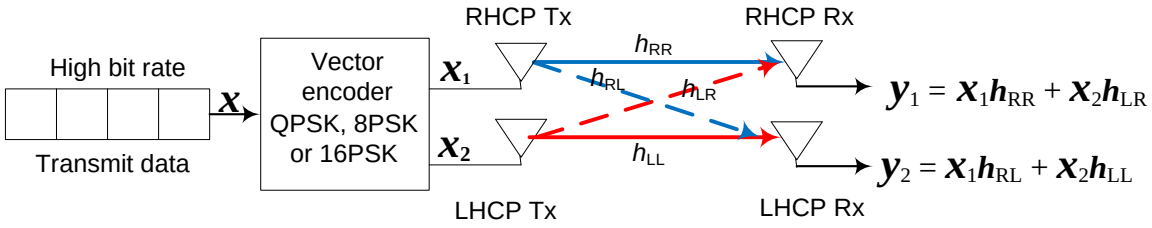

Figure 6.1: High level diagram of DCPM architecture

At the receiver land mobile terminal, from equation (2.1) and using Figure 6.1, observe that the instantaneous overall input-output relationship for the DCPM scheme is given by:

$$\boldsymbol{y} = y_1 + y_2 = x_1 h_{RR} + x_2 h_{LR} + x_1 h_{RL} + x_2 h_{LL} + \boldsymbol{n}, \tag{6.1}$$

where the wanted terms are $x_1 h_{RR}$ and $x_2 h_{LL}$ and the intra-system interference terms are $x_1 h_{RL}$ and $x_2 h_{LR}$; $\boldsymbol{n}$ is the noise vector = (n_1, n_2, n_3, n_4) present in each of the four sub-channels. Note that the intra-system interference directly depends on the orthogonal polarised antennas ability to reject oppositely polarised signals and also on the channel's preponderance to depolarise the transmit signal. Hence, an important factor in the choice of channel equalisation technique is how significant are the $x_1 h_{RL}$ and $x_2 h_{LR}$ terms compared with the $x_1 h_{RR}$ and $x_2 h_{LL}$ terms. Recall that the dual circular polarised channel matrix is given by:

$$\mathbf{H} = \begin{bmatrix} h_{RR} & h_{RL} \\ h_{LR} & h_{LL} \end{bmatrix} = \begin{bmatrix} h_{11} & h_{12} \\ h_{21} & h_{22} \end{bmatrix}. \tag{6.2}$$

The channel effects of equation (6.2) plus the noise term need to be removed from the receive signal, and this can be done using either linear unordered or recursive equalisation techniques. How to implement linear unordered ZF and MMSE channel equalisation was explained in the BER simulations of section 3.2.5, while the process of implementing ordered successive ZF interference cancellation uses the algorithm given in [86] as follows:

Recursion initialisation:

$$i = 1$$

$$\mathbf{G}_i = \mathbf{H}^+$$

$$k_i = \text{argmin}_j \left\| (\mathbf{G}_i)_j \right\|^2$$

Recursion:

$$wk_i = (\mathbf{G}_i)k_i$$

$$yk_i = w_{k_i}^T r_i$$

$$\hat{a}k_i = Q(yk_i)$$

$$r_{i+1} = r_i - \hat{a}k_i(\mathbf{H})k_i$$

$$\mathbf{G}_{i+1} = \mathbf{H}_{k_i}^{\pm}$$

$$k_{i+1} = \text{argmin}_{j \notin (k_1 \ldots\ldots k_i)} \left\| (\mathbf{G}_{i+1})_j \right\|^2$$

$$i = i + 1, \tag{6.3}$$

where $\mathbf{G}_{i,i=1}$ is a matrix of ZF channel weights obtained from the first step Moore-Penrose pseudo-inversion (given as $\mathbf{H}^+$) of $\mathbf{H}$. k_1 is the index number of the column of weights that correspond to the sub-channel with the best post detection SNR. Thus wk_i are the weights of the column with the best SNR, yk_i are the equalised received bits, $\hat{a}k_i$ are the quantised equalised received bits and r_{i+1} is the received signal after subtracting the equalised component. $\mathbf{G}_{i+1}$ is the pseudo-inverse of the depleted channel. In summary, equation (6.3) progressively chooses and eliminates the sub-channel with the next best SNR and the process is based on the receiver having perfect channel state information. Using the

notation developed in chapter 3 to explicitly show how the channel weights are employed in suppressing intra-system interference, equation (6.3) is presented in discrete baseband matrix form as follows:

1. Compute the ZF channel weights by inverting **H** according to equation (3.2) to get:

$$\mathbf{G}_Z = \begin{bmatrix} w_{11} & w_{21} \\ w_{12} & w_{22} \end{bmatrix}. \tag{6.4}$$

2. Determine the column with the best post detection SNR; for example column 2 containing weights w_{21} and w_{22}.

3. Using the weights computed from the column chosen in step 2, equalise the channel as follows:

$$\mathbf{y}_{eq} = \boldsymbol{w}_2^T \boldsymbol{y} = \begin{bmatrix} w_{21} & w_{22} \end{bmatrix} \begin{bmatrix} y_1 \\ y_2 \end{bmatrix} = \begin{bmatrix} w_{21} y_1 + w_{22} y_2 \end{bmatrix}. \tag{6.5}$$

4. Subtract $\mathbf{Y}_{\text{eq}}$ (which is a subset of the received signal that has been equalised and quantised) from the overall received signal:

$$\mathbf{y} = \mathbf{y} - \mathbf{y}_{eq} = \begin{bmatrix} y_1 \\ y_2 \end{bmatrix} - \begin{bmatrix} 0 \\ w_{21} y_1 + w_{22} y_2 \end{bmatrix}. \tag{6.6}$$

   Equation (6.6) completely eliminates y_2 leaving only y_1, so the new channel matrix reduces to: $\begin{bmatrix} x_1 h_{11} & x_2 h_{21} \\ 0 & 0 \end{bmatrix}$, where the zero terms represent the components of y_2 that have been removed.

5. Loop back to step 1 to compute the weights of the remaining channel and equalise as necessary.

The steps given in 1 to 5 above provide a straight forward way to implement the ordered successive ZF algorithm in MATLAB. Also, the compact disc accompanying reference [34] provides robust MATLAB scripts for implementing ZF-OSIC. As can be observed in the above algorithm, only the interference components are removed and any available noise is amplified [8]. Though co-located and of the same design, orthogonally polarised

receive antennas (as proposed for the DCPM scheme) have been known to exhibit slightly different radiation patterns due to imperfect antenna manufacture. This phenomenon partly accounts for the sometimes dissimilar receive power of the two sub-channels and thus requiring that the row with the strongest SNR should always to be correctly determined in step 2 so as to achieve optimal interference cancellation.

Implementing ordered successive MMSE equalisation follows the same procedure as with the ZF equalisation; the only difference being that the channel inversion of step 1 is performed in order to simultaneously suppress both the interference and noise. Therefore the MMSE channel weights are obtained by pseudo-inverting both **H** and the SINR terms as shown in equation (3.4).

One of the assumptions underlying the choice of equalisation schemes for DCPM, which would be validated using simulations in the next section, is that even though ZF is inferior to MMSE, its BER performance should very closely approach that of MMSE because of the high correlation and minimal interference in line of sight (LOS) propagation. It is only when propagation conditions become more challenging, as during severe obstructed line of sight (OLOS1), OLOS2 and NLOS type fading that the more computationally complex MMSE may become more advantageous. Note that as earlier mentioned in chapter 5, OLOS1 describes a large scale channel fading state where the co-polar and cross-polar components are mainly attenuated by vegetative matter. In this fading state, and similar to the vegetation propagation measurements of [127],[128] and the ITU-R recommendations for attenuation in vegetation [129], the co-polar components are attenuated by between 2 dB and 21dB from their LOS level (depending on the depth of foliage and the relative velocity between transmitter and receiver) while the cross-polar components are attenuated by more than 10dB. OLOS2 fading occurs in suburban and urban areas and is characterised by the cross-polar components, though attenuated, being stronger than the co-polar components. Such channel fading conditions are quite rare but significant instances of it have been observed in the measurements earlier described in chapter 4 and from the measurement results of [5].

6.1.1 Scope of DCPM Simulations

Wireless communication applications for which DCPM can be put to use are many; however, this thesis focuses on the LMS broadcast channel for which ETSI's digital video broadcasting standardisation activities is presently gathering momentum. Therefore following the DVB-SH and DVB-NGH recommendations [77], the receiver architecture proposed for DCPM-enabled devices was shown in Figure 2.7 and based on a single satellite single user scenario, Figure 6.2 below shows a block diagram of the BER simulations carried out in this chapter.

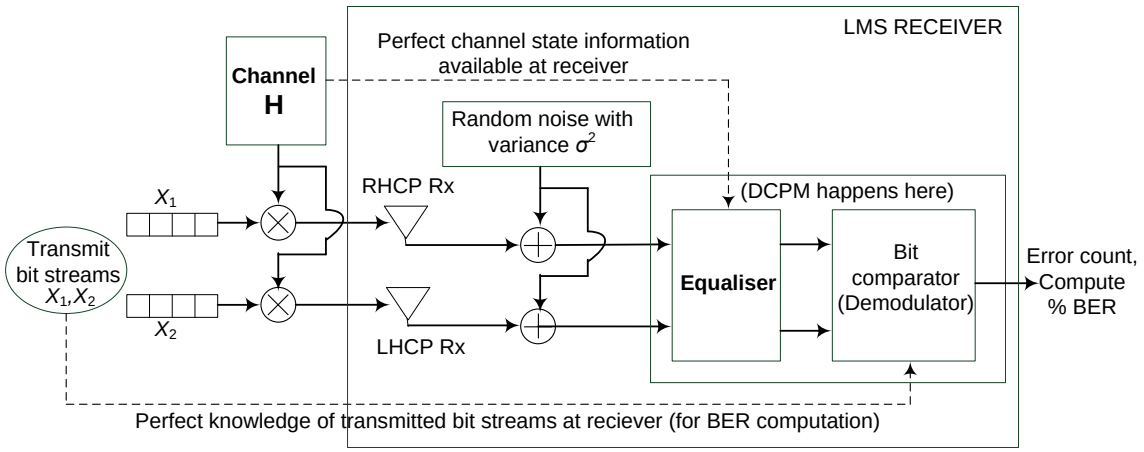

Figure 6.2: Block diagram showing how BER computation is implemented for a DVB-SH-type receiver

An explanation of the BER simulations procedure is as follows.

1. Two randomly generated and QPSK modulated bit streams, X_1 and X_2, are transmitted from each of the satellite's dual circular polarised antennas. Both the in-phase and quadrature-phase components of the bits are transmitted with a fixed energy given by E_B.
2. Using matrix multiplication, the effects of the modelled complex channel, **H**, is induced on the transmitted bits. This multiplication affects both the amplitude and phase of the transmitted bit streams.
3. At the receiver, random noise with variance σ^2 and power density N_0 is added to the received bit stream. The variance of the noise power density is gradually

reduced to get ascending values of energy per bit to noise power density ratios (E_b/N_0).

4. The receiver, having perfect channel state information tries to remove the effects of the channel on the transmitted bit stream using ZF and MMSE. Note that steps 1, 2 and 4 have already been explained in great detail in Section 6.1.
5. The originally transmitted bit streams are then compared with the demodulated/decoded bits. Erroneously decoded bits are counted and the bit error rate is determined.

As can be observed with Figures 2.7 and 6.2 are compared, not all aspects of the receiver are considered in this thesis since this research concentrates on physical layer aspects. Therefore, with the receiver having perfect channel state information as stated in step 4 above, there is no need to consider the pilot signalling and channel estimation aspects. Also, it is assumed that the satellite operates from a geostationary orbit, which allows the effects of Doppler shift to be easily compensated. Other assumptions are as follows:

1. Only the satellite reception mode is considered although the DVB-SH receiver is capable of seamlessly moving between satellite and Complementary Ground Coverage (CGC) reception.
2. Orthogonal circular polarisation provides the only means of sub-channel independence.
3. Only QPSK modulation is considered since it has been recommended in [76] that QPSK at a code rate of 1/3 is optimal at maximising the satellite link margin. The absolute BER of higher order modulation schemes would be progressively worse than that of QPSK. However, if the other recommended modulation schemes (8PSK and 16APSK) are used in comparing the performance of different equalisation schemes, they would give in relative terms the same results as QPSK.
4. Time interleaving and turbo coding aspects are not considered since they are as add-ons and only serve to improve the bit error rates. Note that the adoption of time interleaving techniques (both physical layer and link layer) depend on the available memory and battery life restrictions. While time interleaving and forward error correction turbo codes reduce the effective transmission rates

(capacity), they have been shown in [130] to increase satellite-only error free reception time of DVB-SH systems by more than 10%.

6.2 Bit Error Rate Simulations for the Dual Circular Polarised LMS Channel

The aim of this section is to compare the bit error rates of ZF and MMSE equalisation when used within the DCPM framework under different channel fading conditions. Also included for benchmarking purposes are the bit error rate curves of the optimal exhaustive search MLSE equalisation scheme and BER curves for when equalisation is not used. This last addition explores the advantage that orthogonal circular polarisation alone can bring to mobile DCPM-enabled LMS receivers. All the simulations in this section, except otherwise stated, make use of the channel model developed in chapter 5 and QPSK modulation. To set the stage for subsequent BER plots, Figure 6.3 shows linear ZF, MMSE, MLSE and 'no equalisation' BER curves for the measured and modelled dual circular polarised LOS channel while Figure 6.4 shows the BER curves for when the channel is NLOS. The bracket terms in the legend of the figures: (mod) and (mea) respectively represent error rates derived from modelled channel data and the BER from measured channel data. Observe in Figure 6.3 that the measured and modelled channel BER curves of the respective equalisation schemes are very closely correlated and this serves as a further verification of the accuracy of the model. Also observe that as expected, MLSE gives the best performance, achieving a BER of 10^{-3} at an E_b/N_0 of about 12.6dB for the LOS channel. ZF and MMSE achieve the same BER at a slightly higher E_b/N_0 of 14.0dB and 13.8dB respectively. In the same LOS channel, 'no equalisation' does amazingly well, achieving a BER of 10^{-3} at an E_b/N_0 of 16dB. Of particular significance in this channel is the fact that 'no equalisation' outperforms ZF at E_b/N_0 values less than 7dB. Observe that at low E_b/N_0 values, all the error probability (BER) curves including that of the theoretical AWGN channel tend towards the worst case value of 0.5. The difference between the optimal MLSE BER curve and that of the theoretical AWGN channel BER at higher E_b/N_0 is mainly due to the channel attenuation effects which cannot be completely removed by equalisation. Increasing the channel Rice factor

would make the equalised channel BER curves to tend towards that of the AWGN channel.

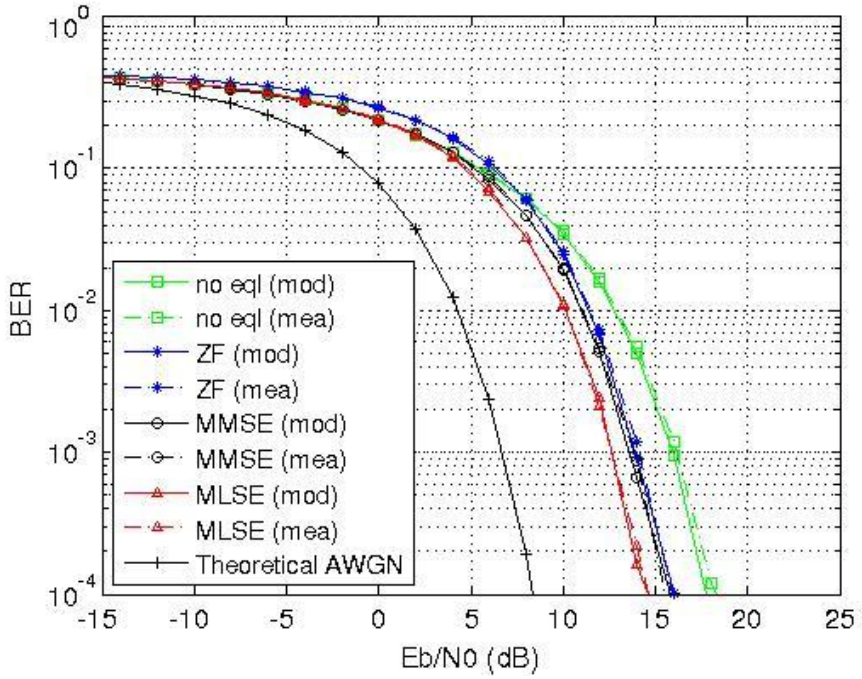

Figure 6.3: BER curves for linear unordered ZF and MMSE, exhaustive search MLSE and 'no equalisation' in the LOS measured and modelled channels

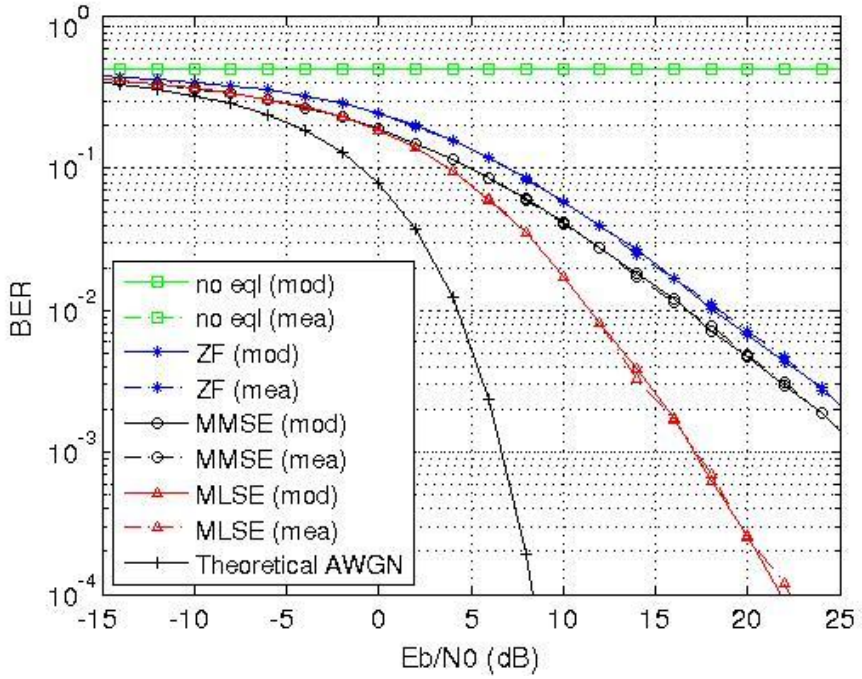

Figure 6.4: BER curves for linear unordered ZF and MMSE, exhaustive search MLSE and 'no equalisation' in the NLOS/Rayleigh measured and modelled channels

The BER for the NLOS/Rayleigh channel shown in Figure 6.4 is several orders of magnitude worse than that of the LOS channel. Observe that increasing the E_b/N_0 in this channel has almost no effect on the bit error rate when 'no equalisation' is used. An agreement between measured and modelled channel bit error rates once again indicates the accuracy of the model.

Table 6-1: Average channel parameters for BER curves of Figure 6.3 to Figure 6.6

Channel type	**Average co-polar Rice factor**	**Average cross-polar Rice factor**	**Average co-polar cross correlation coefficient**	**Average cross-polar cross correlation coefficient**	**Average power level relative to LOS**			
					h_{RR}	h_{RL}	h_{LR}	h_{LL}
LOS	17dB	10dB	0.96	0.87	0dB	-8dB	-7dB	0dB
NLOS	-4dB	-8dB	0.43	0.45	-33dB	-35dB	-34dB	-32dB

The average Rice factors and the co-polar and cross-polar channel cross correlation for the channel data sections used in plotting Figures 6.3 and 6.4 are given in Table 6-1. Also included in the table are the average RHCP and LHCP co- and cross-polar sub-channel levels, which should be pointed out are balanced. A channel is described as balanced when the level of its co-polar RHCP sub-channel (h_{RR}) is roughly equal to the level of its co-polar LHCP sub-channel (h_{LL}); the same equal levels applies to the cross polar sub-channels of a balanced dual circular polarised channel.

In all dual circular polarised LMS channels with balanced branch powers and especially when the channel state information is completely known at the receiver, no advantage is expected from the use of ordered successive interference cancellation (OSIC) either in the ZF or MMSE mode. This has been proven in Figures 6.5 and 6.6, which show BER curves for ordered successive interference cancellation. Observe that these are almost identical to their linear unordered interference cancellation counterparts of Figures 6.3 and 6.4 respectively. These results are not surprising because channel weights, particularly for ZF, are obtained by pseudo-inverting the channel matrix and when this matrix is known and the channel is in LOS fading, interference elimination by the unordered linear ZF achieves its optimal performance, same as with successive interference cancellation. With this insight, subsequent sections of this chapter will explore the BER rates when the channel fading is both balanced and unbalanced and is

predominantly in each of the four fading states (described by the proposed model). This is done in order to determine if successive interference cancellation is superior to linear interference elimination for DCPM implementation.

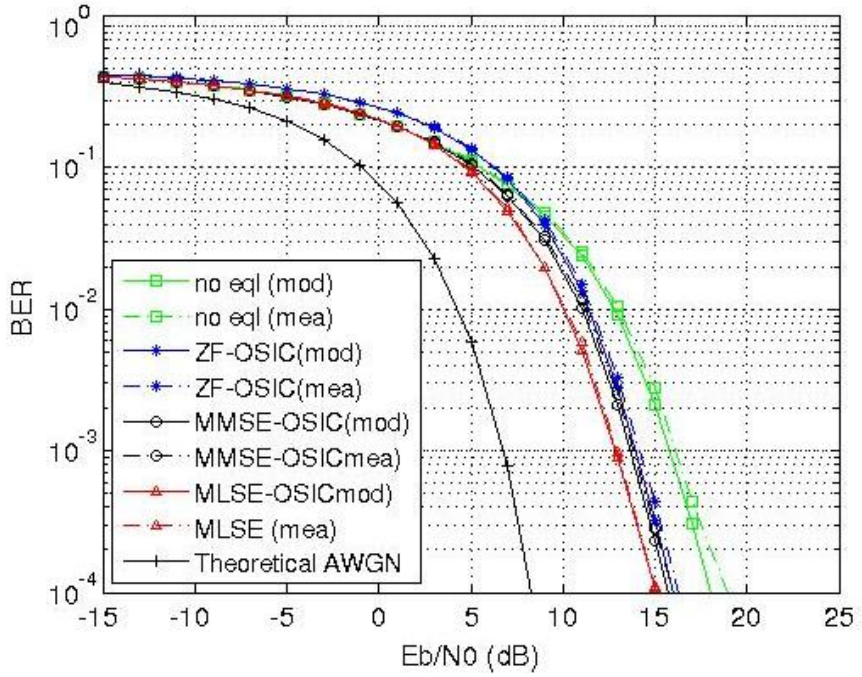

Figure 6.5: BER curves for ordered successive interference cancellation ZF and MMSE, exhaustive search MLSE and 'no equalisation' in the LOS channel

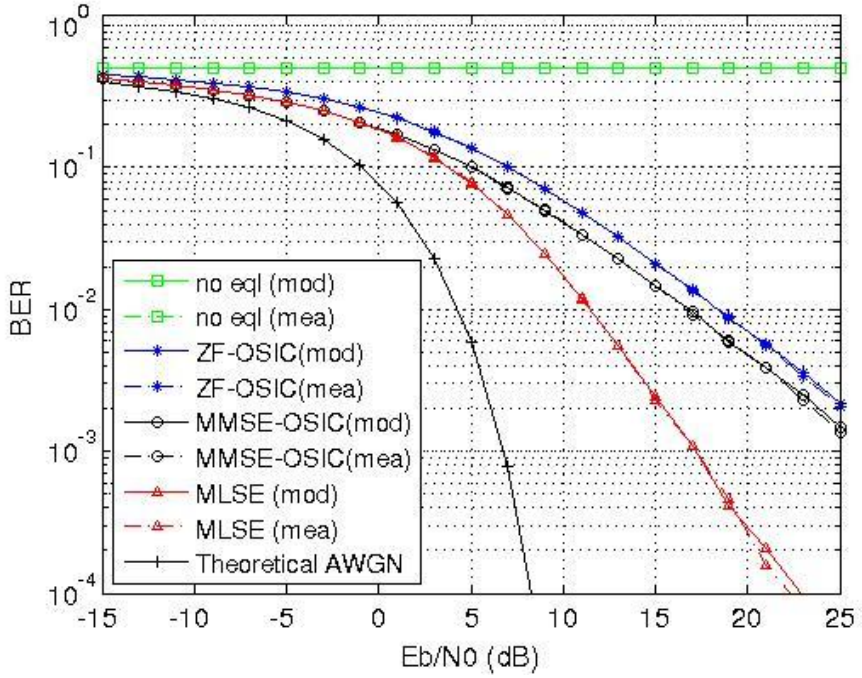

Figure 6.6: BER curves for ordered successive interference cancellation ZF and MMSE, exhaustive search MLSE and 'no equalisation' in the NLOS/Rayleigh channel

6.2.1 The Dual Circular Polarised LMS LOS Channel

Some parameters of the LOS fading channel have already been given in Table 6-1 in the previous section while the rest of the parameters used in simulating this channel are provided in Table 6-2. This subsection expands on the earlier simulations by specifying two types of LOS fading conditions: Scenario A, when the co- and cross- polar branch powers (sub-channels) are balanced and Scenario B, when there is a significant imbalance between the two co-polar branches. A difference between the co-polar branch powers invariably creates some imbalance between the two cross-polar branch powers and in the case of a handheld LMS receiver, branch power imbalance is usually caused by obstructing one of the antennas while handling the device. Theoretically, two other possible scenarios exist, these are: Scenario C, when the co-polar branches are balanced but with unbalanced cross-polar branches and Scenario D, when both co- and cross-polar branches are unbalanced. Scenario C is not presented in this thesis because of its very low probability of occurrence while scenario D is very similar to scenario B. Besides, the BER characteristics of scenarios C and D are very similar to those of scenarios A and B since the co-polar branches–with their usually much larger magnitudes compared the cross-polar branches–dominate the BER performance of dual circular polarised LOS channels. Scenario A has already been shown as part of Figures 6.3 and 6.5 and will not be repeated here.

Table 6-2: Channel parameters for Scenarios A and B of the dual circular polarised LOS channel

	$\mathbf{H_{XPD\text{-}XPC} \odot H_{LOS}}$ **Coherently received component (model input)**	**Correlation coefficients (model input)**		$\mathbf{H_{RiceF}}$ **Average Rice factor in dB (model input)**	$\mathbf{H_{LOS}}$ **Average path loss relative to LOS in dB (estimated)**
		Co-polar channels cross correlation	**Cross-polar channels cross correlation**		
Scenario A	$\begin{bmatrix} 1.0 & \sqrt{0.2} \\ \sqrt{0.2} & 1.0 \end{bmatrix}$	$\begin{bmatrix} 1.0 & 0.96 \\ 0.96 & 1.0 \end{bmatrix}$	$\begin{bmatrix} 1.0 & 0.82 \\ 0.82 & 1.0 \end{bmatrix}$	$\begin{bmatrix} 15 & 7 \\ 7 & 15 \end{bmatrix}$	$\begin{bmatrix} -0.1 & -7.4 \\ -7.4 & -0.1 \end{bmatrix}$
Scenario B	$\begin{bmatrix} 1 & \sqrt{0.2} \times 0.7^{\dagger} \\ \sqrt{0.2} & 0.7^{\dagger} \end{bmatrix}$	$\begin{bmatrix} 1.0 & 0.96 \\ 0.96 & 1.0 \end{bmatrix}$	$\begin{bmatrix} 1.0 & 0.82 \\ 0.82 & 1.0 \end{bmatrix}$	$\begin{bmatrix} 15 & 7 \\ 7 & 15 \end{bmatrix}$	$\begin{bmatrix} -0.1 & -7.4 \\ -7.4 & -6.3 \end{bmatrix}$

† 0.7 represents a 1.54dB reduction in the coherently received LHCP component. Using the channel model defined in equation (5.2), the values in the rightmost column were computed from the generated channel data. Note that the standard deviation of the multipath components in this case was set at 0.1

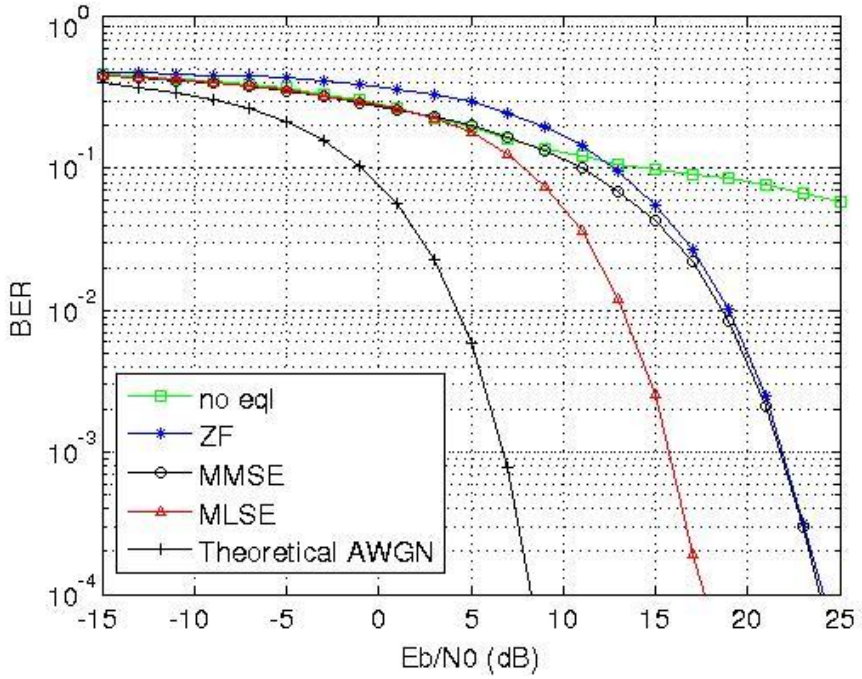

Figure 6.7: BER curves for linear unordered ZF and MMSE, exhaustive search MLSE and 'no equalisation' in the LOS channel Scenario B (unbalanced sub-channels)

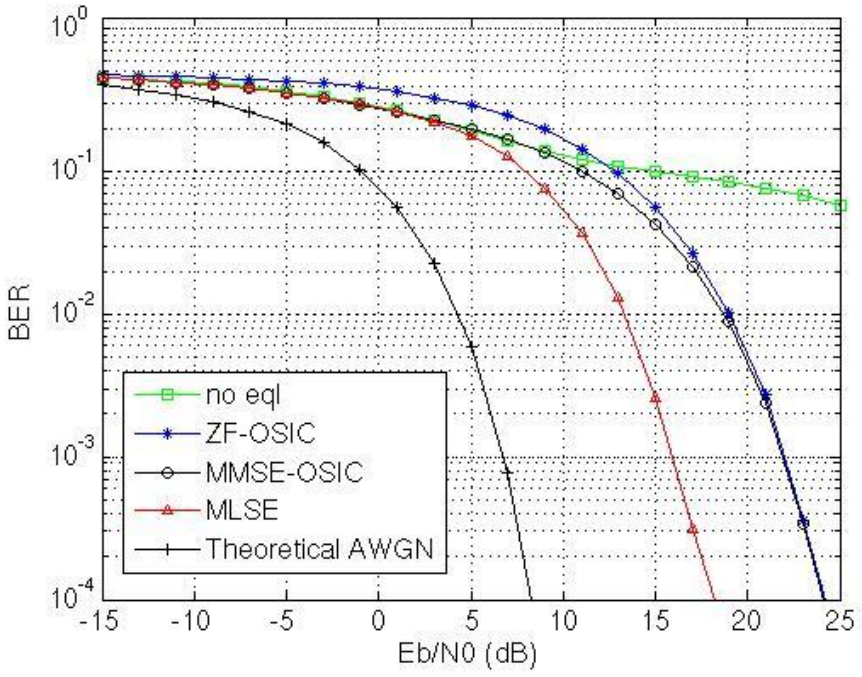

Figure 6.8: BER curves for ordered successive interference cancellation ZF and MMSE, exhaustive search MLSE and 'no equalisation' in the LOS channel Scenario B (unbalanced sub-channels)

6.2.1.1 Discussions on the BER performance of ZF-OSIC and MMSE-OSIC equalisation on the LOS channel

What is immediately obvious in the balanced and unbalanced LOS channels is degradation in the BER performance of all three equalisation schemes. Whereas MLSE, MMSE and ZF (both linear unordered and OSIC) achieved 10^{-3} BER at E_b/N_0 rates of 12.6dB, 13.8dB and 14.0dB in the balanced channel respectively, in the unbalanced channel, they achieve the same BER at 15.8dB, 22dB and 22.1dB E_b/N_0. In the worst case being that of ZF, this represents a 8.1dB loss for a 5.23dB* drop in the coherently received h_{LL} sub-channel power relative to the coherent h_{RR} sub-channel. (*see Table 6-2, where 10log (1 – 0.7) = 5.23dB). There is no significant difference between the BER performance of the linear equalisation schemes and their OSIC counterparts. Decoding signals transmitted through unbalanced LOS channels based only on orthogonal polarisations (i.e. 'no equalisation') gives very poor results and as can be observed, a BER of 10^{-3} cannot be achieved within the windowed E_b/N_0.

A salient point to note from the BER results is that orthogonally polarised systems are very sensitive to branch power imbalances. Since most dual polarised antenna systems are designed to be co-located on devices with small form factors, imbalances would be most likely caused by handling of such devices. For example, if a DCPM receiver is held with both hands, one hand may cover/obstruct one of the antennas while the second antenna is left unobstructed. Another potential source of imbalance is non-identical (i.e. the antennas not having the same XPD) radiation patterns of orthogonally polarised antennas. Although the channel modelling chapter of this thesis purposefully avoided using measured channel data from unbalanced data sections to build the channel model, the proposed model can be easily tuned to generate unbalanced channel data for BER and other analysis. This section has given just one example of the infinitely many 'Scenario B' examples to highlight the effects of branch power imbalance on BER.

6.2.2 The Dual Circular Polarised LMS MIMO OLOS1 Channel

The parameters used in modelling the OLOS1 (State 2) channel are given in Table 6-3, where it is shown the values of the XPD-XPC ratio multiplied with the coherently received signal component (relative to the LOS level): $\mathbf{H}_{\text{XPD-XPC}} \odot \mathbf{H}_{\text{LOS}}$. Also shown are

the cross correlation coefficients of the co-polar and the cross-polar channels and their corresponding Rice factors. The given parameters in addition to the state transition probability matrix (not shown) are used as inputs to the channel model of equation (5.2). The channel model then generates time series data from where the values of the fourth column have been computed. As usual, Scenario A is for balanced co- and cross-polar branch powers while Scenario B represents a situation where the co-polar branches powers are not balanced. The results for the BER simulations of linear unordered ZF and MMSE and ZF-OSIC, MMSE-OSIC are shown in Figures 6.9 to 6.12.

Table 6-3: Channel parameters for Scenarios A and B of the dual circular polarised OLOS1 channel

	$\mathbf{H_{XPD\text{-}XPC} \odot H_{LOS}}$ **Coherently received component (model input)**	**Correlation coefficients (model input)**		$\mathbf{H_{RiceF}}$ **Average Rice factor in dB (model input)**	$\mathbf{H_{LOS}}$ **Average path loss relative to LOS in dB (estimated)**
		Co-polar channels cross correlation	**Cross-polar channels cross correlation**		
A	$\begin{bmatrix} 0.9 & \sqrt{0.1} \times 0.9 \\ \sqrt{0.1} \times 0.9 & 0.9 \end{bmatrix}$	$\begin{bmatrix} 1.0 & 0.9 \\ 0.9 & 1.0 \end{bmatrix}$	$\begin{bmatrix} 1.0 & 0.66 \\ 0.66 & 1.0 \end{bmatrix}$	$\begin{bmatrix} 6 & 4 \\ 4 & 6 \end{bmatrix}$	$\begin{bmatrix} -2.9 & -12.4 \\ -12.4 & -2.9 \end{bmatrix}$
B	$\begin{bmatrix} 0.9 & \sqrt{0.1} \times 0.54^{\ddagger} \\ \sqrt{0.1} \times 0.9 & 0.6 \end{bmatrix}$	$\begin{bmatrix} 1.0 & 0.9 \\ 0.9 & 1.0 \end{bmatrix}$	$\begin{bmatrix} 1.0 & 0.66 \\ 0.66 & 1.0 \end{bmatrix}$	$\begin{bmatrix} 6 & 4 \\ 4 & 6 \end{bmatrix}$	$\begin{bmatrix} -2.9 & -12.4 \\ -12.4 & -9.8 \end{bmatrix}$

‡ 0.54 = 0.9×0.6, where 0.9 represents 0.46dB reduction in the coherently received components of all channels due to OLOS1 fading and 0.6 represents a 2.22dB reduction in only the LHCP component (causing the imbalance). Using the channel model defined in equation (5.2), the values in the rightmost column were computed from the generated channel data. Note that the standard deviation of the multipath components in this case was set at 0.2

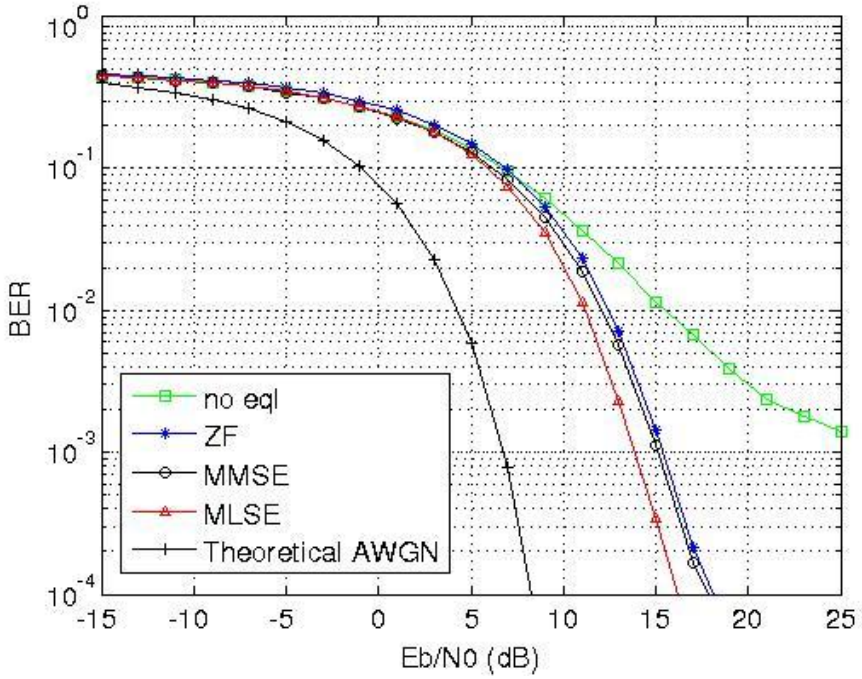

Figure 6.9: BER curves for linear unordered ZF and MMSE, exhaustive search MLSE and 'no equalisation' in the OLOS1 channel Scenario A (balanced sub-channels)

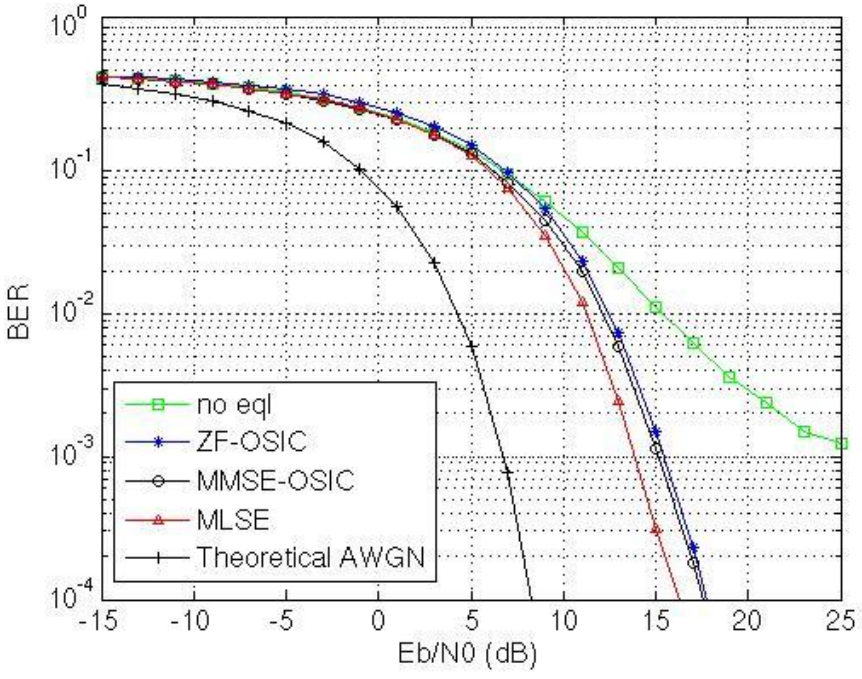

Figure 6.10: BER curves for ordered successive interference cancellation ZF and MMSE, exhaustive search MLSE and 'no equalisation' in the OLOS1 channel Scenario A (balanced sub-channels)

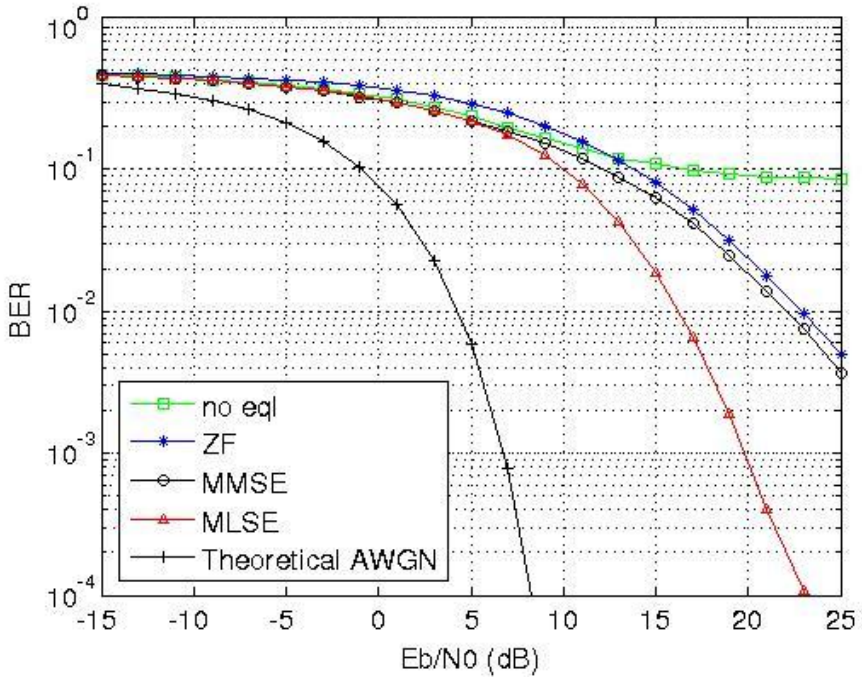

Figure 6.11: BER curves for linear unordered ZF and MMSE, exhaustive search MLSE and 'no equalisation' in the OLOS1 channel Scenario B (unbalanced sub-channels)

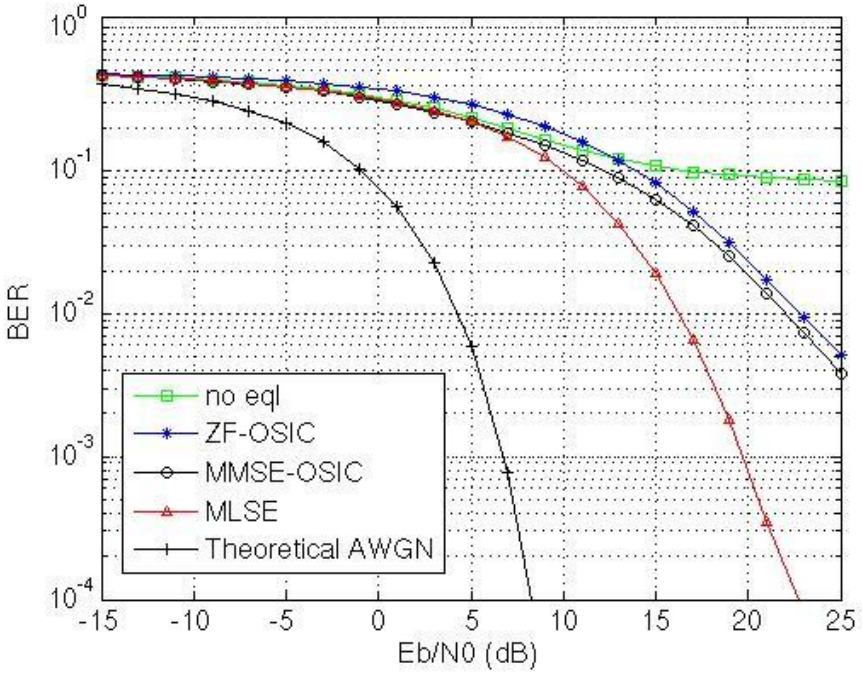

Figure 6.12: BER curves for ordered successive interference cancellation ZF and MMSE, exhaustive search MLSE and 'no equalisation' in the OLOS1 channel Scenario B (unbalanced sub-channels)

6.2.2.1 Discussions on the BER performance of ZF-OSIC and MMSE-OSIC equalisation on the OLOS1 channel

Once again, as was the case with the LOS channel, the biggest effect on BER is caused by branch power imbalance. Neither ZF-OSIC nor MMSE-OSIC is able to improve the BER of the unbalanced channel to match that of the balanced channel. The recursive interference mitigation techniques have failed to provide any significant advantage over linear unordered interference mitigation. As expected, the BER of 'no equalisation' is worse in the OLOS1 channel than in the LOS channel.

Although the OLOS1 channel has better polarisation discrimination than the LOS channel (χ = 0.2 in LOS and χ = 0.1 in OLOS1 – due to the cross-polar components suffering much greater attenuation than their co-polar counterparts), the relatively lower powers of the coherently received co-polar sub-channels (1 for LOS and 0.9 for OLOS1) produces limited effects on the BER of both ZF and MMSE but a much more substantial effect when 'no equalisation' is used. For example, whereas in the balanced LOS channel, to achieve a BER of 10^{-3} requires E_b/N_0 of 13.8dB and 14.1dB for MMSE and ZF respectively, to achieve the same BER in the OLOS1 channel respectively require E_b/N_0 of 15.1dB and 15.4dB. However, when the channel becomes unbalanced, the E_b/N_0 required by MMSE and ZF in the OLOS1 channel to achieve BERs of 10^{-3} both increase to more than 30dB, from the 22.0dB and 22.1dB that was respectively needed in the unbalanced LOS channel. When no equalisation is used, balanced OLOS1 channel achieves a BER of 10^{-2} at an E_b/N_0 of about 15.2dB; in the unbalanced OLOS1 channel, 'no equalisation' may never be able to achieve the bit error rate of 10^{-2}.

The above results once again emphasise the need for co-polar sub-channel powers to be of the same magnitude in order for polarisation multiplexing to succeed. It has also shown that decent BER only using orthogonal circular polarisation decoding is limited to pure LOS channels. Ordered successive interference cancellation does not bring any obvious advantage when channel state information completely available at the receiver.

6.2.3 The Dual Circular Polarised LMS MIMO OLOS2 Channel

The OLOS2 channel state occurs very rarely and is only included in the BER simulations for completeness. In Table 6-4 are the parameters used in simulating this channel and its BER results are shown in Figures 6.13 to 6.16. The OLOS2 fading channel is a more exacting channel state than the previous two cases as can be observed by the parameters in Table 6-4. As expected, the bit error rates for both linear unordered and OSIC equalisations, including MLSE and 'no equalisation' are worse than the previous two cases. Bits decoded with 'no equalisation' are always very close to the worst case value of 0.5, hence the almost horizontal green plot. The use of OSIC in this channel doesn't bring any significant BER advantage over linear unordered equalisation. The important feature about this channel is the fact that MMSE outperforms ZF by about 5dB E_b/N_0 for most of the BER range.

Table 6-4: Channel parameters for Scenarios A and B of the dual circular polarised OLOS2 channel

	$\mathbf{H_{XPD\text{-}XPC} \odot H_{LOS}}$ **Coherently received component (model input)**	**Correlation coefficients (model input)**		$\mathbf{H_{RiceF}}$ **Average Rice factor in dB (model input)**	$\mathbf{H_{LOS}}$ **Average path loss relative to LOS in dB (estimated)**
		Co-polar channels cross correlation	**Cross-polar channels cross correlation**		
A	$\begin{bmatrix} 0.5 & \sqrt{0.5}\times 0.8 \\ \sqrt{0.5}\times 0.8 & 0.5 \end{bmatrix}$	$\begin{bmatrix} 1.0 & 0.58 \\ 0.58 & 1.0 \end{bmatrix}$	$\begin{bmatrix} 1.0 & 0.66 \\ 0.66 & 1.0 \end{bmatrix}$	$\begin{bmatrix} 2 & 4 \\ 4 & 2 \end{bmatrix}$	$\begin{bmatrix} -8.2 & -6.4 \\ -6.4 & -8.1 \end{bmatrix}$
B	$\begin{bmatrix} 0.5 & \sqrt{0.5}\times 0.32^{\S} \\ \sqrt{0.5}\times 0.8 & 0.4 \end{bmatrix}$	$\begin{bmatrix} 1.0 & 0.58 \\ 0.58 & 1.0 \end{bmatrix}$	$\begin{bmatrix} 1.0 & 0.66 \\ 0.66 & 1.0 \end{bmatrix}$	$\begin{bmatrix} 2 & 4 \\ 4 & 2 \end{bmatrix}$	$\begin{bmatrix} -8.1 & -6.4 \\ -6.4 & -18.1 \end{bmatrix}$

[§] 0.32 = 0.8×0.4, where 0.8 represents a 0.97dB reduction in the coherently received components of all channels due to OLOS2 fading and 0.4 represents a 3.98dB reduction in only the LHCP component (causing the imbalance). Using the channel model defined in equation (5.2), the values in the rightmost column were computed from the generated channel data. Note that the standard deviation of the multipath components in this case was set at 0.2.

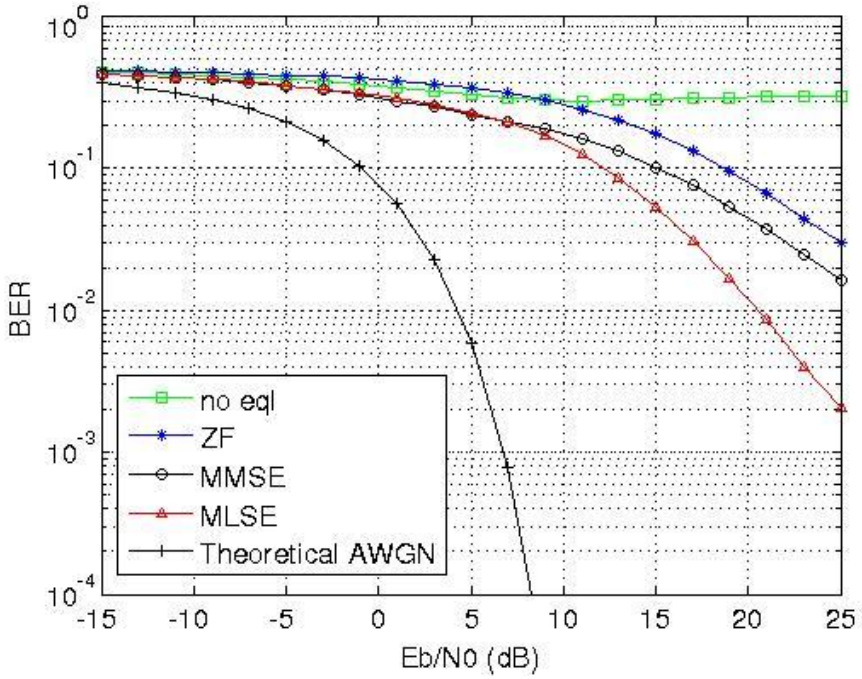

Figure 6.13: BER curves for linear unordered ZF and MMSE, exhaustive search MLSE and 'no equalisation' in the OLOS2 channel Scenario A (balanced sub-channels)

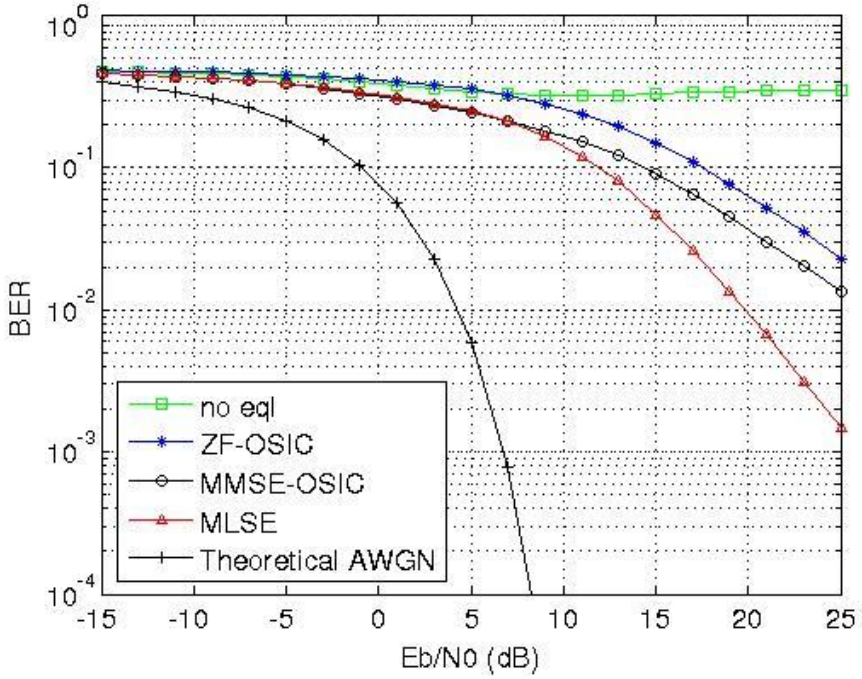

Figure 6.14: BER curves for ordered successive interference cancellation ZF and MMSE, exhaustive search MLSE and 'no equalisation' in the OLOS2 channel Scenario A (balanced sub-channels)

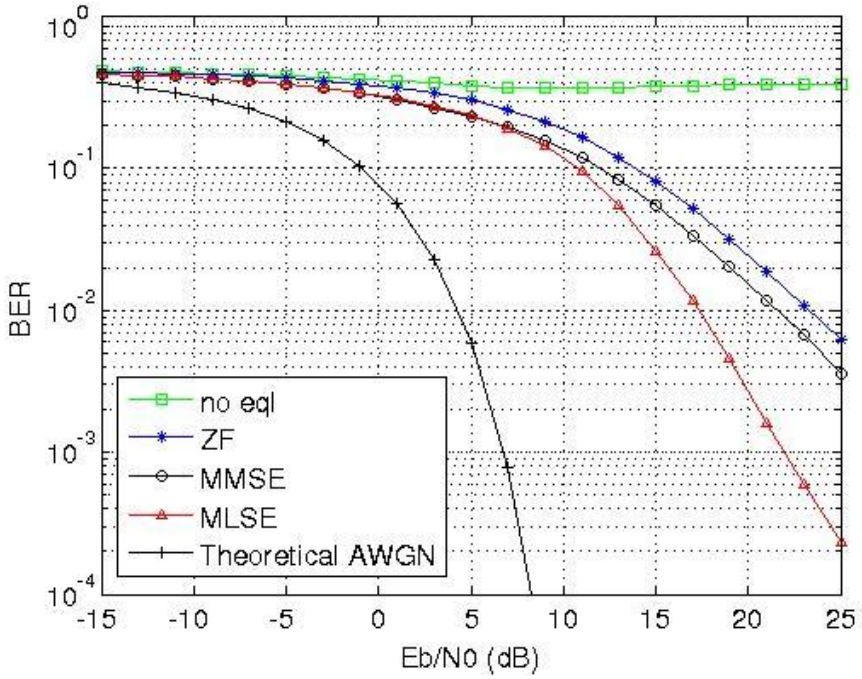

Figure 6.15: BER curves for linear unordered ZF and MMSE, exhaustive search MLSE and 'no equalisation' in the OLOS2 channel Scenario B (unbalanced sub-channels)

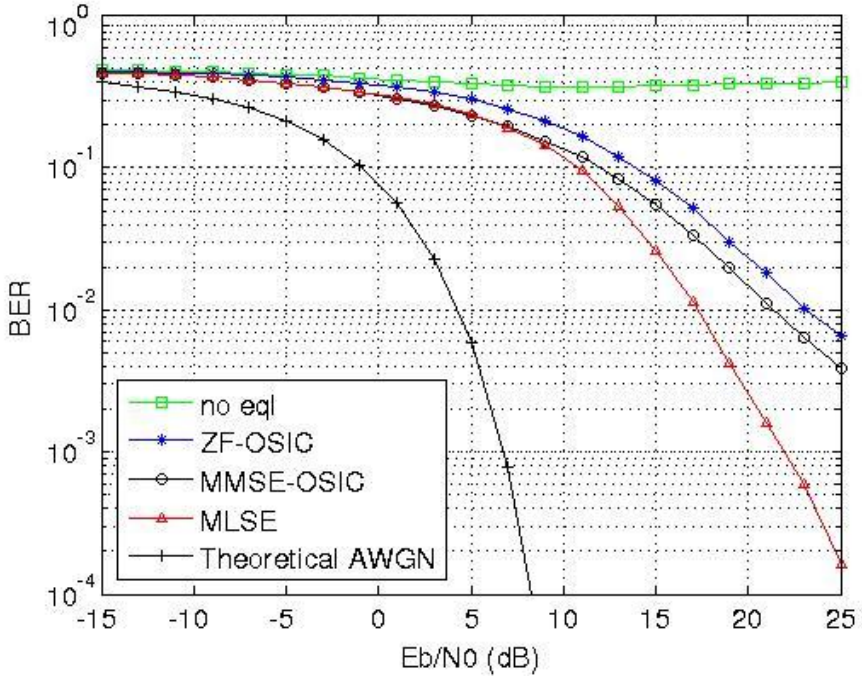

Figure 6.16: BER curves for ordered successive interference cancellation ZF and MMSE, exhaustive search MLSE and 'no equalisation' in the OLOS2 channel Scenario B (unbalanced sub-channels)

6.2.4 The Dual Circular Polarised LMS MIMO NLOS Channel

The NLOS/Rayleigh channel (State 4) is the antithesis of the LOS channel. Here, the LOS component is negligible and an overwhelming majority of the receive signal power comes from multipath components. Some of the parameters of this channel were given in Table 6-1 and the rest are provided in Table 6-5. Since Figures 6.4 and 6.6 already contain components of the balanced NLOS channel, only the unbalanced unordered and OSIC bit error rates of this channel are provided here: see Figures 6.17 and 6.18.

Table 6-5: Channel parameters for Scenarios A and B of the dual circular polarised NLOS channel

	$\mathbf{H_{XPD\text{-}XPC} \odot H_{LOS}}$ **Coherently received component (model input)**	**Correlation coefficients (model input)**		$\mathbf{H_{RiceF}}$ **Average Rice factor in dB (model input)**	$\mathbf{H_{LOS}}$ **Average path loss relative to LOS in dB (estimated)**
		Co-polar channels cross correlation	**Cross-polar channels cross correlation**		
A	$\begin{bmatrix} 0.001 & \sqrt{1} \times 0.001 \\ \sqrt{1} \times 0.001 & 0.001 \end{bmatrix}$	$\begin{bmatrix} 1.0 & 0.32 \\ 0.32 & 1.0 \end{bmatrix}$	$\begin{bmatrix} 1.0 & 0.16 \\ 0.16 & 1.0 \end{bmatrix}$	$\begin{bmatrix} -4 & -8 \\ -8 & -4 \end{bmatrix}$	$\begin{bmatrix} -50.6 & -50.4 \\ -46.6 & -50.8 \end{bmatrix}$
B	$\begin{bmatrix} 0.001 & \sqrt{1} \times 0.001 \\ \sqrt{1} \times 0.001 & 1e-5^{**} \end{bmatrix}$	$\begin{bmatrix} 1.0 & 0.32 \\ 0.32 & 1.0 \end{bmatrix}$	$\begin{bmatrix} 1.0 & 0.16 \\ 0.16 & 1.0 \end{bmatrix}$	$\begin{bmatrix} -4 & -8 \\ -8 & -4 \end{bmatrix}$	$\begin{bmatrix} -49.9 & -57.2 \\ -55.6 & -51.1 \end{bmatrix}$

** This is a totally random channel with negligible coherently received components. Using the channel model of equation (5.2), the standard deviation of the multipath components of this channel was set at 0.3 to get the estimated values shown in the last column.

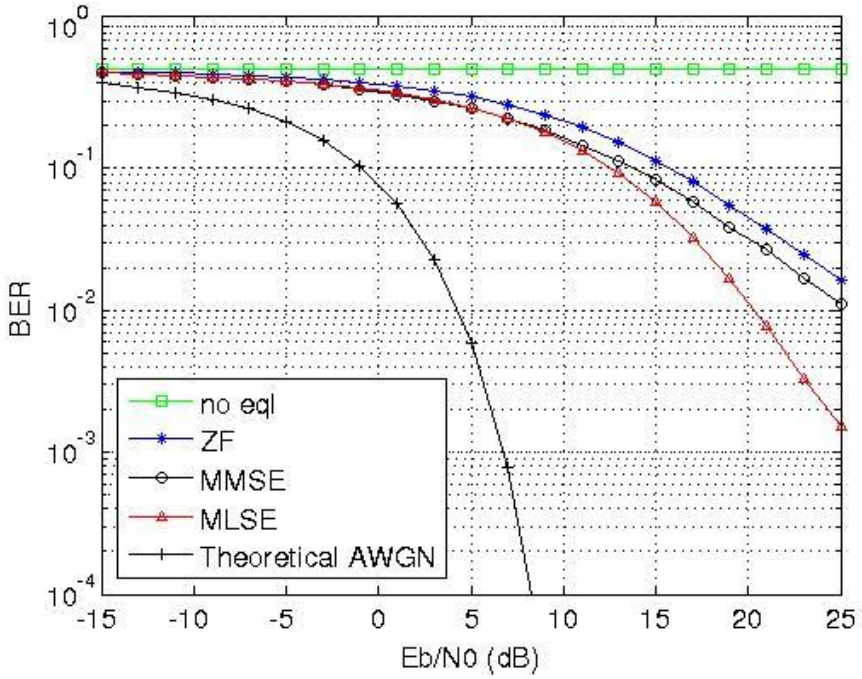

Figure 6.17: BER curves for linear unordered ZF and MMSE, exhaustive search MLSE and 'no equalisation' in the NLOS channel Scenario B (unbalanced sub-channels)

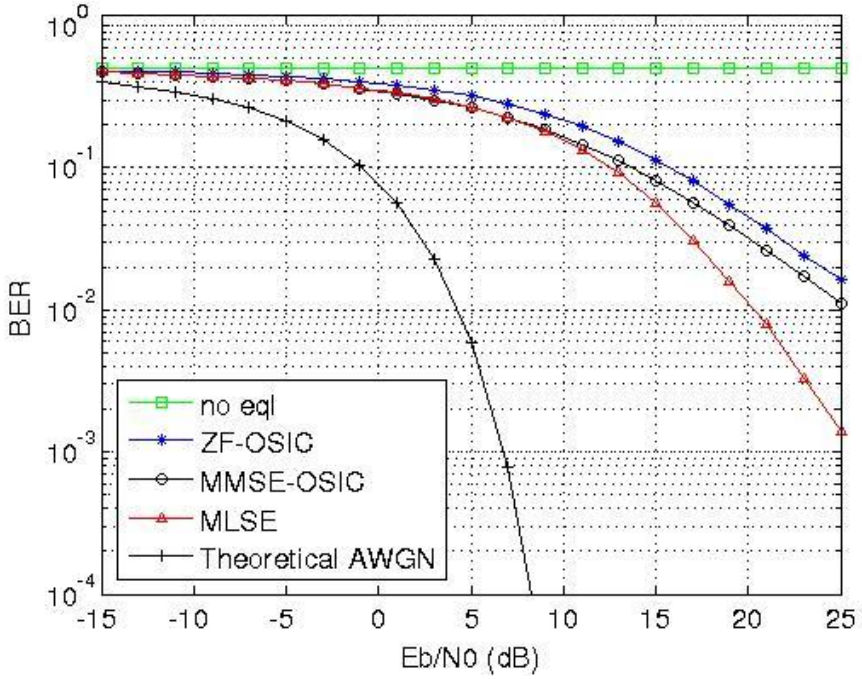

Figure 6.18: BER curves for ordered successive interference cancellation ZF and MMSE, exhaustive search MLSE and 'no equalisation' in the NLOS channel Scenario B (unbalanced sub-channels)

6.2.4.1 Discussions on the BER performance of ZF-OSIC and MMSE-OSIC equalisation on the NLOS channel

The BER in this channel is the worst of the four cases. There is a complete depolarisation in this channel which does not favour any form of polarisation multiplexing. Since most of the received signal power comes from multipath sources, conventional MIMO diversity techniques would fare better in these kinds of channels. A close inspection of the BER plots of the OLOS2 and NLOS channels reveal that their BER performance is very similar. Therefore it is inferred that since conventional MIMO would outperform DCPM in the NLOS channel, there is no need to bother with DCPM in the OLOS2-type channels.

6.2.5 Effects of Channel Correlation and Rice Factor on BER

In order to determine the effects of channel correlation and Rice factor on the BER of receive-only DCPM devices, only two channel states are considered; these are the LOS fading channel and the OLOS1 fading channel. The reason for limiting the analysis to these two channel states is because only these two possess the required polarisation purity suitable for polarisation multiplexing. Also the two channel states are chosen based on their relatively good BER results in the previous sections, where it is shown using Figures 6.4, 6.9 and 6.10 that the BER of DCPM, which is implemented with ZF and MMSE equalisation schemes, approach those achieved using an optimal exhaustive search MLSE equalisation. The Rice factor range used in the simulation of this section is given in Table 6-6 while the corresponding channel cross correlation values and the XPD-XPC factors are given in Table 6-7. The values of correlation to match the Rice factors were computed using equations (5.16) and (5.17) and instances where the Rice factor values fall outside the validated range of the Rice-correlation model, the channel statistics found in Figure 4.29 were used in determining the correct cross correlation values to apply. The results of the BER simulations for the LOS channel are shown in Figures 6.19 to 6.22. In the figures, K_{11} represents the Rice factor of the RHCP co-polar sub-channel while K_{12} stands for the Rice factor of the RHCP cross-polar sub-channel. The BER simulations for both LOS and OLOS1 channels only consider balanced channels, therefore $K_{11} = K_{22}$ and $K_{12} = K_{21}$. As was the case previously, BER from MLSE equalisation are only included for bench marking purposes.

Table 6-6: Rice factor values used in the Rice factor-BER effects simulations

	State 1 (LOS)	**State 2 (OLOS 1)**
Co-polar channels Rice factor range	3dB to 21dB	-5dB to 17dB
Cross-polar channels Rice factor range	-4dB to 14dB	-8dB to 14dB

Table 6-7: Table of complete channel parameters used in the simulations of Rice factor-BER characteristics of the LOS channel

Channel description	**Sub-channel**	**Rice factor in dB**	**Cross correlation coefficient**	**XPD-XPC factor in dB**
Lower end of LOS channel state	Co-polar	3	0.62	6.9
	Cross-polar	-4	0.24	6.9
Intermediate region I of channel state	Co-polar	9	0.90	6.9
	Cross-polar	2	0.46	6.9
Intermediate region II of channel state	Co-polar	15	0.96	6.9
	Cross-polar	8	0.80	6.9
Upper end of LOS channel state	Co-polar	21	0.96	6.9
	Cross-polar	14	0.82	6.9

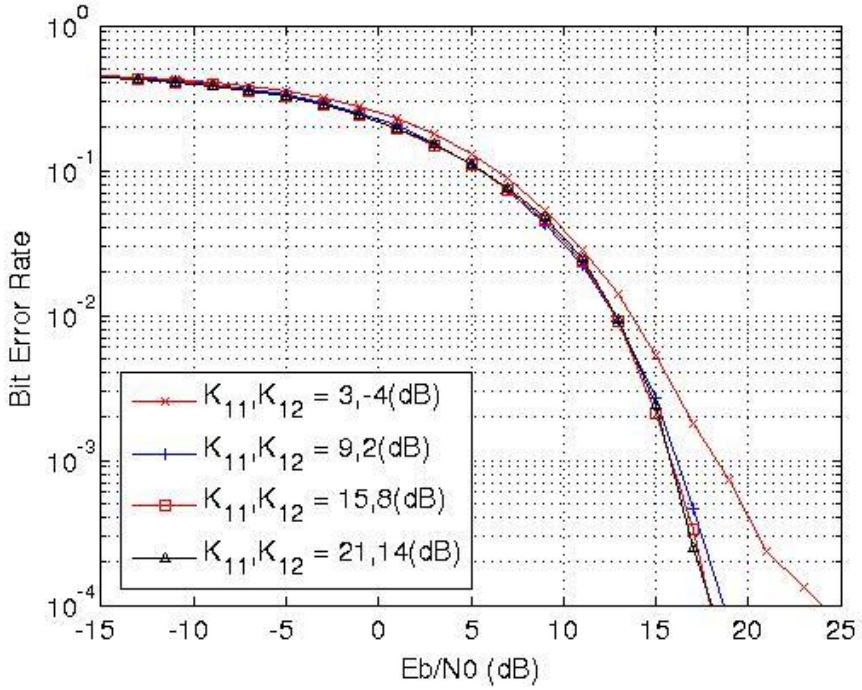

Figure 6.19: Effect of Rice factor on the BER of 'no equalisation' in the LOS channel

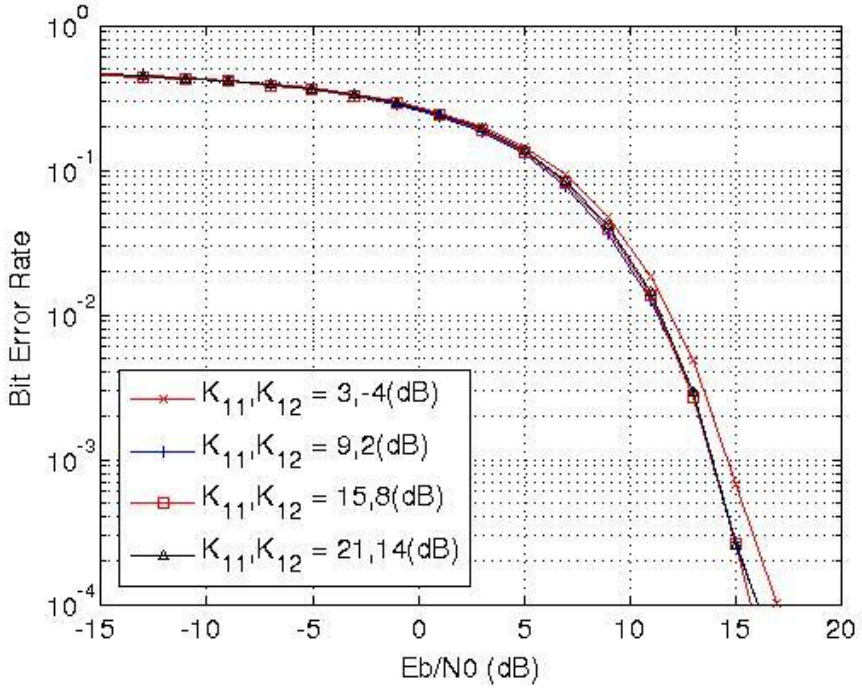

Figure 6.20: Effect of Rice factor on the BER of linear unordered ZF in the LOS channel

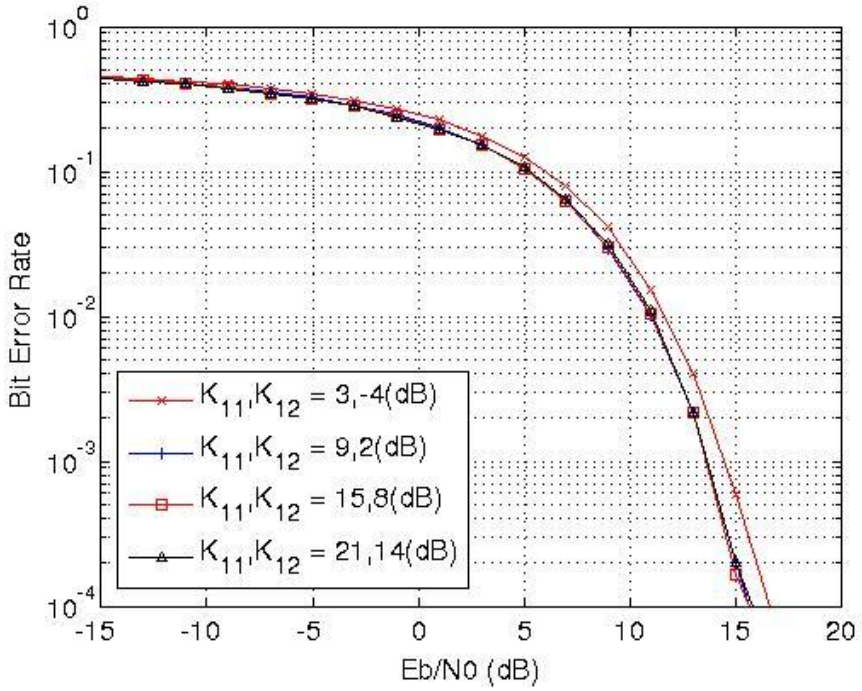

Figure 6.21: Effect of Rice factor on the BER of linear unordered MMSE in the LOS channel

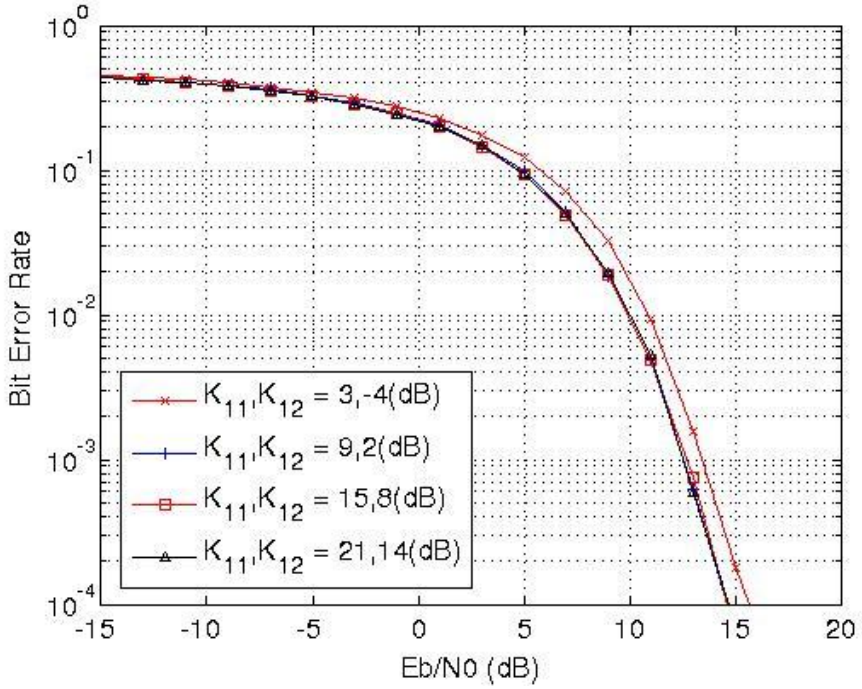

Figure 6.22: Effect of Rice factor on the BER of linear unordered MLSE in the LOS channel

Observe that all four LOS channel BER plots above follow the same trend. Specifically, when the co- and cross-polar Rice factors respectively increase from 3dB and -4dB to 21dB and 14dB, the E_b/N_0 required to achieve a BER of 10^{-2} reduces by at least 1.5dB in all four 'equalisation' modes. However marginal this improvement is, it represents a significant result since this is achieved without resort to any error correction coding.

The same trend repeats itself in the OLOS1 channel where as shown in Figures 6.23 to 6.25, that increasing the co- and cross-polar Rice factor respectively from -5dB and -8dB to 13dB and 10dB gives a minimum E_b/N_0 gain of 10dB (for MLSE equalisation) at 10^{-2} E_b/N_0. As shown in Figure 6.23, it is not even worth attempting to decode transmitted symbols without channel equalisation since a BER of 10^{-2} cannot be achieved even at an E_b/N_0 of 30dB. Interestingly, the simplest of the equalisation schemes, ZF, achieves almost the same BER of 10^{-3} as the more computationally complex MMSE when the E_b/N_0 is 15dB.

Table 6-8: Table of complete channel parameters used in the simulations of Rice factor-BER characteristics of the OLOS1 channel

Channel description	**Sub-channel**	**Rice factor in dB**	**Cross correlation coefficient**	**XPD-XPC factor in dB**
Lower end of OLOS1 channel state	Co-polar	-5	0.28	10
	Cross-polar	-8	0.16	10
Intermediate region I of channel state	Co-polar	1	0.42	10
	Cross-polar	-2	0.24	10
Intermediate region II of channel state	Co-polar	7	0.90	10
	Cross-polar	4	0.66	10
Upper end of OLOS1 channel state	Co-polar	13	0.96	10
	Cross-polar	10	0.83	10

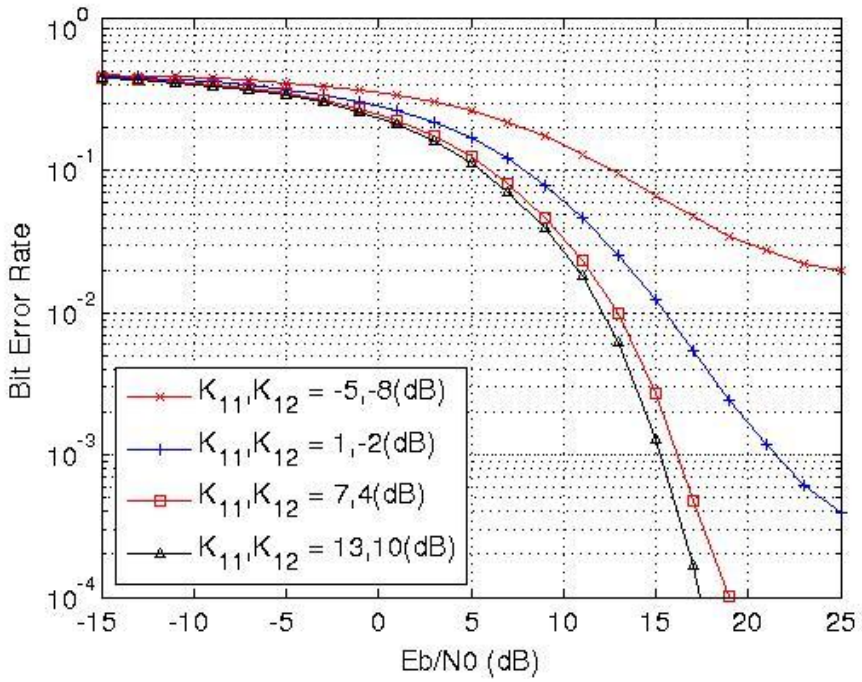

Figure 6.23: Effect of Rice factor on the BER of 'no equalisation' in the OLOS1 channel

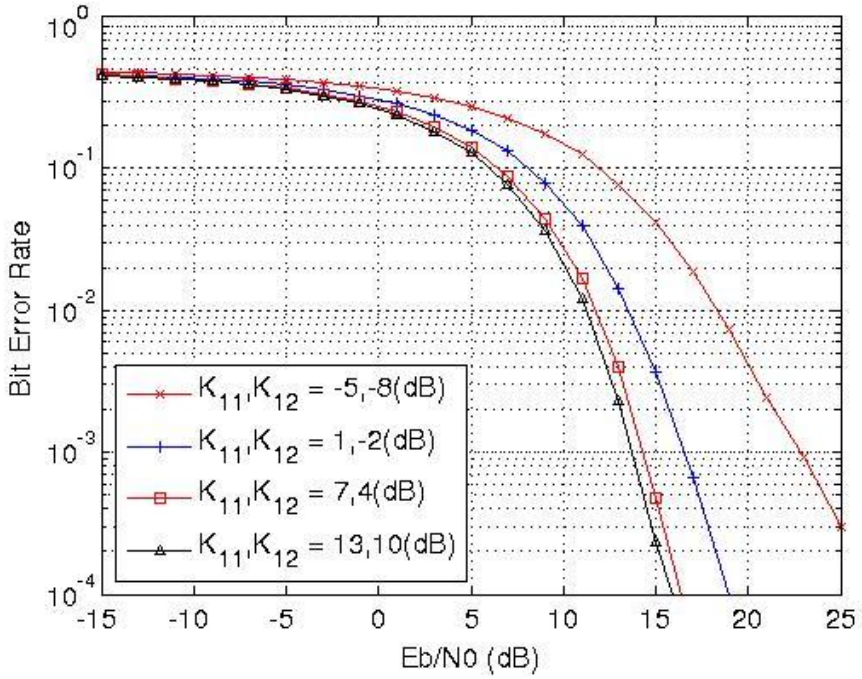

Figure 6.24: Effect of Rice factor on the BER of ZF in the OLOS1 channel

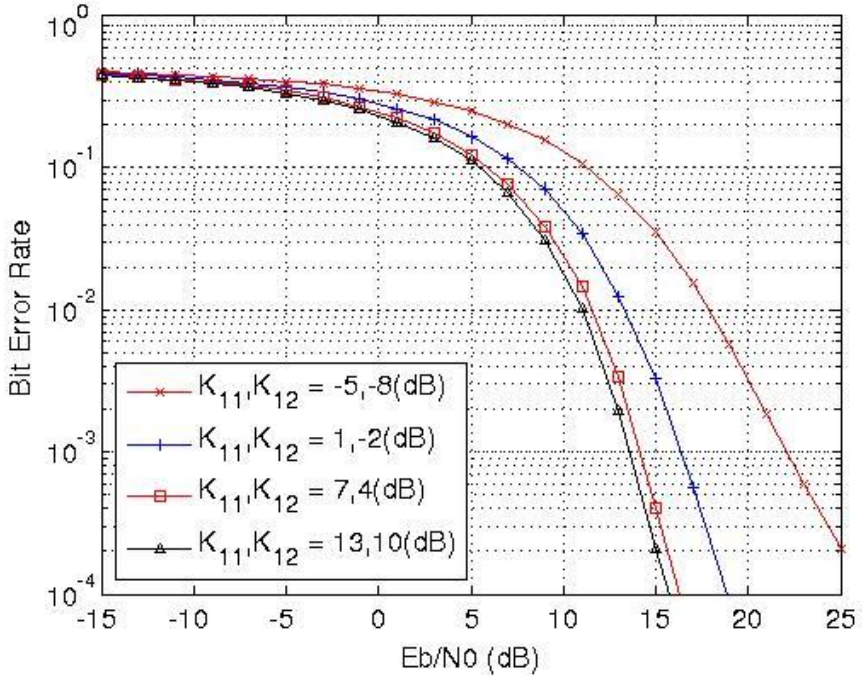

Figure 6.25: Effect of Rice factor on the BER of MMSE in the OLOS1 channel

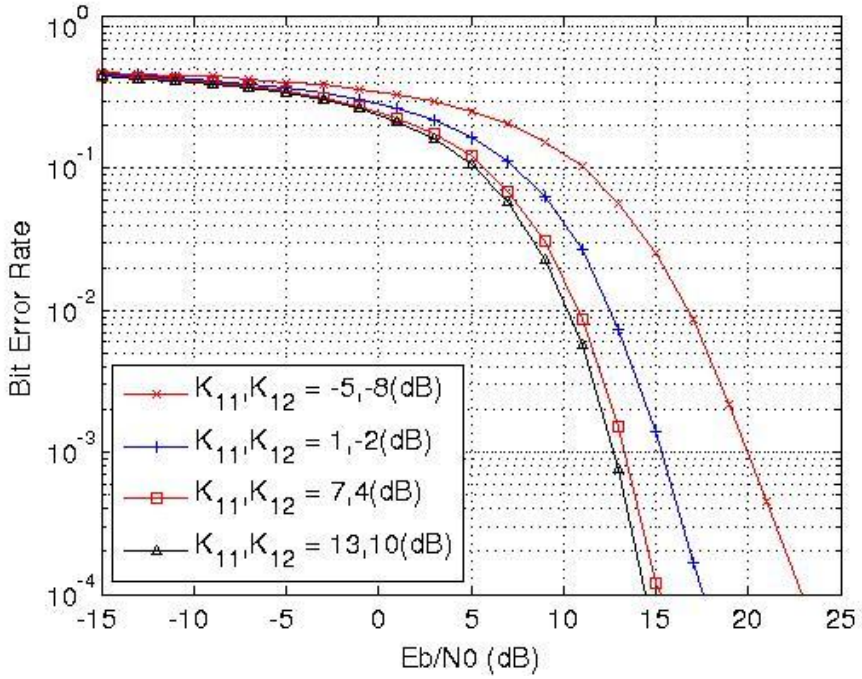

Figure 6.26: Effect of Rice factor on the BER of MLSE in the OLOS1 channel

In order to conclusively determine the most appropriate equalisation scheme to use for DCPM, the BER results of Figures 6.19 to 6.26 and the channel model parameters used in deriving them are summarised into Figures 6.27(a) to (d); their description and implications are as follows:

- Figure 6.27(a) shows the relationship between the co-polar channel Rice factors and the cross-polar channel Rice factors used in the BER simulations, where it can be observed that there is an overlap between the Rice factor of the LOS and OLOS1 channels. However, the main function of the graphs is to show that increasing co-polar channel Rice factors correspond to increasing cross-polar channel Rice factor for both the LOS and OLOS1 fading channel.
- Figure 6.27(b) shows the relationship between the co-polar channel cross correlation and the co-polar channel Rice factor for the LOS and OLOS1 fading channels. Also shown in the same figure is the cross-polar channel cross correlation and their corresponding Rice factor values. This diagram indicates that the co- and cross-polar channel cross correlation coefficients increase with

increasing Rice factor for both LOS and OLOS1 channels and the trend observed in the measured channel data has not been violated.

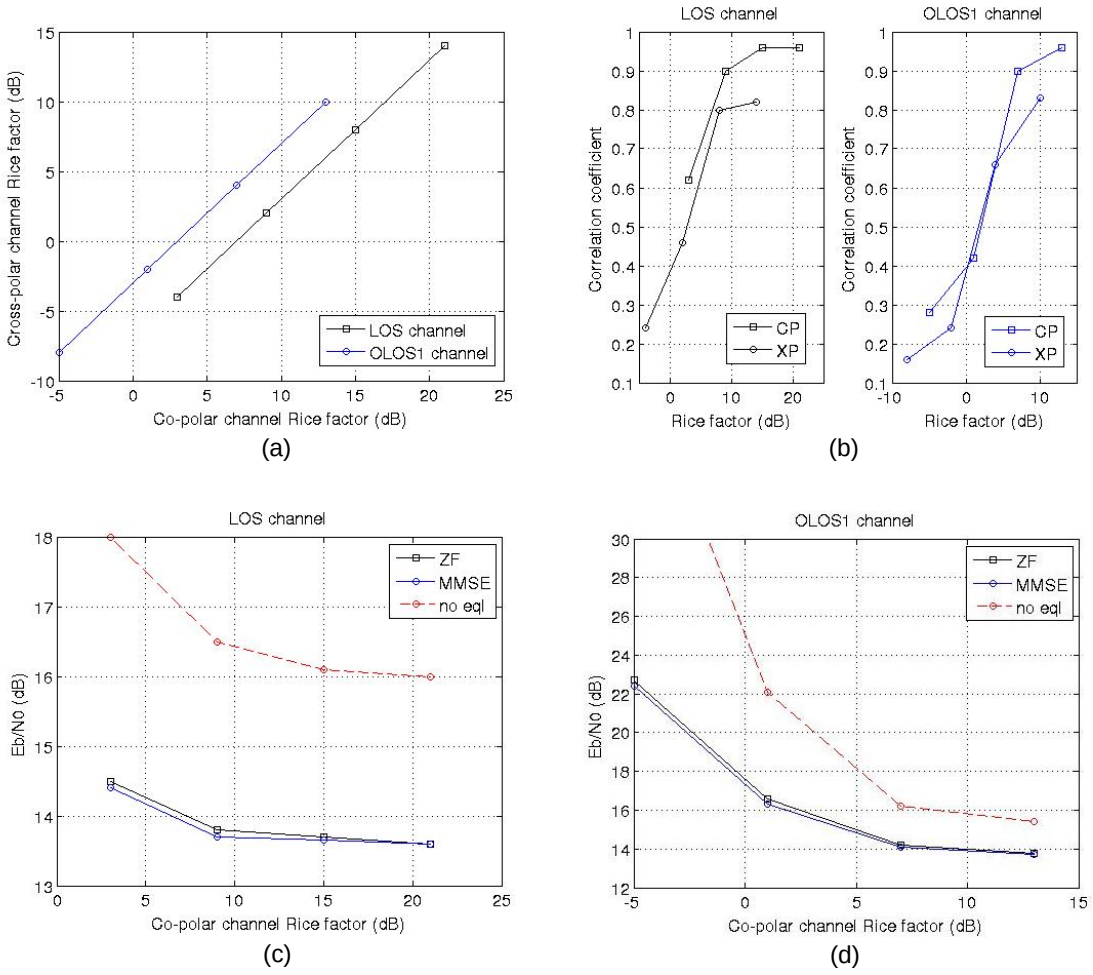

Figure 6.27: Summary of BER simulation results and channel parameters showing: (a) range of co- and cross-polar channel Rice factors, (b) channel correlation coefficients and corresponding Rice factor values, (c) E_b/N_0 and corresponding Rice factor needed by ZF, MMSE and 'no equalisation' equalisation schemes to achieve a BER of 10^{-3} in the LOS channel, (d) E_b/N_0 and corresponding Rice factor needed by ZF, MMSE and 'no equalisation' equalisation schemes to achieve a BER of 10^{-3} in the OLOS1 channel

- Figure 6.27(c) shows the Rice factors and corresponding E_b/N_0 values needed to achieve a BER of 10^{-3} when applying 'no equalisation', ZF and MMSE in a predominantly LOS fading channel. Observe that the E_b/N_0 needed by ZF is within 0.2dB of that required by MMSE for the full simulated Rice factor range. The meagre 0.2dB E_b/N_0 advantage of MMSE over ZF in the LOS channel makes it unsuitable for limited power DCPM devices since its more numerous

computation operations would offset this advantage. Therefore it is recommended that ZF is the equalisation scheme of choice in the highly correlated LOS channel since its lower number of computation operations, despite its 0.2dB E_b/N_0 disadvantage, would better preserve the battery life of DCPM devices.

- Figure 6.27(d) shows the Rice factors and corresponding E_b/N_0 values needed to achieve a BER of 10^{-3} when applying 'no equalisation', ZF and MMSE in channel experiencing OLOS1-type fading. In this channel, the E_b/N_0 required for ZF is within 0.1dB that of MMSE when the Rice factor is above 0dB. Therefore there is no need to bother with the more complex MMSE. ZF should also be the equalisation of choice in the OLOS1 fading channel.

6.3 Recommendations for the use of DCPM in Dual Circular Polarised LMS Channels

Having seen in chapter 3 that polarisation multiplexing can only deliver comparable capacities to conventional MIMO when the polarisation purity of the channel (as characterised by the XPD-XPC) ratio is high, and going by the BER results presented in this chapter, it is recommended that DCPM is only suitable for channels exhibiting LOS and OLOS1-like fading characteristics. More robust but practical channel equalisation schemes like ZF-OSIC and MMSE-OSIC cannot provide better BER than their linear unordered equivalents and hence DCPM receivers do not need to be encumbered with such technologies. However, when the channel tends towards being more OLOS2-like and Rayleigh/NLOS-like, it is recommended that ZF-based DCPM be abandoned due to its poor bit error rates. The technique of choice in such channels should be conventional MIMO since MIMO was originally designed for such multipath-rich channels in the first place. These recommendations are in line with the DVB-SH [40] guidelines, which specifically require that receivers should be able to exploit parallel transmission modes by multiplexing two separate orthogonally polarised data streams during LOS periods and to exploit diversity during OLOS/NLOS propagation. Finally, the recommendations for the operation of dual circular polarised land mobile satellite receiving terminals are summarised as follows:

- Use DCPM with ZF equalisation when channel condition is predominantly LOS and co-polar and cross-polar branch Rice factors are greater than 3dB and -4dB respectively. Based on empirical channel data, these Rice factors correspond to XPD values of at least 7dB and cross correlation coefficients of the two co-polar channels of at least 0.65. Similarly, the cross correlation coefficients of the two cross-polar channels should not be less than 0.20 for good DCPM performance in the LOS channel.

- Only use DCPM in the OLOS1 channel when the co-polar and cross-polar channel Rice factors are greater than 1dB and -2dB respectively and the branch power ratio of the co- and cross-polar channels is close to unity since an imbalance in the branch power ratio adversely affects the BER of ZF. The corresponding correlation coefficients for DCPM to work in this channel type must be at least 0.40 for the co-polar channel and 0.25 for the cross-polar channel while the XPD should be greater than 10dB. If the above channel parameters are not met, DCPM would fail in the OLOS1 channel.

- In all other channels experiencing deep shadowing or obstruction, such as the OLOS2 and NLOS/Rayleigh channels, polarisation multiplexing cannot be beneficially exploited and conventional MIMO diversity techniques become more suitable.

6.4 Conclusions

Using a newly developed dual circular polarised LMS channel model, this chapter embarked on a detailed and extensive analysis of bit error rate simulation results. The effects on equalisation techniques of different channel fading conditions, as exemplified by the channel states of the new channel model, were studied. It was found that ZF-OSIC and MMSE-OSIC do not provide any obvious BER advantage over their linear unordered counterparts and hence should not be applied in DCPM. The effects of Rice factor and the attendant channel correlation were also studied within the LOS and OLOS1 channel states where simulations revealed that increasing Rice factor positively correlates with improved bit error rates. Finally, it was determined that the biggest threat to successful

implementation of DCPM even in the highly favourable LOS channel is an imbalance in channel branch power ratios. The actual causes of these imbalances were however not explored and are left for future researchers to tackle.

The work presented in this chapter and the measurement campaign chapter was compiled into a journal paper titled “Dual Circular Polarization Multiplexing for DVB-SH/NGH Applications”, and is awaiting submission.

Chapter 7

7 Conclusions and Future Work

This research work commenced with the intention of implementing multiple-input multiple-output (MIMO) in the land mobile satellite (LMS) channel. In the course of the literature survey and subsequent research, it was realised that conventional MIMO, employing spatially separated antennas and even of orthogonal circular polarisations, cannot be beneficially adopted from the terrestrial channel into the mostly line of sight (LOS) LMS channel. Therefore, a polarisation multiplexing approach, termed dual circular polarisation multiplexing (DCPM) was proposed as the technique of choice. In order to determine the workability of DCPM, measured channel data from previous campaigns was examined and it was found that high elevation LOS propagation scenarios that are more representative of LMS systems were in short supply. Therefore a series of higher elevation measurement campaigns were carried out to provide the much needed data. Since recorded channel data lacks flexibility of use and can only represent channel fading conditions from which the measurements were taken, a realistic and tractable channel model, based on empirical statistics extracted from the recorded data needed to be developed. The new channel model presented in this thesis has been shown to accurately depict dual circular polarised LMS MIMO channel fading and has been used in bit error rate (BER) simulations to determine the channel equalisation modes most suitable for DCPM implementation.

7.1 Research Contributions

The main contributions of this thesis are as follows: chapter 2 presented various metrics for characterising the MIMO radio channel and provided reasons why most LMS channel models adopt the stochastic modelling approach. A thorough review of available stochastic models of the polarised LMS MIMO channel revealed some weaknesses and their lack of representation of the Rice factor-channel correlation effects. It was posited

that fully incorporating these factors in a tractable channel model would help in uncovering the true potentials of MIMO in orthogonally circular polarised LMS channels.

Since transceivers are the structures through which the benefits of MIMO channels is harnessed, chapter 3 reviewed literature on the popular transceiver architectures, and considering them in the receive-only mode, the intricacies of channel equalisation techniques were laid bare. This allowed for the adoption of two of them – zero forcing and MMSE – for the proposed DCPM. Analysis and preliminary simulations were performed to glean the potential capacity benefits of DCPM compared with conventional MIMO. It was found that polarisation multiplexing can only provide superior capacity to conventional MIMO when the polarisation purity of the orthogonal channels is high and at low SNR values.

Chapter 3 used a basic model to study the effects of polarisation on the capacity and BER of dual circular polarised LMS channels, the best way to understand such channels is by actually measurements and studying the realised data. To this end, a series of measurement campaigns were set up and conducted as described in chapter 4. From the obtained measured channel data, it was concluded that orthogonal circular polarisation, though providing some level of sub-channel independence, cannot provide the enough independent fading needed by conventional MIMO techniques. Also, using polynomial fits to the measured channel data, trends between channel fading variables were uncovered and these were in agreement with earlier and independently obtained channel data.

Building on the trends found in the measured channel data and the on earlier attempts to model the LMS MIMO and terrestrial polarised channels, extensions to the channel model for the dual circular polarised LMS channel was presented in chapter 5. This channel has been validated against measured channel data using first and second order channel fading statistics. Also presented in this chapter is a way to model the relationship between the channel Rice and channel correlation based on empirical fits to measurements.

Chapter 6 made use of the newly developed dual circular polarised LMS channel model to perform extensive BER analysis. These analyses revealed that ZF can provide adequate bit error rates when the channel is mainly LOS and slightly shadowed (OLOS1). Also

uncovered was the fact the ordered successive interference cancellation, either with ZF or MMSE, does not provide significant BER advantage over their linear unordered counterparts. The biggest threat to implementing polarisation multiplexing in the LMS channel comes from branch power imbalances.

Finally, the channel conditions that favour DCPM implementation in the LOS channel were enumerated to include co-polar and cross-polar Rice factors of at least 3dB and -4dB respectively and with the XPD being at least 7dB. The cross correlation coefficient of the two co-polar channels must be at least 0.65 while that of the two cross-polar channels must be at least 0.20. For DCPM to be viable in the OLOS1 channel, the co-polar and cross-polar channel Rice factors must be greater than 1dB and -2dB respectively and the branch power ratio of the two co-polar (and cross-polar) channels should be close to unity while the cross correlation coefficient between the co-polar channels must be at least 0.40 and the cross correlation between the cross-polar channels should be greater than 0.25.

Of the approximately 43km of route travelled during the course of the two measurement campaigns of this thesis, less than 15% of the sampled dual circular polarised LMS channel data met the criteria for good DCPM operability and out of this 15%, 92% of the time was in the rural environment. Since DCPM was intended for rural environments, 92% coverage represents very good results and the remaining 8% is only when the more complex conventional MIMO can be considered.

7.2 Future Work

Based on the findings and the conclusions drawn, the following areas are recommended for future work:

- There was a strict limitation on the interference sources that were considered for the DCPM analysis since the analysis considered a broadcast-only scenario. In addition to the depolarised sub-channel interference considered in this thesis, all other possible sources of interference need to be taken into account. It is especially important for the interference coming from terrestrial sources (the complementary ground components of integrated satellite-terrestrial networks

used for local content insertion) to be considered. However, such additional interference may not be significantly in rural areas where DCPM is most likely to be implemented.

- The BER analysis carried out was limited to uncoded transmissions. This is not usually the case in practice and future work need to factor in the effects of turbo coding, time interleaving and forward error correction schemes in the DCPM system with real time implementation.
- One of the assumptions in this thesis was that pilot signals were transmitted by the satellite and through this, the receiver accurately estimated the channel state information. However, the receiver may not always have an accurate knowledge of the channel and at times this knowledge may be outdated. The effects of having imperfect channel state knowledge should be considered as this would have a significant effect on the DCPM channel equalisation schemes.
- For each of the four channel states defined by the new channel model, chapter 6 considered single cases where there were imbalances in the branch power ratio. The extent of these imbalances (as characterised by varying channel XPC and antenna XPD) and their causes need to be conclusively determined if the application of DCPM is to be further considered.
- Since the proposed channel model employed 'ideal' data from each of the fading states for its development, it was not possible to determine the full extent of Rice factor variability in each of the channels in a single Markov state. To obtain this information, the already available measured channel data needs to be further analysed and where necessary, new measurement campaigns performed to extract the required information.
- Specific antenna effects on the implementation of DCPM, such as those induced by compact co-location of orthogonal circular polarised antennas [97] needs to be studied in greater detail.
- The effects of rainfall and snow attenuation on the BER and capacity of DCPM systems need to be considered.
- Tropospheric and ionospheric effects need to be incorporated into the model for it to be more representative of the LMS channel.

- Other specific environments like maritime and aeronautical mobile environments, with their distinct Doppler characteristics and where the channel fading is characteristically different from the LMS case need to be studied.
- Wideband channel analysis is another important area to consider for further work.
- Finally, both the new channel model and the model describing the Rice factor–channel correlation relationship can be further validated and fine-tuned with the availability of new measured channel data, for example L-band channel measurements.

References

[1] P. R. King and S. Stavrou, "Low Elevation Wideband Land Mobile Satellite MIMO Channel Characteristics," *IEEE Transactions on Wireless Communications,* vol. 6, pp. 2712-2720, 2007.

[2] P. Arapoglou, P. Burzigotti, M. Bertinelli, A. Alamanac, and R. De Gaudenzi, "To MIMO or Not To MIMO in Mobile Satellite Broadcasting Systems," *IEEE Transactions on Wireless Communications,* vol. PP, pp. 1-5, 2011.

[3] P. R. King, "Modelling and Measurement of the Land Mobile Satellite MIMO Radio Propagation Channel," PhD Thesis, University of Surrey, Guildford, UK, 2007.

[4] P. D. Arapoglou, P. Burzigotti, A. B. Alamanac, and R. De Gaudenzi, "Capacity potential of mobile satellite broadcasting systems employing dual polarization per beam," in *5th Advanced satellite multimedia systems conference and the 11th signal processing for space communications workshop*, 2010, pp. 213-220.

[5] E. Eberlein, F. Burkhardt, C. Wagner, A. Heuberger, D. Arndt, and R. Prieto-Cerdeira, "Statistical evaluation of the MIMO gain for LMS channels," in *5th European Conference on Antennas and Propagation*, Rome, Italy, 2011, pp. 2848-2852.

[6] H. Ozcelik and C. Oestges, "Some remarkable properties of diagonally correlated MIMO channels," *IEEE Transactions on Vehicular Technology,* vol. 54, pp. 2143-2145, 2005.

[7] P. D. Arapoglou, K. Liolis, M. Bertinelli, A. Panagopoulos, P. Cottis, and R. De Gaudenzi, "MIMO over Satellite: A Review," *IEEE Communications Surveys & Tutorials,* vol. 13, pp. 27-51, 2011.

[8] A. F. Molisch, *Wireless Communications*. Chichester: John Wiley, 2005.

[9] G. J. Foschini and M. J. Gans, "On limits of wireless communications in a fading environment when using multiple antennas," *Wireless Personal Communications,* vol. 6, pp. 311-335, 1998.

[10] H. Kaibin, J. G. Andrews, and R. W. Heath, "Performance of Orthogonal Beamforming for SDMA With Limited Feedback," *IEEE Transactions on Vehicular Technology,* vol. 58, pp. 152-164, 2009.

[11] T. M. Duman and A. Ghrayeb, *Coding for MIMO Communication Systems*. Chichester: John Wiley, 2007.

[12] L. G. Ordonez, D. P. Palomar, A. Pages-Zamora, and J. Rodriguez Fonollosa, "High-SNR Analytical Performance of Spatial Multiplexing MIMO Systems With CSI," *IEEE Transactions on Signal Processing,* vol. 55, pp. 5447-5463, 2007.

[13] S. R. Saunders and A. Aragon-Zavala, *Antennas and Propagation for Wireless Communication Systems,* 2nd ed. Chichester: John Wiley, 2007.

[14] G. J. Foschini, G. D. Golden, R. A. Valenzuela, and P. W. Wolniansky, "Simplified processing for high spectral efficiency wireless communication employing multi-element arrays," *IEEE Journal on Selected Areas in Communications,* vol. 17, pp. 1841-1852, 1999.

[15] R. W. Heath and A. J. Paulraj, "Switching between diversity and multiplexing in MIMO systems," *IEEE Transactions on Communications,* vol. 53, pp. 962-968, 2005.

[16] R. T. Schwarz, A. Knopp, B. Lankl, D. Ogermann, and C. A. Hofmann, "Optimum-Capacity MIMO Satellite Broadcast System: Conceptual Design for LOS Channels," in *4th Advanced Satellite Mobile Systems*, 2008, pp. 66-71.

[17] R. T. Schwarz, A. Knopp, D. Ogermann, C. A. Hofinann, and B. Lankl, "Optimum-capacity MIMO satellite link for fixed and mobile services," in *International ITG Workshop on Smart Antennas*, 2008, pp. 209-216.

[18] K. Liolis, J. Gomez-Vilardebo, E. Casini, and A. Perez-Neira, "Statistical Modeling of Dual-Polarized MIMO Land Mobile Satellite Channels," *IEEE Transactions on Communications,* vol. 58, pp. 3077-3083, 2010.

[19] B. G. Evans (Ed), *Satellite Communication Systems*, 3rd ed. London, UK: The Instituion of Electrical Engineers, 1999.

[20] M. Ozcelik, N. Czink, and E. Bonek, "What makes a good MIMO channel model?," in *IEEE 61st Vehicular Technology Conference*, 2005, pp. 156-160.

[21] M. Sellathurai, P. Guinand, and J. Lodge, "Space-time coding in mobile Satellite communications using dual-polarized channels," *IEEE Transactions on Vehicular Technology,* vol. 55, pp. 188-199, 2006.

[22] K. Yu and B. Ottersten, "Models for MIMO propagation channels: a review," *Wireless Communications and Mobile Computing,* vol. 2, pp. 653-66, 2002.

[23] P. Kyritsi, D. C. Cox, R. A. Valenzuela, and P. W. Wolniansky, "Correlation analysis based on MIMO channel measurements in an indoor environment," *IEEE Journal on Selected Areas in Communications,* vol. 21, pp. 713-720, 2003.

[24] R. H. Clarke, "A Statistical Theory of Mobile-Radio Reception," *Bell System Technical Journal,* pp. 957-1000, 1966.

[25] T. W. C. Brown and U. M. Ekpe, "When is Clarke's Approximation Valid?," *IEEE Antennas and Propagation Magazine,* vol. 52, pp. 171-181, 2010.

[26] A. M. Tulino, A. Lozano, and S. Verdu, "Impact of antenna correlation on the capacity of multiantenna channels," *IEEE Transactions on Information Theory,* vol. 51, pp. 2491-2509, 2005.

[27] C. Chen-Nee, D. N. C. Tse, J. M. Kahn, and R. A. Valenzuela, "Capacity scaling in MIMO wireless systems under correlated fading," *IEEE Transactions on Information Theory*, vol. 48, pp. 637-650, 2002.

[28] S. Da-Shan, G. J. Foschini, M. J. Gans, and J. M. Kahn, "Fading correlation and its effect on the capacity of multielement antenna systems," *IEEE Transactions on Communications,* vol. 48, pp. 502-513, 2000.

[29] H. Ozcelik and C. Oestges, "Capacity of diagonally correlated MIMO channels," in *IEEE 61st Vehicular Technology Conference*, 2005, pp. 116-120.

[30] C. E. Shannon, "A Mathematical Theory of Communication," *Bell System Technical Journal*, vol. 27, pp. 379-423(Part 1), 623-656(Part 2), 1948.

[31] I. E. Telatar, "Capacity of Multi-antenna Gaussian Channels," *European Transactions on Telecommunications*, vol. 6, pp. 585-595, 1999.

[32] D. Gesbert, M. Shafi, S. Da-shan, P. J. Smith, and A. Naguib, "From theory to practice: an overview of MIMO space-time coded wireless systems," *IEEE Journal on Selected Areas in Communications*, vol. 21, pp. 281-302, 2003.

[33] A. Goldsmith, S. A. Jafar, N. Jindal, and S. Vishwanath, "Capacity limits of MIMO channels," *IEEE Journal on Selected Areas in Communications*, vol. 21, pp. 684-702, 2003.

[34] M. Jankiraman, *Space-Time Codes and MIMO Systems*. Boston: Artech House, 2004.

[35] G. H. Golub and C. F. Van Loan, *Matrix Computations*, 3rd ed. Baltimore: John Hopkins University Press, 1996.

[36] W. Weichselberger, "Spatial Structure of Multiple Antenna Radio Channels. A Signal Processing Viewpoint," PhD, Technical University, Vienna, 2003.

[37] M. Webb, M. Hunukumbure, and M. Beach, "Eigen-Coherence and Link Performance of Closed-Loop 4G Wireless in Measured Outdoor MIMO Channels," *IEEE Transactions on Antennas and Propagation*, vol. 60, pp. 674-681, 2012.

[38] D. G. Brennan, "Linear diversity combining techniques," *Proceedings of the IEEE*, vol. 91, pp. 331-356, 2003.

[39] M. A. N. Parks, G. Butt, M. J. Willis, and B. G. Evans, "Wideband propagation measurements and results at L- and S-bands for personal and mobile satellite communications," in *Fifth International Conference on Satellite Systems for Mobile Communications and Navigation*, 1996, pp. 64-71.

[40] ETSI EN 302-583 V1.1.2, "Digital Video Broadcasting (DVB); Framing Structure, channel coding and modulation for Satellite Services to Handheld devices (SH) below 3 GHz," Feb. 2010.

[41] I. Frigyes, B. Molnar, L. Juhasz, I. Papp, Z. Bodnar, J. Berces, F. Som, and A. Kasa, "Theoretical and experimental characterisation of the satellite-to-indoor radio channel," in *Fifth International Conference on Satellite Systems for Mobile Communications and Navigation*, 1996, pp. 47-50.

[42] C. Oestges and D. Vanhoenacker-Janvier, "A physical-statistical shadowing correlation model and its application to low-Earth-orbit systems," *IEEE Transactions on Vehicular Technology*, vol. 50, pp. 416-421, 2001.

[43] F. Perez-Fontan, N. Jeannin, L. Castanet, H. Mametsa, F. Lacoste, V. Hovinen, M. Schonhuber, F. Teschl, and R. Prieto-Cerdeira, "Statistical and physical-statistical modeling of the land mobile satellite channel at Ku- and Ka-Band," in *5th*

European Conference on Antennas and Propagation, Rome, Italy, 2011, pp. 3393-3397.

[44] C. Tzaras, B. G. Evans, and S. R. Saunders, "Physical-statistical analysis of land mobile-satellite channel," *Electronics Letters,* vol. 34, pp. 1355-1357, 1998.

[45] A. F. Molisch, "A generic model for MIMO wireless propagation channels in macro- and microcells," *IEEE Transactions on Signal Processing,* vol. 52, pp. 61-71, 2004.

[46] P. Petrus, J. H. Reed, and T. S. Rappaport, "Geometrical-based statistical macrocell channel model for mobile environments," *IEEE Transactions on Communications,* vol. 50, pp. 495-502, 2002.

[47] C. Oestges, "A stochastic geometrical vector model of macro- and megacellular communication channels," *IEEE Transactions on Vehicular Technology,* vol. 51, pp. 1352-1360, 2002.

[48] W. Shuangquan, A. Abdi, J. Salo, H. M. El-Sallabi, J. W. Wallace, P. Vainikainen, and M. A. Jensen, "Time-Varying MIMO Channels: Parametric Statistical Modeling and Experimental Results," *IEEE Transactions on Vehicular Technology,* vol. 56, pp. 1949-1963, 2007.

[49] D. Chizhik, J. Ling, P. W. Wolniansky, R. A. Valenzuela, N. Costa, and K. Huber, "Multiple-input-multiple-output measurements and modeling in Manhattan," *IEEE Journal on Selected Areas in Communications,* vol. 21, pp. 321-331, 2003.

[50] J. P. Kermoal, L. Schumacher, K. I. Pedersen, P. E. Mogensen, and F. Frederiksen, "A stochastic MIMO radio channel model with experimental validation," *IEEE Journal on Selected Areas in Communications,* vol. 20, pp. 1211-1226, 2002.

[51] W. Weichselberger, M. Herdin, H. Ozcelik, and E. Bonek, "A stochastic MIMO channel model with joint correlation of both link ends," *IEEE Transactions on Wireless Communications,* vol. 5, pp. 90-100, 2006.

[52] H. Ozcelik, M. Herdin, W. Weichselberger, J. Wallace, and E. Bonek, "Deficiencies of 'Kronecker' MIMO radio channel model," *Electronics Letters,* vol. 39, pp. 1209-1210, 2003.

[53] V. Erceg, H. Sampath, and S. Catreux-Erceg, "Dual-polarization versus single-polarization MIMO channel measurement results and modeling," *IEEE Transactions on Wireless Communications,* vol. 5, pp. 28-33, 2006.

[54] V. R. Anreddy and M. A. Ingram, "Capacity of measured ricean and rayleigh indoor MIMO channels at 2.4 GHz with polarization and spatial diversity," in *IEEE Wireless Communications and Networking Conference,* 2006, pp. 946-951.

[55] P. Horvath and I. Frigyes, "Investigation of the polarization properties of satellite channels with multiple antennas," in *Proceedings of the European Conference on Antennas and Propagation*, Noordwijk, Netherlands, 2006, p. 4 pp.

[56] C. Oestges, B. Clerckx, M. Guillaud, and M. Debbah, "Dual-polarized wireless communications: from propagation models to system performance evaluation," *IEEE Transactions on Wireless Communications,* vol. 7, pp. 4019-4031, 2008.

[57] N. Zorba, M. Realp, M. A. Lagunas, and A. I. Perez-Neira, "Dual polarization for MIMO processing in multibeam satellite systems," in *10th International Workshop on Signal Processing for Space Communications*, 2008, pp. 1-7.

[58] P.-D. Arapoglou, M. Zamkotsian, and P. Cottis, "Dual Polarization MIMO in LMS Broadcasing Systems: Possible Benefits and Challenges," *International Journal of Satellite Communications and Networking*, 2010.

[59] J. H. Chisholm, P. A. Portmann, J. T. Debettencourt, and J. F. Roche, "Investigations of Angular Scattering and Multipath Properties of Tropospheric Propagation of Short Radio Waves beyond the Horizon," *Proceedings of the IRE*, vol. 43, pp. 1317-1335, 1955.

[60] F. P. Fontan, I. S. Lago, R. P. Cerdeira, and A. B. Alamanac, "Consolidation of a Multi-State Narrowband Land Mobile Satellite Channel Model," in *The Second European Conference on European Conference on Antennas and Propagation*, 2007, pp. 1-6.

[61] C. Loo, "A statistical model for a land mobile satellite link," *IEEE Transactions on Vehicular Technology*, vol. 34, pp. 122-127, 1985.

[62] F. P. Fontan, M. Vazquez-Castro, C. E. Cabado, J. P. Garcia, and E. Kubista, "Statistical modeling of the LMS channel," *IEEE Transactions on Vehicular Technology*, vol. 50, pp. 1549-1567, 2001.

[63] R. Prieto-Cerdeira, F. Perez-Fontan, P. Burzigotti, A. Bolea-Alamañac, and I. Sanchez-Lago, "Versatile two-state land mobile satellite channel model with first application to DVB-SH analysis," *International Journal of Satellite Communications and Networking*, vol. 28, pp. 291-315, 2010.

[64] Y. Ma and L. Zhao, "Achievable Performance of Orthogonal STBC Over Spatially Correlated Rician Channels," *IEEE Transactions on Vehicular Technology*, vol. 56, pp. 1251-1261, 2007.

[65] C. Oestges, B. Clerckx, D. Vanhoenacker-Janvier, and A. J. Paulraj, "Impact of fading correlations on MIMO communication systems in geometry-based statistical channel models," *IEEE Transactions on Wireless Communications*, vol. 4, pp. 1112-1120, 2005.

[66] J. L. Glaser and L. P. Faber, "Evaluation of Polarization Diversity Performance," *Proceedings of the IRE*, vol. 41, pp. 1774-1778, 1953.

[67] T. L. Marzetta, "EM algorithm for estimating the parameters of a multivariate complex Rician density for polarimetric SAR," in *International Conference on Acoustics, Speech, and Signal Processing*, 1995, pp. 3651-3654.

[68] D. Greenwood and L. Hanzo, "Characterization of mobile radio channels," R. Steele, Ed., ed London, U.K.: Pentech, 1992, pp. 163-185.

[69] L. J. Greenstein, D. G. Michelson, and V. Erceg, "Moment-method estimation of the Ricean K-factor," *IEEE Communications Letters*, vol. 3, pp. 175-176, 1999.

[70] I. Sarris and A. R. Nix, "A Line-of-Sight Optimised MIMO Architecture for Outdoor Environments," in *IEEE 64th Vehicular Technology Conference*, 2006, pp. 1-5.

[71] T. W. C. Brown and A. Kyrgiazos, "On the small scale modelling aspects of dual polarised land mobile satellite MIMO channels in line of sight and in vehicles," in *5th European Conference on Antennas and Propagation*, Rome, Italy, 2011, pp. 3718-3721.

[72] P. R. King, T. W. C. Brown, A. Kyrgiazos, and B. G. Evans, "Empirical-Stochastic LMS-MIMO Channel Model Implementation and Validation," *IEEE Transactions on Antennas and Propagation*, vol. 60, pp. 606-614, 2012.

[73] K. P. Liolis, J. Gomez-Vilardebo, E. Casini, and A. Perez-Neira, "On the Statistical Modeling of MIMO Land Mobile Satellite Channels: A Consolidated Approach," in *The 27th IET and AIAA International Communications Satellite Systems Conference*, Edinburgh, UK, 2009.

[74] A. A. Abouda, H. M. El-Sallabi, L. Vuokko, and S. G. Haggman, "Performance of Stochastic Kronecker MIMO Radio Channel Model in Urban Microcells," in *IEEE 17th International Symposium on Personal, Indoor and Mobile Radio Communications*, 2006, pp. 1-5.

[75] P. Kelley, "Overview of the DVB-SH specifications," *International Journal of Satellite Communications and Networking*, vol. 27, pp. 198-214, 2009.

[76] N. Chuberre, O. Courseille, P. Laine, L. Roullet, T. Quignon, and M. Tatard, "Hybrid satellite and terrestrial infrastructure for mobile broadcast services delivery: An outlook to the 'Unlimited Mobile TV' system performance," *International Journal of Satellite Communications and Networking*, vol. 26, pp. 405-426, 2008.

[77] DVB Document A120, "Digital Video Broadcasting (DVB); DVB-SH Implementation Guidelines," June 2011.

[78] DVB TM-H NGH v1.0, "DVB-NGH Call for Technologies," 19 Nov. 2009.

[79] DVB TM-H NGHSM055r1 v1.1, "DVB-NGH Study Mission Report TM-H," 25 Nov. 2009.

[80] DVB CM-NGH v1.01, "Commercial Requirements for DVB-NGH," 29 June 2009.

[81] A. J. Paulraj, D. A. Gore, R. U. Nabar, and H. Bolcskei, "An overview of MIMO communications - a key to gigabit wireless," *Proceedings of the IEEE*, vol. 92, pp. 198-218, 2004.

[82] C. Oestges, "Channel correlations and capacity metrics in MIMO dual-polarized Rayleigh and Ricean channels," in *IEEE 60th Vehicular Technology Conference*, 2004, pp. 1453-1457.

[83] K. N. Sivertsen, A. E. L. Liou, A. Emami-Forooshani, and D. G. Michelson, "A first-order model for depolarization of propagating signals by narrowband ricean fading channels," *IEEE Transactions on Wireless Communications*, vol. 8, pp. 3921-3925, 2009.

[84] S. H. Simon and A. L. Moustakas, "Optimizing MIMO antenna systems with channel covariance feedback," *IEEE Journal on Selected Areas in Communications*, vol. 21, pp. 406-417, 2003.

[85] G. J. Foschini, "Layered space-time architecture for wireless communication in a fading environment when using multi-element antennas," *Bell Labs Technical Journal*, vol. 1, pp. 41-59, 1996.

[86] P. W. Wolniansky, G. J. Foschini, G. D. Golden, and R. A. Valenzuela, "V-BLAST: an architecture for realizing very high data rates over the rich-scattering wireless channel," in *URSI International Symposium on Signals, Systems, and Electronics*, 1998, pp. 295-300.

[87] G. D. Golden, C. J. Foschini, R. A. Valenzuela, and P. W. Wolniansky, "Detection algorithm and initial laboratory results using V-BLAST space-time communication architecture," *Electronics Letters*, vol. 35, pp. 14-16, 1999.

[88] S. Yue and X. Xiang-gen, "On fast recursive algorithms for V-BLAST with optimal ordered SIC detection," *IEEE Transactions on Wireless Communications*, vol. 8, pp. 2860-2865, 2009.

[89] Y. Young-Hwan and S. Hyoung-Kyu, "Influence of channel estimation error on layered space-time receivers," *Electronics Letters*, vol. 39, pp. 1008-1010, 2003.

[90] N. Wang and S. D. Blostein, "Approximate Minimum BER Power Allocation for MIMO Spatial Multiplexing Systems," *IEEE Transactions on Communications*, vol. 55, pp. 180-187, 2007.

[91] H. Juan, T. Xiaofeng, and C. Qimei, "Lower Bound of BER in M-QAM MIMO System with Ordered ZF-SIC Receiver," in *IEEE 69th Vehicular Technology Conference, 2009*, 2009, pp. 1-5.

[92] H. Jaesang, K. Kyeongyeon, K. Sangheon, and L. Chungyong, "Link-Adaptive MIMO Systems With Ordered SIC Receiver Using Stream-Ordering Algorithms in Multiuser Environments," *IEEE Transactions on Vehicular Technology*, vol. 57, pp. 3224-3230, 2008.

[93] M. Mohammad and R. Buehrer, "The Effects of Ordering Criteria in Linear Successive Interference Cancellation in CDMA Systems," *IEEE Transactions on Wireless Communications*, vol. 7, pp. 4128-4132, 2008.

[94] J. Akhtar and D. Gesbert, "Spatial multiplexing over correlated MIMO channels with a closed-form precoder," *IEEE Transactions on Wireless Communications*, vol. 4, pp. 2400-2409, 2005.

[95] U. M. Ekpe, T. Brown, and B. G. Evans, "Unleashing the polarisation domain for land mobile satellite MIMO systems," in *3rd European Conference on Antennas and Propagation*, Berlin, Germany, 2009, pp. 2288-2291.

[96] M. F. Mansor, T. W. C. Brown, and B. G. Evans, "A dual circularly polarised Contrawound Quadrifilar Helix Antenna for land mobile satellite MIMO terminal," in *3rd European Conference on Antennas and Propagation*, 2009, pp. 1072-1076.

[97] M. F. B. Mansor, T. W. C. Brown, and B. G. Evans, "Satellite MIMO Measurement With Colocated Quadrifilar Helix Antennas at the Receiver Terminal," *IEEE Antennas and Wireless Propagation Letters*, vol. 9, pp. 712-715, 2010.

[98] C. Oestges, V. Erceg, and A. J. Paulraj, "Propagation modeling of MIMO multipolarized fixed wireless channels," *IEEE Transactions on Vehicular Technology,* vol. 53, pp. 644-654, 2004.

[99] A. Lozano, A. M. Tulino, and S. Verdu, "Multiple-antenna capacity in the low-power regime," *IEEE Transactions on Information Theory,* vol. 49, pp. 2527-2544, 2003.

[100] B. Sklar, *Digital Communications Fundamentals and Applications*, 2nd ed. New Jersey, USA: Prentice Hall, 2001.

[101] H. Bolcskei, D. Gesbert, C. Papadias, and A. van der Veen (Eds), *Space-Time Wireless Systems. From Array Processing to MIMO Communications*. New York: Cambridge University Press, 2006.

[102] R. Kannan, "Improved algorithms for integer programming and related lattice problems," presented at the Proceedings of the fifteenth annual ACM symposium on Theory of computing, 1983.

[103] J. Lagarias, H. Lenstra, and C. Schnorr, "Korkin-Zolotarev bases and successive minima of a lattice and its reciprocal lattice," *Combinatorica,* vol. 10, pp. 333-348, 1990.

[104] M. Pohst, "On the computation of lattice vectors of minimal length, successive minima and reduced bases with applications," *SIGSAM Bull.,* vol. 15, pp. 37-44, 1981.

[105] U. Fincke and M. Pohst, "Improved Methods for Calculating Vectors of Short Length in a Lattice, Including a Complexity Analysis," *Mathematics of Computation*, vol. 44, pp. 463-471, 1985.

[106] T. Heyn, E. Eberlein, D. Arndt, B. Matuz, F. L. Blasco, R. Prieto-Cerdeira, and J. Rivera-Castro, "Mobile satellite channel with angle diversity: The MiLADY project," in *4th European Conference on Antennas and Propagation*, 2010, pp. 1-5.

[107] D. Arndt, A. Ihlow, A. Heuberger, T. Heyn, E. Eberlein, and R. Prieto-Cerdeira, "Mobile satellite broadcasting with angle diversity - performance evaluation based on measurements," in *IEEE International Symposium on Broadband Multimedia Systems and Broadcasting*, 2010, pp. 1-8.

[108] M. P. Ioannidou and D. P. Chrissoulidis, "Depolarization, Scattering, and Attenuation of Circularly Polarized Radio Waves by Spherically Asymmetric Melting Ice Particles," *IEEE Transactions on Geoscience and Remote Sensing,* vol. 45, pp. 367-375, 2007.

[109] J. D. Parsons (Ed.), *The Mobile Radio Propagation Channel,* 2nd ed. Chichester: John Wiley & Sons, 2000.

[110] W. L. Stutzman, *Polarization in Electromagnetic Systems*. Boston: Artech House, 1992.

[111] M. Evans, N. Hastings, and B. Peacock, *Statistical Distributions*, 3rd ed. New York: John Wiley, 2000.

[112] W. Lee and Y. Yeh, "On the Estimation of the Second-Order Statistics of Log Normal Fading in Mobile Radio Environment," *IEEE Transactions on Communications,* vol. 22, pp. 869-873, 1974.

[113] C. Daniel and F. S. Wood, *Fitting Equations to Data*, 2nd ed. New York: John Wiley, 1999.

[114] U. M. Ekpe, T. W. C. Brown, and B. G. Evans, "Channel characteristics analysis of the dual circular polarized land mobile satellite MIMO radio channel," in *IEEE-APS Topical Conference on Antennas and Propagation in Wireless Communications*, Turin, Italy, 2011, pp. 781-784.

[115] U. M. Ekpe, T. W. C. Brown, and B. G. Evans, "Measuring, Modeling and Simulating the Dual Circular Polarized Land Mobile Satellite MIMO Radio Channel for DVB-SH/NGH Applications," *IEEE Transactions on Wireless Communications,* 2012.

[116] M. S. Bartlett, "Fitting a Straight Line When Both Variables are Subject to Error," *Biometrics*, vol. 5, pp. 207-212, 1949.

[117] F. P. Fontan and P. M. Espineira, *Modeling the Wireless Propagation Channel: A Simulation Approach with MATLAB*. Chichester: John Wiley, 2008.

[118] A. Kyrgiazos, "Land mobile satellite MIMO: Channel modelling for in vehicle line of sight links," MSc Dissertation, University of Surrey, Guildford, UK, 2010.

[119] E. Lutz, D. Cygan, M. Dippold, F. Dolainsky, and W. Papke, "The land mobile satellite communication channel-recording, statistics, and channel model," *IEEE Transactions on Vehicular Technology,* vol. 40, pp. 375-386, 1991.

[120] N. J. Higham, "Cholesky Factorization," *Wiley Interdisciplinary Reviews: Computational Statistics,* vol. 1, pp. 251-254, 2009.

[121] C. Loo, "Further results on the statistics of propagation data at L-band (1542 MHz) for mobile satellite communications," in *IEEE 41st Vehicular Technology Conference*, 1991, pp. 51-56.

[122] C. Oestges and B. Clerckx, *MIMO Wireless Communications: From Real-World Propagation to Space-Time Code Design*. Oxford: Academic Press, 2007.

[123] P. J. Huber, *Robust Statistics*. New York: John Wiley, 1981.

[124] Z. B. Alfassi, Z. Boger, and Y. Ronen, "Outliers," in *Statistical Treatment of Analytical Data*, ed: Blackwell Publishing Ltd., 2009, pp. 68-73.

[125] W. C. Jakes, *Microwave Mobile Communications*. London: Wiley, 1974.

[126] A. N. Baker, "Frequency reuse in land mobile-satellite systems," in *IEE Colloquium on Land Mobile Satellite Systems*, 1992, pp. 5/1-5/5.

[127] S. Perras and L. Bouchard, "Fading characteristics of RF signals due to foliage in frequency bands from 2 to 60 GHz," in *The 5th International Symposium on Wireless Personal Multimedia Communications*, 2002, pp. 267-271.

[128] M. H. Hashim and S. Stavrou, "Measurements and modelling of wind influence on radiowave propagation through vegetation," *IEEE Transactions on Wireless Communications,* vol. 5, pp. 1055-1064, 2006.

[129] Recommendation ITU-R P.833-3, "Attenuation in Vegetation," *The ITU Radio Communication Assembly*, 2001.

[130] S. A. Wilkus, J. D. Bailey, D. G. Brown, R. Dave, R. L. Dorn, J. Hanriot, M. Hoffman, A. Kulkarni, C. S. Lee, L. R. Meader, J. M. Polakovic, and J. Sullivan, "Field Measurements of a Hybrid DVB-SH Single Frequency Network With an Inclined Satellite Orbit," *IEEE Transactions on Broadcasting*, vol. 56, pp. 523-531, 2010.

Appendix

Link Budget Analysis

To ensure that measurement campaigns are successfully conducted, link budget analysis must first be performed. The following represents a link budget analysis carried out for the Newlands Corner measurement campaign. It is important that at maximum measurement distance, there is enough impulse response dynamic range (IRDR) to accommodate the channel effects of shadowing and small scale fading. Factors considered are

1. The emulated satellite's effective isotropic radiated power (EIRP), which is given as transmit power plus transmit antenna gain.
2. The Free Space Loss (FSL), which is given as:

   $$20log\left(\frac{4\pi d}{\lambda}\right),$$

   where d = 1400 metres is the maximum distance between the transmit and receive antennas and using a centre frequency of 2.43GHz gives λ = 0.12m
3. Receiver sensitivity is given in the Elektrobit (channel sounder) user manual as:

   $$n_{therm} + 10\log(BW) + n_{sys},$$

   where n_{therm} is the thermal noise of the sounder's resistors, given as -174dBm/Hz;
   BW is the null to null bandwidth, which is 50MHz;
   n_{sys} is system noise figure of the channel sounder, which is specified as 3dB.
4. The channel sounder processing gain is given as:

   $$10\log(N_C),$$

   where N_C is the number of chips per code (also known as code length), which is 63 for the Newlands Corner measurements.
5. The theoretically available impulse response dynamic range (IRDR) is then given as

   EIRP – FSL – Receiver Sensitivity + Processing Gain,

   which amounts to 35dBm – 103.3dB + 94dBm + 17.9dB = **43.6dB.**